

STATEMENT OF ORIGINALITY

The experimental work in this thesis has been carried out by the author in the Department of Chemistry at the University of Leicester between September 2003 and August 2006. This work has not previously been published or submitted for any other degree at this or any other university.

Signed:  Date: 7/12/06

Thesis submitted for the degree of

Doctor of Philosophy

at the University of Leicester

by

Donna Jade Palmer MChem (Leicester)

Department of Chemistry

University of Leicester



**University of
Leicester**

September 2006

UMI Number: U220717

All rights reserved

INFORMATION TO ALL USERS

The quality of this reproduction is dependent upon the quality of the copy submitted.

In the unlikely event that the author did not send a complete manuscript and there are missing pages, these will be noted. Also, if material had to be removed, a note will indicate the deletion.



UMI U220717

Published by ProQuest LLC 2013. Copyright in the Dissertation held by the Author.
Microform Edition © ProQuest LLC.

All rights reserved. This work is protected against
unauthorized copying under Title 17, United States Code.



ProQuest LLC
789 East Eisenhower Parkway
P.O. Box 1346
Ann Arbor, MI 48106-1346

STATEMENT OF ORIGINALITY

The experimental work in this thesis has been carried out by the author in the Department of Chemistry at the University of Leicester between September 2003 and August 2006. The work has not been submitted, and is not presently being submitted, for any other degree at this or any other university.

Signed 

Date 7/12/06

Donna Palmer
University of Leicester
University Road,
Leicester.
LE1 7RH

SOLUTE EFFECTS ON THE PROPERTIES OF SUPERCRITICAL SOLUTIONS

DONNA JADE PALMER

UNIVERSITY OF LEICESTER

2006

ABSTRACT

Supercritical (sc) fluids are extensively used for material processing and carbon dioxide is the most commonly used solvent. In these solutions, solute-solvent interactions consist primarily of Van der Waals forces. By employing more polar solvents high concentrations of polar solutes can be dissolved, resulting in more ordered solutions. This has an effect on clustering and mass transport. The aim of this thesis is to investigate solute-solute-solvent interactions in sc difluoromethane and to quantify the effect on solution viscosity for the first time. Chapter One provides a general introduction to sc fluids and details of the experimental work are described in Chapter Two.

The local composition about a solvatochromic probe has been measured as a function of pressure and the Kamlet-Taft polarisability/dipolarity and hydrogen bond donor parameters are presented in Chapter Three. Variations in these solvent properties are understood in terms of solute aggregation and a model for solvation considering the relative solute-solvent interactions is proposed.

In Chapter Four the use of a piezoelectric quartz crystal as a reliable high-pressure viscometer is proposed and used to determine the viscosity of sc solutions as a function of pressure and solute polarity. A modification of the Dole-Jones equation is used to model the viscosity of simple sc solutions and the volume fraction of solute is shown to be the key factor affecting solution viscosity.

Rapid expansion of supercritical solutions (RESS) is a technique used to reduce particle size and alter morphology of pharmaceuticals. Many pharmaceuticals are polar compounds or salts, which suffer from low solubility in sc carbon dioxide. Chapter Five presents the applicability of sc difluoromethane for precipitation of materials by RESS. For the first time, a number of compounds with different polarities are processed. Qualitative trends in particle morphology are explained in terms of solute aggregation and solution viscosity.

ACKNOWLEDGEMENTS

The first person I would like to thank is my supervisor Prof. Andrew Abbott. Over the past three years his ideas, support and patience have been invaluable to me. His unwavering optimism and enthusiasm have allowed me to go further and in directions I would have never believed possible.

I would like to show my appreciation to the members of the Abbott group for their support and discussion, especially my partner in crime Miss Mistry. Rob, Glen and John get special mentions for supporting me with my extra curricular activities. Thanks also go to Karl, Katy and the Hillman group, specifically Samantha, for their ideas and help with some of the techniques that have been new to me. I would also like to thank Eric Hope, Andrew West and both past and present members of the Fluorine group, I have often considered myself as a surrogate member.

Without the knowledge and commitment of the workshop guys, John Weale, Carl Schieferstein and especially Keith Wilkinson, none of my experiments would have ever got running and I would have never been able to 'push the button'. I will be truly disappointed if I don't continue to see Keith out and about on a Saturday night. A big thank you must also go to all those in the department that have helped me at some point during my time in Leicester.

Special thanks go to my parents and sister for their support and understanding. It may have taken me a little longer but I have finished 'school' and am heading out into the big wide world of work at the same time as my little sister. Finally a huge thank you goes to Simon who has inadvertently shared all the ups and downs of the past three years. No matter how many times I say thank you it still won't be enough. I hope this proves I haven't spent the past three years watching daytime television and shopping.

'Do they give a Noble Prize for attempted chemistry?'

- "Sideshow" Bob Terwilliger

CONTENTS

	PAGE
CHAPTER ONE Introduction	1
1.1 Supercritical Fluids	2
1.2 Industrial Applications of Supercritical Fluids	4
1.2.1 Chromatography	4
1.2.2 Extraction and Separation Processes	5
1.2.3 Chemical Reactions	7
1.2.4 Materials Processing	9
1.3 Hydrofluorocarbons	14
1.4 Project Outline	18
1.5 References	19
CHAPTER TWO Experimental	25
2.1 Materials	26
2.1.1 Solvents	26
2.1.2 Solutes	26
2.1.3 Solvatochromic Probes	26
2.1.4 Electrochemical Reagents	26
2.1.5 Piezoelectric Quartz Crystal Modification materials	27
2.2 Instrumentation	27
2.2.1 High Pressure Apparatus	27
2.2.2 UV-Visible Cell	28
2.2.3 Electrochemical Cell	28
2.2.4 RESS Apparatus	30
2.3 Experimental Procedure	33
2.3.1 Visual Observations	33
2.3.2 Solvatochromic Shift Measurements	33
2.3.3 Viscosity Measurements	34
2.3.4 Diffusion Coefficient Measurements	34
2.3.5 RESS Experiments	35
2.4 Piezoelectric Quartz Crystal Modification Procedure	36
2.4.1 Non-electrolyte Solute Investigations	36
2.4.2 Electrolyte Solute Investigations	38
2.5 References	38
CHAPTER THREE Probing Solute Clustering in Supercritical Solutions Using Solvatochromic Parameters	39
3.1 Introduction	40
3.1.1 Solvatochromism	40
3.1.2 The Kamlet and Taft Polarisability/dipolarity π^* Parameter	42
3.1.3 Hydrogen Bonding and the Hydrogen Bond Donor Parameter α	45
3.2 Results and Discussion	49
3.2.1 Polarisability Parameter π^*	50
3.2.2 Hydrogen Bond Donor Properties α	60
3.3 Conclusion	69
3.4 References	70

	PAGE
CHAPTER FOUR Determination of the Viscosity of Supercritical Solutions	73
4.1 Introduction	74
4.1.1 Viscosity	75
4.1.2 The Piezoelectric Quartz Crystal Resonator	78
4.2 Results and Discussion	86
4.2.1 Technique and Method Design	86
4.2.2 Non-electrolyte Solutions	94
4.2.3 Electrolyte Solutions	106
4.2.4 Electrochemistry in Supercritical Electrolyte Solutions	117
4.3 Conclusion	121
4.4 Reference	122
CHAPTER FIVE Solute Precipitation from Supercritical Solutions	127
5.1 Introduction	128
5.1.1 Rapid Expansion of Supercritical Solutions	128
5.1.2 Design of Particle Formation System	139
5.2 Results and Discussion	142
5.2.1 Effect of Extraction Pressure	146
5.2.2 Slow Expansion of Supercritical Solutions	154
5.2.3 Effect of Pre-expansion Temperature	159
5.2.4 Effect of Supercritical Solvent	167
5.3 Conclusion	169
5.4 References	170
CHAPTER SIX Summary and Future Work	173
6.1 Summary	174
6.1.1 Probing Solute Clustering in Supercritical Solutions	174
6.1.2 Determination of the Viscosity of Supercritical Solutions	174
6.1.3 Solute Precipitation from Supercritical Solutions	175
6.2 Future Work	176
6.2.1 Structure of Supercritical Solutions	176
6.2.2 Analysis of the Conductivity and Viscosity of Supercritical Solutions	176
6.2.3 Particle Size Analysis	176
APPENDIX	177

Chapter One

INTRODUCTION

-
- 1.1 Supercritical Fluids
 - 1.2 Industrial Applications of Supercritical Fluids
 - 1.2.1 Chromatography
 - 1.2.2 Extraction and Separation Processes
 - 1.2.3 Chemical Reactions
 - 1.2.4 Materials Processing
 - 1.3 Hydrofluorocarbons
 - 1.4 Project Outline
 - 1.5 References
-

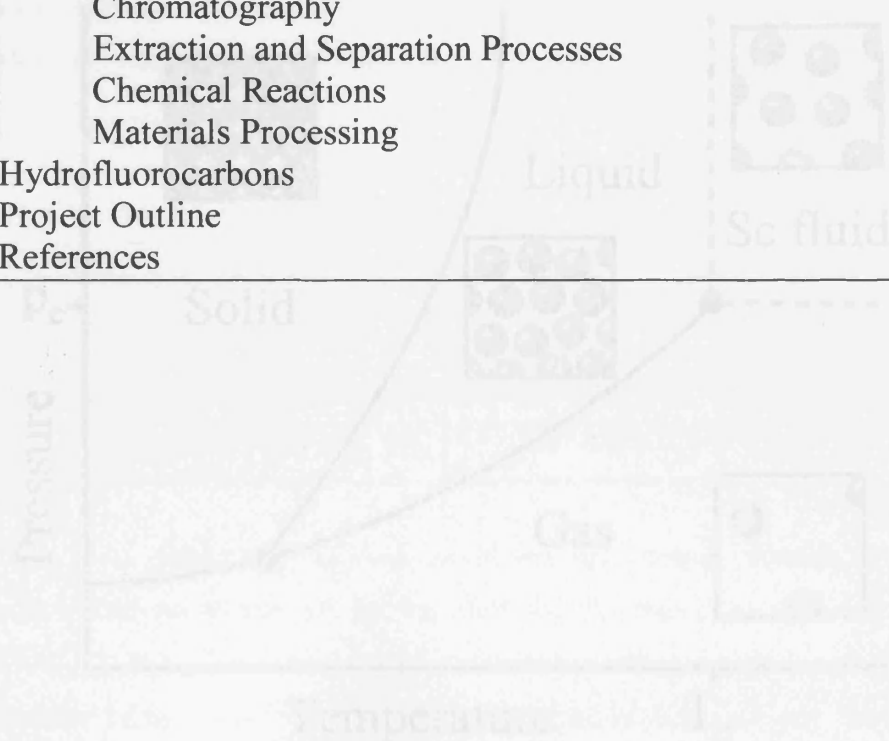


Figure 1.1 Phase diagram of a pure substance.

1.1 Supercritical Fluids

The existence of supercritical (sc) fluids has been known for more than a century¹ and, in the last few decades, their enhanced solvent characteristics and applications as reaction media have had rejuvenated interest. This can be attributed to a movement to find cleaner and more sustainable solvent systems as alternatives to solvents such as volatile organic solvents (VOCs), currently most often used in industry and academia. Applications of supercritical fluids include extraction and separation,^{2,3} chemical synthesis⁴⁻⁶ and materials processing.⁷⁻⁹ Over the past decade, a number of books have been published^{2,3,5} and, in 1999 an extensive review covering many aspects of supercritical fluid research was published.¹⁰

For a pure material a sc fluid is defined as a substance that exists above its critical pressure (p_c) and critical temperature (T_c), but below the pressure required to condense it into a solid.¹¹ Figure 1.1 represents a typical phase diagram, clearly showing the areas where a substance exists as a solid, liquid, gas or sc fluid.

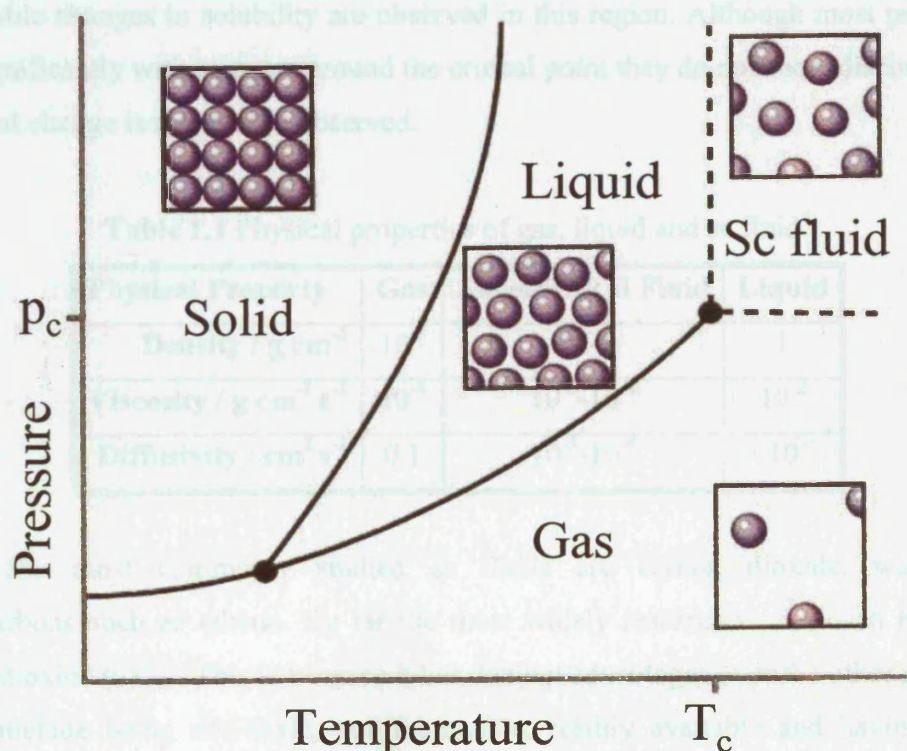


Figure 1.1 Phase diagram of a pure substance

The properties of a sc fluid are often described as being intermediate between those of a gas and a liquid. However, there are exceptions and not all physical properties are intermediate between those of a gas and a liquid. Compressibility and heat capacity are much higher near the critical point than they are in gases or liquids. A comparison of some typical values of selected physical properties of sc fluids, gases and liquids is shown in Table 1.1. At high pressures and temperatures, molecules possess high kinetic energy similar to that of a gas. For this reason, diffusivity and mass transport properties are enhanced compared to liquids. Conversely, the density of a sc fluid is similar to that of a liquid, which means solvent molecules have a large interaction with solutes. Hence, it is not surprising that density gives an indication of the solvating power of a sc fluid. In simple terms the transport properties of sc fluids are similar to gases whereas their solvating properties are more akin to liquids.

Fluid density is a highly tunable function of pressure. Therefore solubility and other density-dependent properties, such as viscosity and relative permittivity, can be easily manipulated with variations in pressure. Close to the critical point, a dramatic change in density occurs with a relatively small change in pressure. As a result, remarkable changes in solubility are observed in this region. Although most properties vary significantly with pressure around the critical point they do not show discontinuity; a gradual change is more often observed.

Table 1.1 Physical properties of gas, liquid and sc fluid⁴

Physical Property	Gas	Supercritical Fluid	Liquid
Density / g cm^{-3}	10^{-3}	0.1-1	1
Viscosity / $\text{g cm}^{-1} \text{s}^{-1}$	10^{-4}	10^{-3} - 10^{-4}	10^{-2}
Diffusivity / $\text{cm}^2 \text{s}^{-1}$	0.1	10^{-3} - 10^{-4}	$<10^{-5}$

The most commonly studied sc fluids are carbon dioxide, water and hydrocarbons such as ethane. By far the most widely researched and used has been carbon dioxide (CO_2). This is because it has distinct advantages over the other solvents, which include being non-toxic, non-flammable, readily available and having easily accessible critical constants ($p_c = 73.08 \text{ bar}$, $T_c = 31.1 \text{ }^\circ\text{C}$).⁵ Unfortunately, due to the low polarity of CO_2 , its applications are limited to low-to-medium molecular weight, non-polar solutes, where solubilities have been reported as between 0.1 and 10 mol %.¹²

The main disadvantage of using sc CO₂ and fluids such as ethane is that they are non-polar. The addition of a co-solvent or modifier, such as methanol or acetone, may enhance the solvating power to allow the dissolution of a number of polar solutes.¹³⁻¹⁵ Unfortunately this has a number of disadvantages associated with it, namely the critical temperature is increased and the modifier is frequently left as a residue in the product. This may cause problems if, for example, the product is to be used for human consumption.¹⁶⁻¹⁸

In general, the greater the polarity of a substance, the greater is its critical temperature.⁶ The high polarity of water makes it an ideal sc solvent and the properties of sc water are very different to those of liquid water. For example, the reduced dielectric constant allows high solubility of organic solutes and reduced solubility of inorganic solutes. Unfortunately, water has extremely high critical constants ($p_c = 220.5$ bar, $T_c = 374$ °C),¹⁹ that make it undesirable for widespread industrial use. Studies have also shown near critical water to be a highly corrosive medium.^{20,21} Nevertheless, reactions in sc water have been performed²² and sc water has been studied extensively for applications in the treatment of organic waste. Several supercritical water oxidation (SCWO) plants are in operation worldwide.²³

In the last decade it has been suggested that hydrofluorocarbons (HFCs) could be used as alternative sc fluids.²⁴ These compounds are non-toxic, inert, more polar than CO₂ and still possess reasonably low critical constants.

1.2 Industrial Applications of Supercritical Fluids

The unique tuneability of the solvent properties of sc fluids by simple manipulation of temperature and/or pressure offers a means of control and selectivity for various chemical applications. This has led to their exploitation in a number of applications including chromatography (section 1.2.1), extraction (section 1.2.2), reaction processes (section 1.2.3) and materials processing (section 1.2.4).

1.2.1 Chromatography

In the 1960s it was recognised that sc mobile phases could be employed in chromatographic analysis.²⁵ Supercritical fluid chromatography (SFC) uses sc gases as a mobile phase to transport compound mixtures over the stationary phase. The solvating power of the mobile phase is determined by its density, which can easily be modified by varying the pressure. Due to the enhanced mass transport properties in sc fluids, a

mixture of high molecular mass compounds can be dissolved and efficiently separated at relatively low temperatures. SFC is therefore an important analytical technique that can provide information on solubility and partitioning behaviour of a wide range of molecular mass compounds, which is essential in designing chemical processes. The theory and fundamentals of SFC has been reviewed by Hupe *et al.*²⁶

Early studies of SFC included the separation of oligomers,²⁷ polystyrene²⁸ and high molecular weight compounds.²⁹ Analysis of aromatics in diesel fuel³⁰ and plant materials³¹ has also been studied by this technique. A recent review by Chester and Pinkston describes some of the most recent applications of SFC.³² These include food related separations, work with natural products and applications in forensic science.^{33,34}

The most commonly employed mobile phase in SFC is sc CO₂, but modifiers are often added to this non-polar fluid to change the solvating strength of the mobile phase.³⁵⁻³⁷ Using a more polar sc fluid can increase the solvent strength of a mobile phase and some research groups have examined the use of 1,1,1,2-tetrafluoroethane in both the liquid and sc state.^{38,39} It was reported that for many separations 1,1,1,2-tetrafluoroethane offers better separation than sc CO₂. In addition, the scale-up of SFC processes employing 1,1,1,2-tetrafluoroethane as sc solvent is potentially easier and less expensive than that employing sc CO₂ due to the lower pressures required to achieve sc conditions.³⁹

1.2.2 Extraction and Separation Processes

An ideal extraction method should be rapid, simple and cost effective. The substrate should be recovered without loss or degradation and be ready for direct analysis without the need for additional concentration or fractionation steps. In addition, no auxiliary waste should be produced. Liquid solvent extraction techniques fail to meet a number of these criteria but supercritical fluid extraction (SFE) has emerged as a promising alternative. This is because solvent properties of sc fluids, such as solvating power, can change significantly with only modest changes in temperature or pressure. This allows the solvent to be tuned to maximise solubility or “extractability” of a substrate.^{2,3}

The extractability of a particular compound is governed by different molecular interactions (i.e. solute-solvent interactions versus solute-solute or solute-matrix interactions). Over the last few decades the solubilities of solids and liquids in sc fluids has been studied extensively. Knowledge of the solubility of a compound in a sc fluid

gives an indication of the extractability of that compound from the sc solvent. This is important in process design and is influenced by the chemical functionality of substrate, nature of solvent and operating conditions.

Approximately 98 % of SFE processes employ sc CO₂ as the extracting solvent. This is due to its relatively low critical parameters, environmentally benign nature and its low cost. Alternatively a more polar fluid may be used as the extracting solvent.

From the 1960s onwards researchers have explored the potential of SFE to extract spices,^{40,41} herbs,⁴² coffee^{2,3,43} and tea,^{2,3,44} predominately using sc CO₂. The extraction of hops,⁴⁵⁻⁴⁷ cholesterol from food products,⁴⁸⁻⁵⁰ perfumes and flavours from natural products⁵¹ and unsaturated fatty acids from fish oils^{52,53} using SFE has also been investigated. Today there are a number of large-scale SFE processes in operation around the world. Table 1.2 shows the number and locations of commercial SFE plants as of 2000.²³ The largest of these processes are the decaffeination of coffee and tea and the extraction of hops. Switching from previous extraction methods to SFE has reduced the amounts of undesirable residues left in products. For example, tetrachloromethane was previously used to decaffeinate coffee and dichloromethane was employed in the extraction of hops. Both of these compounds have been suggested to be carcinogens and toxic to humans.⁵⁴ The treatment of decontaminated soil and waste⁵⁵⁻⁵⁷ and cleaning of metals, plastics, ceramics and optical materials²³ have also been investigated and SFE is a promising alternative to the current processes that are used.

In synthetic chemistry, SFE is an attractive alternative to conventional methods of purification for pharmaceuticals, vitamins and high value products.⁵⁸ However, it is mainly restricted to the food industry for the extraction of natural products.⁵⁹ In some cases SFE is also used for the fractionation of products.⁶⁰ An example of this is paprika extraction where oleoresins are separated in the first step, which is followed by the separation of aroma and essential oils.⁶¹ A similar process is used for Rosemary extraction. Here the antioxidants are separated from the aroma and essential oils.⁶²

Supercritical fluid extraction is still a rapidly growing area of research and another potential application is the purification of polymers. This takes advantage of the variation in polymer solubility governed by chain length and operating conditions. SFE has also been applied to the textile industry as an alternative for dyeing materials. The dyestuff is dissolved in the sc fluid and the mixture is capable of penetrating the whole fibre. By controlled depressurisation the dyestuff remains in the fibre and no residual

solvent is left in the sample.⁶³ The works of McHugh and Krukonis² and Taylor³ provide a more detailed treatment of the basics and applications of SFE.

Table 1.2 Commercial SFE plants as of 2000.²³

Commercial Application	Number Of Plants	America	Asia/Australia	Europe
Coffee and Tea	5	1	0	4
Hops	7	4	1	2
Nicotine	3	1	1	1
Chemistry	5	3	1	1
Environmental	5	2	3	0
Spices	12	1	5	6
Fats and oils	8	0	4	5
Medical Products	7	0	1	6
Flavours	7	0	3	4
Total	59	12	18	29

1.2.3 Chemical Reactions

In the early nineteenth century Baron Cagniard de La Tour noted the reactivity of near critical water.⁶⁴ Following his pioneering work a number of reactions in sc H₂O were investigated and are reviewed by Morey.⁶⁵ Despite this, it has not been until the past few decades that research into the use of sc fluids as reaction media has grown significantly.

The unique combination of gas-like diffusivity and viscosity, liquid-like density and tuneable solvating power and polarity with a sc fluid allow different types of reactions to benefit particularly from specific fluid properties.⁵ This area has been reviewed by Jessop and Leitner, covering a wide range of reactions including organometallic, organic, photochemical and catalytic. The majority have utilised sc CO₂ and, to a lesser extent, sc H₂O.⁵

Many reactions that occur in sc fluids can occur in liquid solvents, but there are numerous examples where the use of a sc fluid can cause the rate of reaction to increase. There are several factors that account for this effect but it is not always easy to identify the dominant contributor. The low viscosity of sc fluids allows diffusion-

controlled processes, such as free radical and enzymatic reactions, to proceed at higher rates than in liquids.⁶⁶ Solvent polarity has also been shown to have an influence on the rates of reactions.⁶⁷ In addition, reaction rates are known to change exponentially with temperature and high temperatures are usually involved in sc synthesis. Fox *et al.*⁶⁸ demonstrated that the rate of Michael addition of piperidine to methyl propiolate in polar sc fluoroform (CHF₃) and non-polar sc ethane depends on fluid density. A difference in rate constants was observed between the two solvents and this was attributed to the reaction dependence on the solvent dielectric constant. The reaction proceeds through a highly polar transition state and this is better stabilised in the more polar sc CHF₃ solvent.

A number of studies have shown that product selectivity in sc reactions is strongly dependent on fluid density and, as a result, was found to be greater than for those reported in conventional solvents.⁶⁹ These studies have encouraged researchers to examine the influence of either bulk or local density variations on stoichiometric reactions.⁷⁰⁻⁷² An example is the Diels-Alder reaction, where endo/exo and ortho/para selectivity appears to be controlled to some extent by variations in bulk density. Paulaitis and Alexander examined the effect of sc CO₂ pressure on the reaction rate of maleic anhydride and isoprene.⁶⁹ The reaction mechanism was thought to be the same irrespective of the solvent medium and results showed the reaction rate increased with solvent pressure. Later Kim and Johnston carried out the Diels-Alder reaction of cyclopentadiene and methyl acrylate. Both endo and exo products are formed although selectivity for the endo product was found to increase with fluid density. This was attributed to the differences in dipole moments between the endo and exo products, the endo being the more polar of the two.⁷³

Sc fluids have no surface tension and will diffuse rapidly to occupy the entire volume of a system. As a result, if other gases are introduced to the system they will be completely miscible with the sc fluid. Processes such as hydrogenation,^{5,74-76} hydroformylation^{5,77} and oxidation^{5,78} take advantage of this complete miscibility. Another example of a sc chemical reaction is the sc water oxidation (SCWO) process.⁷⁹⁻⁸¹ This technique employs sc H₂O to achieve complete oxidation of organic wastes found in many industrial wastewater streams.

The industrial uses of sc fluids as reaction media are becoming more widespread and examples include the synthesis of ammonia and low-density polyethylene. Recently, the first multi-purpose industrial-scale sc fluid plant was commissioned

(Thomas Swan & Co. Ltd., County Durham, UK).⁸² Reactions carried out at the Thomas Swan plant include hydrogenations,⁸³ Friedel-Crafts alkylations,⁸⁴ hydroformylations,⁸⁵ esterifications⁸⁵ and etherifications.⁸⁶

1.2.4 Materials Processing

One of the largest areas of sc fluid research is concerned with the processing of materials such as polymers and pharmaceuticals. Ipatiev reported the earliest research into polymer processing with sc fluids at the beginning of the twentieth century,⁸⁷ discovering that when ethylene is heated above its critical temperature it oligomerises into higher molecular mass alkanes. Since this initial work, many studies have been conducted on polymer synthesis using sc fluids and a number of reviews have been published.^{7,8,88}

The high diffusivity, low viscosity and lack of surface tension of sc fluids means they are capable of being adsorbed into polymers. This results in swelling of the polymer and changes the mechanical and physical properties of the material. The most important of these effects is the reduction of the glass transition temperature, T_g , of glassy polymers. This process is known as plasticization and many polymer-processing operations take advantage of this effect.⁸⁹

Within a swollen polymer diffusion rates are greatly enhanced. This has advantages in polymer synthesis, as the enhanced diffusion of monomers within the swollen polymer allows polymerisation to occur within the polymer matrix. It has been shown that a range of polymer blends can be made by infusion of a styrene monomer and an initiator into several polymers including polychlorotrifluoroethylene (PCTFE), polymethylpentane (PMP) and polyethylene (PE).^{90,91} Another application which takes advantage of the enhanced diffusivity in swollen polymers is impregnation. Berens demonstrated that compressed CO₂ could be used to accelerate the rate of adsorption of additives into a number of glassy polymers in comparison to conventional methods.⁹² Many types of additives have been successfully impregnated into polymers these include organometallic compounds,⁹³ metal complexes⁹⁴ and dyestuffs.⁹⁵ This area has been reviewed in detail by Kazarian.⁹

In certain polymers, plasticization caused by swelling a polymer with a sc fluid may induce crystallisation. This will occur when induced mobility in the polymer chains allows rearrangement into kinetically-favoured configurations forming crystallites.⁹ Several research groups have shown that sc CO₂ can be used to change the

degree of crystallinity in poly(ethylene terephthalate) (PET).^{91,96-100} The degree of crystallinity affects the gas permeability of the material. This is particularly important as materials based on PET are widely used in the production of drink bottles and synthetic polyester fibres. The crystallinity of polyester fibres will affect the ability to dye the material and the morphology will determine the mechanical properties of the fibres.

When a polymer is swollen with a sc fluid the viscosity of the polymer can be greatly reduced. This can be beneficial for polymer extrusion processes. Conventional methods have a large energy requirement and employ heat and plasticizers to reduce the polymer viscosity. The increased temperatures can lead to polymer degradation and the plasticizers often remain in the end product, which affects its properties and performance.

A further application of sc fluids to polymer modification is polymer foaming. The resultant materials have widespread applications from use as heat insulators to vehicle parts and cushioning materials in furniture. Polymer foaming is achieved using substances called blowing agents. Before chlorofluorocarbons (CFCs) were implicated as the primary agent responsible for ozone depletion they were used extensively. Since the phase-out of these compounds, hydrofluorocarbons (HFCs) have been researched as potential replacements. This is because they retain many of the properties of CFCs, such as low toxicity and high solubility within the polymer material, but do not contribute to ozone depletion.¹⁰¹ One of the most important factors that influences the final properties of the foam is the solubility of the blowing agent in the polymer. Computer simulations have shown that the solubility can affect the bubble size, size distribution and density of the foam.¹⁰²

In addition to polymer modifications, sc fluids have been used to alter the size and shape of materials. This is significantly important for the pharmaceutical industry, as there are problems associated with the conventional methods employed to reduce the particle size such as milling, grinding, sublimation and recrystallisation from solution; for example many substrates are unstable under conventional milling conditions and, in recrystallisation, products can be easily contaminated with the solvent. The unique solvent properties of sc fluids such as low viscosity, high diffusivity and tuneable solubility allow them to hold a distinct advantage over these conventional methods.

The simplest method of precipitating a solid from a sc fluid is to allow the fluid to cool and liquefy. The remaining solid may then be recovered by conventional filtration

or evaporation. This method does not allow for control over the size and morphology of the solid and consequently a number of techniques have been developed.¹⁰³⁻¹⁰⁶ These can be divided into three broad groups: Precipitation from sc solutions; precipitation from a saturated solution using sc fluid as a non-solvent or anti-solvent; and precipitation from gas saturated solutions. A summary of the different methods of particle preparation using sc fluids is shown in Table 1.3.

Process	Acronym	Solute	Solvent	Anti-solvent	Mechanism of Particle Precipitation	Factors Affecting Particle Morphology
Rapid expansion of supercritical solutions	RESS	Material	Pure or modified sc fluid	Absent	Loss of sc fluid solvent power after rapid expansion	Temperature, extraction pressure, pre-expansion, collection vessel, orifice design
Particles from gas-saturated solutions	PGSS	Compressed gas / sc fluid	Melt of material	Absent	Phase change in solute and Joule-Thomson cooling	Temperature, reaction pressure, pre-expansion, collection vessel, orifice design
Gas anti-solvent system	GAS	Material	Liquid organic solvent	Compressed gas / sc fluid	Volumetric expansion of solvent by anti-solvent	Temperature, pressure, solvent, rate and extent of addition, reaction vessel
Precipitation using compressed anti-solvent	PCA	Material	Liquid organic solvent	Compressed gas / sc fluid	Extraction of solvent and solvent evaporation into anti-solvent	Temperature, pressure, solvent, rate of addition, reaction vessel
Aerosol solvent extraction system	ASES	Material	Liquid organic solvent	Compressed gas / sc fluid	Extraction of solvent and solvent evaporation into anti-solvent	Temperature, pressure, solvent, rate of addition, reaction vessel
Supercritical anti-solvent system	SAS	Material	Liquid organic solvent	Sc fluid	Extraction of solvent and solvent evaporation into anti-solvent	Temperature, pressure, solvent, rate of addition, reaction vessel
Solution enhanced dispersion by supercritical fluids	SEDS	Material	Liquid organic solvent	Sc fluid	Dispersion of solute into solvent, extraction of solvent and solvent evaporation into anti-solvent	Temperature, reaction pressure, solvent, flow rate, orifice design

Table 1.3 Summary of sc fluid particle formation processes 103-106

In the nineteenth century, Hannay and Hogarth¹ reported that the expansion of a solution of CoCl_2 in sc ethanol led to a snow-like precipitation of the dissolved cobalt salt, but it was not until the late 1980s that the rapid expansion of a supercritical solution (RESS) process was developed. Smith *et al.* presented a wide range of fine powdered materials that could be formed by sc fluid expansion.¹⁰⁷ The concept of the process is relatively simple and involves dissolving a solute in a sc fluid followed by rapid expansion of the sc solution across an orifice into a low-pressure chamber. This causes supersaturation of the solute, homogeneous nucleation and particle formation. By varying parameters such as pressure, temperature and orifice geometry, particles with different sizes and morphologies may be obtained. Advantages of RESS are that it is a solvent free process, very fine particles can be produced, down to the nanometer scale, and the particles have a controllable and narrow size distribution. This can be of particular importance in drug delivery systems where inhalation and retention of drugs in the body need to be optimised. The RESS technique is also very rapid and thus allowing the isolation of compounds that usually decompose by other techniques. The major disadvantage of this technique is the large sc fluid to solid ratio that is required as the solubility of most materials in the more commonly employed sc fluids is low.

The application of sc fluids as anti-solvents is an alternative recrystallisation technique for processing solids that are insoluble in sc fluids. There are several variations that exist, including precipitation with compressed antisolvent (PCA), gas anti-solvent system (GAS) and solution-enhanced dispersion by supercritical fluids (SEDS). These processes differ in the way contact between solution and anti-solvent is achieved. The method using sc anti-solvents exploits the ability of gases to dissolve in organic liquids. The dissolution of the anti-solvent lowers the solvent power of the liquid for the solute in solution, hence causing the material to precipitate. This is similar to the well-established use of aliphatic hydrocarbons to precipitate materials from a more polar organic solvent. The GAS or supercritical antisolvent (SAS) processes involve mixing a solution with a dense gas so that the expanded solution has a lower solvent strength to the pure solution. The mixture will become supersaturated and the solute precipitates. Aerosol solvent extraction systems (ASES) involve injecting a solution through a nozzle into a vessel containing a dense gas. The liquid solvent power is reduced by a large volume expansion and causes supersaturation and consequent particle formation. Advantages of anti-solvent processes are that particles of very small size are formed that can be easily controlled. There have been numerous publications to

show that sc anti-solvent processes can be used to recrystallise a variety of materials, for example polymers, pharmaceuticals and dyes.¹⁰³ The main disadvantages are that they are batch processes and require the use of organic solvents.

More recently, a method for particle formation called particles from gas-saturated solutions (PGSS) has been developed. This process avoids the problems of product and gas recovery sometimes encountered with RESS or GAS techniques. The sc fluid is solubilised or emulsified in a molten or liquid-suspended material. When expanded through a nozzle, the sc fluid comes out of solution and disperses the material into fine particles or droplets. This technique is ideal for materials that are not soluble in the sc fluid but can absorb large concentrations such as some polymers. The simplicity of the PGSS process has led to low processing costs and a wide variety of products can be treated. Several applications of this technique have been found in spray coating of paints and pigmented polymers for automotive topcoats, furniture lacquers and aerospace and corrosion coatings.¹⁰³

1.3 Hydrofluorocarbons

Since the discovery of the ‘ozone hole’ over Antarctica in the mid-1980s, a number of substances have been held responsible for ozone depletion. As a result, the Montreal Protocol¹⁰¹ stipulated that the production and consumption of ozone-depleting compounds were to be phased out by 2005. This has been successfully achieved and, in 2005, the Kyoto Protocol came into force. This agreement includes the requirement to reduce the emissions of several greenhouse gases including CO₂ and HFCs to approximately 5 % of their 1990 values by 2008.

One class of ozone-depleting compounds are CFCs. These were used in a variety of applications including refrigeration, air-conditioning, insulation and medical products. An alternative class of compounds that has been extensively researched as a replacement for CFCs are HFCs and today several are employed as refrigerants and propellants.^{108,109} Some of these HFCs are shown in Table 1.4.

As HFCs retain many of the desired properties of CFCs an intensive research and assessment program was conducted in 1989 by the Alternative Fluorocarbons Environmental Acceptability Study (AFEAS) to assess their environmental effects.¹⁰¹ It was concluded that HFCs are largely removed in the lower atmosphere by natural processes. Hydroxyl radicals break down most to form simple, inorganic species already present in the atmosphere. As a consequence, the ozone depletion potential

(ODP) of all HFCs is zero.¹¹⁰ However, some HFCs have the ability to form trifluoroacetyl halides. These compounds may dissolve in water and form trifluoroacetate (TFA) salts.¹¹¹ Low concentrations of these salts are already present in rain and seawater and may be degraded by microorganisms naturally present in sediment and soils. Although further testing continues it has been suggested that these salts do not pose a threat to the environment.¹¹²

The destruction of HFCs in the lower atmosphere, along with their relatively short lifetime, means they do not accumulate and consequently have a smaller potential contribution to the greenhouse effect. This greatly reduces their global warming potential (GWP). A comparison of atmospheric lifetime for CO₂ and a number of HFC and CFC compounds is shown in Table 1.5. The rate of removal of CO₂ varies significantly because several removal processes exist. Although atmospheric decay rates of HFCs do vary the lifetimes are significantly lower than that of CO₂. Furthermore, when compared to the alternatives, HFCs promote the efficient use of energy in their areas of application. In most cases, when the direct and indirect contributions to global warming from emissions are compared, HFCs are the most energy efficient and safest available.

Table 1.4 Common uses for several HFCs^{113,114}

Hydrofluorocarbon	Abbreviation	Flammability	Application
Difluoromethane	HFC 32	Flammable	Refrigeration Blends
Pentafluoroethane	HFC 125	Non-flammable	Refrigeration Blends
1,1,1,2-Tetrafluoroethane	HFC 134a	Non-flammable	Refrigeration, Aerosol, Foam Blowing, Medical
1,1,1-Trifluoroethane	HFC 143a	Flammable	Refrigeration Blends
1,1-Difluoroethane	HFC 152a	Flammable	General Aerosol
1,1,1,2,3,3,3-Heptafluoropropane	HFC 227ea	Non-flammable	Fire Fighting Agent, Aerosol Propellant
1,1,1,3,3,3-Hexafluoropropane	HFC 236fa	Non-flammable	Foam Blowing

Table 1.5 Atmospheric lifetimes of CO₂ and some selected CFCs and HFCs¹¹⁵

Compound	Abbreviation	Estimated Atmospheric Lifetime / years
Carbon dioxide	CO ₂	50 – 500
Trichlorofluoromethane	CFC 11	45
Dichlorodifluoromethane	CFC 12	100
1,2-Dichlorotetrafluoroethane	CFC 114	300
Chloropentafluoroethane	CFC 115	1700
1,1-Difluoroethane	HFC 152a	1.4
Difluoromethane	HFC 32	5
1,1,1,2-Tetrafluoroethane	HFC 134a	13.8
1,1,1,2,3,3,3-heptafluoropropane	HFC 227ea	33

In addition to the refrigeration and propellant industries HFCs have been examined for use in dry-cleaning,¹¹⁶ natural product extraction³⁸ and HPLC mobile phases.^{39,117}

In the last few years numerous applications for the use of HFCs as solvents have been explored and it has been suggested that, in some cases, they could be employed as an alternative to using sc CO₂.³⁸ In the past decade research has shown that several HFC fluids are relatively polar solvents with accessible critical constants.¹¹⁸⁻¹²⁰ These HFCs are readily available, non-toxic, inert and can be efficiently used on their own, or in conjunction with CO₂, as sc solvents for both extraction and reactions. The three most commonly researched HFCs are shown in Table 1.6. A number of conventional solvents are also shown for comparison.

In recent years, Abbott and co-workers have extensively investigated and characterised the solvent properties of difluoromethane (CH₂F₂) and 1,1,1,2-tetrafluoroethane (CF₃CH₂F).^{121,122} The solubilities of a range of aromatic hydrocarbons and unsaturated carboxylic acids have been shown to be greater in sc CH₂F₂ than in the more commonly used sc CO₂. The Kamlet-Taft solvatochromic shift parameters were used to characterise the solvent properties and both HFC solvents were shown to exhibit significant hydrogen bond donating properties.^{123,124} In addition, the use of CH₂F₂ for polymer modification was investigated. It was found that the fluid had a higher solubility than CO₂ in the samples studied.¹²⁵

Table 1.6 Critical data and properties of some common HFCs^{108,109,126-128}

Hydrocarbon	Abbreviation	T _c / °C	p _c / bar	μ / D
1,1,1,2-Tetrafluoroethane	HFC 134a	101.21	40.59	2.058
Difluoromethane	HFC 32	78.26	57.82	1.987
Pentafluoroethane	HFC 125	66.33	36.29	1.563
Toluene	N/A	318.80	41.06	0.31
Dichloromethane	DCM	273.00	61.71	1.14
Ethyl Acetate	N/A	250.30	37.81	1.82

1.4 Project Outline

The majority of sc fluid applications have focussed on the use of sc CO₂ because of its readily-accessible critical constants, environmental compatibility and low cost. However, the low solubility of polar species in sc CO₂ limits the solutes that can be used. In recent years it has been highlighted that HFC fluids such as CH₂F₂ and CF₃CH₂F have accessible critical constants and can be used as an alternative to sc CO₂.³⁸ Research has shown these solvents are relatively polar, exhibit significant change in polarisability with pressure and are strong hydrogen bond donors close to the critical pressure.^{118-120,123,124} These solvent properties are more tuneable than sc CO₂, hence it may be possible to examine specific solvent effects in HFCs that are not observed in sc CO₂. Here, CH₂F₂ has been employed as the sc fluid to explore the interactions with dissolved solutes and associated solvent properties.

Since the work by Eckert and co-workers¹²⁹ in the early 1980s, a great deal of attention has been given to the local sc solvent environment. Many spectroscopic techniques such as infrared and fluorescence spectroscopies have been used to probe the local sc solvent environment around a solute.^{130,131} These investigations have shown that, close to the critical density, there is considerable local density augmentation about the solute when the solute-solvent interactions are attractive. The work presented here is the first to measure the effect of solute clustering on solution polarity. Solvent polarisability/dipolarity and hydrogen bond donor characteristics have been measured as a function of pressure when solutes with varying degrees of polarity are solubilised.

In the second part of this research the bulk solution property of viscosity is examined. This is the first concerted study of solution viscosity with a range of solute polarities. A novel technique has been employed, which relates the shift in resonant frequency of a quartz crystal resonator to the viscosity of its surroundings. The viscosity of several sc solutions has been measured as a function of pressure and the trends explained in terms of solute clustering indicated by the solvatochromic measurements.

The final part of this study aims to examine the effects solvent properties such as viscosity and clustering have on the morphology of a material when it is precipitated from a sc solution. A technique called rapid expansion of supercritical solutions, or RESS, is used and process parameters such as extraction pressure and pre-expansion temperature have been systematically varied. The precipitated material is analysed by scanning electron microscopy and qualitative trends presented.

1.5 References

1. Hannay, J. B.; Hogarth, J. *Proc. R. Soc. London* **1879**, *29*, 324.
2. McHugh, M.; Krukonis, V. J. *Supercritical Fluid Extraction*, 2nd ed.; Butterworth-Heinemann: Boston, **1994**.
3. Taylor, L. T. *Supercritical Fluid Extraction*; Wiley: New York, **1996**.
4. Oakes, R. S.; Clifford, A. A.; Rayner, C. M. *J. Chem Soc. Perkin Trans. 1*, **2001**, 917.
5. Jessop, P. G.; Leitner, W. *Chemical Synthesis using Supercritical Fluids*; Wiley-VCH: Weinheim, **1999**.
6. Savage, P. F.; Goplan, S.; Mizan, T. I.; Martino, C. J.; Brook, E. E. *AIChE J.* **1995**, *41*, 1723.
7. Cooper, A. I. *J. Mater. Chem.* **2000**, *10*, 207.
8. Kendall, J. L.; Canelas, D. A.; Young, J. L.; DeSimone, J. M. *Chem. Rev.* **1999**, *99*, 543.
9. Kazarian, S. G. *Polym. Sci. Ser. C*, **2000**, *42*, 78.
10. Noyori, R. *Chem. Rev.* **1999**, *99*, 353.
11. Stanley, H. E. *Phase Transitions and Critical Phenomena*; Clarendon press: Oxford, **1987**.
12. Bartle, K. D.; Clifford, A. A.; Jafar, S. A.; Shilstone, G. F. *J. Phys. Chem. Ref. Data*, **1991**, *20*, 713.
13. Dobbs, J. M.; Johnston, K. P. *Ind. Eng. Chem. Res.* **1987**, *26*, 1476.
14. Ting, S. S. T.; Macnaughton, S. J.; Tomasko, D. L.; Foster, N. R. *Ind. Eng. Chem. Res.* **1993**, *32*, 1471.
15. Zhang, X.; Han, B.; Hou, Z.; Zhang, J.; Liu, Z.; Jiang, T.; He, J.; Li, H. *Chem. Eur. J.* **2002**, *8*, 5107.
16. Anitescu, G.; Tavlarides, L. L. *J. Supercrit. Fluid.* **1997**, *11*, 37.
17. Anitescu, G.; Tavlarides, L. L. *J. Supercrit. Fluid.* **1999**, *14*, 197.
18. Foster, N. R.; Singh, H.; Yun, J. S. L.; Tomasko, D. L.; MacNaughton, S. J. *Ind. Eng. Chem. Res.* **1993**, *32*, 2849.
19. Reid, R. C.; Prausnitz, J. M.; Poling, B. E. *The Properties of Gases and Liquids*; 4th ed.; McGraw-Hill: New York, **1987**.
20. Berry, W. E. *Int. Corros. Conf. Ser.* **1976**, *NACE-4*, 48.
21. Vermilyea, D. A.; Indig, M. E. *J. Electrochem. Soc.* **1972**, *119*, 39.
22. Darr, J.; Poliakoff, M. *Chem Rev.* **1999**, *99*, 495.

23. Socrates Intensive Program on High Pressure Chemical Engineering Processes: Basics and Applications, Barcelona, 2004.
24. Olsen, S. A.; Tallman, D. E. *Anal. Chem.* **1996**, *68*, 2054.
25. Klesper, E.; Corwin, A. H.; Turner, D. A. *J. Org. Chem.* **1962**, *27*, 700.
26. Hupe, K. P.; McNair, H. M.; Kok, W. T.; Bruin, G. J.; Poppe, H.; Poole, C.; Chester, T. L.; Wimalasena, R. L.; Wilson, G. S. *LC-GC*, **1992**, *10*, 211.
27. Schmitz, F. P.; Klesper, E. *Polymer Bulletin*, **1981**, *14*, 679.
28. Schmitz, F. P. *Polymer Comm.* **1983**, *24*, 142.
29. Jackson, W. P.; Markides, K. E.; Lee, M. L. *J. High Resolut. Chromatogr. Chromatogr. Comm.* **1986**, *9*, 213.
30. Brooks, M. W.; Uden, P. C. *J. Chromatogr.* **1993**, *637*, 179.
31. Namiesnik, J.; Gorecki, T. *JPC-J. Planar Chromat-Mod. TLC*, **2000**, *13*, 404.
32. Chester, T. L.; Pinkston, J. D. *Anal. Chem.* **2002**, *74*, 2801.
33. Radcliffe, C.; Maguire, K.; Lockwood, B. *J. Biochem. Biophys. Methods*, **2000**, *43*, 261.
34. McAvoy, Y.; Dost, K.; Jones, D. C.; Cole, M. D.; George, M. W.; Davidson, G. *Forensic Science International*, **1999**, *99*, 123.
35. Pyo, D. *Microchem. J.* **2001**, *68*, 183.
36. Gritti, F.; Felix, G.; Archard, M.-F.; Hardouin, F. *Chromatographia*, **2001**, *53*, 201.
37. Brenner, B. A. *Anal. Chem.* **1998**, *70*, 4594.
38. Corr, S. *J. Fluorine Chem.* **2002**, *118*, 55.
39. Vayisoglu-Giray, E. S.; Johnson, B. R.; Frere, B. G. A. M.; Bartle, K. D.; Clifford, A. A. *Fuel*, **1998**, *77*, 1533.
40. Illes, V.; Daood, H. G.; Biacs, P. A.; Gnayfeed, M. H.; Meszaros, B. *J. Chromatogr. Sci.* **1999**, *37*, 345.
41. Lack, E.; Seidlitz, H. *Process Technol. Proc.* **1996**, *12*, 253.
42. Ma, X.; Yu, X.; Zheng, Z.; Mao, J. *Chromatographia*, **1991**, *32*, 40.
43. Dean, J. R.; Liu, B.; Ludkin, E. *Methods Biotechnol.* **2000**, *13*, 17.
44. Chang, C. J.; Chiu, K.-L.; Chen, Y.-L. *Food Chem.* **1999**, *69*, 109.
45. Smith, G. W. *Eur Patent Appl.* **1995**, EP679419.
46. Verschuene, M.; Sandra, P.; David, F. *J. Chromatogr. Sci.* **1992**, *30*, 388.
47. Sieves, U.; Eggers, R. *Chem. Eng. Proc.* **1996**, *35*, 239.
48. Jimenez-Carbona, M. M.; Luque de Castro, M. D. *Anal. Chem.* **1998**, *70*, 2100.

49. Wehling, R. L. *Adv. App. Biotechnol. Ser.* **1991**, *12*, 133.
50. Froning, G. W. *Adv. App. Biotechnol. Ser.* **1991**, *12*, 277.
51. Hawthorne, S. B.; Krieger, M. S.; Miller, D. J. *Anal. Chem.* **1988**, *60*, 472.
52. Imanishi, N.; Fukuzato, R.; Furuta, S.; Ikawa, N. *R&D. Research and Development, Kobe Steel Ltd.* **1989**, *39*, 29.
53. Lucien, F. P.; Liong, K. K.; Cotton, N. J.; MacNaughton, S. J.; Foster, N. R. *Australas. Biotechnol.* **1993**, *3*, 143.
54. *Dictionary of Substances and their Effects*; Gangolli, S. Eds; Royal Society of Chemistry: Cambridge, **1999**.
55. Laiten, A.; Michaux, A.; Aaltanen, O. *Environ. Technol.* **1994**, *15*, 715.
56. Misch, B.; Firus, A.; Brunner, G. *J. Supercrit. Fluid.* **2000**, *17*, 227.
57. Sahle-Demessie, E. *Environ. Technol.* **2000**, *21*, 447.
58. Chester, T. L.; Pinkston, J. D.; Raynie, D. E. *Anal. Chem.* **1998**, *70*, 301.
59. Steyler, D. *Separation Processes in the Food and Biotechnology Industries*; Woodhead: Cambridge, **1996**, pp 17-64.
60. Zosel, K. *Angew. Chem. Int. Ed. Engl.* **1978**, *17*, 702.
61. Vesper, H.; Nitz, S. *Adv. Food Sci.* **1997**, *17*, 172.
62. Senorans, F. J.; Ibanez, E.; Cavero, S.; Tabera, J.; Reglero, G. *J. Chromatogr. A*, **2000**, *870*, 491.
63. Montero, G. A.; Smith, C. B.; Hendrix, W. A.; Butcher, D. L. *Ind. Eng. Chem. Res.* **2000**, *39*, 4806.
64. Cagniard de La Tour, C. *Ann. Chim. Phys.* **1822**, 127.
65. Morey, G. W.; Niggli, P. *J. Am. Chem. Soc.* **1913**, *35*, 1086.
66. Mesiano, A. J.; Beckman, E. J.; Russell, A. J. *Chem. Rev.* **1999**, *99*, 623.
67. Zhang, X.; Sui, Q.; Han, B.; Yan, H.; Wang, Y. *J. Supercrit. Fluid.* **2000**, *17*, 171.
68. Rhodes, T. A.; O'Shea, K.; Bennett, G.; Johnston, K. P.; Fox, M. A. *J. Phys. Chem.* **1995**, *99*, 9903.
69. Paulaitis, M. E.; Alexander, G. C. *Pure Appl. Chem.* **1987**, *59*, 61.
70. Reaves, J. T.; Roberts, C. B. *J. Chem. Soc. Chem. Eng. Comm.* **1999**, *171*, 117.
71. Dillow, A. K.; Brown, J. S.; Liotta, C. L.; Eckert, C. A. *J. Phys. Chem. A*, **1998**, *102*, 7609.
72. Thompson, R. L.; Glaser, R.; Bush, D.; Liotta, C. L.; Eckert, C. A. *Ind. Eng. Chem. Res.* **1999**, *38*, 4220.
73. Kim, S.; Johnston, K. P. *J. Chem. Soc. Chem. Eng. Comm.* **1988**, *63*, 49.

74. Tsang, C. Y.; Streett, W. B. *Chem. Eng. Sci.* **1981**, *36*, 993.
75. Jessop, P. G.; Hsiao, Y.; Ikariya, T.; Noyori, R. *J. Am. Chem. Soc.* **1996**, *118*, 344.
76. Xiao, J.; Nefkens, S. C. A.; Jessop, P. G.; Ikariya, T.; Noyori, R. *Tetrahedron Lett.* **1996**, *37*, 2813.
77. Koch, D.; Leitner, W. *J. Am. Chem. Soc.* **1998**, *120*, 13398.
78. Nelson, W. M.; Puri, I. K. *Ind. Eng. Chem. Res.* **1997**, *36*, 3449.
79. Kritzer, P.; Dinjus, E. *J. Chem. Eng.* **2001**, *83*, 207.
80. Koda, S.; Kanno, N.; Fujiwara, H. *Ind. Eng. Chem. Res.* **2001**, *40*, 3861.
81. Portela, J. R.; Nebot, E.; de la Ossa, E. M. *J. Supercrit. Fluid.* **2001**, *21*, 135.
82. <http://www.thomas-swan.co.uk>.
83. Licence, P.; Ke, J.; Sokolova, K.; Ross, S. K.; Poliakov, M. *Green Chem.* **2003**, *5*, 99.
84. Hitzler, M. G.; Smail, F. G.; Ross, S. K.; Poliakov, M. *Chem. Comm.* **1998**, *3*, 359.
85. Hyde, J. R.; Licence, P.; Carter, D.; Poliakov, M. *Applied Cat.* **2001**, *222*, 119.
86. Walsh, B.; Hyde, J. R.; Licence, P.; Poliakov, M. *Green Chem.* **2005**, *7*, 456.
87. Ipatiev, V.; Rutala, O. *Ber. Dtsch. Chem.* **1913**, *46*, 1748.
88. Cooper, A. I.; DeSimone, J. M. *Curr. Opin. Solid State Mat. Sci.* **1996**, *1*, 761.
89. Alessi, P.; Cortesi, A.; Kikic, L.; Vecchione, F. *J. Appl. Polym. Sci.* **2003**, *88*, 2189.
90. Watkins, J. J.; McCarthy, T. J. *Macromolecules*, **1994**, *27*, 4845.
91. Muth, O.; Hirth, T.; Vogel, H. *J. Supercrit. Fluid.* **2000**, *17*, 65.
92. Berens, A. R.; Huvard, G. S.; Korsmeyer, R. W.; Kunig, R. W. *J. Appl. Polym. Sci.* **1992**, *46*, 231.
93. Poliakov, M.; Howdle, S. M.; Kazarian, S. G. *Angew. Chem. Int. Ed. Engl.* **1995**, *34*, 1275.
94. Watkins, J. J.; McCarthy, T. J. *J. Chem. Mater.* **1995**, *7*, 1991.
95. Von Schnitzler, J.; Eggers, R. *J. Supercrit. Fluid.* **1999**, *16*, 81.
96. Zhong, Z.; Zheng, S.; Mi, Y. *Polymer*, **1999**, *40*, 3829.
97. Mensitieri, G.; Del Nobile, N. A.; Guerra, G.; Apicella, A.; Al Ghatta, H. *Polym. Eng. Sci.* **1995**, *35*, 506.
98. Kazarian, S. G.; Brantley, N. H.; Exckert, C. A. *Vibr. Spectrosc.* **1999**, *19*, 277.
99. Mizoguchi, K.; Hirose, T.; Naito, Y.; Kamiya, Y. *Polymer*, **1987**, *28*, 1298.
100. Lambert, S. M.; Paulaitis, M. E. *J. Supercrit. Fluid.* **1991**, *14*, 15.

101. <http://www.afeas.org>.
102. Shafi, M. A.; Joshi, K.; Flumerfelt, R. W. *Chem. Eng. Sci.* **1997**, *52*, 635.
103. Jung, J.; Perrut, M. *J. Supercrit. Fluid.* **2001**, *20*, 179.
104. Knez, Z.; Weidner, E. *Curr. Opin. Solid State Mater. Sci.* **2003**, *7*, 353.
105. Ye, X.; Wai, C. M. *J. Chem. Ed.* **2003**, *80*, 198.
106. Cansell, F.; Aymonier, C.; Loppinet-Serabi, A. *Curr. Opin. Solid State Mater. Sci.* **2003**, *7*, 331.
107. Matson, D. W.; Fulton, J. L.; Peterson, R. C.; Smith, R. D. *Ind. Eng. Chem. Res.* **1987**, *26*, 2298.
108. Meyer, C. W.; Morrison, G. *J. Phys. Chem.* **1991**, *95*, 3860.
109. Meyer, C. W.; Morrison, G. *J. Chem. Eng. Data*, **1991**, *36*, 409.
110. Ravishankara, A. R. *Science* **1994**, *263*, 71.
111. Frank, H.; Christoph, E. H.; Holm-Hansen, O.; Bullister, J. L. *Environ. Sci. Technol.* **2002**, *36*, 12.
112. Boutonnet, J. C. *Environmental Risk Assessment of Trifluoroacetic Acid; Human and Ecological Risk Assessment*, **1999**, *5*, 59.
113. Noakes, T. *J. Fluorine Chem.* **2002**, *118*, 35.
114. Tsai, W.-T. *Chemosphere*, **2005**, *61*, 1539.
115. <http://www.grida.no/>
116. Woerlee, G. F.; Van Roosmalen, M.; Breijer, A.; Van Ganswijk, J. W.; Wichhart, M. *PCT Int. Appl.* **2003**, pp 21.
117. Cantrell, G. O.; Blackwell, J. A. *J. Chromatogr. A*, **1997**, *782*, 237.
118. Abbott, A. P.; Eardley, C. A. *J. Phys. Chem. B*, **1998**, *102*, 8574.
119. Abbott, A. P.; Eardley, C. A.; Tooth, R. J. *J. Chem. Eng. Data*, **1999**, *44*, 112.
120. Abbott, A. P.; Eardley, C. A. *J. Phys. Chem. B*, **1999**, *103*, 2504.
121. Abbott, A. P.; Eltringham, W.; Hope, E. G.; Nicola, M. *Green Chem.* **2005**, *7*, 210.
122. Abbott, A. P.; Corr, S.; Durling, N. E.; Hope, E. G. *J. Chem. Eng. Data*, **2002**, *47*, 900.
123. Abbott, A. P.; Corr, S.; Durling, N. E.; Hope, E. G. *J. Phys. Chem. B*, **2003**, *107*, 10628.
124. Abbott, A. P.; Eardley, C. A.; Scheirer, J. E. *Phys. Chem. Chem. Phys.* **2001**, *3*, 3722.

125. Abbott, A. P.; Eltringham, W.; Hillman, A. R.; Hope, E. G. *J. Polym. Sci.* **2006**, *44*, 1072.
126. Tillner-Roth, R.; Baehr, H. D. *J. Phys. Chem. Ref. Data*, **1994**, *23*, 657.
127. Tillner-Roth, R.; Yokozeki, A. *J. Phys. Chem. Ref. Data*, **1997**, *26*, 1273.
128. *Organic Solvents Physical Properties and Methods of purification*, 4th Ed.; Riddick, J. A.; Bunger, W. B.; Sakanl, T. K., Eds.; Techniques of Chemistry; Wiley: New York, **1986**; Vol. 2.
129. Eckert, C. A.; Ziger, D. H.; Johnston, K. P.; Ellison, T. K. *Fluid Phase Equilib.* **1983**, *14*, 167.
130. Blitz, J. P.; Yonker, C. R.; Smith, R. D. *J. Phys. Chem.* **1989**, *93*, 6661.
131. Heitz, M. P.; Bright, F. V. *J. Phys. Chem.* **1996**, *100*, 6889.

Chapter Two

The solutes employed in this work and their purity, molecular mass and melting points are shown in Table 2.1. Each solute was used as received.

EXPERIMENTAL

Table 2.1 Solutes investigated in this work

Solute	Company	Molecular Mass	Melting Point/°C	Purity/%
Naphthalene	Purac	128.17	80-82	99
2,2,2-Trifluoroethanol	Purac	138.13	124-126	99
1,2-Dichloroethane	Aldrich	136.15	120-122	99
1,2-Dichlorobenzene	Aldrich	146.96	179-182	99
1,2-Dichloroethane	Aldrich	136.15	120-122	99

2.1 Materials

2.1.1 Solvents

2.1.2 Solutes

2.1.3 Solvatochromic Probes

2.1.4 Electrochemical Reagents

2.1.5 Piezoelectric Quartz Crystal Modification Materials

2.2 Instrumentation

2.2.1 High Pressure Apparatus

2.2.2 UV-Visible Cell

2.2.3 Electrochemical Cell

2.2.4 RESS Apparatus

2.3 Experimental Procedure

2.3.1 Visual Observations

2.3.2 Solvatochromic Shift Measurements

2.3.3 Viscosity Measurements

2.3.4 Diffusion Coefficient Measurements

2.3.5 RESS Experiments

2.4 Piezoelectric Quartz Crystal Modification Procedure

2.4.1 Non-electrolyte Solute Investigations

2.4.2 Electrolyte Solute Investigations

2.5 References

2.1 Materials

2.1.1 Solvents

Difluoromethane was obtained from Ineos Fluor and carbon dioxide from BOC Limited. Both were used as received (purity > 99.9 %). All other solvents were obtained from Fischer (purity > 99.9 %) and used directly as received.

2.1.2 Solutes

The solutes employed in this work and their purity, molecular mass and melting points are shown in Table 2.1. Each solute was used as received.

Table 2.1 Solutes investigated in this work

Solute	Company	Molecular Mass	Melting Point / °C	Purity / %
Naphthalene	Fisons	128.17	80-82	98
<i>o</i> -hydroxybenzoic acid	Fisons	138.13	158-160	97
<i>p</i> -toluic acid	Aldrich	136.15	180-182	98
Tetrabutylammonium tetrafluoroborate	Fluka	329.28	159-162	99
Anthracene	Aldrich	178.23	216-218	99

2.1.3 Solvatochromic Probes

The solvatochromic dyes Nile blue A Oxazone (Nile Red) (Aldrich, 99 %) and *N,N*-dimethylindoaniline (Phenol Blue) (Aldrich, 97 %) were used as received. Dye concentrations ranged from 10^{-5} to 10^{-6} mol dm⁻³ such that solute-solute interactions could be ignored.

2.1.4 Electrochemical Reagents

Tetrabutylammonium tetrafluoroborate (TBABF₄) (Fluka, electrochemical grade, 99 %) was used as the electrolyte and ferrocene (Fluka, 98 %) as the electroactive species, each were used as received.

2.1.5 Piezoelectric Quartz Crystal Modification Materials

1-Butanethiol (Aldrich, > 99 %) and ethanol (VWR, > 99.9%) were both used as received. Scotch-Weld™ epoxy structural adhesive was obtained from 3M and used to coat one side of a crystal for the electrolyte solute studies.

2.2 Instrumentation

2.2.1 High Pressure Apparatus

An example of the high-pressure apparatus used is shown in Figure 2.1. Prior to each experiment the cell was purged with the appropriate gas. Pressure was applied using a model P50-series piston controlled pump (Thar Technologies inc.; Pittsburgh, PA) and monitored (± 2 bar) using a Swagelok manometer. At the centre of the cell the tip of an iron/constantan thermocouple was in contact with the solvent and a constant temperature (± 0.5 °C) was retained using a CAL 9300-controlled heater.

The cell was constructed from 316 stainless steel and had a working pressure of 300 bar. Burst discs rated to 400 bar were fitted for safety. The internal volume of the cell was approximately 37 cm³. To provide the high-pressure seal between the head and base of the cell a viton 90 O-ring and PTFE ring were employed and the electrical feedthroughs (RS Components Ltd.) were sealed with Swagelok fittings.

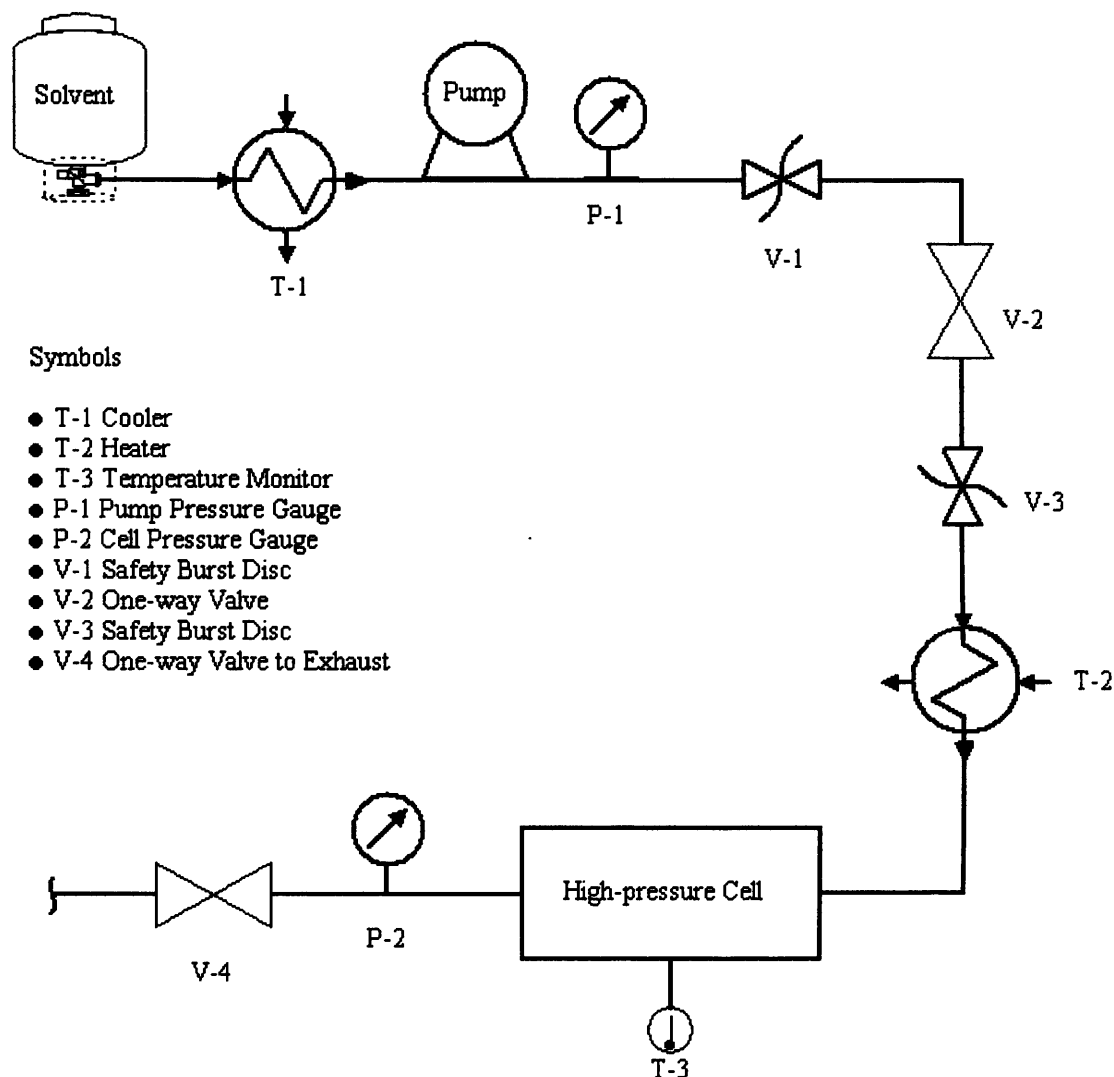


Figure 2.1 Schematic diagram of high pressure equipment

2.2.2 UV-visible Cell

A Shimadzu Model UV-1601 Spectrophotometer was used to measure the solvatochromic shift of Nile Red and Phenol Blue in the visible absorbance region. The optical high-pressure cell is shown in Figure 2.2. The cell was constructed from 316 stainless steel with 1 cm thick sapphire windows. The gas seals were made from Teflon. The cell path length was 6 cm and the cell volume was 100 cm³. Light was fed into and out of the high-pressure cell by fibre-optic cables (Hellma, Müllheim, FRG) fitted with a 662 QX prism adapter.

2.2.3 Electrochemical Cell

The cell was designed to be double ended so both electrochemical and viscosity data may be obtained simultaneously (Figure 2.3).

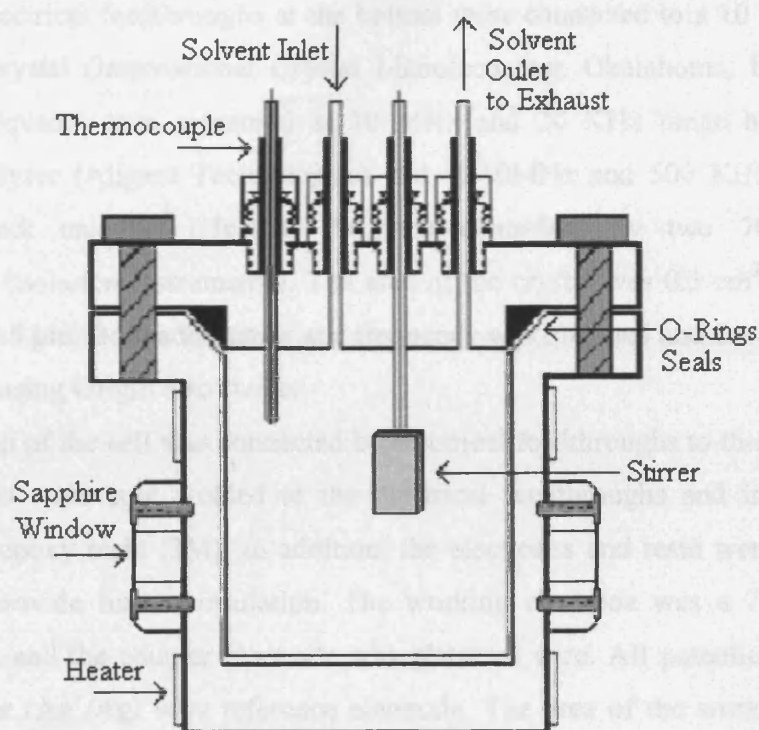


Figure 2.2 High-pressure optical cell for solvatochromic measurements

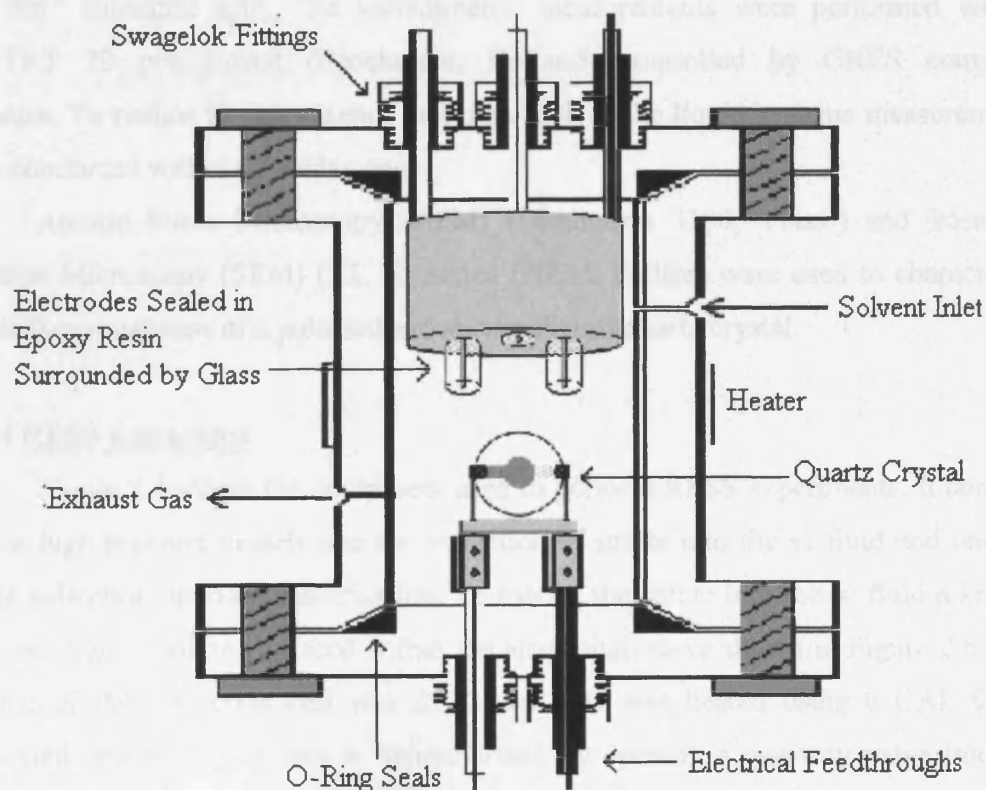


Figure 2.3 Electrochemical cell

The electrical feedthroughs at the bottom were connected to a 10 MHz AT-cut gold quartz crystal (International Crystal Manufacturing; Okalahoma, USA), whose oscillating frequency was measured at 10 MHz and 20 KHz range by a E5061A Network Analyser (Aligent Technologies) and at 10MHz and 500 KHz range by a 8751A network analyser (Hewlett Packard) controlled by two 7060 systems voltammeters (Solarton instruments). The area of the crystal was 0.3 cm^2 and it had a thickness of $< 5 \text{ }\mu\text{m}$. Both admittance and frequency was obtained and the data acquired was analysed using Origin 6 software.

The top of the cell was connected by electrical feedthroughs to three electrodes. The electrodes were spot welded to the electrical feedthroughs and insulated with Scotch-Weld epoxy resin (3M). In addition, the electrodes and resin were surrounded by glass to provide further insulation. The working electrode was a $7.85 \times 10^{-3} \text{ cm}^2$ platinum disk and the counter electrode was platinum wire. All potentials are quoted versus a silver (Ag^+/Ag) wire reference electrode. The area of the working electrode was calculated by voltammetry, using an aqueous solution of $0.03 \text{ mol dm}^{-3} \text{ K}_3\text{Fe}(\text{CN})_6$ and $0.5 \text{ mol dm}^{-3} \text{ KNO}_3$ at $25 \text{ }^\circ\text{C}$ and was polished with $1 \text{ }\mu\text{m}$ alumina and cycled in 0.1 mol dm^{-3} sulphuric acid. The voltammetric measurements were performed with a PGSTAT 20 potentiostat (Ecochemie, Holland) controlled by GRES computer software. To reduce iR interference and distortion in the liquid systems measurements were conducted within a Faraday cage.

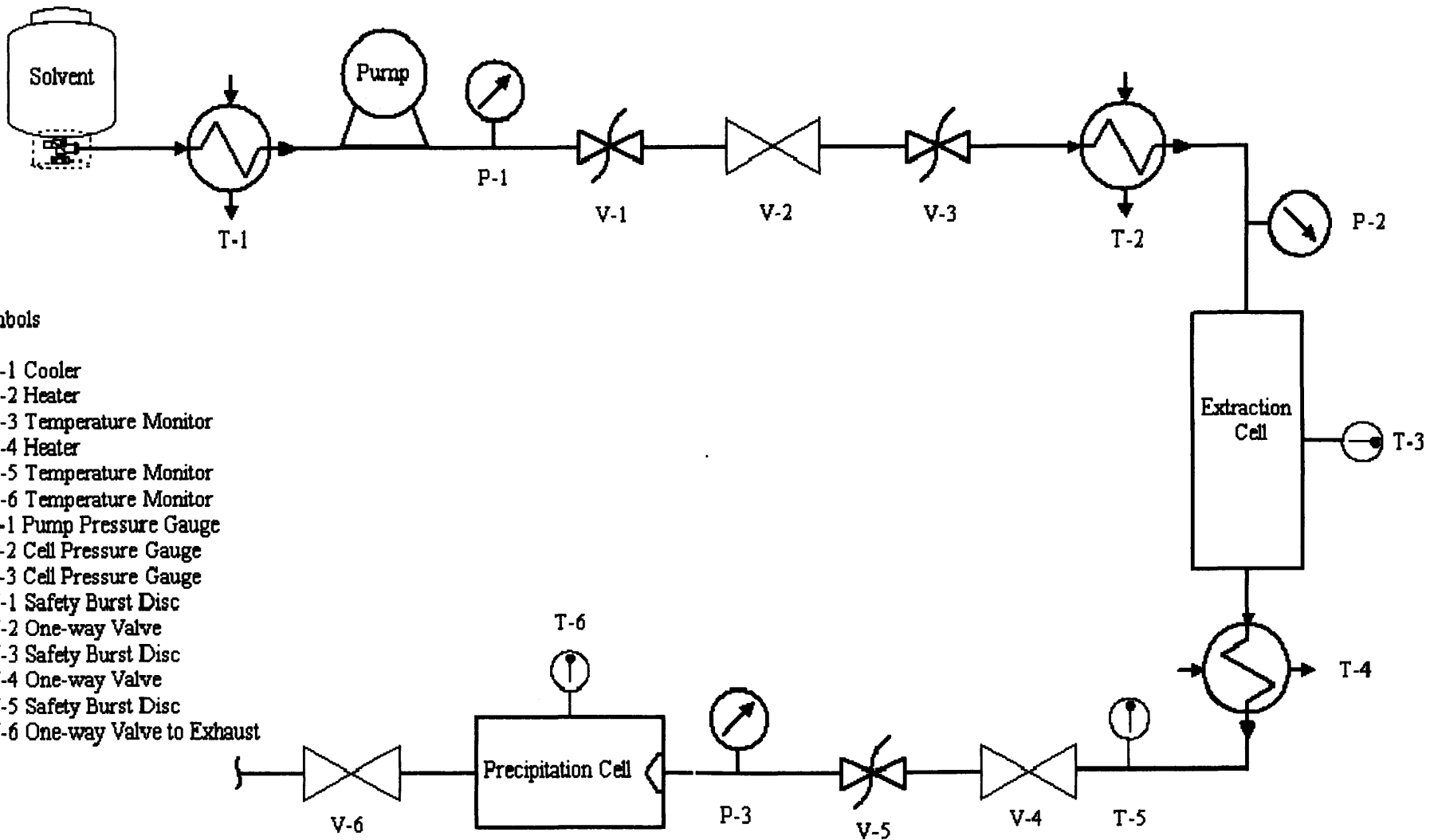
Atomic Force Microscopy (AFM) (Dimension 3100, Veeco) and Scanning Electron Microscopy (SEM) (XL 30 Series ESEM, Philips) were used to characterise the surface roughness of a polished and an unpolished quartz crystal.

2.2.4 RESS Apparatus

Figure 2.4 shows the equipment used to perform RESS experiments. It consists of two high-pressure vessels one for extraction of solute into the sc fluid and one for solute collection upon depressurisation. To extract the solute into the sc fluid a known concentration of solute is placed within the aluminium sieve shown in Figure 2.6. The volume of the extraction cell was 22.52 cm^3 and was heated using a CAL 9300-controlled heater. The system is depressurised by opening a one-way valve into the collection cell that was kept at atmospheric pressure. At the exit of the valve a nozzle was fitted. This was a piece of stainless steel with a $300 \text{ }\mu\text{m}$ diameter hole drilled through it. It was possible to heat the interconnecting tubing between the extraction

vessel and the depressurisation valve using Thermomelt heater wire (Infroheat) controlled by a Carel heat controller. The tubing was insulated with 25 ml Rockwool insulator and aluminium foil. To ensure a constant temperature was retained (± 0.5 °C), an iron/constantan thermocouple was in contact with the solution.

A sample vial was mounted in the collection vessel to gather the samples for analysis. On the lid of the sample vial was a SEM specimen stub with an adhesive carbon disk affixed to the surface. The stub could easily be removed and the samples were analysed by SEM using low pressure wet mode. To minimise the effects of charging of the solutes, samples were coated with a thin layer of gold (approximately 22.5 nm) using an Edwards Scancoat (Edwards Laboratories, Milpitas, CA) six Pirani 501 (at 45 mV, 0.7 kV, for 90 sec) prior to analysis.



Symbols

- T-1 Cooler
- T-2 Heater
- T-3 Temperature Monitor
- T-4 Heater
- T-5 Temperature Monitor
- T-6 Temperature Monitor
- P-1 Pump Pressure Gauge
- P-2 Cell Pressure Gauge
- P-3 Cell Pressure Gauge
- V-1 Safety Burst Disc
- V-2 One-way Valve
- V-3 Safety Burst Disc
- V-4 One-way Valve
- V-5 Safety Burst Disc
- V-6 One-way Valve to Exhaust

Figure 2.4 Schematic diagram of RESS apparatus

2.3 Experimental Procedure

2.3.1 Visual Observations

To assess whether a sc solution is homogeneous an optical view cell was employed. The sc system was set up in a small cylindrical cell of 9.08 cm³ that contained a 1 cm thick sapphire window at either end (Figure 2.5). To make the visual observations the cell was loaded with the solute and subsequently heated and pressurised to the required conditions.



Figure 2.5 High-pressure optical cell used for visual observations

2.3.2 Solvatochromic Shift Measurements

The optical cell shown in Figure 2.2 was used to measure the solvatochromic shift of two indicator dyes at various pressures and 90 °C. The cell was heated to the required temperature and a small amount of dye was loaded into the cell. The cell was then pressurised to the desired conditions. The system was left to equilibrate for 20 minutes then the absorbance spectra were taken as described in section 2.2.2. The wavelength of absorbance maximum was calculated from an average of three spectra and data were found to vary by no more than 0.5 %.

2.3.3 Viscosity Measurements

The quartz crystal was calibrated from known viscosity and density data.¹⁻⁴ Measurements in liquid media were made using a glass electrochemical vessel. The quartz crystal was fixed to the underside of the cell with silicone adhesive (Dow Corning) such that only one side was exposed to the solvent. To perform measurements in aqueous solution the crystal was suspended in a sample vial filled with the solution. The sample vial was placed in a water-bath and held at a constant temperature (± 0.5 °C) until the oscillating frequency remained constant, spectra were then taken.

For high-pressure viscosity measurements, the electrochemical cell shown in Figure 2.3 was loaded with the appropriate quantity of solute and subsequently heated and pressurised to the desired conditions. The system was allowed to equilibrate until steady oscillation of the crystal was observed at which point the spectra were taken. The oscillation frequency maximum was calculated from an average of three spectra and data were found to vary by no more than 1 %.

Viscosity measurements in liquid solvents and sc difluoromethane-electrolyte solutions were performed using a modified 10 MHz gold quartz crystal and measured on a 8751A network analyser (Hewlett Packard) controlled by two 7060 system voltmeters (Solarton instruments) at an oscillating frequency of 10 MHz and 500 KHz range. Measurements in aqueous solutions and sc difluoromethane-non-electrolyte solutions were made using a E5061A Network Analyser (Aligent Technologies) at an oscillating frequency of 10 MHz and 20 KHz range. Variations in both admittance and oscillating frequency were observed. Variations in oscillating frequency were related to the density-viscosity product of the solution by an extension to the Sauerbrey equation as described in Chapter Four.

2.3.4 Diffusion Coefficient Measurements

Electrochemical investigations performed in the cell shown in Figure 2.3 were carried out using a μ Autolab (Ecochemie, Holland). The cell was loaded with the electrolyte and electroactive species and subsequently heated to the required temperature. The system was then pressurised and allowed to equilibrate for 20 minutes. The electrolyte was tetrabutylammonium tetrafluoroborate and ferrocene was employed as the electroactive species.

The working electrode was a 10 μ m platinum disk microelectrode (CH Components) and the counter electrode was platinum wire. All potentials are quoted

versus a silver (Ag^+/Ag) wire reference electrode. The half wave potentials were determined using cyclic voltammetry at a sweep rate of 10 mV s^{-1} . Diffusion coefficients were obtained from the following equation

$$i_p = 4nFDcr \quad (2.1)$$

where i_p is the limiting current, n is the number of electrons, F is Faradays constant, c is concentration of the electroactive probe employed, r is radius of the working electrode and D is the diffusion coefficient.

2.3.5 RESS Experiments

A schematic diagram of the equipment set up is shown in Figure 2.4 and described in section 2.2.4. To perform an experiment a known quantity of solute was loaded into the aluminium sieve shown in Figure 2.6 and placed inside the extraction cell. The cell was heated and pressurised to the desired conditions and allowed to equilibrate for up to an hour. For a number of experiments the interconnecting tubing between the extraction cell and the depressurisation valve was heated to $140 \text{ }^\circ\text{C}$. In other experiments the tubing was not heated. To depressurise the system a one-way valve was opened to the collection cell, which was kept under atmospheric conditions. The solution entered the collection cell through a nozzle where the spray of particles was collected on a carbon disk adhered to a SEM specimen stub. To prevent sublimation the samples were kept in a freezer ($-17 \text{ }^\circ\text{C}$) until analysis by SEM was performed.

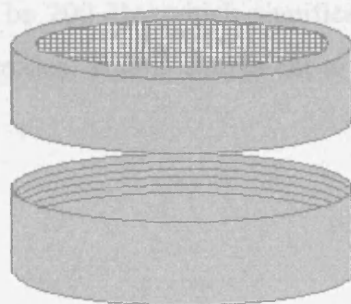


Figure 2.6 Aluminium sieve used to contain solutes for RESS experiments

Salicylic acid precipitate was obtained from liquid dichloromethane by dissolving 0.01 mol dm^{-3} salicylic acid in dichloromethane over a heating mantle. Rapid cooling was achieved by immersing the vessel in dry ice until a precipitate appeared

whereas a second batch was allowed to cool to room temperature and immersed in ice until a precipitate appeared. In both cases the precipitate was subsequently filtered and collected for imaging by SEM.

2.4 Piezoelectric Quartz Crystal Modification Procedure

2.4.1 Non-electrolyte Solute Investigations

A layer of butanethiol was adsorbed onto the gold electrode surface of a quartz crystal. To do this a quartz crystal was first cleaned with dilute HNO₃ solution. The crystal was then placed in a solution of 0.02 mol dm⁻³ 1-butanethiol in ethanol for 36 hours. On removal from the solution the crystal was rinsed with ethanol. The resonant frequency of the crystal was measured prior to and after the thiolation process. The shift in oscillating frequency was calculated and related to the mass deposited onto the electrode surface by the Sauerbrey equation

$$\Delta f = \frac{-2f_0^2 \Delta m}{A(\rho_q \mu_q)^{1/2}} \quad (2.2)$$

where Δf is the shift in resonant frequency, f_0 is the fundamental frequency of the crystal, Δm is the change in mass at the electrode surface, A is the piezoelectrically active crystal area or electrode area, μ_q is the shear modulus of quartz and ρ_q is the density of quartz which have values of 2.947×10^{11} g cm⁻¹ s⁻² and 2.648 g cm⁻³, respectively.

Figure 2.7 shows an admittance-frequency plot for a crystal prior to and after the thiolation process, where admittance is the inverse of impedance. The shift in resonant frequency was calculated to be 200 Hz, which signifies a mass of 2.02 ng cm⁻² was deposited onto the gold electrodes. This is equivalent to an approximate coverage of 2 monolayers.

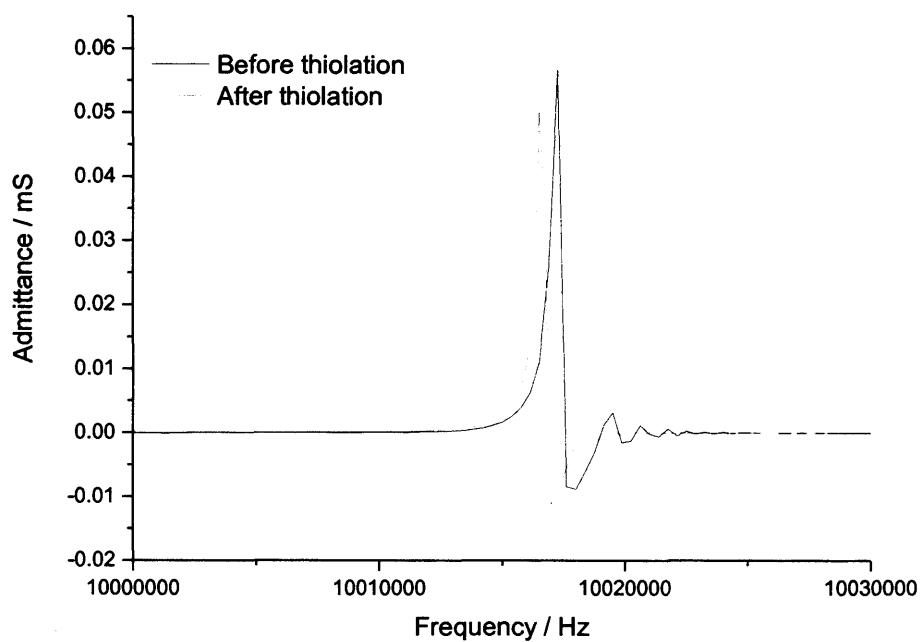


Figure 2.7 Frequency-admittance plot for a quartz crystal before and after thiolation (where admittance is equal to impedance⁻¹)

2.4.2 Electrolyte Solute Investigations

Scotch-Weld™ epoxy resin was mixed according to instructions and a thin layer was manually applied to the surface of one gold electrode with a craft pick. Coverage of the electrode was examined by visual inspection and the resonant frequency of the crystal was used to confirm the layer was sufficiently thin.

2.5 References

1. Tillner-Roth, R.; Yokozeki, A. *J. Phys. Chem. Ref. Data*, **1997**, *26*, 1273.
2. *Organic Solvents Physical Properties and Methods of purification*, 4th Ed.; Riddick, J. A.; Bunger, W. B.; Sakani, T. K., Eds.; Techniques of Chemistry; Wiley: New York, **1986**; Vol. 2.
3. James, C. J.; Mulcahy, D. E.; Steel, B. J. *J. Phys. D: Appl. Phys.* **1984**, *17*, 225.
4. *CRC Handbook of Chemistry and Physics*, 63rd Ed.; Weast, R. C., Eds.; CRC Press: Boca Raton, Florida, **1982**; pp F-11, F-40.

Chapter Three

PROBING SOLUTE CLUSTERING IN SUPERCRITICAL SOLUTIONS USING SOLVATOCHROMATIC PARAMETERS

3.1	Introduction	
3.1.1	Solvatochromism	
3.1.2	The Kamlet and Taft Polarisability/dipolarity Parameter π^*	
3.1.3	Hydrogen Bonding and the Hydrogen Bond Donor Parameter α	
3.2	Results and Discussion	
3.2.1	Polarisability Parameter π^*	
3.2.2	Hydrogen Bond Donor Properties α	
3.3	Conclusions	(3.1)
3.4	References	

most stable nuclear configurations, it is deduced from the Franck-Condon principle that immediately following an electronic transition the final state, or the Franck-Condon state, cannot be reached because nuclei require considerable more time than electrons to rearrange to their most stable configuration (approximately 10^{-12} s and 10^{-15} s, respectively). Therefore, both the initial relaxed and final Franck-Condon states have the same geometry pattern.

In an absorption or emission process the initial (S_0) and final (S_1) states are linked by a radiative transition. In Figure 3.1 an upward transition corresponding to absorption ($S_0 \rightarrow S_1$) of energy under gas phase conditions ($\epsilon_{0,g}$) and when the molecule is surrounded by a medium ($\epsilon_{0,m}$) is depicted. In this case, each electronic

3.1 Introduction

It has been widely accepted that in a sc fluid solution the local density of solvent around a solute molecule can be much higher than that of the bulk value. This phenomenon has been termed ‘local density augmentation’ or ‘clustering’.¹ In this chapter, the solvent properties of the local environment surrounding a solute are considered.

Over the past two decades a significant amount of research has been conducted using spectroscopic techniques to probe the microenvironment of the solute molecule, commonly referred to as the cybotactic region.²⁻¹¹ From measurements of solvatochromic shifts, it is possible to determine the polarisability/dipolarity parameter, π^* , and to obtain information about specific solute-solvent interactions such as the hydrogen bond donor (HBD) and/or acceptor (HBA) abilities of the solvent.¹¹

3.1.1 Solvatochromism

Solvatochromism can be defined as the influence of a medium on the electronic absorption and emission spectra of molecules.¹² The displacement of the electronic spectrum for a specific solute in different solvents is known as a solvatochromic shift and is associated with the absolute and relative energies of the electronic excited states of the molecule. Each of these electronic states has a specific energy, denoted E . In quantum mechanics the Schrödinger equation relates this energy to the wavefunction, Ψ , and the Hamiltonian operator, H , by¹³

$$H\Psi = E\Psi \quad (3.1)$$

For an isolated molecule the initial relaxed electronic states correspond to the most stable nuclear configurations. It is deduced from the Franck-Condon principle that immediately following an electronic transition the final state, or the Franck-Condon state, cannot be relaxed because nuclei require considerable more time than electrons do to rearrange to their most stable configuration (approximately 10^{-12} s and 10^{-16} s respectively). Therefore, both the initial relaxed and final Franck-Condon states have the same solvation pattern.

In an absorption or emission process the initial (S_0) and final (S_1) states are linked by a radiative transition. In Figure 3.1 an upward transition corresponding to absorption ($S_0 \rightarrow S_1$) of energy under gas phase conditions ($h\nu_{\text{vac}}$) and when the molecule is surrounded by a medium ($h\nu_{\text{sol}}$) is depicted. In this case, each electronic

state can be stabilised or destabilised by a specific amount of energy known as the solvation energy, E_s . This solvation energy is dependent on the polarity of the medium and it is the difference between the solvation energies of the initial and final state (E_s^0 and E_s^1 , respectively) that causes a solvatochromic shift. Positive solvatochromism is the term used to describe a bathochromic (red) shift in the absorption or emission spectra with increasing solvent polarity and in contrast, negative solvatochromism describes a hypsochromic (blue) shift with increasing solvent polarity.

Solvatochromic shifts can be used to describe the relative energies of the electronic states of a molecule. From these measurements, it is possible to determine a number of the physical properties of the molecule such as the dipole moment and polarisability. In addition, it is possible to obtain information about specific interactions such as hydrogen bonding.

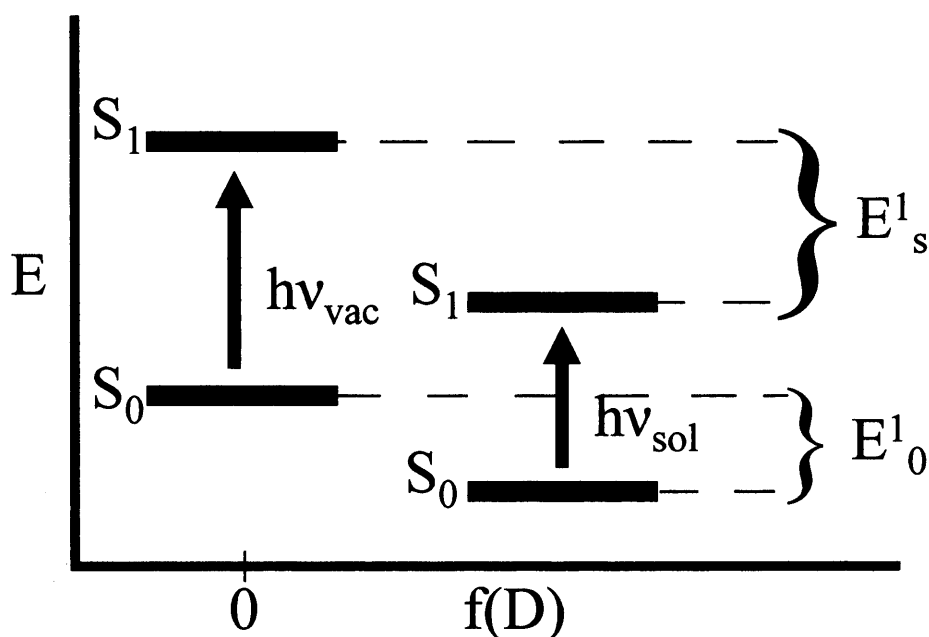


Figure 3.1 Solvatochromic shift energy diagram for the case of a vacuum and a solvent $f(D)$ is the Onsager solvent polarity function $2(\epsilon - 1)/(2\epsilon + 1)$

3.1.2 The Kamlet and Taft Polarisability/Dipolarity Parameter π^*

Solvation can be described as the surrounding of an individual molecule or ion with a shell of solvent molecules. This solvent shell is a direct consequence of intermolecular forces between the solute and solvent. Alternatively, solvation can be defined quantitatively as the energy of interaction between a solute and a solvent. The solvation energy of a solute, E_s , for non-specific interactions can be expressed as

$$E_s = P_M \times \pi_s \quad (3.2)$$

where P_M and π_s are the ‘polarity’ of the solute molecule, M, and the solvent respectively.¹² This theoretical approach works well for non-specific interactions and several physical constants including dielectric constant and permanent dipole moment have been used to assess the effects of a medium on solvation. However, difficulties arise when specific solute-solvent interactions such as hydrogen bonding and electron-pair donor or acceptor interactions occur. For this reason, several empirical solvent polarity scales have been developed that take into account the presence or absence of these specific interactions.¹⁴

In 1948, Winstein introduced the first empirical parameter of ‘solvent ionising power’ known as the Y scale. A number of years later it was proposed that solvatochromic dyes could be used as visual indicators of solvent polarity but it was not until 1958 that Kosower set up the first spectroscopic solvent polarity scale. This was called the Z scale and used the solvent-sensitive intermolecular charge-transfer (CT) absorption of 1-ethyl-4-(methoxycarbonyl)pyridinium iodide. Since then, many solvent polarity scales based on ultraviolet (UV)-visible or near infra-red (IR) spectroscopy have been devised.

A significant proportion of these empirical scales use a single-parameter approach, where the non-specific and specific interactions ‘mix’ into a single solvent parameter. The most widely used is the $E_T(30)$ scale, which is based on the negative solvatochromic shift of the intramolecular CT absorption band of a pyridinium N -phenolate betaine dye. The solubility of this molecule in both polar and non-polar solvents allows this scale to cover a large range of solvents, although anomalies in protic hydrogen-bonding solvents have been shown to occur.¹⁵

The major limitation of the single parameter polarity scales is the mixing of non-specific and specific interactions. It is assumed that the interaction between the solvatochromic dye and the solvent molecules is the same as the interaction with the

solute under investigation. To overcome this problem a number of multi-parameter correlation equations have been developed. These consist of four single empirical parameters each of which measures a specific aspect of the solvation capability of the solvent such as its polarisability, dipolarity, Lewis acidity and Lewis basicity. One of the most-commonly used multi-parameter scales is the π^* scale of solvent polarisability/dipolarity.^{16,17}

The π^* scale relies on a linear solvation energy relationship (LSER) correlating a number of solvent effects on a solute.¹⁸ The relationship has the general form

$$XYZ = XYZ_0 + a\alpha + b\beta + h\delta_H + SPPE \quad (3.3)$$

where XYZ and XYZ_0 represent a solvent-dependent property of the system such as reaction rate, equilibrium constant or a position or intensity of spectral absorption in a given solvent and in a standard reference solvent, respectively. The α term is a measure of the ability of the bulk solvent to act as a hydrogen bond donor (HBD) towards a solute, whereas β is a measure of the hydrogen bond acceptor (HBA) properties of the solvent.^{19,20} The a and b parameters are the corresponding hydrogen bonding constants associated with the solute. The parameter δ_H is known as the Hildebrand solubility parameter and is a measure of the solvent-solvent interactions that are broken in creating a cavity for the solute. h is the corresponding solute parameter.²¹ The solvent polarity/polarisability effect ($SPPE$) is represented by the $SPPE$ term.

Kamlet, Taft and co-workers used the LSER in Equation 3.3 to correlate the solvent induced shift in peak position of a UV-visible absorption maximum of an indicator solute in a liquid solvent with characteristic values of the HBD, HBA and $SPPE$ parameters for various solvents. They showed that the $SPPE$ term could be expressed by the parameter π^* , which measures the ability of the solvent to stabilize a neighbouring charge or a dipole by virtue of its dielectric interactions. The name of the parameters originates from solvatochromic effects on $p \rightarrow \pi^*$ and $\pi \rightarrow \pi^*$ electronic spectral transitions.

Substitution of the π^* term for the $SPPE$ term into Equation 3.3 leads to

$$XYZ = XYZ_0 + s(\pi^* + \rho\delta) + a\alpha + b\beta + h\delta_H \quad (3.4)$$

where s represents the susceptibility of XYZ to changing $SPPE$ and is a constant characteristic of the solute. The quantity δ is a polarisability correction term equal to 0.0 for non-halogenated aliphatics, 0.5 for halogenated aliphatics and 1.0 for aromatic solvents. When the electronic spectrum is shifted to lower frequencies

(bathochromically) with increasing solvent polarity, the coefficient of the δ term, α , is equal to zero and, therefore, δ can be neglected.

Under a number of conditions it is possible to simplify Equation 3.4. According to the Franck-Condon principle, the ground and electronic excited states of an indicator molecule in UV-visible spectroscopy occupy the same volume. As a consequence, the h parameter is zero and the δ_H term in Equation 3.4 can be ignored. In addition, if the solvents under consideration are non-HBD, the α term can be ignored and conversely, if the solvents are non-HBA, the β term can be ignored. Hence, the four-parameter Equation 3.4 can be reduced to a three-, two-, or even a one-parameter equation of the form

$$\nu_{\max} = \nu_0 + s\pi^* \quad (3.5)$$

where ν_{\max} is the wavenumber of maximum absorbance in the UV-visible spectrum and ν_0 is the reference wavenumber of maximum absorbance determined for a standard solvent (cyclohexane).

Since the initial work with seven nitroaromatic indicator solutes¹⁸ an arbitrary π^* scale of solvent polarities has been established. Values of π^* in the scale include 0.0 for non-polar cyclohexane and a π^* of 1.0 for polar dimethyl sulphoxide. This scale has been expanded and refined with the addition of other solvatochromatic indicators, and its success has led to the characterisation of over 250 liquid solvents.²²

In comparison, there have been relatively few studies conducted that characterise the dipolarity/polarisability π^* parameter of sc fluids.¹¹ Of those that have been undertaken, mainly low polarity solvents, such as CO₂ and NO₂ have been studied, where the contribution of hydrogen bonding to solvent polarity is small.

The first investigation into the π^* parameter of a sc solvent was conducted by Sigman *et al.*²³ π^* values were measured for a number of solvatochromic indicator solutes in sc CO₂ and it was found that the values were less than those for cyclohexane, indicating that sc CO₂ is a very non-polar fluid. In addition, the π^* parameter was shown to increase with the solvent density in the sc region. The relationship between π^* and solvent density has been reported by many other authors for a variety of sc solvents including N₂O, NH₃, Xe, CClF₃ and ethane.²⁴⁻²⁷ Solvatochromic studies have also been carried out in near critical and sc water and ethanol.²⁸⁻³¹ These solvents were found to have a wide range of solvent strength, which can be readily and continuously tuned by temperature and pressure changes.

A number of research groups have investigated solvatochromic shifts for fluorinated sc solvents. Lagalante *et al.* used two probe molecules, 4-nitroanisole and 4-nitrophenol, to calculate the π^* values of ethane and six fluorinated ethane solvents in the sub-critical and sc region.³² Once again it was found that the π^* parameter increases with solvent density. For the solvents studied, trends in the π^* values were related to the degree of fluorination about the ethane molecule. Three further sc HFCs, including CH_2F_2 and $\text{CF}_3\text{CH}_2\text{F}$ have been investigated by Abbott and Eardley.³³⁻³⁵ In this work, the change in π^* with reduced density was explained in terms of local density augmentation and a Van der Waals model was used to predict the changes in solvent properties.

In addition to the aforementioned studies, Abbott and co-workers examined the solvent properties of $\text{CO}_2/\text{CF}_3\text{CH}_2\text{F}$ mixtures by measuring π^* values at a range of temperatures, pressures and $\text{CF}_3\text{CH}_2\text{F}$ mole fractions.³⁶ They discovered that a mixture of 30 mol % $\text{CF}_3\text{CH}_2\text{F}$ in CO_2 has similar π^* values to that of bulk $\text{CF}_3\text{CH}_2\text{F}$ at high densities. A number of other authors have investigated the solvent properties of sc mixtures and shown that there is preferential solvation of the solute by the more polar solvent in the mixture. As pressure is increased, the local composition of this polar constituent is found to steadily decrease.³⁷⁻⁴²

3.1.3 Hydrogen Bonding and the Hydrogen Bond Donor Parameter α

A hydrogen bond is a donor-acceptor interaction that specifically involves a hydrogen atom. This attractive interaction between two species may be either intermolecular or intramolecular and is commonly represented by a broken line as shown in Figure 3.2.⁴³

Hydrogen bonds are formed between small and highly electronegative atoms, commonly N or O. When the electronegativity of species A relative to H in an A—H covalent bond (Figure 3.2) is such as to withdraw electrons and leave the proton partially unshielded, the A—H bond becomes capable of donating the proton. In order to interact with this donor bond the acceptor species, B, must possess a lone pair of electrons or polarisable π electrons. The strength of a hydrogen bond is found to be approximately 20 kJ mol^{-1} , which is similar in strength to a Van der Waals attraction. However, a hydrogen bond is directional and this can give rise to discrete recognisable units which consist of two or more single molecules.

Hydrogen bonds have been proposed as an explanation for, among other effects, the high boiling points of compounds containing the groups -OH, -NH₂ or -NH- compared with isomeric molecules with no hydrogen directly attached to the oxygen or nitrogen atom.

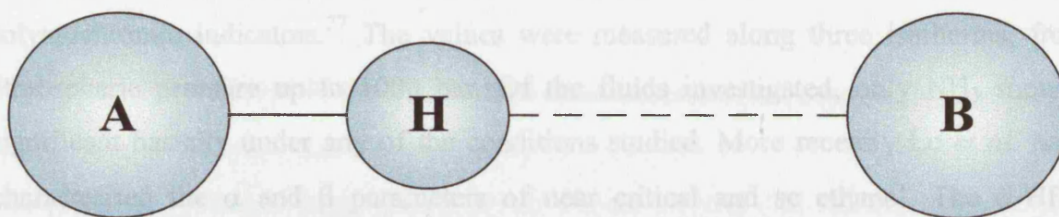


Figure 3.2 Representation of a hydrogen bond

Kamlet and Taft showed that the strength of a hydrogen bond can be measured via UV-visible spectral data by using a solvatochromic comparison method. This method was successfully used to construct a β -scale of solvent HBA basicities and an α -scale of HBD acidities.^{19,20} These hydrogen bond interactions can be accounted for by modifying Equation 3.5 to

$$\nu_{\max} = \nu_0 + s\pi^* + a\alpha + b\beta \quad (3.6)$$

where α and β are measures of HBD acidity and HBA basicity respectively, and a , b and s are the corresponding susceptibility constants.

The solvatochromic comparison method can be used to determine α values by comparison of solvent-induced shifts of the longest wavelength $\pi \rightarrow \pi^*$ absorption band of two similar probe molecules. Only one of these must be able to act as a HBA towards HBD solvents. The corresponding β values may be determined by an analogous method, where one of the probe molecules should act as a HBD towards solvents. Values of α and β for a number of liquid solvents have been reported by Kamlet and Taft^{19,20} and more recently by Marcus.^{44,45}

A number of authors have examined how the α and β scales change with density under sc conditions. Kim and Johnston used UV-visible spectroscopy to examine the HBD ability of sc fluoroform with the solvatochromic probe phenol blue.³¹ It was shown that hydrogen bond interactions were well developed at the critical density but did not change significantly at higher pressures. In a further study, Bennett and Johnston employed the spectroscopic probes acetone and benzophenone to characterize the HBD strength of sc water. They also showed that hydrogen bonding can persist in sc

media at low densities and augment the local density of water about the probe molecules.⁴⁶

Sigman *et al.* reported β values in sc CO₂. These values were found to be constant in the density range investigated.²³ The HBA strength of five sc fluids, CO₂, N₂O, CClF₃, SF₆ and NH₃ were examined by Maiwald and Schneider, using five solvatochromic indicators.²⁷ The values were measured along three isotherms, from atmospheric pressure up to 1000 bar. Of the fluids investigated, only NH₃ showed significant basicity under any of the conditions studied. More recently Lu *et al.* have characterised the α and β parameters of near critical and sc ethanol. The α -HBD properties were found to decrease with increasing pressure and temperature, whereas the β -HBA properties were found to be small and relatively invariant with pressure in the sc region.²⁹

Lagalante and co-workers measured β for six fluorinated ethane solvents in their liquid and sc states.³² The average β values were found to be negative over the density range studied and were interpreted as the inability of the solvents to act as hydrogen bond acceptors. Eardley reported preliminary results for the determination of α in liquid and sc CF₃CH₂F based on the π^* values that were determined experimentally and the π^* and β values reported by Lagalante *et al.*³² Assuming the reported π^* and β values are accurate, Eardley calculated the α values as a function of temperature and pressure using Equation 3.6.⁴⁷ However, these results presented a number of inconsistencies. It was shown that α and hence the hydrogen bond donating ability of the solvent increased with the temperature of the system from liquid to supercritical conditions; generally the hydrogen bond donor strength of a solvent decreases with temperature at a given density.^{31,46}

More recently, Abbott and Durling characterized the Kamlet-Taft π^* , α and β parameters for liquid and sc CF₃CH₂F and CH₂F₂ as a function of temperature and pressure. Three solvatochromic probe molecules, Nile Red, 4-nitroaniline and *N,N*-dimethyl-4-nitroaniline, were employed to calculate α and β values by the solvatochromic comparison method.⁴⁸ Both solvents were shown to have significant hydrogen bonding properties, which exhibit the characteristic decrease with increasing pressure. The polarity parameters were found to be larger for CF₃CH₂F, which has the larger dipole moment. For both solvents, β values were small and positive and similar to those reported by Lu *et al.* for sc ethanol.²⁹ These results are contradictory to those

published by Lagalante,³² however the discrepancy is thought to be due to the assumption Lagalante and co-workers made regarding the indicator solute 4-nitroanisole: It was considered not to be not capable of acting as a hydrogen bond acceptor. Abbott and Durling found that at high pressures, under sc conditions, the HBD α -parameter decreased with increasing temperature. However, at pressures below 100 bar, α values were found to increase with increasing temperature. This was attributed to the change in the equilibrium between solvent-solvent and solvent-solute interactions. A strong correlation between the parameters π^* and α was shown. This was found to change significantly when solvent-solvent interactions are reduced indicating that, at densities where the solvation sheath is incomplete, preferential solvation around the polar moieties of the probe molecule may occur.

In addition to the investigations discussed above, many other spectroscopic studies, such as infrared²⁻⁷ and fluorescence,⁸⁻¹⁰ have shown that, close to the critical temperature and density, the local solvent density around a solute molecule is found to be higher than the actual bulk value. The extent of enhanced solvent density about the solute has frequently been calculated by computer simulations,^{1,49,50} integral equation formulations⁴⁰ or compressible electrostatic continuum methods.⁵¹

Here, the aim is to obtain the first data for the polarisability/dipolarity π^* parameter and the hydrogen bond donor acidity parameter, α for three solid solutes dissolved in sc CH_2F_2 . The solutes investigated are *o*-hydroxybenzoic acid (salicylic acid), naphthalene and *p*-methylbenzoic acid (*p*-toluic acid). Successful results will allow a range of solute-solute and solute-solvent interactions to be evaluated. It is known that salicylic acid is capable of forming hydrogen bonded dimers, whereas naphthalene is non-polar. It is thought that these differences should have an appreciable influence on the π^* and α polarity parameters.

3.2 Results and Discussion

Two solvatochromic probes were employed to investigate the variations in π^* and α parameters for three solutes as a function of pressure. These were Nile blue Oxazone (Nile Red) and *N,N*-dimethylindoaniline (Phenol Blue) and are shown in Figure 3.3. It was not possible to obtain values for the β parameter because no suitable solvatochromic dye with sufficient absorption in a region free of overlap or interference from the absorption spectrum of the solute could be obtained. The three solutes under investigation, salicylic acid, naphthalene and *p*-toluic acid, all exhibited an absorption maximum at wavelengths below 400 nm.

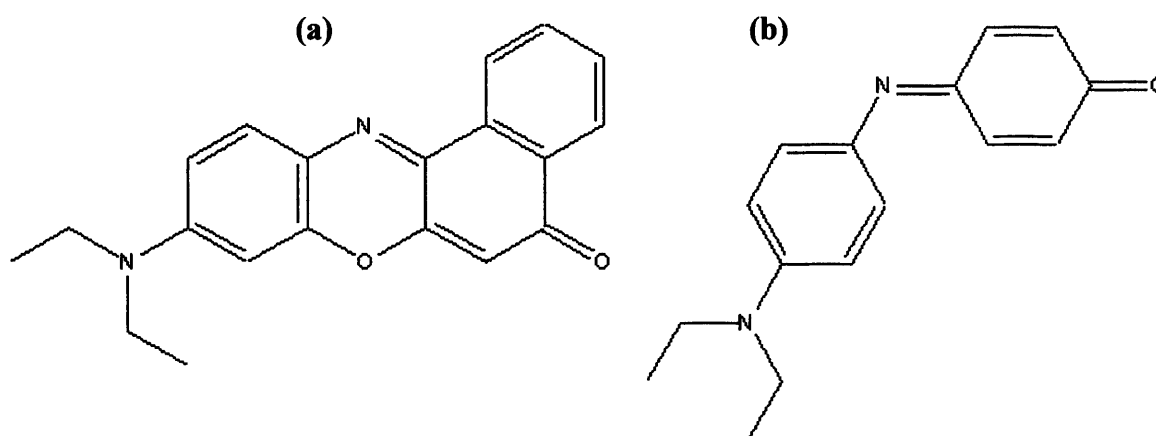


Figure 3.3 Structures of (a) Nile Red and (b) Phenol Blue

According to Equation 3.6, to obtain the parameters π^* , α and β from measured solvatochromic shift data, the susceptibility constants *a*, *b* and *s* are required. In order to obtain these, the absorption spectra of the solvatochromic dyes in 13 liquid solvents of different polarity and solvent type (HBD, HBA and non-hydrogen bonding (NHB)) were measured. The data were fitted to Equation 3.6 using a multiple regression analysis. However, poor correlation was obtained by this method. This is thought to be due to the discrepancy in the literature values of π^* and α and the purity of the solvents examined.

Consequently, an alternative method to obtain the susceptibility constants was required. The wavelength of absorption maxima, ν_{\max} , for the probe molecules in CH₂F₂ as a function of pressure at 90 °C were measured and fitted to the data previously published by Abbott and Durling.⁴⁸ The susceptibility constants *a* and *s* were obtained by this method with excellent correlations for each dye (Table 3.1). For comparison, the

measured and calculated ν_{\max} values using the susceptibility constants shown in Table 3.1 are given in Table 1 of the Appendix. This approach is valid since the aim of the process is to determine relative changes in polarity parameters with pressure. Example UV-visible absorption spectra are shown in Figure 1 of the Appendix.

Table 3.1 Susceptibility constants for the solvatochromic probes employed

Solvatochromic Probe	a value	s value	ν_0	R^2 value
Nile Red	1.180	-1.437	19.923	0.999
Phenol Blue	2.629	-1.765	18.048	0.993

3.2.1 Polarisability Parameter π^*

The pressure dependence of π^* for CH_2F_2 was first characterised by Abbott and Eardley using Nile red as an indicator solute.³²⁻³⁴ More recently, Abbott and Durling obtained the susceptibility constants a, b and s for three solvatochromic dyes and calculated the corresponding π^* , α and β values for $\text{CF}_3\text{CH}_2\text{F}$ and CH_2F_2 as a function of temperature and pressure.⁴⁸ A good correlation with previously reported π^* values was obtained using the solvatochromic comparison method. Figure 3.4 shows the calculated π^* values for CH_2F_2 at 90 °C as a function of pressure measured in this work. For comparison, the previously published π^* results by Abbott and Durling are also shown.⁴⁸

Figure 3.5 shows how π^* for the three 0.01 mol dm⁻³ solute systems varies with pressure. For comparison, the π^* parameter for the pure CH_2F_2 sc fluid is also shown. It is clear that the addition of a solute to the sc fluid alters the interactions of the solvent molecules with the probe dye. The difference in π^* values, $\Delta\pi^*$, between the pure sc fluid and the 0.01 mol dm⁻³ solute systems is shown in Figure 3.6.

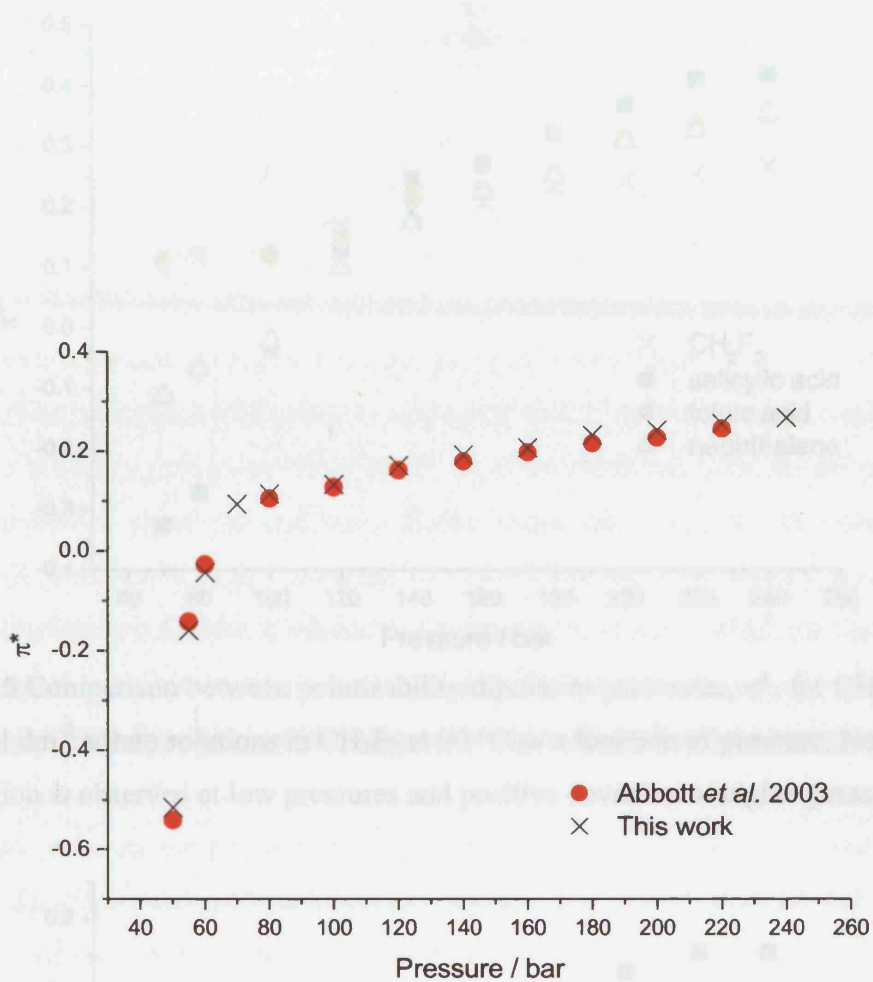


Figure 3.4 Comparison between the polarisability/dipolarity parameter, π^* , for CH_2F_2 at 90 °C as a function of pressure for this work and those previously published⁴⁸

Chapter Three – Probing Solute Clustering in Supercritical Solutions Using Solvatochromic Parameters

Salicylic acid causes the largest deviation in π^* from that of the pure fluid.

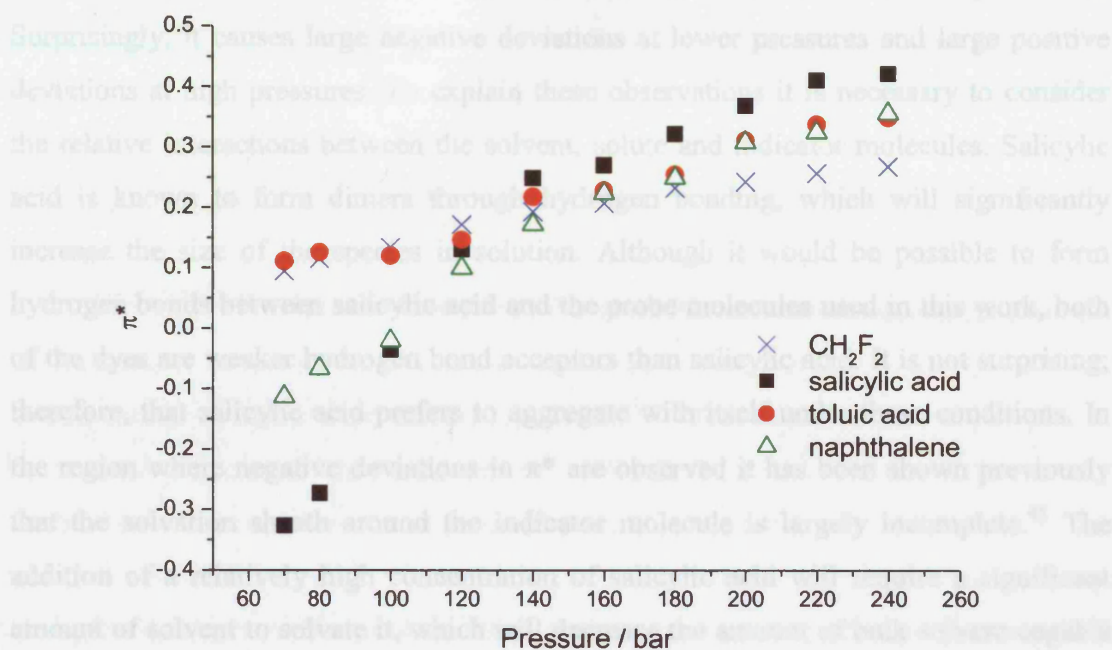


Figure 3.5 Comparison between polarisability/dipolarity parameter, π^* , for CH_2F_2 and 0.01 mol dm^{-3} solute solutions in CH_2F_2 at $90 \text{ }^\circ\text{C}$ as a function of pressure. Negative deviation is observed at low pressures and positive deviation at higher pressures

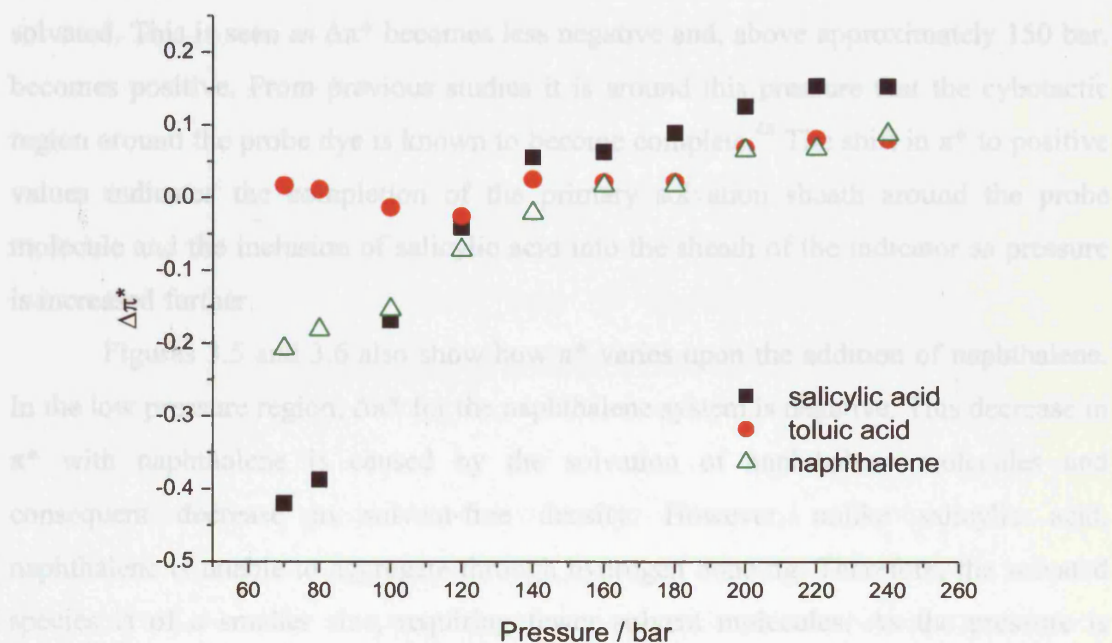


Figure 3.6 Change in polarisability/dipolarity parameter, $\Delta\pi^*$, for 0.01 mol dm^{-3} solutes in CH_2F_2 at $90 \text{ }^\circ\text{C}$ as a function of pressure. Note that salicylic acid exhibits greatest change in π^* at both low and high pressures

Salicylic acid causes the largest deviation in π^* from that of the pure fluid. Surprisingly, it causes large negative deviations at lower pressures and large positive deviations at high pressures. To explain these observations it is necessary to consider the relative interactions between the solvent, solute and indicator molecules. Salicylic acid is known to form dimers through hydrogen bonding, which will significantly increase the size of the species in solution. Although it would be possible to form hydrogen bonds between salicylic acid and the probe molecules used in this work, both of the dyes are weaker hydrogen bond acceptors than salicylic acid. It is not surprising; therefore, that salicylic acid prefers to aggregate with itself under these conditions. In the region where negative deviations in π^* are observed it has been shown previously that the solvation sheath around the indicator molecule is largely incomplete.⁴⁸ The addition of a relatively high concentration of salicylic acid will require a significant amount of solvent to solvate it, which will decrease the amount of bulk solvent capable of solvating the indicator and hence π^* appears to fall. As the pressure is increased, hydrogen bonding decreases and the association between the salicylic acid molecules is reduced. The salicylic acid dimers break up and the increase in free solvent molecules allows the probe molecule, as well as the individual salicylic acid molecules, to be solvated. This is seen as $\Delta\pi^*$ becomes less negative and, above approximately 150 bar, becomes positive. From previous studies it is around this pressure that the cybotactic region around the probe dye is known to become complete.⁴⁸ The shift in π^* to positive values indicates the completion of the primary solvation sheath around the probe molecule and the inclusion of salicylic acid into the sheath of the indicator as pressure is increased further.

Figures 3.5 and 3.6 also show how π^* varies upon the addition of naphthalene. In the low pressure region, $\Delta\pi^*$ for the naphthalene system is negative. This decrease in π^* with naphthalene is caused by the solvation of naphthalene molecules and consequent decrease in solvent-free density. However, unlike salicylic acid, naphthalene is unable to aggregate through hydrogen bonding. Therefore, the solvated species is of a smaller size, requiring fewer solvent molecules. As the pressure is increased, a similar trend in increasing $\Delta\pi^*$ exists. Above around 150 bar, $\Delta\pi^*$ becomes positive, indicating that the cybotactic region around the probe molecule is complete and naphthalene molecules become included in the solvation sheath. For naphthalene no specific dipole-dipole interactions occur, hence naphthalene is less likely to be

incorporated in the solvation sphere and the apparent decrease in π^* at low pressure results from the decreased concentration of unassociated solvent molecules. The increased π^* at higher pressures is again due to an increased solvation density arising from the dissolution of solute.

In contrast to these results the pattern exhibited by toluic acid is somewhat different. $\Delta\pi^*$ does not change significantly with pressure and is positive in the low pressure region. This suggests that there is no competition between the probe molecule and toluic acid for the solvent molecules. It has previously been shown that the addition of co-solvents to sc fluids can increase π^* values.³⁶⁻⁴² This work has shown that there is preferential clustering of the co-solvent around the probe molecule at low pressures and as the pressure is increased it is replaced by the solvent molecules. However, in the current work the increase in π^* is not as significant as would be expected if preferential clustering of toluic acid around the probe molecule was solely present. Toluic acid is not known to form aggregates like salicylic acid, but it is capable of hydrogen bonding and could solvate the probe molecules used in this work. If these associated species were present in the low pressure region (below 150 bar) the observed slight increase in $\Delta\pi^*$ would be accounted for. When pressure is increased the association between these species is weakened.

The data for 0.001 mol dm⁻³ solute solutions is shown in Figures 3.7 and 3.8. Similar trends to the 0.01 mol dm⁻³ solutions are observed, although more scatter in the data is present. This indicates that, even at lower concentrations, the same solute-solute interactions and variations in solvation are present. Measurements were also taken at concentrations of 0.0001 mol dm⁻³, these are displayed in Tables 2 to 4 of the Appendix. Although scatter in the data increased at lower concentrations, similar trends were observed and show that the variations in π^* are independent of the solute concentration.

Many research groups have shown that three distinct density regions exist with marked changes occurring in solvent properties at reduced densities, ρ_r , of approximately 1 and 2.³³⁻³⁶ These changes are ascribed to local density augmentation as discussed previously.

Figures 3.9 and 3.10 show the dependency of $\Delta\pi^*$ on reduced density ($\rho_r = \rho/\rho_c$ where ρ_c for CH₂F₂ was taken to be 0.424 g cm⁻³) at 0.01 mol dm⁻³ and 0.001 mol dm⁻³ respectively. Although data below $\rho_r = 1$ and above $\rho_r = 2$ are limited, a noticeable

Chapter Three – Probing Solute Clustering in Supercritical Solutions Using Solvatochromic Parameters

change in the shape of the plot is observed over the pressure range studied. For dilute sc fluid solutions the bulk fluid density and local solute density about the probe molecule have been shown to be similar in the liquid-like region ($\rho_r > 2$). The data presented here for different solutes is shown to converge with a steep slope close to this region. This is in agreement with the bulk density being akin to the local density around the indicator dye. Below this region, (approximately $1 < \rho_r < 2$), the local solvent density about the probe molecule is believed to be considerably higher than the bulk value. This is evident from the decrease in the slope and again is present in the systems investigated here. The slope in the gas-like region of a dilute sc fluid ($\rho_r < 1$) has been shown to again increase. This trend suggests that the local density approaches that of the bulk as ρ_r tends to zero. Although data in this region is more limited, it is in this region that the distinction between the three solutes becomes even more apparent as they appear to diverge. The overall shape of the plots indicates that local density augmentation occurs with each of the solute systems.

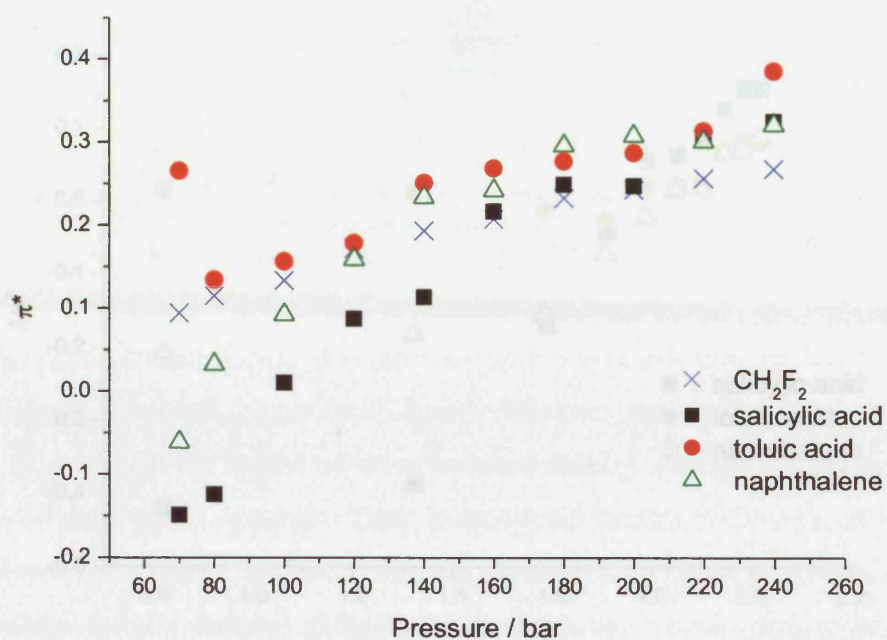


Figure 3.7 Comparison between polarisability/dipolarity parameter, π^* , for CH_2F_2 and $0.001 \text{ mol dm}^{-3}$ solute solutions in CH_2F_2 at $90 \text{ }^\circ\text{C}$ as a function of pressure

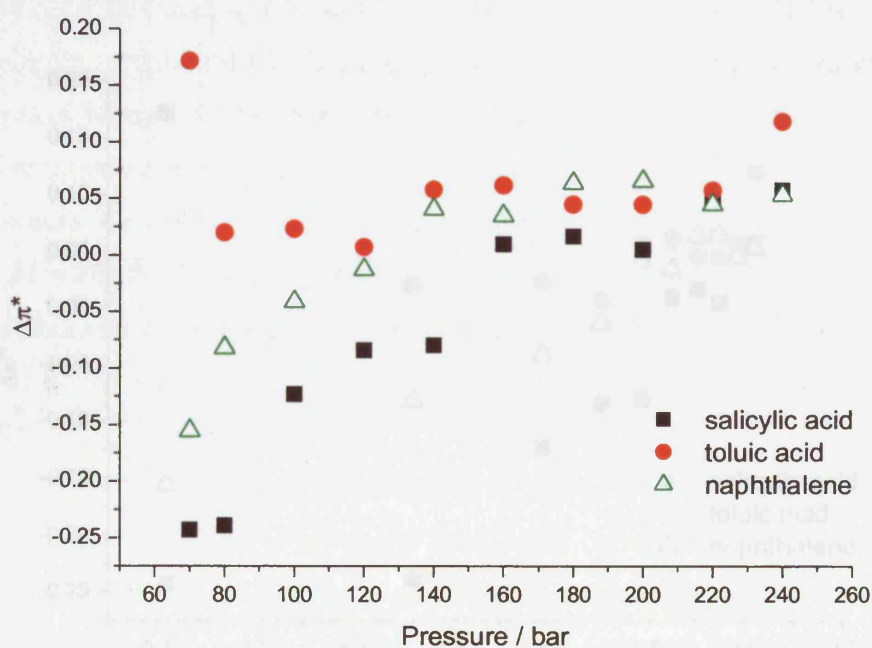


Figure 3.8 Change in polarisability/dipolarity parameter, $\Delta\pi^*$, for $0.001 \text{ mol dm}^{-3}$ solutes in CH_2F_2 at $90 \text{ }^\circ\text{C}$ as a function of pressure. Trends displayed are similar to those for 0.01 mol dm^{-3}

Chapter Three – Probing Solute Clustering in Supercritical Solutions Using Solvatochromic Parameters

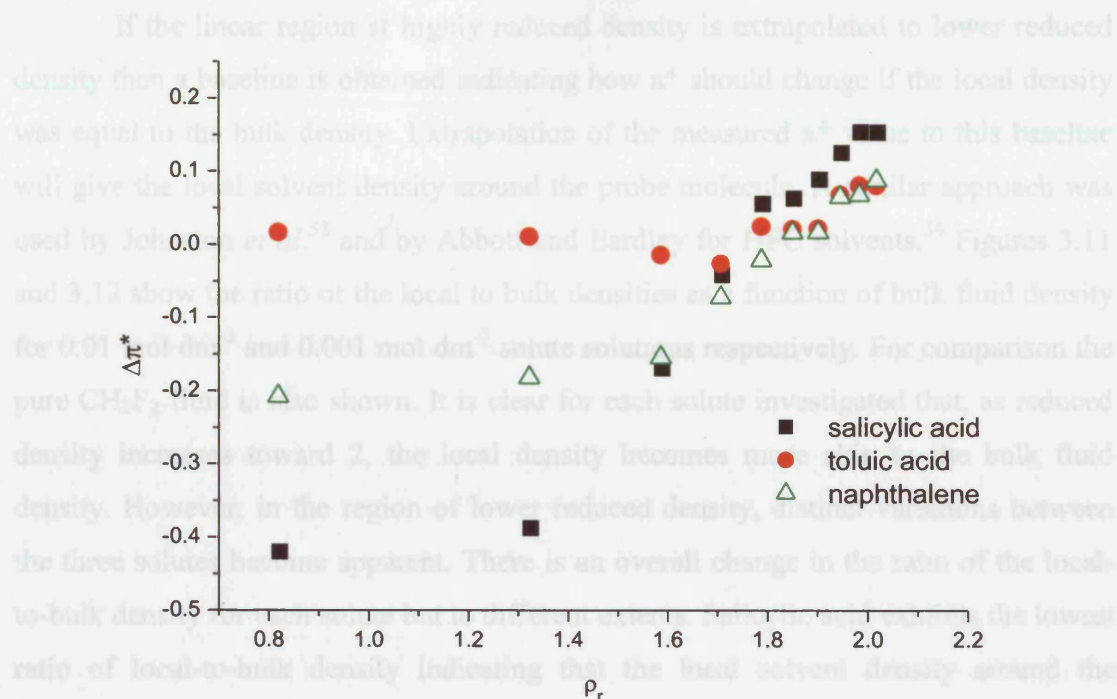


Figure 3.9 Change in polarisability/dipolarity parameter, $\Delta\pi^*$, for 0.01 mol dm⁻³ solutes in CH₂F₂ at 90 °C as a function of reduced density. The convergence of data at high ρ_r values indicates that each solute behaves the same in this region

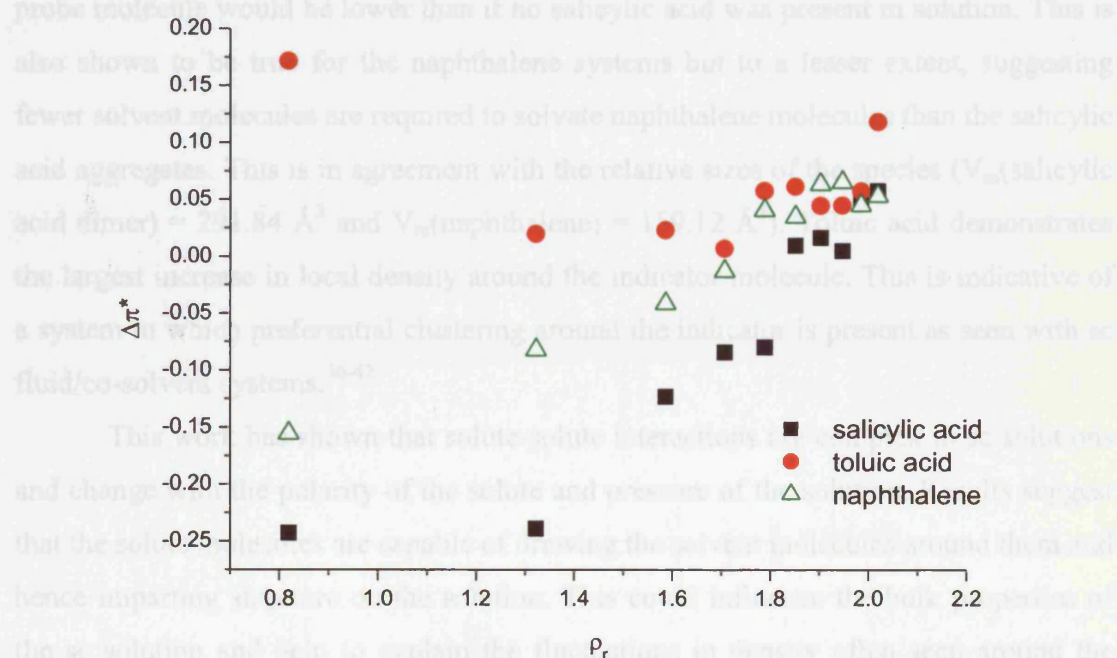


Figure 3.10 Change in polarisability/dipolarity parameter, $\Delta\pi^*$, for 0.001 mol dm⁻³ solutes in CH₂F₂ at 90 °C as a function of reduced density. As observed for 0.01 mol dm⁻³ solute solutions differences between each solute are pronounced at low ρ_r values

If the linear region at highly reduced density is extrapolated to lower reduced density then a baseline is obtained indicating how π^* should change if the local density was equal to the bulk density. Extrapolation of the measured π^* value to this baseline will give the local solvent density around the probe molecule. A similar approach was used by Johnston *et al.*⁵² and by Abbott and Eardley for HFC solvents.³⁴ Figures 3.11 and 3.12 show the ratio of the local to bulk densities as a function of bulk fluid density for 0.01 mol dm⁻³ and 0.001 mol dm⁻³ solute solutions respectively. For comparison the pure CH₂F₂ fluid is also shown. It is clear for each solute investigated that, as reduced density increases toward 2, the local density becomes more akin to the bulk fluid density. However, in the region of lower reduced density, distinct variations between the three solutes become apparent. There is an overall change in the ratio of the local-to-bulk density for each solute but to different extents. Salicylic acid exhibits the lowest ratio of local-to-bulk density indicating that the local solvent density around the indicator molecule is greater than the bulk fluid density, but this is not as great as those for naphthalene or toluic acid. This is in agreement with the variations in $\Delta\pi^*$ because, if at pressures below approximately 150 bar ($\rho_r = 1.82$) the solvent molecules are effectively used up solvating salicylic acid dimers, the local solvent density around the probe molecule would be lower than if no salicylic acid was present in solution. This is also shown to be true for the naphthalene systems but to a lesser extent, suggesting fewer solvent molecules are required to solvate naphthalene molecules than the salicylic acid aggregates. This is in agreement with the relative sizes of the species ($V_m(\text{salicylic acid dimer}) = 291.84 \text{ \AA}^3$ and $V_m(\text{naphthalene}) = 159.12 \text{ \AA}^3$). Toluic acid demonstrates the largest increase in local density around the indicator molecule. This is indicative of a system in which preferential clustering around the indicator is present as seen with sc fluid/co-solvent systems.³⁶⁻⁴²

This work has shown that solute-solute interactions are complex in sc solutions and change with the polarity of the solute and pressure of the solution. Results suggest that the solute molecules are capable of drawing the solvent molecules around them and hence imparting structure on the solution. This could influence the bulk properties of the sc solution and help to explain the fluctuations in density often seen around the critical point.

3.2.3 Hydrogen Bond Donor Properties

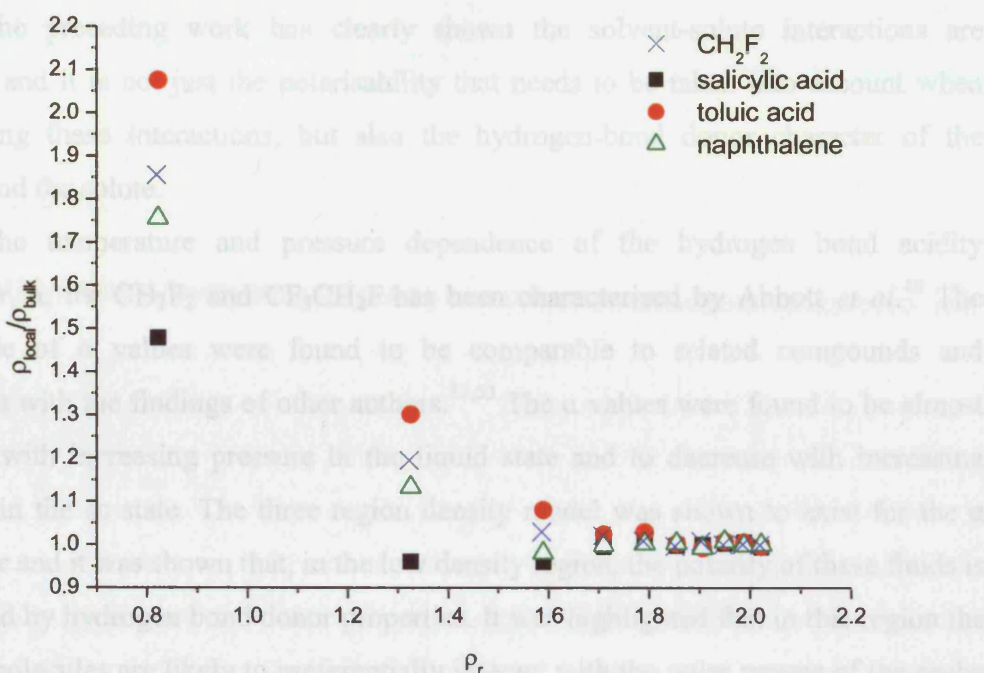


Figure 3.11 Comparison between the ratio of local to bulk density as a function of reduced density for CH₂F₂ and 0.01 mol dm⁻³ solute solutions. A reduction in local density around probe molecule is exhibited by salicylic acid and naphthalene

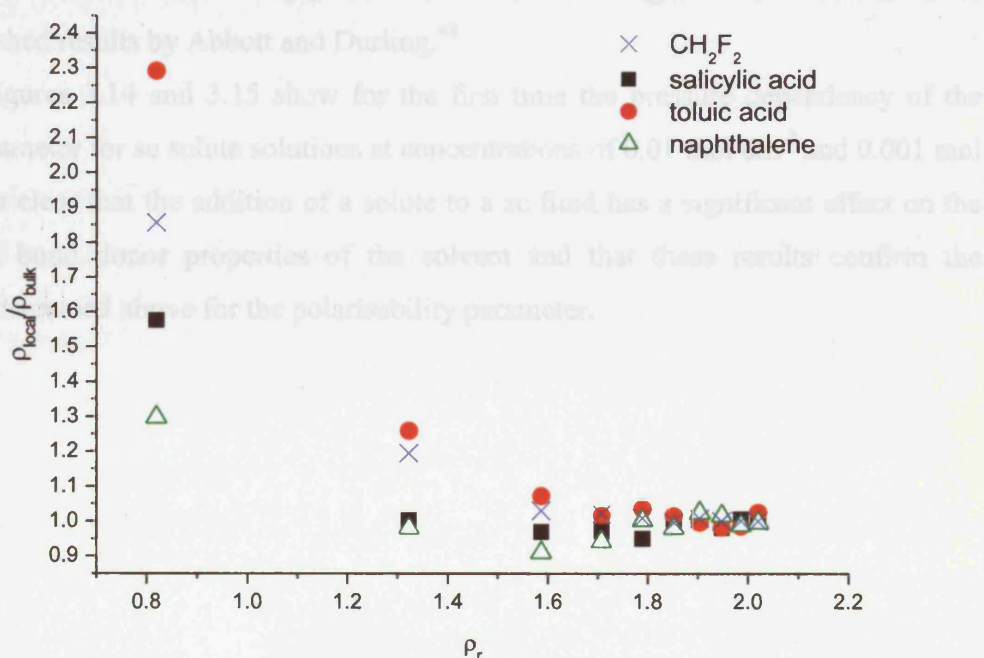


Figure 3.12 Comparison between the ratio of local to bulk density as a function of reduced density for 0.001 mol dm⁻³ solutes. A similar trend to 0.01 mol dm⁻³ solutions is observed. At high values of ρ_r there is no increase in local density around the probe

3.2.2 Hydrogen Bond Donor Properties α

The preceding work has clearly shown the solvent-solute interactions are complex and it is not just the polarisability that needs to be taken into account when considering these interactions, but also the hydrogen-bond donor character of the solvent and the solute.

The temperature and pressure dependence of the hydrogen bond acidity parameter, α , for CH_2F_2 and $\text{CF}_3\text{CH}_2\text{F}$ has been characterised by Abbott *et al.*⁴⁸ The magnitude of α values were found to be comparable to related compounds and consistent with the findings of other authors.^{32,53} The α values were found to be almost constant with increasing pressure in the liquid state and to decrease with increasing pressure in the sc state. The three region density model was shown to exist for the α parameter and it was shown that, in the low density region, the polarity of these fluids is dominated by hydrogen bond donor properties. It was highlighted that in this region the solvent molecules are likely to preferentially interact with the polar groups of the probe molecules. These findings support the work of other authors.¹

Here, the solvatochromic probes Nile Red and Phenol Blue were again used to obtain the acidity parameter for the three sc solute solutions as a function of pressure. The calculated α values for CH_2F_2 at 90 °C are shown in Figure 3.13. Also shown are the published results by Abbott and Durling.⁴⁸

Figures 3.14 and 3.15 show for the first time the pressure dependency of the HBD parameter for sc solute solutions at concentrations of 0.01 mol dm⁻³ and 0.001 mol dm⁻³. It is clear that the addition of a solute to a sc fluid has a significant effect on the hydrogen bond donor properties of the solvent and that these results confirm the findings discussed above for the polarisability parameter.



Figure 3.13 Comparison of hydrogen bond donor acidity, α , values for CH_2F_2 at 90°C as a function of pressure measured in this work and those previously published⁴⁸

Chapter Three – Probing Solute Clustering in Supercritical Solutions Using Solvatochromic Parameters

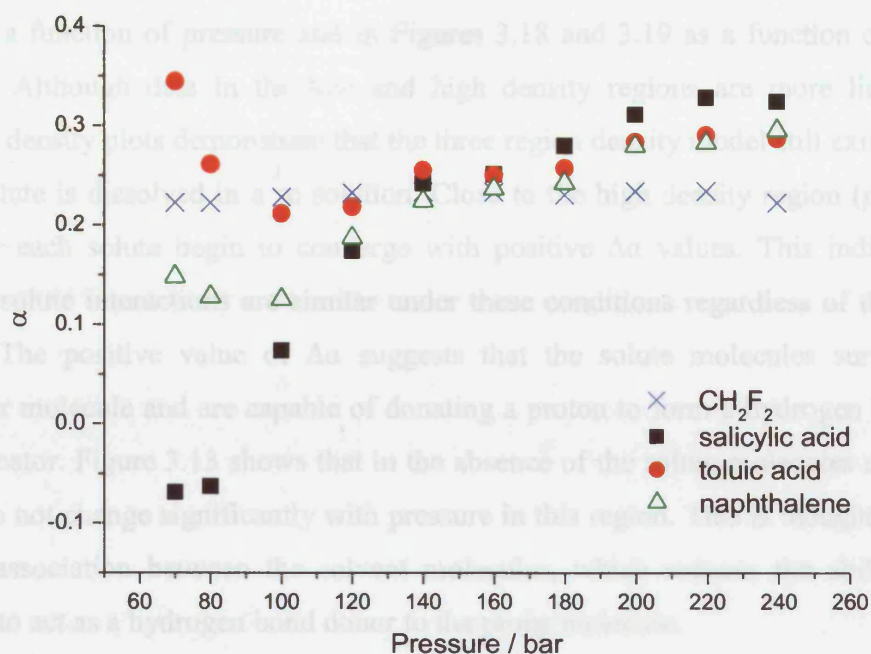


Figure 3.14 Comparison between hydrogen bond donor acidity, α , values for CH_2F_2 and 0.01 mol dm^{-3} solute solutions in CH_2F_2 at $90 \text{ }^\circ\text{C}$ as a function of pressure. Note there is negative deviation at low pressures and positive deviation at higher pressures

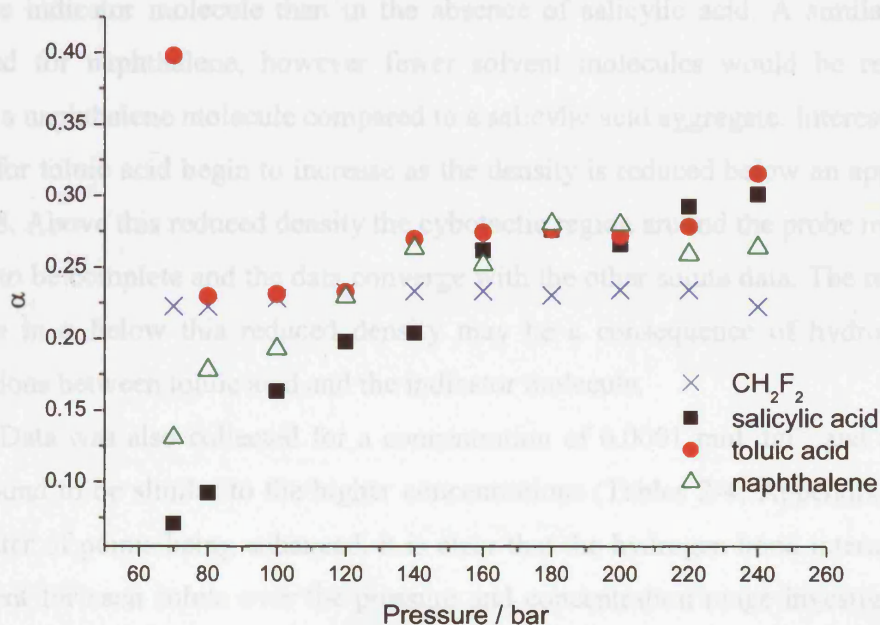


Figure 3.15 Comparison between the hydrogen bond donor acidity, α , values for CH_2F_2 and $0.001 \text{ mol dm}^{-3}$ solute solutions in CH_2F_2 at $90 \text{ }^\circ\text{C}$ as a function of pressure. A similar trend to 0.01 mol dm^{-3} solutions is observed

The change in α with respect to the pure fluid, $\Delta\alpha$, is shown in Figures 3.16 and 3.17 as a function of pressure and in Figures 3.18 and 3.19 as a function of reduced density. Although data in the low and high density regions are more limited, the reduced density plots demonstrate that the three region density model still exists when a solid solute is dissolved in a sc solution. Close to the high density region ($\rho_r > 2$) the data for each solute begin to converge with positive $\Delta\alpha$ values. This indicates that solvent-solute interactions are similar under these conditions regardless of the type of solute. The positive value of $\Delta\alpha$ suggests that the solute molecules surround the indicator molecule and are capable of donating a proton to form a hydrogen bond with the indicator. Figure 3.13 shows that in the absence of the solute molecules α has been found to not change significantly with pressure in this region. This is thought to be due to self-association between the solvent molecules, which reduces the ability of the solvent to act as a hydrogen bond donor to the probe molecule.

Figures 3.16 to 3.19 show that at lower pressures and densities ($\rho_r < 2$) the trend for each solute becomes different. Salicylic acid is shown to cause a considerable reduction in α with respect to the pure fluid. This could be caused by the interactions of the solvent molecules with the highly associated salicylic molecules present under these conditions. This would mean that there are fewer solvent molecules available to interact with the indicator molecule than in the absence of salicylic acid. A similar trend is observed for naphthalene, however fewer solvent molecules would be required to solvate a naphthalene molecule compared to a salicylic acid aggregate. Interestingly, $\Delta\alpha$ values for toluic acid begin to increase as the density is reduced below an approximate ρ_r of 1.8. Above this reduced density the cybotactic region around the probe molecule is known to be complete and the data converge with the other solute data. The remarkable increase in α below this reduced density may be a consequence of hydrogen bond interactions between toluic acid and the indicator molecule.

Data was also collected for a concentration of $0.0001 \text{ mol dm}^{-3}$ and the trends were found to be similar to the higher concentrations (Tables 2-4, Appendix). Despite the scatter of points being enhanced, it is clear that the hydrogen bond interactions are consistent for each solute over the pressure and concentration range investigated. It is also clear from Figures 3.5-3.8 and 3.14-3.17 that the trends for α and π^* are similar with pressure.

Chapter Three – Probing Solute Clustering in Supercritical Solutions Using Solvatochromic Parameters

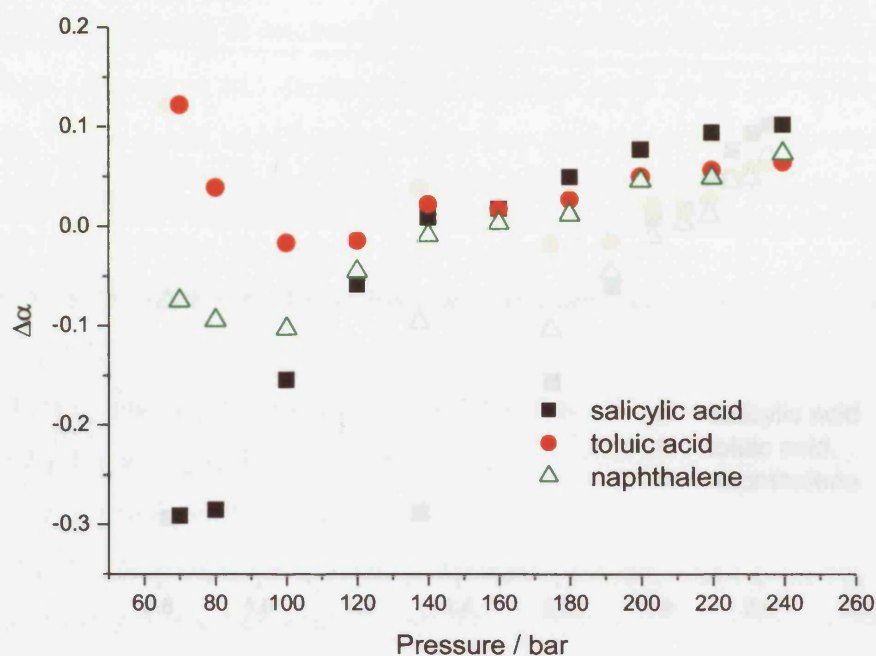


Figure 3.16 Change in hydrogen bond acidity, $\Delta\alpha$, for 0.01 mol dm^{-3} solutes in CH_2F_2 at 90°C as a function of pressure. Note that salicylic acid exhibits the largest change

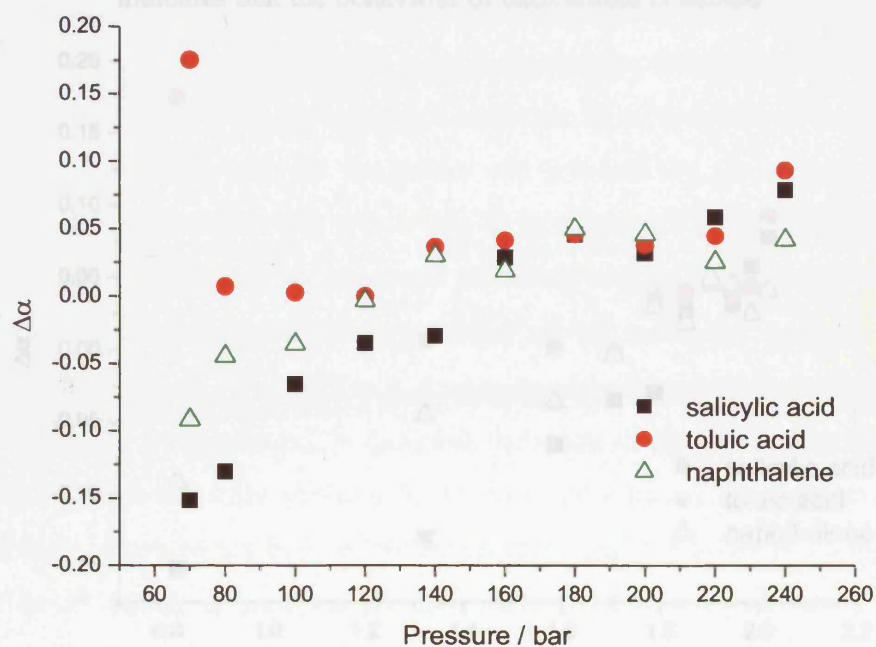


Figure 3.17 Change in hydrogen bond acidity, $\Delta\alpha$, for $0.001 \text{ mol dm}^{-3}$ solutes in CH_2F_2 at 90°C as a function of pressure. A similar trend is displayed to the 0.01 mol dm^{-3} solutions

Chapter Three – Probing Solute Clustering in Supercritical Solutions Using Solvatochromic Parameters

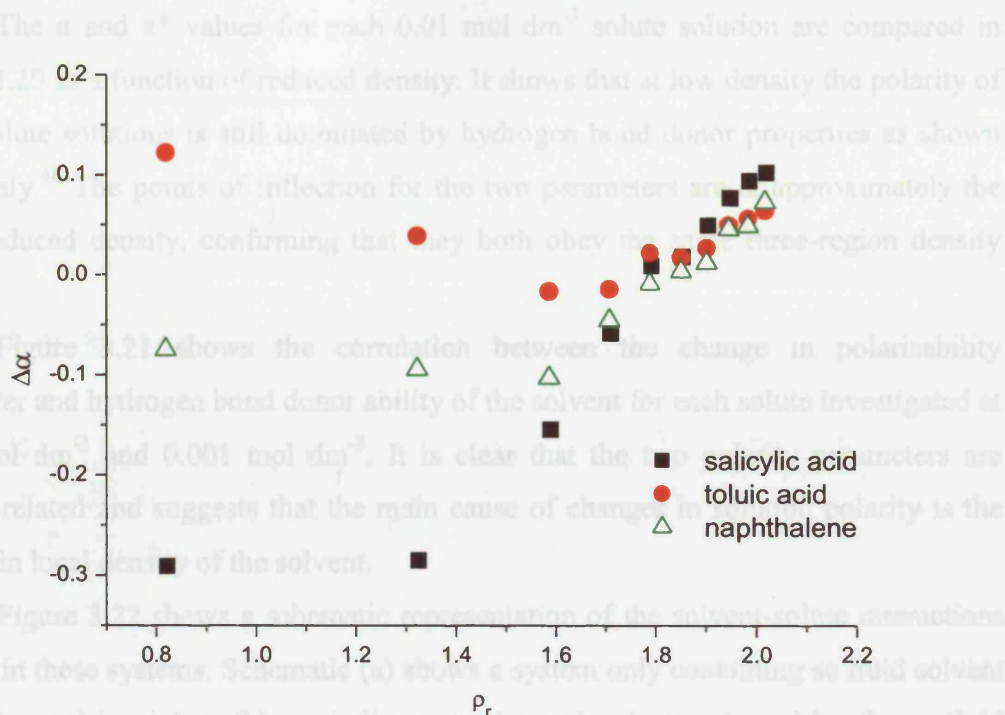


Figure 3.18 Change in hydrogen bond acidity, $\Delta\alpha$, for 0.01 mol dm⁻³ solutes in CH₂F₂ at 90 °C as a function of reduced density. The convergence of data at high values indicates that the behaviour of each solute is similar

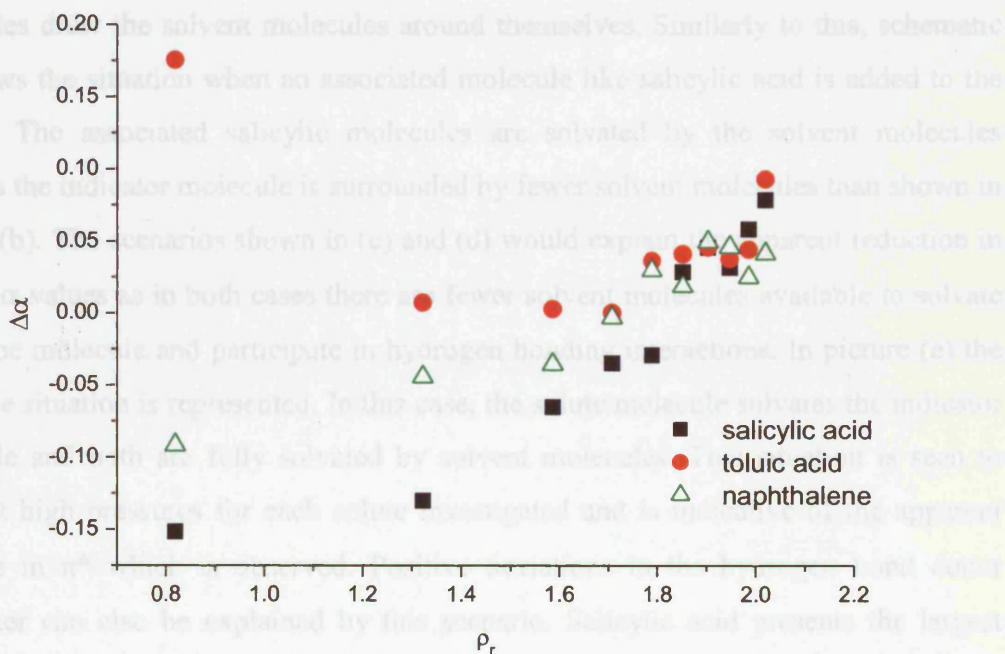


Figure 3.19 Change in hydrogen bond acidity, $\Delta\alpha$, for 0.001 mol dm⁻³ solutes in CH₂F₂ at 90 °C as a function of reduced density. As with 0.01 mol dm⁻³ solutions the divergence at low values is a result of the differences between each solute

The α and π^* values for each 0.01 mol dm⁻³ solute solution are compared in Figure 3.20 as a function of reduced density. It shows that at low density the polarity of these solute solutions is still dominated by hydrogen bond donor properties as shown previously.⁴⁸ The points of inflection for the two parameters are at approximately the same reduced density, confirming that they both obey the same three-region density model.

Figure 3.21 shows the correlation between the change in polarisability parameter and hydrogen bond donor ability of the solvent for each solute investigated at 0.01 mol dm⁻³ and 0.001 mol dm⁻³. It is clear that the two polarity parameters are closely related and suggests that the main cause of changes in solution polarity is the change in local density of the solvent.

Figure 3.22 shows a schematic representation of the solvent-solute interactions present in these systems. Schematic (a) shows a system only containing sc fluid solvent molecules and in picture (b), an indicator probe molecule is solvated by the sc fluid molecules. Picture (c) represents the scenario when an unassociated solute molecule like naphthalene is present in solution along with the indicator molecule. The solvent density around the indicator molecule is lower than in (b) as the naphthalene solute molecules draw the solvent molecules around themselves. Similarly to this, schematic (d) shows the situation when an associated molecule like salicylic acid is added to the system. The associated salicylic molecules are solvated by the solvent molecules whereas the indicator molecule is surrounded by fewer solvent molecules than shown in picture (b). The scenarios shown in (c) and (d) would explain the apparent reduction in π^* and α values as in both cases there are fewer solvent molecules available to solvate the probe molecule and participate in hydrogen bonding interactions. In picture (e) the converse situation is represented. In this case, the solute molecule solvates the indicator molecule and both are fully solvated by solvent molecules. This situation is seen to occur at high pressures for each solute investigated and is indicative of the apparent increase in π^* which is observed. Positive deviations in the hydrogen bond donor parameter can also be explained by this scenario. Salicylic acid presents the largest positive deviation in α and is capable of hydrogen bond interactions with the indicator molecules.

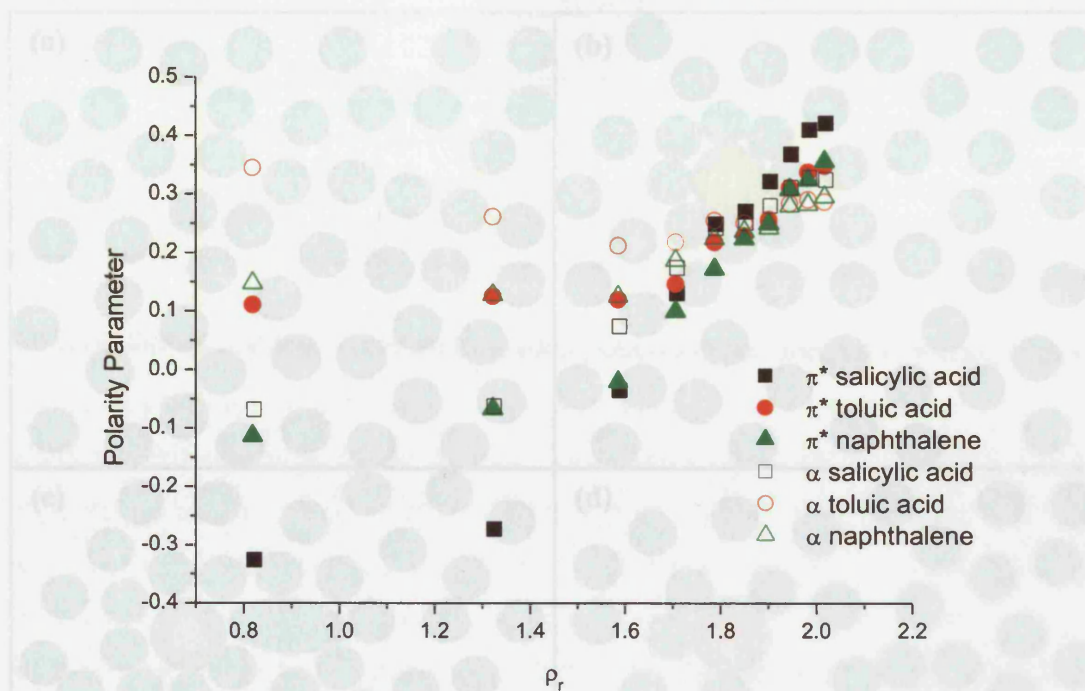


Figure 3.20 Polarity parameters π^* and α as a function of reduced density for 0.01 mol dm^{-3} solute solutions showing the three region density model is apparent and that solution polarity is dominated by hydrogen bonding properties

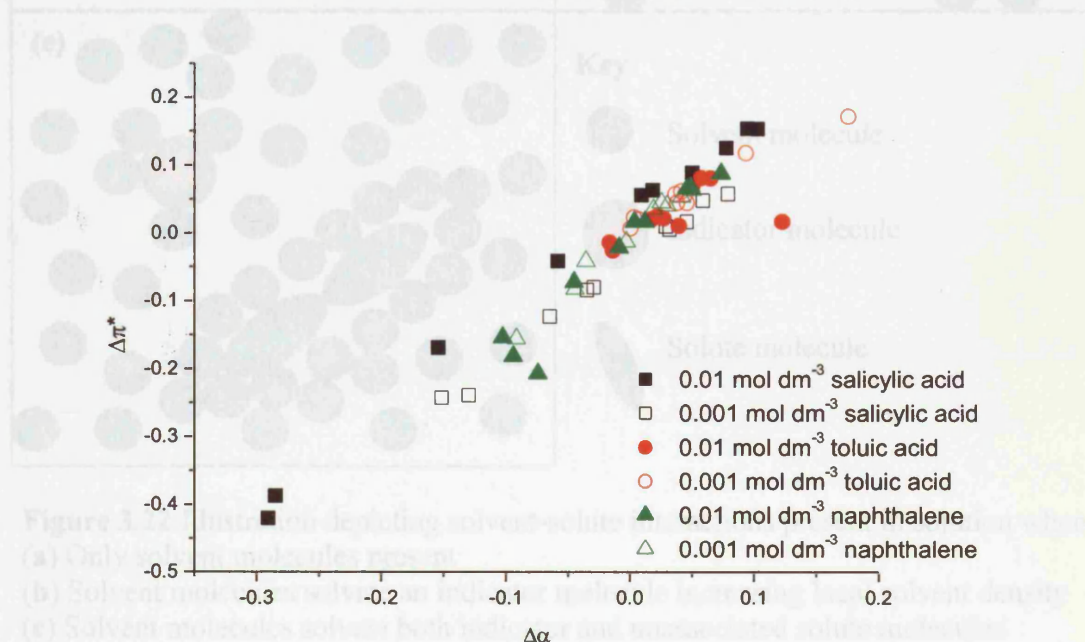


Figure 3.21 Correlation between $\Delta\pi^*$ and $\Delta\alpha$ for solute solutions at solute concentrations of 0.01 mol dm^{-3} and $0.001 \text{ mol dm}^{-3}$ indicating that the main cause of change in solution polarity is the change in local density of the solvent

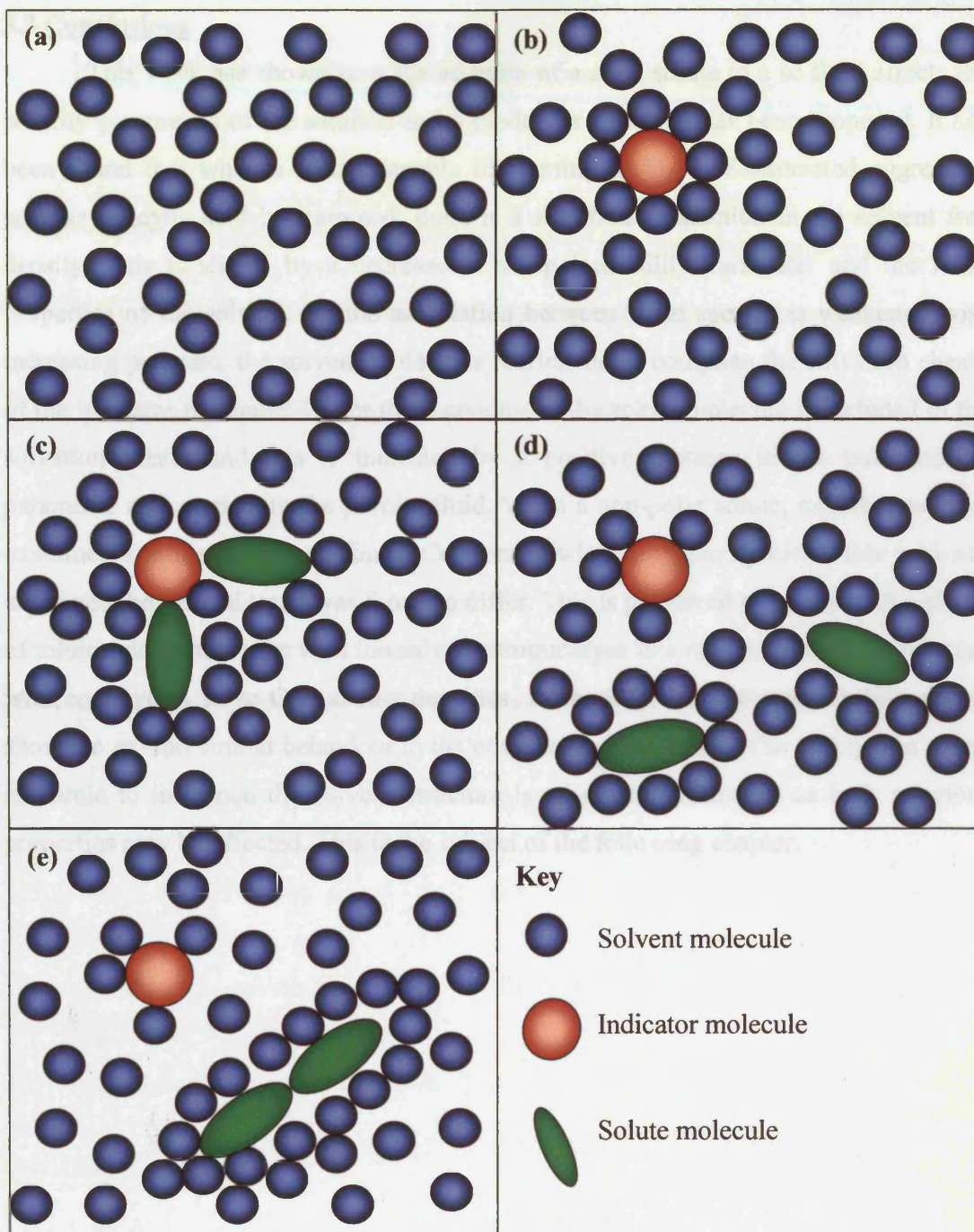


Figure 3.22 Illustration depicting solvent-solute interactions present in solution when
(a) Only solvent molecules present
(b) Solvent molecules solvate an indicator molecule increasing local solvent density
(c) Solvent molecules solvate both indicator and unassociated solute molecules reducing solvent density around the indicator, for example naphthalene
(d) Solvent molecules solvate both indicator and self-associated solute molecules like salicylic acid, reducing solvent density around the indicator molecule
(e) Solvent molecules and solute molecules surround the indicator molecule increasing local density around the indicator molecule

3.3 Conclusions

This work has shown how the addition of a solid solute to a sc fluid affects the polarity parameters of the solution and a model for solvation has been proposed. It has been found that when a solute capable of forming highly self-associated aggregates such as salicylic acid is examined, there is a significant reduction in the solvent free density. This is shown by a decrease in the polarisability parameter and the HBD properties of the solvent. As the association between these species is weakened with increasing pressure, the solvent molecules reorientate to complete the solvation sheath of the indicator molecule. Under these conditions the solute molecule is included in the solvation sheath and this is indicated by a positive increase in the polarisability parameter with respect to the pure sc fluid. When a non-polar solute, naphthalene, was examined a similar trend was found. Conversely when the polar species toluic acid was examined the general trend was found to differ. This is perceived to be due to the ability of toluic acid to associate with the solvatochromic dyes in a manner similar to that seen with co-solvents in sc CO₂ at low densities. In the high density region toluic acid is shown to exhibit similar behaviour to the other solutes examined. The ability of a solute molecule to influence the solvent structure is of great significance as bulk solutions properties may be affected. This is the subject of the following chapter.

3.4 References

1. Tucker, S. C. *Chem. Rev.* **1999**, *99*, 391.
2. Blitz, J. P.; Yonker, C. R.; Smith, R. D. *J. Phys. Chem.* **1989**, *93*, 6661.
3. Ikushima, Y.; Saito, N.; Arai, M. *J. Phys. Chem.* **1992**, *96*, 2293.
4. Gupta, R. B.; Combes, J. R.; Johnston, K. P. *J. Phys. Chem.* **1993**, *97*, 707.
5. Bulgarevich, D. S.; Sako, T.; Sugeta, T.; Otake, K.; Takebayashi, Y.; Kamizawa, C.; Horikawa, Y.; Kato, M. *Ind. Eng. Chem. Res.* **2002**, *41*, 2074.
6. Bulgarevich, D. S.; Otake, K.; Sako, T.; Sugeta, T.; Takebayashi, Y.; Kamizawa, C.; Shintani, D.; Negishi, A.; Tsuruni, C. *J. Chem. Phys.* **2002**, *116*, 1995.
7. Barlow, S. J.; Bondarenko, G. V.; Gorbaty, Y. E.; Yamaguchi, T.; Poliakov, M. *J. Phys. Chem. A*, **2002**, *106*, 10452.
8. Brennecke, J. F.; Tomasko, D. L.; Peshkin, J.; Eckert, C. A. *Ind. Eng. Chem. Res.* **1990**, *29*, 1682.
9. Betts, T. A.; Zagrobelny, J.; Bright, F. V. *J. Am. Chem. Soc.* **1992**, *114*, 8163.
10. Heitz, M. P.; Bright, F. V. *J. Phys. Chem.* **1996**, *100*, 6889.
11. Marcus, Y. *J. Phys. Org. Chem.* **2005**, *18*, 373.
12. Suppan, P.; Ghoneim, N. *Solvatochromism*; Royal Society of Chemistry: Cambridge, **1997**.
13. Atkins, P. W. *Physical Chemistry*, 6th Ed.; Oxford University Press: Oxford, **1996**.
14. Reichardt, C. *Solvent and Solvent Effects in Organic Chemistry*, 2 Ed.; VCH Publishers: Weinheim, **1988**.
15. Reichardt, C. *Chem Rev.* **1994**, *94*, 2319.
16. Taft R, W.; Abboud, J.-L. M.; Kamlet, M. J.; Abraham, M. H. *J. Soln. Chem.* **1985**, *14*, 153.
17. Kamlet, M. J.; Taft, R. W.; Abboud, J.-L. M. *Prog. Phys. Org. Chem.* **1981**, *13*, 485.
18. Kamlet, M. J.; Abboud, J.-L. M.; Taft, R. W. *J. Am. Chem. Soc.* **1977**, *99*, 6027.
19. Kamlet, M. J.; Abboud, J.-L. M.; Taft, R. W. *J. Am. Chem. Soc.* **1976**, *98*, 377.
20. Kamlet, M. J.; Abboud, J.-L. M.; Taft, R. W. *J. Am. Chem. Soc.* **1976**, *98*, 2886.
21. Hildebrand, J. H.; Scott, R. L. *The Solubility of Non-Electrolytes*, 3rd Ed.; Dover Publisher: New York, **1964**.
22. Kamlet, M. J.; Taft, R. W.; Abboud, J.-L. M.; Abraham, M. H. *J. Org. Chem.* **1983**, *48*, 2877.

**Chapter Three – Probing Solute Clustering in Supercritical
Solutions Using Solvatochromic Parameters**

23. Sigman, M. E.; Lindley, S. M.; Leffler, J. E. *J. Am. Chem. Soc.* **1985**, *107*, 1471.
24. Yonker, C. R.; Frye, S. L.; Kalkwarf, D. R.; Smith, R. D. *J. Phys. Chem.* **1986**, *90*, 3022.
25. Smith, R. D.; Frye, S. L.; Yonker, C. R.; Gale, R. W. *J. Phys. Chem.* **1987**, *91*, 3059.
26. O'Neill, M. L.; Kruus, P.; Burk, R. C. *Can. J. Chem.* **1993**, *71*, 1834.
27. Maiwald, M.; Schneider, G. M. *Ber. Bunsen. Phys. Chem.* **1998**, *102*, 960.
28. Lu, J.; Brown, J. S.; Boughner, E. C.; Liotta, C. L.; Eckert, C. A. *Ind. Eng. Chem. Res.* **2002**, *41*, 2835.
29. Lu, J.; Boughner, E. C.; Liotta, C. L.; Eckert, C. A. *Fluid Phase Equilib.* **2002**, *198*, 37.
30. Minami, K.; Mizuta, M.; Suzuki, M.; Aizawa, T.; Arai, K. *Phys. Chem. Chem. Phys.* **2006**, *8*, 2257.
31. Kim, S.; Johnston, K. P. *Ind. Eng. Chem. Res.* **1987**, *26*, 1206.
32. Lagalante, A. F.; Hall, R. L.; Bruno, T. J. *J. Phys. Chem. B*, **1998**, *102*, 6601.
33. Abbott, A. P.; Eardley, C. A. *J. Phys. Chem. B*, **1998**, *102*, 8574.
34. Abbott, A. P.; Eardley, C. A. *J. Phys. Chem. B*, **1999**, *103*, 2504.
35. Abbott, A. P.; Eardley, C. A.; Scheirer, J. E. *Phys. Chem. Chem. Phys.* **2001**, *3*, 3722.
36. Abbott, A. P.; Eardley, C. A.; Scheirer, J. E. *J. Phys. Chem. B*, **1999**, *103*, 8790.
37. Yonker, C. R.; Smith, R. D. *J. Phys. Chem.* **1988**, *92*, 2374.
38. Kim, S.; Johnston, K. P. *AIChE J.* **1987**, *33*, 1603.
39. Sun, Y.-P.; Bennett, G.; Johnston, K. P.; Fox, M. A. *J. Phys. Chem.* **1992**, *96*, 10001.
40. Zhang, J.; Lee, L. L.; Brennecke, J. F. *J. Phys. Chem.* **1995**, *99*, 9268.
41. Kelley, S. P.; Lemert, R. M. *AIChE J.* **1996**, *42*, 2047.
42. Chen, J.; Shen, D.; Wu, W.; Han, B.; Wang, B.; Sun, D. *J. Chem. Phys.* **2005**, *122*, 204508.
43. Jeffrey, G. A. *An Introduction to Hydrogen Bonding*; Oxford University Press: New York, **1997**.
44. Marcus, Y. *Chem. Soc. Rev.* **1993**, *22*, 409.
45. Marcus, Y. *J. Soln. Chem.* **1991**, *20*, 929.
46. Bennett, G. E.; Johnston, K. P. *J. Phys. Chem.* **1994**, *98*, 441.
47. Eardley, C. A. PhD Thesis, University of Leicester, Leicester, **1999**.

**Chapter Three – Probing Solute Clustering in Supercritical
Solutions Using Solvatochromic Parameters**

48. Abbott, A. P.; Corr, S.; Durling, N. E.; Hope, E. G. *J. Phys. Chem. B*, **2003**, *107*, 10628.
49. Adams, J. E. *J. Phys. Chem. B*, **1998**, *102*, 7455.
50. Ingrosso, F.; Ladanyi, B. M.; Mennucci, B.; Scalmani, G. *J. Phys. Chem. B*, **2006**, *110*, 10120.
51. Yonker, C. R.; Smith, R. D. *J. Phys. Chem.* **1988**, *92*, 236.
52. Johnston, K. P.; Kim, S.; Combes, J. *ACS Symp. Ser.*, **1989**, *406*, 52.
53. Corr, S. *J. Fluor. Chem.* **2002**, *118*, 55.

4.1 Introduction

Supercritical fluids are generally considered to have low viscosities. Many substances, however, exhibit a significant increase in viscosity related to the critical point. For example, carbon dioxide, a non-polar fluid with a critical temperature of 31.1°C and a critical pressure of 73.8 bar, exhibits a sharp increase in viscosity over the pressure range 10–30 bar, which possesses a quadrupole moment and a density of 0.927 g cm⁻³ at 300 bar, exhibits a more significant change in viscosity with increasing pressure. This variation is also true for dipolar CH₂F₂ (ρ = 0.895 g cm⁻³ at 300 bar).

DETERMINATION OF THE VISCOSITY OF SUPERCRITICAL SOLUTIONS

The viscosity of supercritical fluids has rarely been studied. Here a novel technique for the determination of the viscosity of supercritical fluids is described and the effect of solutes is investigated.

4.1	Introduction
4.1.1	Viscosity
4.1.2	The Piezoelectric Quartz Crystal Resonator
4.2	Results and Discussion
4.2.1	Technique and Method Design
4.2.2	Non-electrolyte Solutions
4.2.3	Electrolyte Solutions
4.2.4	Electrochemistry in Supercritical Electrolyte Solutions
4.3	Conclusions
4.4	References

0.0002

0.0001

Pressure / bar

Figure 4.1 Variation in fluid viscosity with pressure at T = 4.25 (above T_c)

4.1 Introduction

Supercritical fluids are primarily of interest because of their low viscosities. Many authors have examined the viscosity of pure sc fluids and shown that it is clearly related to the density, ρ , of the fluid.¹⁻³ Figure 4.1 illustrates how the viscosity of three fluids varies with pressure at the same reduced temperature, T_r (where $T_r = T/T_c$). The viscosity of non-polar helium ($\rho = 0.164 \text{ g cm}^{-3}$ at 300 bar) does not alter significantly over the pressure range. In contrast CO_2 , which possesses a quadrupole moment and a density of 0.927 g cm^{-3} at 300 bar, exhibits a more significant change in viscosity with increasing pressure. This variation is also true for dipolar CH_2F_2 ($\rho = 0.893 \text{ g cm}^{-3}$ at 300 bar).

The properties of sc fluid solutions and the effect of solutes on viscosity have rarely been studied. Here a novel technique to measure viscosity of sc fluid solutions is described and the effect of solutes is examined.

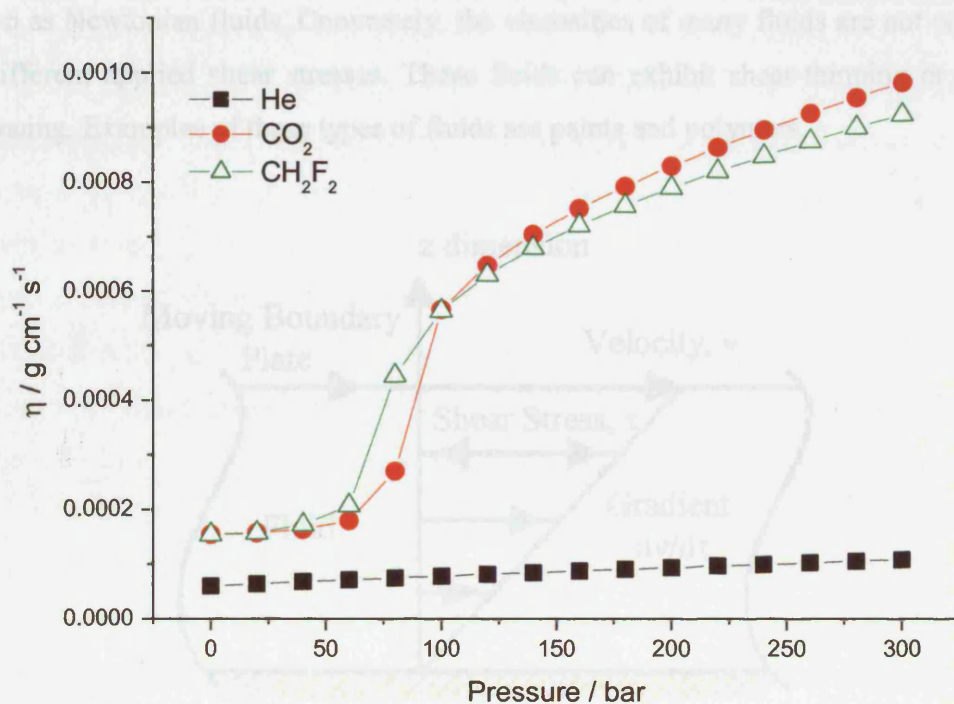


Figure 4.1 Variation in fluid viscosity with pressure at $T_r = 1.15$ (where $T_r = T/T_c$)¹⁻³

4.1.1 Viscosity

In 1687 Newton proposed that the rate of deformation, also known as the shear rate, is proportional to the shearing stress. This can easily be explained by considering a fluid that is sandwiched between two parallel plates set at a distance, dz , apart (Figure 4.2). If the upper plate moves with a velocity, dv , in comparison to the lower plate there will be a small resisting force over the plate area due to viscous frictional effects in the fluid. This force per unit area of plate is known as the shear stress, τ , and is given by

$$\tau = \eta \frac{dv}{dz} \quad (4.1)$$

where the proportionality constant, η , is the dynamic viscosity. This is a measure of the resistance to flow and varies from one fluid to another. The common SI units of viscosity are Pa s, N m⁻² s or g cm⁻² s, which are called poise, P. The sub multiple of centipoises, cP, is commonly encountered where 1cP is equal to 1mPa s.

According to Equation 4.1 viscosity is independent of the shear rate. This is true for ideal fluids such as water, ethanol, glycerine and benzene and these fluids are known as Newtonian fluids. Conversely, the viscosities of many fluids are not constant for different applied shear stresses. These fluids can exhibit shear-thinning or shear-thickening. Examples of these types of fluids are paints and polymers.

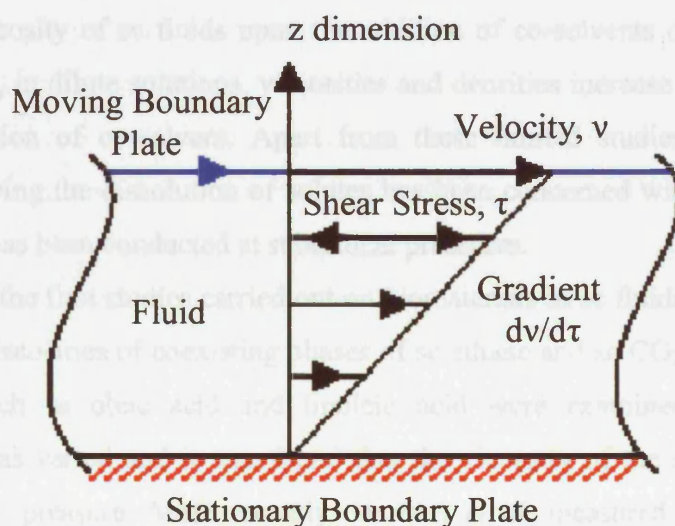


Figure 4.2 Schematic representation of laminar shear of fluid between two plates

To perform measurements under ambient conditions, a wide range of viscometers are commercially available and fall into three main categories; capillary, rotational and moving body.^{4,5} Capillary flow methods involve measuring the flow rate of a fluid as it is fed through a fine-bore tube. The viscosity is determined from the flow time. Rotational viscometers employ two cylinders that are separated by the fluid. The relative movements of these cylinders produce a shearing action and the torque required to produce a given angular velocity is a measure of the viscosity. The third type determines the fluid viscosity from the rate of movement or fall of a body such as a ball or rod through the fluid.

Viscosity measurements under sc conditions can be more challenging to perform because there are experimental difficulties with working at both high temperatures and pressures. Despite this, a range of techniques have become available to study high pressure viscosity. These include the oscillating-disk viscometer,⁶ high-pressure capillary viscometer^{7,8} and the vibrating quartz crystal viscometer.^{9,10} However, the most common is the falling-body type viscometer,¹¹⁻¹³ in which the time taken for a body to fall a known distance in a tube filled with the fluid is measured.

Although several groups have measured the viscosity of fluids at high pressure and temperature^{6,10} there has been relatively little work done on the effects on viscosity of solutes dissolved in sc fluids. A number of research groups have examined the changes in viscosity of sc fluids upon the addition of co-solvents or modifiers.^{14,15} It was found that, in dilute solutions, viscosities and densities increase with size, polarity and concentration of co-solvent. Apart from these limited studies, the majority of research involving the dissolution of solutes has been concerned with biomolecules or polymers and has been conducted at subcritical pressures.

One of the first studies carried out on biomaterials in sc fluids was by Peter and Jakob.¹⁶ The viscosities of coexisting phases of sc ethane and sc CO₂ with a number of fatty acids such as oleic acid and linoleic acid were examined. The fatty acid composition was varied and it was found that the viscosity of the sc phase increased with increasing pressure. More recently, Harriott *et al.* measured and modelled the viscosities of several sc CO₂/lipid mixtures by high-pressure capillary viscometry.^{7,8} The viscosities of solubilised methyl oleate and oleic acid as a function of concentration, up to 5 weight %, and temperature were explored. Relative viscosities ($\eta_r = \eta/\eta_0$) increased linearly with concentration and were found to be no greater than 1.21 for either solute. It was concluded that the addition of oleic acid causes a three-fold

increase in viscosity when compared to the addition of the same weight percent of methyl oleate. The viscosity dependence on methyl oleate and anhydrous milk fat (AMF) mass fraction in sc CO₂ was also measured. This dependence was found to be linear with the greatest increase in viscosity found at the highest mass fraction of solute. Prior to this work, the group had investigated the viscosities of several fatty acids and fatty acid esters saturated with sc CO₂.⁷ Results showed that the viscosities of the liquid phase methylated fatty acids decreased as the pressure was increased. Both the fatty acids and AMF also experienced a viscosity reduction. However, in comparison with the methylated fatty acids, this was lower at higher pressures.

Over the past three decades research into high-pressure polymer solutions has grown significantly. Kiran and co-workers have carried out the most extensive research into the viscosity of these solutions. A falling-body type viscometer was employed to determine the temperature and pressure dependence of viscosity and density of several high-pressure alkanes.¹³ The effect on solution viscosity of several polymers in both sub and sc alkanes and sc CO₂ was also investigated. Studies include: poly(dimethylsiloxane) (PDMS) in sc CO₂,¹⁷ polyethylene (PE) in *n*-pentane¹⁸ and polystyrene (PS) in near critical and sc *n*-butane, sub-critical *n*-hexane and sub-critical methylcyclohexane.¹⁹ In each case it was found that viscosity increases linearly with pressure. For solutions of sc CO₂/PDMS, viscosities were found to increase with pressure and polymer concentration and decrease with temperature. The corresponding relative viscosities ranged from approximately 1 to 1.50 at the highest PDMS weight percent. More recently, work was carried out at the critical polymer concentration for PDMS in sc CO₂ and PE in sub-critical *n*-pentane.^{17,18} At the temperatures and pressures investigated the corresponding relative viscosities were approximately 2 for sc CO₂/PDMS solutions and ranged from 18 to 26 for *n*-pentane/PE solutions. Mertsch and Wolf have also investigated solutions of PDMS in sc CO₂.¹² Five concentrations of PDMS at pressures from 100 to 700 bar were examined using a rolling-ball and rotational viscometer.

A number of studies have looked into the reverse of this process where sc CO₂ is added to a polymer melt in order to decrease its viscosity. This process has applications in extrusion, foaming and impregnation processes. At pressures up to 350 bar, Kiran and Yeo examined PS solutions in toluene and sc CO₂ as a function of polymer composition and CO₂ content.²⁰ It was found that the solution viscosity varied linearly with pressure and polymer concentration. The largest reduction in viscosity was

observed for the lowest temperature and highest weight percent of polymer. When correlated with density, different viscosities were observed at the same density depending on the CO₂ content. Other research groups have investigated the reduction of viscosity of PS with sc CO₂.^{21,22}

All of the systems studied to date have been carried out in non-polar sc fluids and have reported modest increases in viscosity. In addition, the solutes studied have been non-polar and hence would be expected to cause only modest ordering in the sc solution. The aim of this work was to design a reliable viscometer capable of measuring viscosities of sc fluid solutions up to 300 bar and this technique would be used to study the effect of a variety of solutes on the viscosity of sc CH₂F₂. The ideal measuring procedure would be simple, inexpensive and allow direct *in situ* measurements of the system to be taken.

4.1.2 The Piezoelectric Quartz Crystal Resonator

In 1880 Jacques and Pierre Curie discovered that, by applying a mechanical stress to the surface of certain crystals such as tourmaline, rochelle salt (NaKC₄H₄O₆·4H₂O) and quartz, an electrical potential is produced across the crystal. The magnitude of this electrical potential is proportional to the applied stress. This phenomenon is called the piezoelectric effect, derived from the Greek word piezein meaning 'to press'.

In a piezoelectric material, the positive and negative electric charges are separated, but symmetrically distributed, so that the crystal overall is electrically neutral (Figure 4.3a). If a mechanical stress is applied to the material, the lattice symmetry is disturbed and the centre of gravity of positive and negative charges in the material are separated. For example, in Figure 4.3b the material lattice has been elongated along the Y-axis resulting in charge asymmetry. There are net movements along the X-axis, negative charges to the left and positive charges to the right, generating a voltage across the material. If the properties of a material are the same in both directions along any line it will possess a centre of symmetry and is not capable of deforming in the manner caused by the piezoelectric effect.

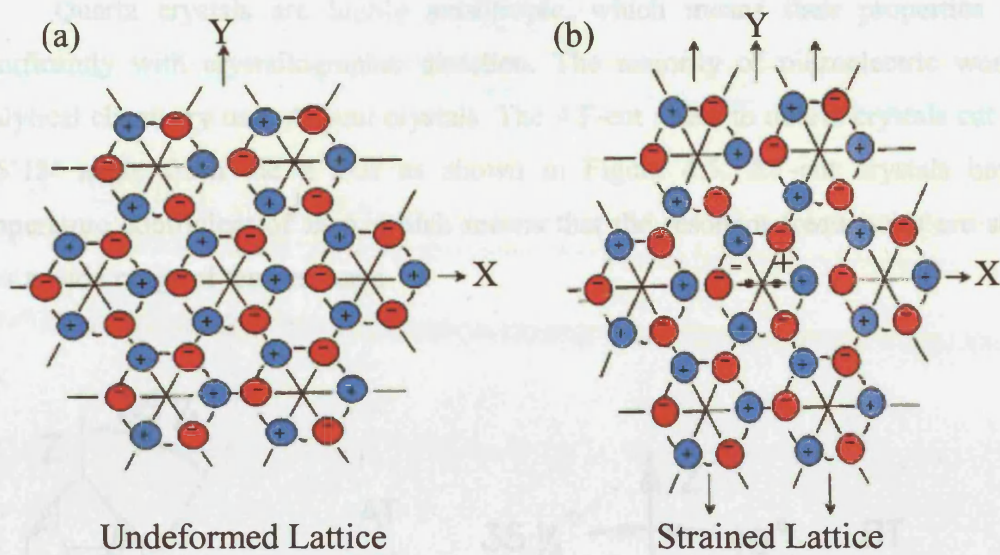


Figure 4.3 Schematic diagram to represent the piezoelectric effect²³

(a) Undeformed electrically neutral lattice

(b) Strained lattice showing charge asymmetry which generates a voltage across the material

It is the reverse of this phenomenon termed the converse piezoelectric effect (Figure 4.4) that is the basis of the piezoelectric quartz crystal (PQC); A voltage is applied across the crystal which induces reorientation of the dipoles resulting in lattice strain and deformation of the material. In the case of quartz, if the voltage applied is an alternating potential a mechanical oscillation of a standing shear wave is produced across the quartz at a characteristic vibrational frequency. This is the crystal's natural resonant frequency and is sensitive to minute changes in the crystal. It is dependent on physical properties such as cut, density, size and shear modulus and the environment surrounding the crystal.

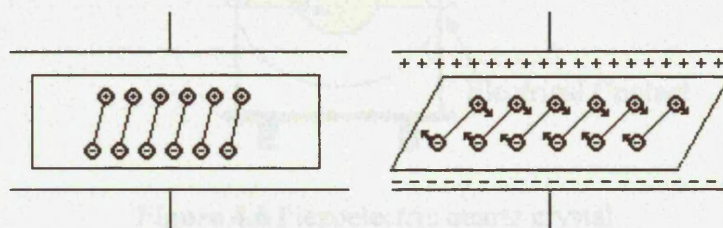


Figure 4.4 Schematic representation of the converse piezoelectric effect^{24,25}

Quartz crystals are highly anisotropic, which means their properties vary significantly with crystallographic direction. The majority of piezoelectric work in analytical chemistry uses AT-cut crystals. The AT-cut refers to quartz crystals cut at a $+35^{\circ}15'$ angle from the z axis as shown in Figure 4.5. AT-cut crystals have a temperature coefficient of zero, which means that the resonant frequencies are stable over a wide range of temperatures.

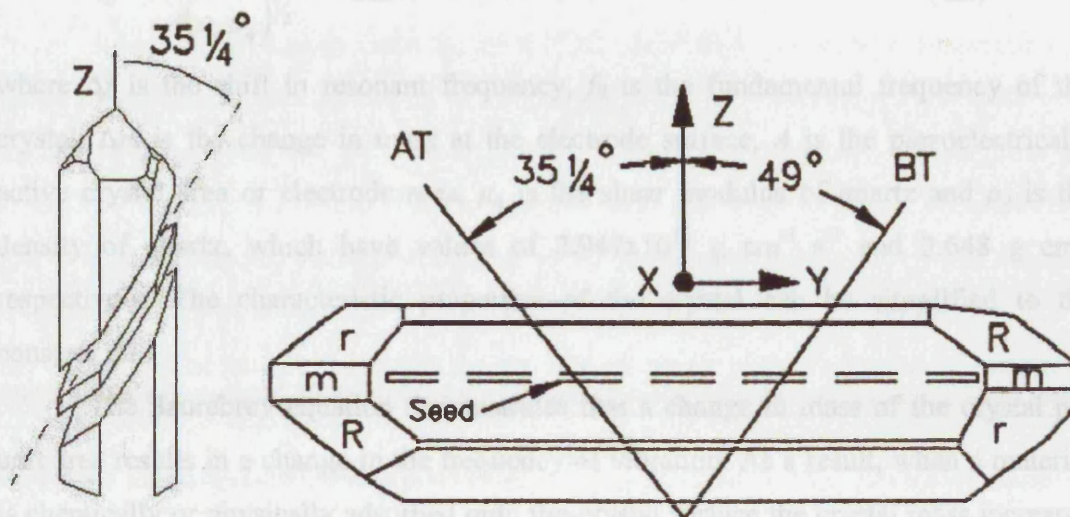


Figure 4.5 Schematic diagram of AT-cut crystal

A quartz crystal resonator (QCR) is a thin quartz disk sandwiched between two metal electrodes that are prepared by thermal evaporation onto the quartz surface (Figure 4.6). Only the region between the electrodes is piezoelectrically active.

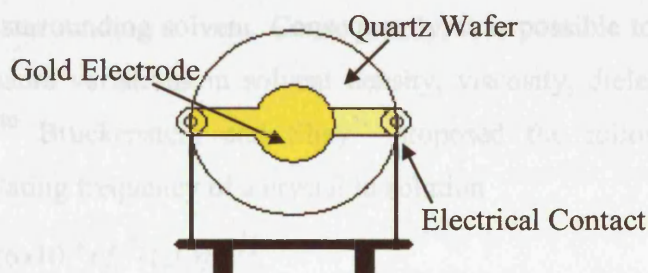


Figure 4.6 Piezoelectric quartz crystal

A variety of applications exist for the PQC including use as a chemical or biological sensor^{26,27} and for electrochemical studies into interfacial properties of

films.²⁸ By far the most common application of the PQC is as a micro or nanobalance. Here, changes in mass of the crystal or thin film coatings adhered to the crystal surface are examined. When a crystal is used in this manner it is referred to as quartz crystal microbalance, QCM. The Saurebrey equation, developed in the 1950s, describes the mass sensitivity of the resonant frequency of the crystal, which decreases as the mass of the crystal increases.

$$\Delta f = \frac{-2f_0^2 \Delta m}{A(\rho_q \mu_q)^{1/2}} = -C\Delta m \quad (4.2)$$

where Δf is the shift in resonant frequency, f_0 is the fundamental frequency of the crystal, Δm is the change in mass at the electrode surface, A is the piezoelectrically active crystal area or electrode area, μ_q is the shear modulus of quartz and ρ_q is the density of quartz, which have values of $2.947 \times 10^{11} \text{ g cm}^{-1} \text{ s}^{-2}$ and 2.648 g cm^{-3} respectively. The characteristic properties of the crystal can be simplified to the constant C .

The Saurebrey equation demonstrates that a change in mass of the crystal per unit area results in a change in the frequency of vibration. As a result, when a material is chemically or physically adsorbed onto the crystal surface the crystal mass increases and results in a corresponding change to the resonant frequency. When the limit of mass that can be added is reached the crystal will cease to oscillate. Hence, it is assumed that any mass absorbed will be less than the mass of the crystal. In addition, it is assumed that the mass is firmly attached to the crystal and rigid, implying that it resonates with the crystal.

In liquid media the oscillating frequency of a crystal will depend on the properties of the surrounding solvent. Consequently, it is possible to employ the PQC technique to measure variations in solvent density, viscosity, dielectric constant and conductivity.^{24,29,30} Bruckenstein and Shay³¹ proposed the following equation to describe the oscillating frequency of a crystal in solution

$$\Delta f = -2.26 \times 10^{-6} n f_0^{3/2} (\rho_f \eta_f)^{1/2} \quad (4.3)$$

where n is the number of faces of the crystal exposed to the solution and ρ_f and η_f are the density and viscosity of the surrounding fluid. Kanazawa and Gordon introduced a similar physical model (Equation 4.4).³² This model couples the shear wave in the quartz crystal to a damped shear wave in the viscous fluid and was derived in terms of the material parameters of the fluid and the crystal.

$$\Delta f = -\eta f_0^{3/2} \left(\frac{\rho_f \eta_f}{\pi \rho_q \mu_q} \right)^{1/2} \quad (4.4)$$

Despite the differences in these models, they both display the same linear correlation between the density-viscosity product of the solvent, $(\rho_f \eta_f)$ and shift in resonant frequency. This relationship has been examined by several research groups and a number of these have employed the PQC as a reliable viscometer.³³ The fluids studied range from aqueous sugar and polymer solutions³⁴ to industrial oils³⁵ and blood.^{36,37}

When the frequency response of a PQC under high pressure is examined it is found that the resonance frequency is not only affected by the viscosity and density of the surrounding fluid but also the hydrostatic pressure. Stockbridge investigated the change in resonant frequency when a crystal is exposed to gases at low pressures.³⁸ It was concluded that three effects contribute to the experimental frequency shift. The first is caused by pressure and due to the increasing stiffness of the quartz as pressure is increased. The second is due to the density and viscosity of the surrounding gas, while the third effect is caused by gas sorption to the electrode surface. Therefore the overall frequency shift, Δf_{exp} , may be expressed by

$$\Delta f_{exp} = \Delta f_p + \Delta f_\eta + \Delta f_m \quad (4.5)$$

where Δf_p is the frequency shift due to pressure, Δf_η is the shift due to the viscosity and density of the surrounding fluid and Δf_m is the frequency due to mass changes through adsorption. Each of these terms may be evaluated if the appropriate values are known. Stockbridge showed that the frequency change caused by the compression effect increases linearly with pressure. The gradient of this dependence is independent of the nature of the fluid and is proportional to the fundamental frequency of the crystal, f_0 .

$$\Delta f_p = f_0 \alpha P \quad (4.6)$$

α is the proportionality constant and can be evaluated from the linear gradient of a frequency-versus-pressure plot of a non-adsorbing gas such as helium. Park *et al.*³⁹ showed that α decreases with increasing temperature and proposed the following equation for α , expressed in MPa⁻¹ and temperature, T, in °C

$$\alpha = 1.095 \times 10^{-5} - 2 \times 10^{-8} T \quad (4.7)$$

α values were estimated from extrapolations of the elastic modulus of the quartz crystal with pressure at a number of temperatures. It was highlighted that α values are dependent on viscosity loading of the surrounding fluid but, within the temperature

range under consideration Equation 4.7 may be used to obtain a value for α with a negligible error.

The next term in Equation 4.5 is Δf_η and can be calculated in a similar manner to the liquid state by Equations 4.3 or 4.4. The final term in Equation 4.5 is due to mass addition to the crystal and can be calculated by the Sauerbrey Equation (Equation 4.2). However, it is more commonly obtained by evaluating all of the other terms in Equation 4.5. Otake *et al.* applied this analysis to examine the frequency change of a silver electrode deposited on a quartz crystal in sc CO₂.⁴⁰ The pressure dependencies of resonance frequencies in helium and nitrogen gases were measured to calculate the value of α . This was found to be in excellent agreement with the value calculated by Equation 4.7. Δf_η was evaluated from literature data. It was therefore possible to calculate Δf_m by rearranging Equation 4.5. The mass of CO₂ adsorbed to the silver electrode surface could be extracted from Equation 4.2 and, subsequently, the number of layers of CO₂ molecules adsorbed onto the surface was calculated. Discrepancies with previously published work were highlighted and attributed to the roughness of the electrode surface.

By employing the same technique, Guigard and co-workers measured the solubilities of two metal chelates in sc CO₂ solutions.⁴¹ A known mass of solute was deposited onto the surface of a crystal and the change in frequency monitored as the solute was dissolved in sc CO₂.

For perfectly smooth surfaces, the shift in resonant frequency is proportional to the square root of the viscosity-density product of the solution as shown by Equations 4.3 and 4.4. However, when the crystal surface is rough, the response is found to be somewhat different. It is thought that the solution may partially or completely fill the surface features and become constrained. Under these conditions the solution may behave as a rigidly deposited mass. To minimise the effects due to surface roughness, highly polished quartz crystals are used. Urbakh and Daikhin remarked that many research groups have neglected the effects of surface roughness at the crystal-fluid interface. The significance of surface roughness on frequency shifts was emphasised and shown to dramatically alter resonance frequencies in both the liquid state and at high pressures.⁴² Three types of surface were examined with varying textures from rough to polished. The gases used were specifically chosen so adsorption would not occur; therefore frequency changes due to mass effects were negligible. Effects due to pressure, viscosity and density were calculated from literature data thus all the terms in

Equation 4.5 were accounted for. It was concluded that the residual frequency shift was due to the surface morphology of the crystal. By including frequency shift effects caused by surface morphology, Δf_r , Equation 4.5 becomes

$$\Delta f_{\text{exp}} = \Delta f_p + \Delta f_\eta + \Delta f_m + \Delta f_r \quad (4.8)$$

Although it is difficult to analyse surface roughness because it is random by nature, a theory for a number of limiting cases was proposed as shown in Figure 4.7. Surface roughness was shown to be related to the density of the fluid. In these studies, surface roughness was characterised by scanning tunnelling microscopy (STM).

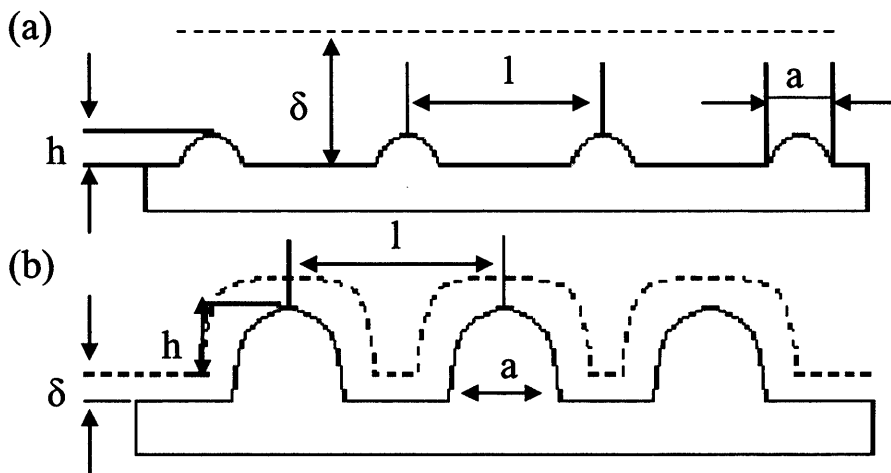


Figure 4.7 Schematic representation of PQC roughness characterised by average height, h , lateral length, a , and the distance between surface inhomogeneities, l and decay length, δ , which is the thickness of the surrounding fluid that is driven to move by the vibrating crystal

(a) Slightly rough surface $h / \delta \ll 1$; (b) Highly rough surface $h / \delta \gg 1$ ⁴²

More recently Grant *et al.* examined the response of a PQC in high pressure CO₂.⁴³ The frequency response of a number of crystals made from different materials with varying degrees of roughness was evaluated. Crystal surfaces were characterised by Atomic Force Microscopy (AFM) and the parameters depicted in Figure 4.7 were obtained. To account for roughness effects a model similar to that proposed by Urbakh⁴² was used and a roughness-frequency correlation factor was defined. It was found that adsorption of gaseous CO₂ was independent of surface roughness and electrode type. Conversely when sc CO₂ was examined, only the polished crystals were able to give accurate adsorption values. The remaining crystals required adjustments to

the frequency shifts to account for roughness effects. The adsorption values obtained were much lower than those estimated by either Otake⁴⁰ or Guigard⁴¹ and this was attributed to the consideration of roughness effects. Park and co-workers also examined the effects of surface roughness on the resonant frequency shift.³⁹ Surface morphologies of an etched and a polished surface were examined by AFM. In calculations a term to describe the surface roughness was used and its value was evaluated by fitting theoretical calculations to experimental results. The polished surface had a value of zero because the roughness was much lower than the diffusion length but the value for the etched surface was found to be much higher and indicated that the frequency shift was strongly dependent on roughness.

In addition to the abovementioned studies a number of other groups have examined the applications of the PQC under sc conditions. By far the most common application has been to measure the solubility of gases in polymers. Gases studied include CO₂ and, more recently, CH₂F₂.^{44,45} These experiments were performed by coating the PQC surface with a polymer film and measuring the frequency change when exposed to different pressures of a chosen gas. Subsequently, the mass of gas absorbed per mass of polymer as a function of pressure can be calculated and further information on plasticization and polymer swelling can be determined. It has also been possible to measure the kinetics of gas sorption by monitoring the change in frequency shift over a period of time. Alternatively, Poliakoff and co-workers have employed a PQC to determine phase behaviour of sc CO₂, sc ethane and sc CO₂ mixtures as a function of solvent density and viscosity.^{46,47}

It has been shown that using a PQC is a simple and convenient method to obtain reliable *in situ* measurements. Depending on the cut of the crystal employed, they can be stable over a wide temperature range and can be used at extremely high pressures. The majority of studies have been concerned with the use of PQC's for a range of sensor applications in the liquid and gaseous states. Despite investigations under sc conditions being more limited they have shown great potential as a sensor to monitor solubility and phase behaviour.

Here, the potential of using a PQC to measure viscosity of sc fluids and to apply the technique to sc fluid solutions is fully assessed. Information on the viscosity of sc fluid solutions is valuable in understanding the factors that influence solute-solute and solute-solvent interactions when solutes are dissolved in sc fluids.

4.2 Results and Discussion

4.2.1 Technique and Method Design

To ascertain whether a piezoelectric quartz crystal could be used as a viscometer under sc conditions it was essential to first investigate the frequency response of a crystal under ambient conditions. This was carried out in a number of liquid solvents with a range of viscosities from acetone ($0.003 \text{ g cm}^{-1} \text{ s}^{-1}$) to 2-methyl-2-propanol ($0.044 \text{ g cm}^{-1} \text{ s}^{-1}$). These measurements were obtained using the equipment described in Section 2.3.3, in which only one side of the crystal is exposed to the solvent in question. A poor correlation was found between the frequency shift and density-viscosity product for these solvents. It was thought that this was due to interactions of the solvent with the gold electrode. Problems associated with adsorption, wetting and solvent trapping which would lead to contamination were thought to be possible.

To circumvent these interferences the frequency response of a crystal submerged in water was measured as the temperature was systematically altered. This work was thought to be more accurate because both sides of the crystal were exposed to the solvent as would be the case under high pressure conditions and there is no risk of contamination of the crystal because only one solvent is used. To obtain readings in high viscosity fluids a number of aqueous sucrose solutions of different concentrations were also examined under ambient conditions. These aqueous results (Figure 4.8) show an excellent correlation ($R > 0.99$) and indicate that the technique is applicable.

The high pressure vessel described in Section 2.2.3 was used to make measurements under sc conditions. It was found that the accuracy of the data was strongly related to the sensitivity of the measuring equipment. Frequency shifts in liquid media and of polymer gas sorption under high pressure were not sensitive enough to acquire the shifts in frequency of a crystal as a function of pressure. Once the appropriate degree of sensitivity had been established, the response of a crystal was monitored over a range of pressures at constant temperature ($90 \text{ }^\circ\text{C}$). Figure 4.9 shows the frequency-admittance plots obtained. It is clear that as pressure is increased the shape of the curve significantly changes especially as the critical pressure is reached ($\text{CH}_2\text{F}_2 \text{ } p_c = 57 \text{ bar}$). The dampening of curves (decrease in admittance) is due to an increase in the resistance of the fluid as pressure is increased. This effect was also apparent in aqueous solutions under ambient conditions and is attributed to the viscoelastic properties of the solvent.

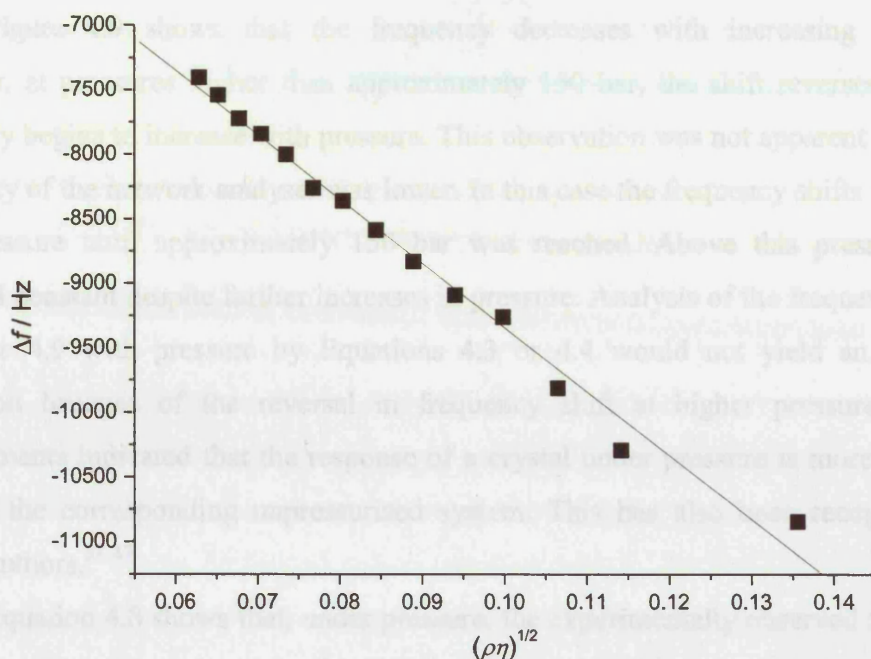


Figure 4.8 Calibration of density-viscosity product and frequency shift for aqueous systems as a function of temperature and sucrose concentration

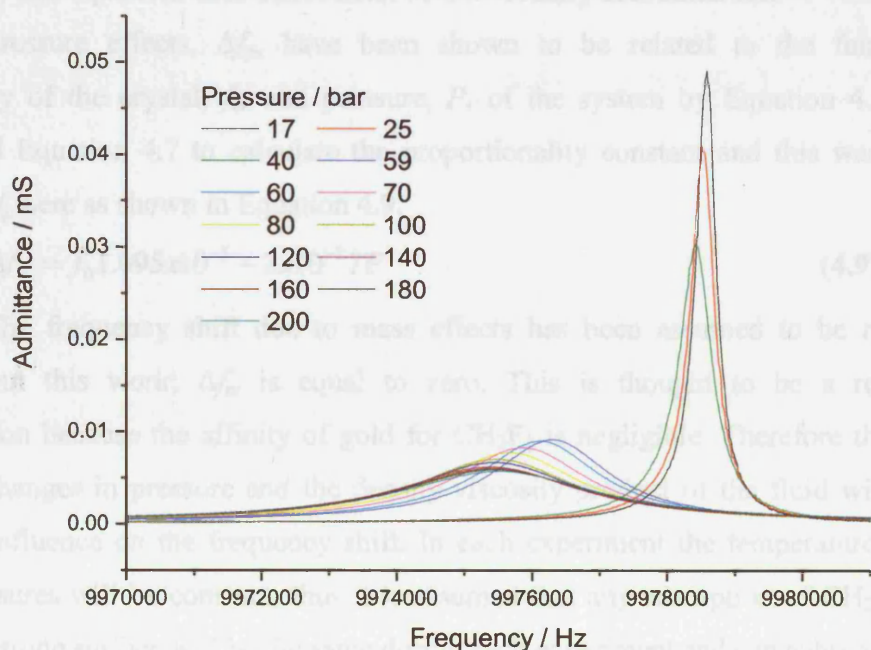


Figure 4.9 Frequency-admittance responses for CH_2F_2 at $90\text{ }^\circ\text{C}$ as a function of pressure. Both admittance and frequency decrease with increasing pressure. Above 150 bar frequency is observed to increase with increasing pressure

Figure 4.9 shows that the frequency decreases with increasing pressure. However, at pressures higher than approximately 150 bar, the shift reverses and the frequency begins to increase with pressure. This observation was not apparent when the sensitivity of the network analyser was lower. In this case the frequency shifts increased with pressure until approximately 150 bar was reached. Above this pressure they remained constant despite further increases in pressure. Analysis of the frequency shifts in Figure 4.9 with pressure by Equations 4.3 or 4.4 would not yield an accurate calibration because of the reversal in frequency shift at higher pressures. These measurements indicated that the response of a crystal under pressure is more complex than for the corresponding unpressurised system. This has also been recognised by several authors.³⁸⁻⁴³

Equation 4.8 shows that, under pressure, the experimentally observed frequency shift, Δf_{exp} , is equal to the sum of individual frequency shifts caused by a number of effects. These effects are due to pressure, mass loading, the viscosity of the surrounding fluid and crystal surface morphology. To evaluate the frequency shifts observed in CH_2F_2 by this equation, each effect must be individually accounted for.

Pressure effects, Δf_p , have been shown to be related to the fundamental frequency of the crystal, f_0 , and pressure, P , of the system by Equation 4.6. Park³⁹ proposed Equation 4.7 to calculate the proportionality constant and this was used to obtain Δf_p here as shown in Equation 4.9.

$$\Delta f_p = f_0 1.095 \times 10^{-5} - 2 \times 10^{-8} TP \quad (4.9)$$

The frequency shift due to mass effects has been assumed to be negligible throughout this work; Δf_m is equal to zero. This is thought to be a reasonable assumption because the affinity of gold for CH_2F_2 is negligible. Therefore the effects due to changes in pressure and the density-viscosity product of the fluid will have a greater influence on the frequency shift. In each experiment the temperature, solvent and pressures will be constant, thus it is assumed that any adsorption of CH_2F_2 to the gold electrode surface will be the same during each experiment and can subsequently be considered as constant.

Viscosity loading effects are related to the density-viscosity product of the fluid ($\rho_f \eta_f$) by Equations 4.3 and 4.4. Viscosity and density values for CH_2F_2 at 90 °C at each pressure were obtained from the literature³ and used in the equations to calculate Δf_η .

Frequency shifts that result from the surface morphology of the crystal, Δf_r , will vary from crystal to crystal. It has been shown that these effects can be minimised by using polished crystals. However, in this study unpolished crystals were used. Analysis of the surface morphology of both an unpolished and a polished crystal was performed using atomic force microscopy (AFM) and scanning electron microscopy (SEM). The results are shown in Figures 4.10 and 4.11. Recently Hillman and Daisley have characterised the surface features of unpolished and polished crystals similar to those used in this work.⁴⁸ They calculated that the average surface features sizes are 140 nm and 20 nm for the unpolished and polished crystals respectively. These values are in good agreement with the observable pore sizes on the AFM and SEM images.

To assess the potential inaccuracies from using unpolished crystals the calibration analysis was performed with a polished crystal. The results were not found to deviate significantly from those obtained previously. Therefore, it was decided that it was reasonable to assume Δf_r would have a negligible contribution to Δf_{exp} and remain constant throughout the experiments.

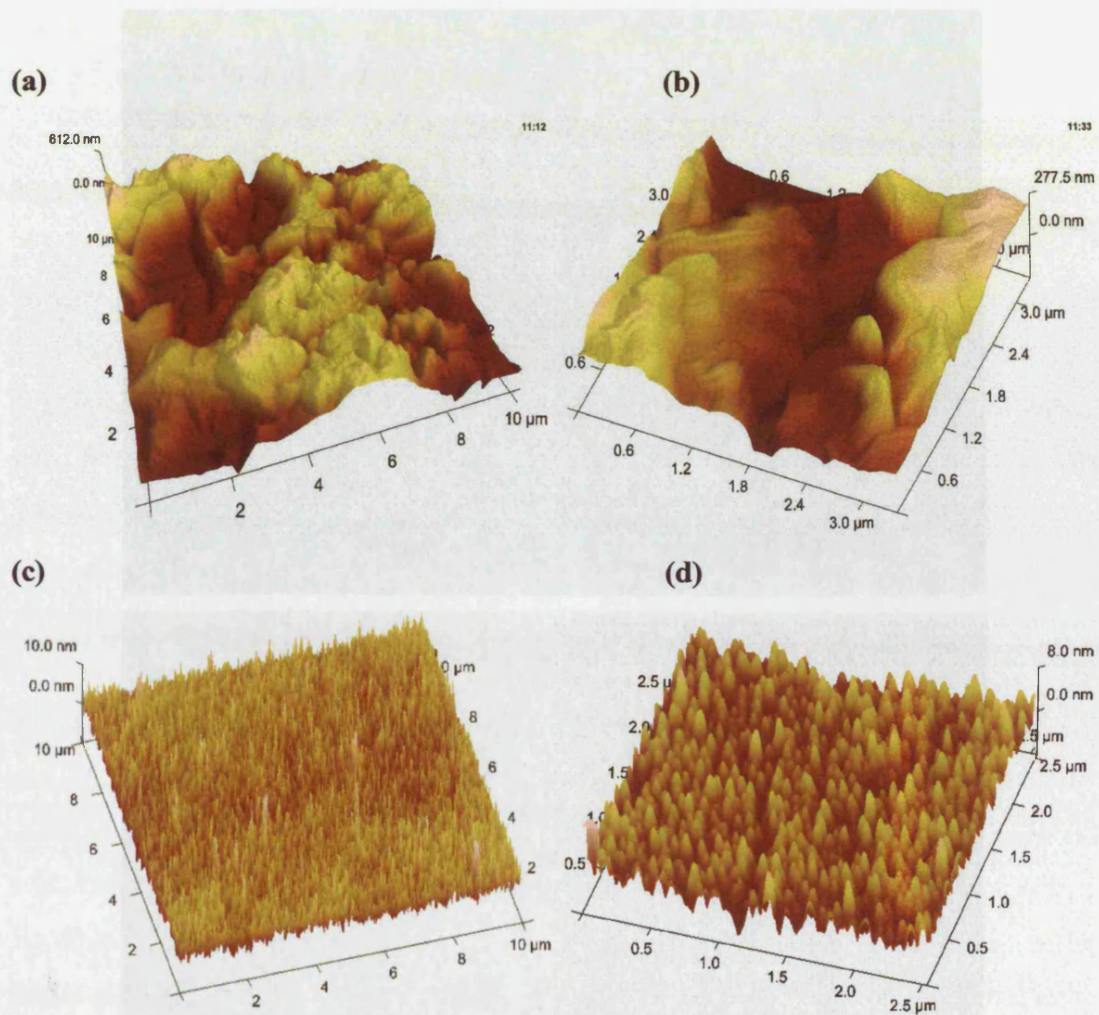


Figure 4.10 Atomic force microscopy images at different magnifications for (a) and (b) Unpolished quartz crystal, surface features approximately 140 nm (c) and (d) Polished quartz crystal, surface features approximately 20 nm

Chapter Four – Determination of the Viscosity of Supercritical Solutions

When each of the γ terms that contribute to Equation 4.8 are accounted for and compared, (Figure 4.12) it is clear that pressure effects have a large influence on Δf_{app} . This has also been observed by other authors.¹¹⁻¹³ Equation 4.4 can be rearranged

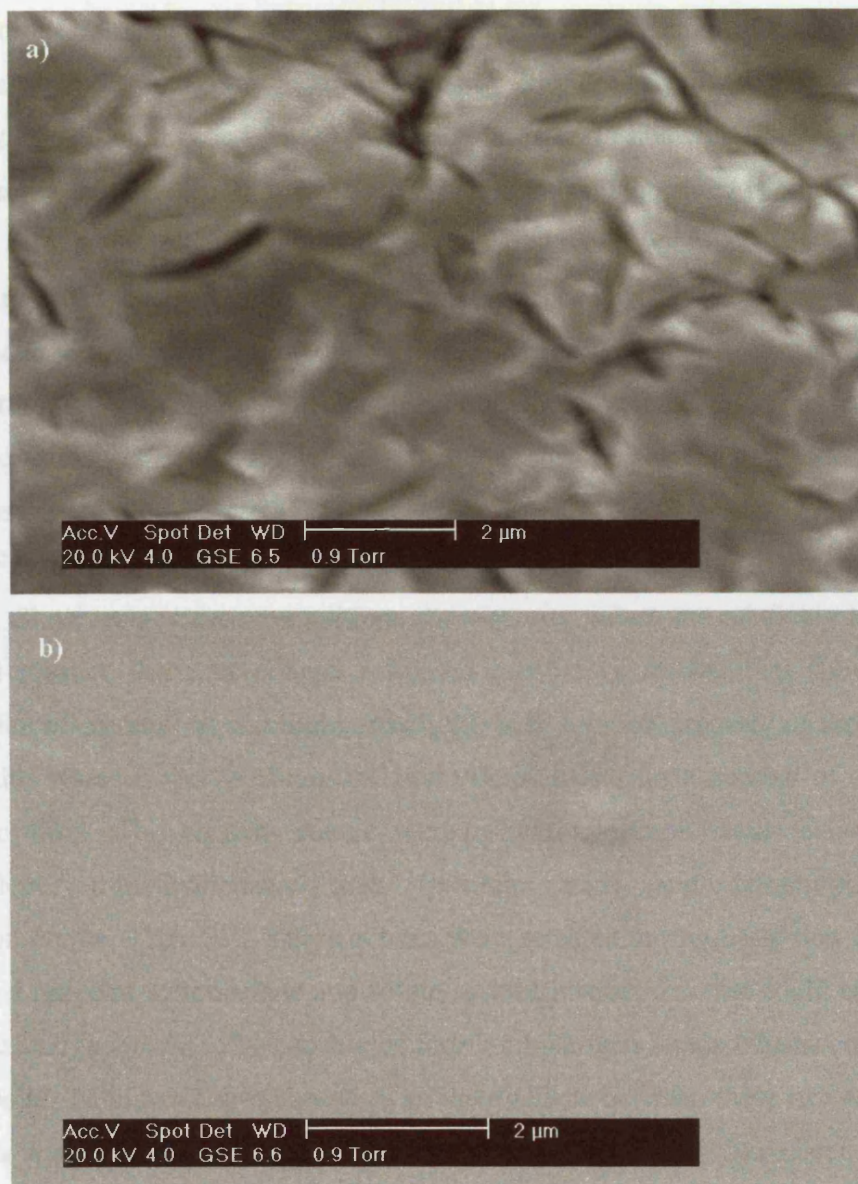


Figure 4.11 SEM images of
(a) Unpolished quartz crystal
(b) Polished quartz crystal

When each of the effects that contribute to Equation 4.8 are accounted for and compared, (Figure 4.12) it is clear that pressure effects have a large influence on Δf_{exp} . This has also been observed by other authors.³⁸⁻⁴³ Equation 4.8 can be rearranged leading to the formation of a calibration plot for Δf_{η} as a function of solution viscosity and density. In a solution of unknown viscosity, providing the density of the system is known, this calibration can be used to obtain viscosity. In this work the total density of the system is calculated from the solvent density, which is obtained from the literature,³ and the amount of solute added to the system of known volume. This calculation is thought to be reasonable due to the experimental procedure undertaken. The solute was first loaded into the high pressure vessel, which was then heated to the required temperature. After an appropriate amount of time to allow the cell to reach equilibrium, and the crystal to achieve a stable resonant frequency, the solvent was added to the cell and pressurised to the desired value.

Figure 4.13 shows how the viscosity of CH_2F_2 varies with increasing pressure. As with all solvents under sc conditions the viscosity values are relatively low (Figure 4.1). At present, there have been a limited number of studies that show how the dissolution of material in a sc fluid affects the bulk solution property of viscosity. The aim of this research was to obtain the first viscosity data for a number of solutes in a polar sc fluid. The chosen solutes were *o*-hydroxybenzoic acid (salicylic acid), naphthalene, *p*-methylbenzoic acid (*p*-toluic acid) and tetrabutylammonium tetrafluoroborate, TBA BF_4 . These solutes were selected on the basis that they would produce a range of solute-solute and solute-solvent interactions that could be explored. Salicylic acid is known to be capable of forming hydrogen bonds whereas naphthalene is non-polar. Toluic acid was chosen as an intermediate between these two compounds. TBA BF_4 is an electrolyte whose conductive properties in CH_2F_2 have been previously investigated and is known to form both ion pairs and triple ions as a function of pressure.⁴⁹ Consequently it would be interesting to discover what effects these might have on solution viscosity.

4.1.7 Non-electrolyte Solutions

Three non-electrolyte solutions were prepared in $\text{sc CH}_2\text{F}_2$, these were acetic acid, nitric acid and H_2SO_4 . The solubility of each solute in $\text{sc CH}_2\text{F}_2$ has been previously determined, it was not possible to determine the sc solute solutions were made up in the sc solvent. It is confirmed the homogeneity, a further step was to determine the solubility of each solute in $\text{sc CH}_2\text{F}_2$ at different pressures, this was done by measuring the change in the refractive index of the solution. The refractive index was measured into the sc cell, and the pressure of CH_2F_2 was varied from 15 to 50 bar. The refractive index of the solution was measured at each pressure and the refractive index of the pure solvent was measured at the same pressure. The refractive index of the solution was measured at each pressure and the refractive index of the pure solvent was measured at the same pressure. The refractive index of the solution was measured at each pressure and the refractive index of the pure solvent was measured at the same pressure.

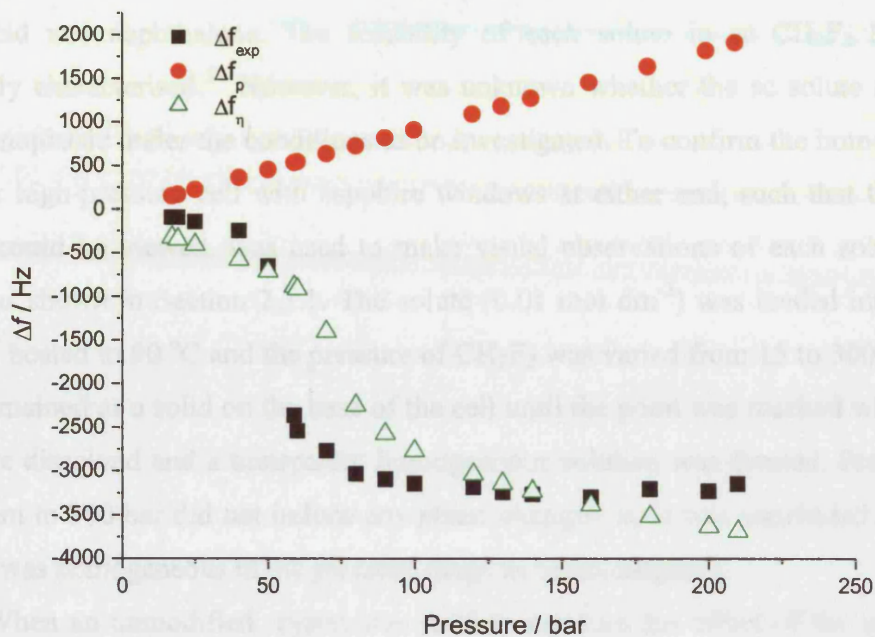


Figure 4.12 Shift in resonance frequency contributing to Δf_{exp} From Equation 4.5 for PQC as a function of pressure at 90 °C using literature viscosity and density data

Various researchers have taken advantage of this to investigate adsorption processes and rates. It was, therefore, proposed that the adsorption of nitrate ions to the surface of the gold electrode. The adsorption of nitrate ions to the surface of the gold electrode is not reversible and the adsorption rate changes with time. Although this is a common phenomenon, it is not always observed in the frequency shift. Although this is a common phenomenon, it is not always observed in the frequency shift. Although this is a common phenomenon, it is not always observed in the frequency shift. Although this is a common phenomenon, it is not always observed in the frequency shift.

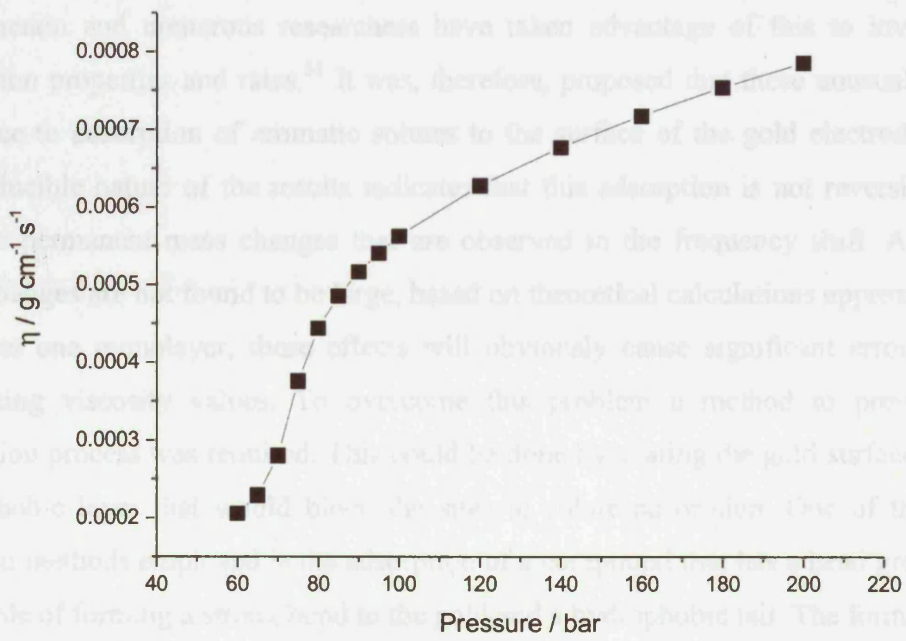


Figure 4.13 Viscosity of CH_2F_2 at 90 °C as a function of pressure³

4.2.2 Non-electrolyte Solutions

Three non-electrolytes were examined in sc CH_2F_2 , these were salicylic acid, toluic acid and naphthalene. The solubility of each solute in sc CH_2F_2 has been previously characterised.⁵⁰ However, it was unknown whether the sc solute solutions were monophasic under the conditions to be investigated. To confirm the homogeneity, a tubular high-pressure cell with sapphire windows at either end, such that the entire volume could be viewed, was used to make visual observations of each solute in sc CH_2F_2 , as shown in Section 2.3.1. The solute (0.01 mol dm^{-3}) was loaded into the 10 cm^3 cell, heated to $90 \text{ }^\circ\text{C}$ and the pressure of CH_2F_2 was varied from 15 to 300 bar. The solute remained as a solid on the base of the cell until the point was reached whereupon the solute dissolved and a transparent homogeneous solution was formed. Pressurising the system to 300 bar did not induce any phase changes, so it was concluded that each solution was homogeneous in the pressure range to be investigated.

When an unmodified crystal was used to measure the effect of the solutes on solution viscosity the results were unexpected. There were no discernible patterns for either the frequency shift as a function of pressure or the change in the type of solute employed. In addition, the results were irreproducible. The electrodes on the piezoelectric crystals used in this work were formed by splutter coating with gold particles. Adsorption to gold, especially of aromatic compounds, is a renowned phenomenon and numerous researchers have taken advantage of this to investigate adsorption properties and rates.⁵¹ It was, therefore, proposed that these unusual results were due to adsorption of aromatic solutes to the surface of the gold electrodes. The irreproducible nature of the results indicates that this adsorption is not reversible and leads to permanent mass changes that are observed in the frequency shift. Although these changes are not found to be large, based on theoretical calculations approximately less than one monolayer, these effects will obviously cause significant errors when calculating viscosity values. To overcome this problem a method to prevent the adsorption process was required. This could be done by coating the gold surface with a hydrophobic layer that would block the sites to solute adsorption. One of the most common methods employed is the adsorption of a compound that has a head group that is capable of forming a strong bond to the gold and a hydrophobic tail. The formation of gold-sulphur bonds is known to be facile and they are stable over a wide range temperatures and pressures. Chemisorption of butanethiol to the gold electrode surface would prevent the adsorption of solutes and eliminate the corresponding artefacts. The

experimental procedure for crystal thiolation and calculations for the estimation of gold coverage is described in Section 2.4.1.

After thiolating the crystal the calibration procedure was repeated to confirm that the technique was feasible. It was found that crystal thiolation did not alter the outcome of the calibration process and would, therefore, be suitable to use in this investigation. It must be noted that in order to prevent inaccuracies resulting from contamination a different crystal was used for each solute. The resonant frequency was measured prior to and after thiolating each crystal and to avoid errors owing to the use of a number of crystals the calibration procedure was performed for each crystal prior to solute experiments.

The change in crystal admittance was related to the solution viscosity by using literature viscosity and density data for CH₂F₂ at constant temperature as a function of pressure.³ Figure 4.14 shows a calibration plot obtained giving a line of best fit of

$$\Delta f = -1.09 \times 10^5 (\pm 2.16 \times 10^3) (\eta \rho)^{1/2} + -1860 (\pm 50) \quad (4.10)$$

where Δf is the change in admittance from the quartz crystal in contact with the sc solution compared to the value obtained in contact with air, ρ is the solution density and η is the solution viscosity. Good correlations were obtained for all data with each crystal ($R > 0.98$).

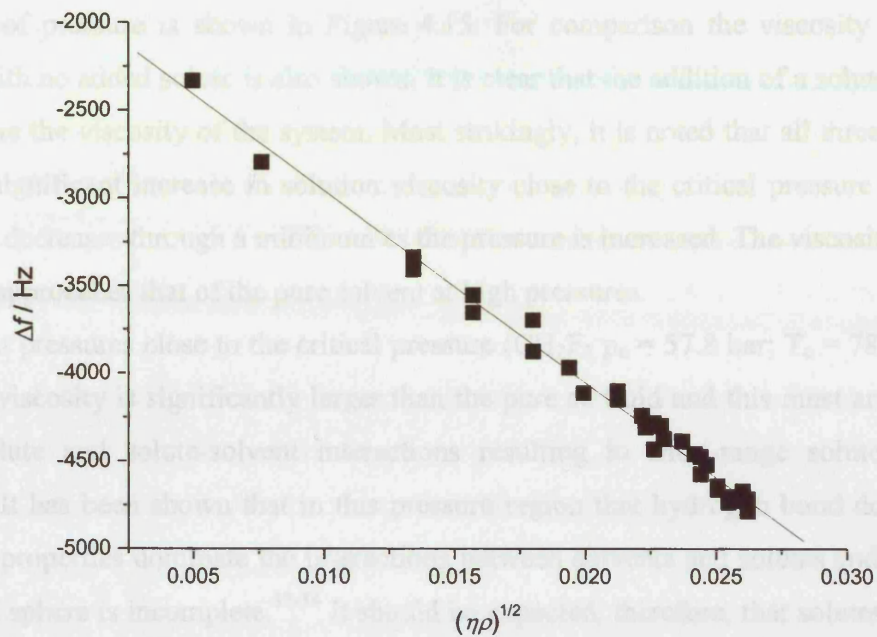


Figure 4.14 Calibration plot for PQC at 90 °C used with solute *p*-toluic acid

$$\Delta f = -1.09 \times 10^5 (\pm 2.16 \times 10^3) (\eta\rho)^{1/2} + -1860 (\pm 50)$$

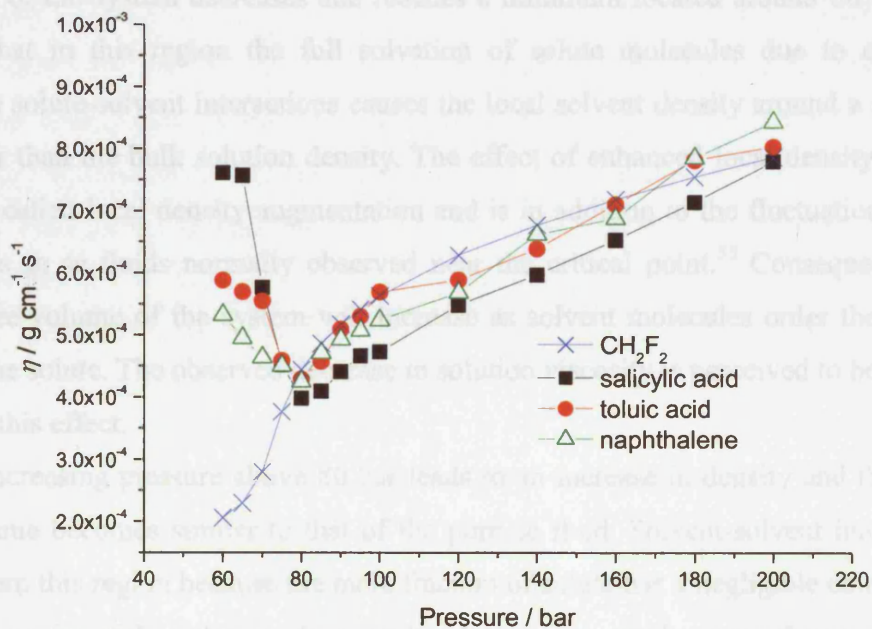


Figure 4.15 Comparison between CH_2F_2 viscosity and CH_2F_2 solution viscosity with 0.01 mol dm^{-3} solute at $90 \text{ }^\circ\text{C}$ as a function of pressure. A large increase in solution viscosity at low pressures is observed and is different for each solute

The data for CH₂F₂ solutions containing 0.01 mol dm⁻³ of each solute as a function of pressure is shown in Figure 4.15. For comparison the viscosity of pure CH₂F₂ with no added solute is also shown. It is clear that the addition of a solute to a sc fluid alters the viscosity of the system. Most strikingly, it is noted that all three solutes cause a significant increase in solution viscosity close to the critical pressure and the viscosity decreases through a minimum as the pressure is increased. The viscosity of the solution approaches that of the pure solvent at high pressures.

At pressures close to the critical pressure (CH₂F₂ p_c = 57.8 bar; T_c = 78 °C) the solution viscosity is significantly larger than the pure sc fluid and this must arise from solute-solute and solute-solvent interactions resulting in short-range solute-solvent clusters. It has been shown that in this pressure region that hydrogen bond donor and acceptor properties dominate the interactions between solvents and solutes and that the solvation sphere is incomplete.⁵²⁻⁵⁴ It should be expected, therefore, that solutes such as salicylic acid should impart significant structure to the solution.

When the pressure is increased the number of solvent molecules in the system also increases. These solvent molecules will solvate the solute-solute clusters, completing the solvation sheath around solute molecules and breaking up the interactions between solute molecules. Figure 4.15 shows that it is in this region that the viscosity of the system decreases and reaches a minimum located around 80 bar. It is known that in this region the full solvation of solute molecules due to enhanced attractive solute-solvent interactions causes the local solvent density around a solute to be higher than the bulk solution density. The effect of enhanced local density about a solute is called local density augmentation and is in addition to the fluctuations of the properties in sc fluids normally observed near the critical point.⁵⁵ Consequently, the molar free volume of the system will increase as solvent molecules order themselves around the solute. The observed decrease in solution viscosity is perceived to be a direct result of this effect.

Increasing pressure above 80 bar leads to an increase in density and the molar free volume becomes similar to that of the pure sc fluid. Solvent-solvent interactions will govern this region because the mole fraction of solute has a negligible contribution on the viscosity of the solution. As a result solution viscosity becomes the same as that of the pure sc solvent i.e. solvent-solvent interactions dominate over solvent-solute.

Figure 4.16 shows the values of relative viscosity, η_r , for the same systems (where $\eta_r = \eta/\eta_0$). These values are higher than those in studies of polymers or fatty

acids in sc CO₂.¹⁶⁻¹⁹ This is not surprising as both solute-solute and solute-solvent interactions will be limited between these non-polar solutes and non-polar fluids, therefore not causing significant structuring of the fluid. As expected, the relative viscosities in Figure 4.16 decrease to a value of one as pressure and density are increased and the viscosity becomes similar to that of the pure fluid. This indicates that, at high pressures and densities, solute molecules do not impart any structure to the fluid. In contrast, in the low pressure region the solute molecules have a role in ordering the fluid and causing the system to have structure.

The effect of a dissolved solute on viscosity has commonly been analysed using the Dole-Jones equation⁵⁶

$$\eta_r = 1 + Ac^{1/2} + Bc \quad (4.11)$$

where η_r is the relative viscosity ($\eta_r = \eta/\eta_0$), c is concentration and A and B are constants. The A coefficient arises from ion-ion interactions and, for non-electrolytes, will have a value of zero.⁵⁷ The B coefficient is related to the size and shape of solute molecules and describes the effect of the solute on the solvent structure. Negative B values result from breaking up the solvent structure whereas positive values imply the solution is more ordered than the pure solvent. For non-electrolyte systems Equation 4.11 can be simplified to

$$\eta_r = 1 + Bc \quad (4.12)$$

There have been relatively few studies to analyse the effect of non-electrolytes using the Dole-Jones relationship and none have employed solvents under sc conditions. The studies that have been conducted have examined the effect of solutes in aqueous, polar and non-polar solvents.⁵⁸⁻⁶⁴ The majority of high pressure viscosity investigations have focussed on modelling the phase behaviour and viscosity.^{7,8} In addition, activation volumes for high pressure polymer solutions have commonly been estimated from viscosity data.^{12,17}

Chapter Four – Determination of the Viscosity of Supercritical Solutions

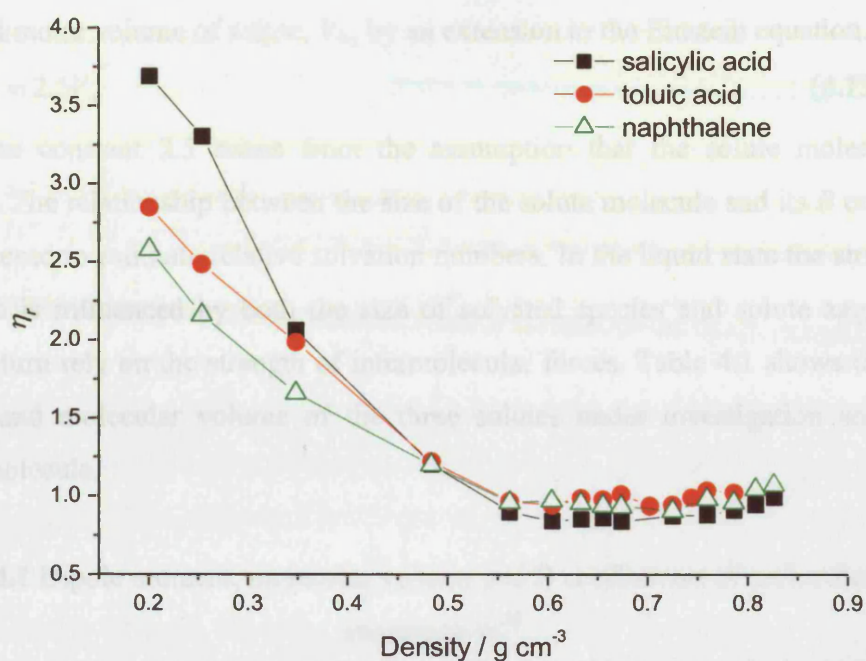


Figure 4.16 Relative viscosity ($\eta_r = \eta/\eta_0$) of 0.01 mol dm^{-3} CH_2F_2 solute solutions at 90°C as a function of density ($\rho_c = 0.424 \text{ g cm}^{-3}$)

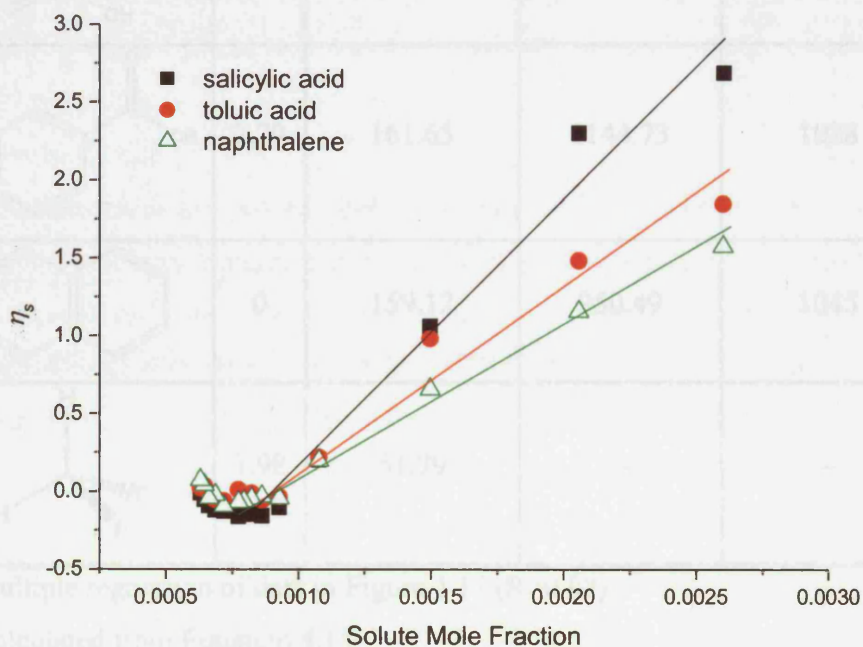


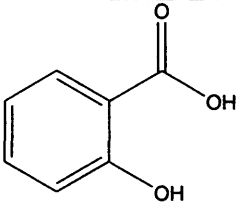
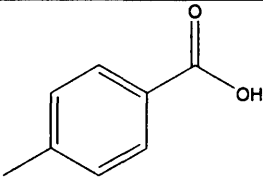
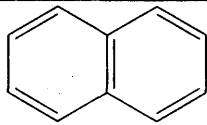
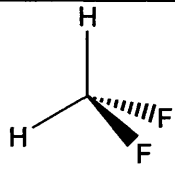
Figure 4.17 Specific viscosity ($\eta_s = \eta_r - 1$) of CH_2F_2 solute solutions at 90°C as a function of solute mole fraction. At high mole fractions corresponding to low pressure region solute-solute interactions dominate

For non-electrolyte molecules the B coefficient has commonly been related to the partial molar volume of solute, V_m , by an extension to the Einstein equation.⁵⁸⁻⁶⁴

$$B = 2.5V_m \quad (4.13)$$

The constant 2.5 arises from the assumption that the solute molecules are spherical. The relationship between the size of the solute molecule and its B coefficient has been used to estimate relative solvation numbers. In the liquid state the structure of a solution is influenced by both the size of solvated species and solute aggregation, which in turn rely on the strength of intermolecular forces. Table 4.1 shows the dipole moment and molecular volume of the three solutes under investigation and CH_2F_2 solvent molecule.

Table 4.1 Dipole moment, molecular volume and B coefficients of molecules under investigation⁶⁵

Molecule	μ / D	$V_m / \text{\AA}^3$	B coefficient ^a	B' coefficient ^b
	2.21	149.37 (dimer 291.84)	1749.61	1115
	2.79	161.65	1144.73	1028
	0	159.12	950.49	1045
	1.98	51.79	–	–

^a Multiple regression of data in Figure 4.17 ($R > 0.98$)

^b Calculated from Equation 4.15

The assumptions used in Equations 4.12 and 4.13 are slightly different in sc fluids as the concentration of the solute remains constant and it is the concentration of solvent that changes hence an analogous form of Equation 4.12 can be written

$$\eta_r = 1 + B'x \quad (4.14)$$

Figure 4.17 shows how the specific viscosity, η_s , (where $\eta_s = (\eta - \eta_0)/\eta_0 = \eta_r - 1$) varies with mole fraction of solute, x . It can be seen that there are clearly two pressure regimes: At high mole fractions, corresponding to the low pressure region, positive slopes are observed which fit well to Equation 4.14 indicating that the fluid is more ordered than the pure solvent. Below 0.001 mole fraction the slopes are approximately zero which suggests that the solute no longer has any significant influence on the overall structure of the fluid and the viscosity is similar to that of the pure solvent. Hence, it can be concluded that there are two types of pressure regime above and below a critical mole fraction whereby at high solute mole fractions the solute-solute interactions dominate and at low mole fractions solvent-solvent interactions dominate. It would appear from Figure 4.17 that the critical mole fraction is solute independent and must be controlled by solvent-solvent interactions.

The B' coefficient in Equation 4.14 is not the partial molar volume but rather it must be related to the fraction of the volume occupied by the solute in the vessel. Assuming that larger solutes will have a larger effect upon solution viscosity it is logical to suggest that

$$B' = 1/(V_m N_A c) \quad (4.15)$$

where V_m is the molecular volume and N_A is the Avogadro constant. Table 4.1 shows that for the three solutes studied in this work very good agreement is obtained between the values calculated using Equation 4.15 and those obtained experimentally from Figure 4.17. The slight discrepancy observed for salicylic acid is probably due to the dimerisation of the solute through hydrogen bonding and the change in solvation of the dimer.

Assuming each molecule is spherical in shape and the packing of CH_2F_2 molecules around the solute follows a cubic close packing arrangement, the number of solvent molecules required to solvate an individual solute molecule is estimated to be between 18 and 19 molecules. Depending on the solute, the individual solvated molecule will have an estimated radius of approximately 8 Å. However, these calculations do not take solute aggregation into account. Salicylic acid is known to

dimerise through hydrogen bonding, which would significantly increase the number of solvent molecules in the surrounding sheath (approximately 24) and the overall size of the solvated species. At present, it is unknown whether toluic acid will form similar dimers or higher aggregates, further increasing the solvation number. In addition to hydrogen bonding it is possible that the solute molecules could aggregate via π -stacking interactions because of the presence of an aromatic ring. This is the only type of solute-solute interaction that may be present between naphthalene molecules as it does not possess a dipole moment (Table 4.1). These solute-solute interactions will impart long-range order and structuring onto the surrounding solvent molecules. This is evident from the positive slopes at high mole fractions of solute (Figure 4.16 and 4.17).

In addition to solute-solute interactions it is possible that the solvent-solute interactions influence the viscosity response found. Solvent molecules may fill more than the primary solvation sheath around salicylic acid even at low pressures and non-polar naphthalene may not require a full sheath to dissolve.

Similar trends are found when the solute concentration is reduced to $0.001 \text{ mol dm}^{-3}$ as shown in Tables 5-7 of the Appendix. This indicates that even at relatively low concentrations the solute plays an important role in imparting structure to the solution.

The fact that sc solutions are relatively viscous close to the critical pressure can be used to explain many observations. In the low-pressure region, between 60 and 80 bar, this research shows that appreciable changes in solution viscosity occur with small variations in pressure. The viscosity is first observed to be at a maximum and rapidly decreases to a minimum as the pressure is increased. This suggests that the velocity of solutes will also vary, therefore it is expected that solution properties such as reaction kinetics would be significantly altered around this region. Several authors have examined reactions in sc fluids and found enhanced reaction rates at pressures just above the critical point. Most of these investigations have involved the use of non-polar sc fluids such as CO_2 , although a number of authors have investigated more polar fluids. The only reaction carried out in CH_2F_2 for which kinetic data are available is the Friedel-Crafts alkylation reaction of anisole with *t*-butylchloride in sc CH_2F_2 and sc CO_2 .⁶⁶ Abbott and Durling found that reaction rates were greater in sc CH_2F_2 due to the increased solvent polarity. Rate constants were observed to reach a maximum at c a. 80 bar, which corresponds to the minimum solution viscosity in Figure 4.15. They concluded that the dielectric constant of the solution was the controlling influence on the reaction. Figure 4.18 shows a plot of solution viscosity data taken from Figure 4.15

Chapter Four – Determination of the Viscosity of Supercritical Solutions

against the reaction rate constant for the reaction of anisole ($\mu = 1.25$ D) with *t*-butylchloride ($\mu = 2.15$ D) in sc CH_2F_2 .⁶⁶ Very good correlation is obtained showing that the solution viscosity is affecting the reaction rate. While the solutes used in the Friedel-Crafts reaction are clearly different from salicylic acid ($\mu = 2.21$ D) the dipole moments are similar and hence the dipole-dipole interactions would be comparable.

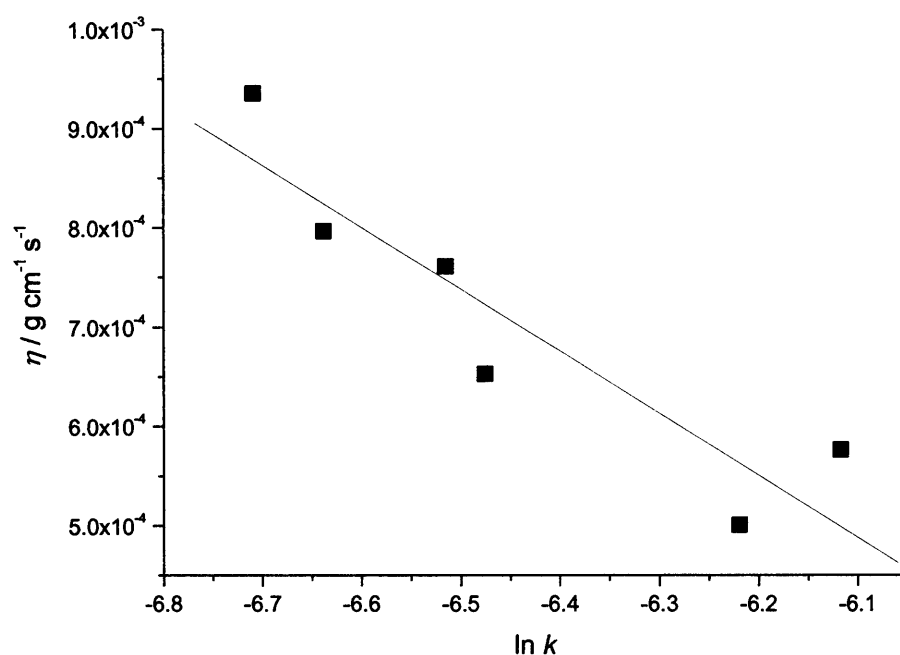


Figure 4.18 Plot of viscosity data from Figure 4.15 versus the reaction rate constant for the reaction of anisole with *t*-butylchloride in sc CH₂F₂.⁶⁶ Linear correlation indicates solution viscosity is affecting the reaction rate

Many other groups have observed a maximum in reaction rate constant close to the critical pressure. Rhodes *et al.* compared the reaction kinetics of a Michael addition in non-polar sc ethane to the more polar sc fluoroform.⁶⁷ Near the critical point the reaction rate in sc ethane was observed to increase as a result of solute-solute clustering. It was thought that this increase could not be due to solvent-solute clustering as solvent density had little effect on the kinetics of the reaction. In sc fluoroform solvent-solute clustering was proposed to be the reason for the changes in rate constant near the critical point. However, below the critical density solute-solute clustering was thought to dominate.

Ellington *et al.* have conducted a number of investigations into the effect of local density reaction rates.^{68,69} Apparent bimolecular rate constants were calculated and found to exhibit a remarkable 25-fold increase with a decrease in pressure. It was argued that the local concentration of reactants exceeded the average bulk and this could account for the enhanced rate constants at low pressures. Measurements of local composition and density showed this to be true.

More recently, Hou and co-workers calculated the apparent equilibrium constant for an esterification reaction in sc CO₂.⁷⁰ The results showed that, at low pressures, the equilibrium constant increased with pressure reaching a maximum in the critical region. This observed increase at low pressures was explained with respect to the degree of clustering at these pressures. At high pressures, where clustering is insignificant the equilibrium constant was found to be close to that of the reaction in the absence of CO₂.

The Diels-Alder reaction has also been the focus of a number of investigators.⁷¹⁻⁷³ The clustering of solvent molecules with reactants and the activated complex was proposed to be the reason for the enhanced reaction rates around the critical region.

Pronounced solvent effects have also been observed for hydrogen bonding interactions in sc SF₆. The equilibrium for methanol-triethylamine association increased as the pressure decreased towards the critical point. The complex was stabilized at lower densities where the degree of hydrogen bonding is enhanced due to solute-solute clustering.⁷⁴

To further evaluate these findings the following section examines the effect of an electrolyte in sc CH₂F₂. The composition and size of the ionic species formed in solution are known hence the relationship with solution viscosity can be evaluated.

4.2.3 Electrolyte Solutions

The electrolyte investigated was tetrabutylammonium tetrafluoroborate, TBABF₄. It was chosen because a number of electrochemical studies employing this electrolyte have been performed in sc CH₂F₂.⁷⁵⁻⁷⁷ Furthermore the conductivity of sc CH₂F₂ using TBABF₄ has been determined.⁴⁹

To ensure that the electrolyte was soluble and that the resultant solution was homogeneous the system was again viewed in the high-pressure cell with sapphire windows. TBABF₄ (0.03 mol dm⁻³) was placed in a 10 cm³ cell and the pressure of CH₂F₂ was varied from 15 to 300 bar. When CH₂F₂ (15 bar) was first introduced to the cell at 90 °C, the electrolyte immediately liquefied to form a dense liquid at the base of the cell despite the CH₂F₂ being in the gaseous state. The cell temperature was 70 °C below the melting point of the electrolyte (159-162 °C) and the volume of the observed liquid phase was not too dissimilar to that of the solid (Figure 4.19b). In general, the melting point of a solid increases with increasing pressure. However, in the presence of a sc fluid the melting point of the solid is found to decrease with increasing pressure.⁷⁸ The reason for this observation is that, as pressure increases, more and more of the gas dissolves in the dense liquid phase and subsequently the temperature required to melt the solid is reduced. Such effects have also been observed by other groups with CO₂ and ethane; however, the effect is not fully understood.⁷⁹⁻⁸⁴ Wightman *et al.* performed electrochemical studies in sc CO₂ using water as a co-solvent.⁸⁵ They found that in the presence of water, the electrolyte tetrahexylammonium hexafluorophosphate ((THA)PF₆) formed a molten salt layer. Analysis of this layer by near infra-red spectroscopy found that it contained CO₂ dissolved in the liquid electrolyte. In a subsequent study they presented cryoscopic data for the similar electrolyte tetrahexylammonium nitrate ((THA)NO₃).⁸⁶ The cryoscopic constant for the liquid electrolyte was found to be large and could explain similar observations of other authors.⁸⁷ The freezing point depressions of (THA)NO₃ under CO₂, N₂O and argon were investigated as a function of gas pressure and excellent linear correlations were obtained. In the case of TBABF₄ with CH₂F₂, it is assumed that the electrolyte forms a clathrate with the gas molecules coordinating strongly to the ions, decreasing the lattice energy and causing the complex to melt. This observation is not unique, as the same electrolyte also forms a complex of this type with non-polar liquids such as toluene.⁸⁷ The observation that this occurs with a gaseous fluid demonstrates the high affinity of the electrolyte for CH₂F₂. This dense liquid phase remains until the pressure is raised

above 95 bar in the sc region whereupon it becomes completely miscible and the whole solution becomes transparent (Figure 4.19c). Pressurising the cell to 300 bar did not induce any further phase changes and hence all further studies were confined to pressures above 100 bar where the fluid is known to be homogeneous.

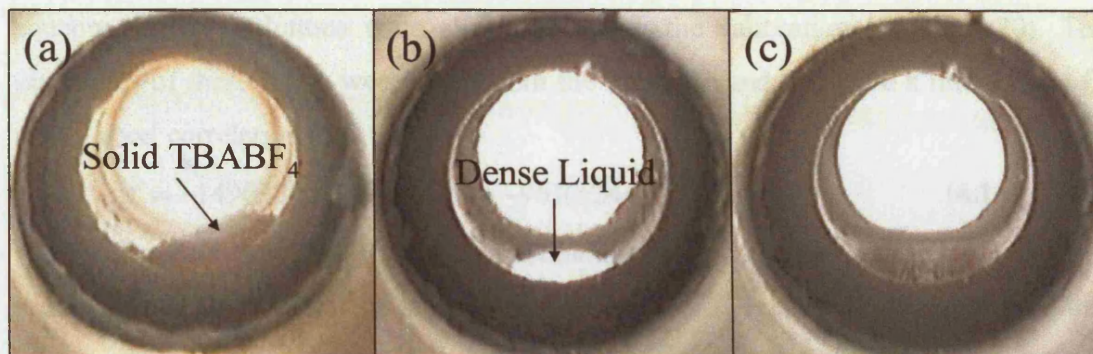


Figure 4.19 Phase behaviour of TBABF₄ and CH₂F₂ at 90 °C

(a) Solid TBABF₄

(b) TBABF₄ and 15 bar CH₂F₂ form dense liquid phase

(c) TBABF₄ and 95 bar CH₂F₂ a single homogeneous solution observed

To investigate the effect that the electrolyte has on solution viscosity it was found that the PQC needed to be modified in a different manner to the non-electrolyte solutes. When an unmodified crystal was analysed in the sc electrolyte solution the admittance was found to increase with pressure. This is the reverse of what is normally observed. Solutions of TBABF₄ in CH₂F₂ are known to be conductive so it was thought that interferences arising from solution conductivity were being observed.⁴⁹ This is a reasonable assumption because interferences of this kind were not observed with the non-electrolyte solutes. In addition the frequency response for solutions of a non-ionic surfactant was investigated and the normal response was observed. To circumvent this interference it was thought that if one side of the quartz crystal was not exposed to the electrolytic solution the conductivity would not be measured. Thus a method of blocking one side of the crystal was necessary. Several ideas were proposed including placing a glass covering over one electrode and coating one electrode with a non-conducting film. It was decided to coat the electrode surface on one side of a crystal with a thin layer of a non-conducting polymer. This was confirmed by visual inspection of the crystal and measuring the shift in resonant frequency. It was vital that a thin layer

of polymer was applied to the crystal, as an overload in mass would prevent the crystal oscillating.

As with the previous studies, the modified crystal was calibrated using pure CH₂F₂ at different pressures. However, the data obtained for TBABF₄ solution were found to be much higher in value than pure CH₂F₂ so measurements for water and aqueous sucrose solutions were also included in the calibration (Figure 4.20). The viscosities of these fluids were taken from the literature and this gave a line of best fit with a good correlation ($r > 0.98$).

$$\Delta f = -149630(\pm 4119)(\eta\rho)^{1/2} + -961(\pm 244) \quad (4.16)$$

The data for CH₂F₂ solutions containing various concentrations of TBABF₄ were obtained as a function of pressure and are shown in Figure 4.21. It can be seen that incorporation of the quaternary ammonium electrolyte results in a significant increase in solution viscosity even at relatively low concentrations. Given that in pure CH₂F₂ the viscosity ranges from 5.63×10^{-4} to 9.19×10^{-4} g cm⁻¹ s⁻¹ over the pressure range 100 to 260 bar, the data in Figure 4.21 represent relative viscosities in the range from 8 to 32 depending on the pressure and concentration (Figure 4.22). This shows that the addition of 0.03 mol dm⁻³ of electrolyte increases the viscosity such that it is more akin to a liquid solution. The increase in relative viscosity is considerably greater than those found for the previous studies for fatty acids or polymers in scCO₂.¹⁶⁻¹⁹ This is not surprising given that CO₂ has no dipole moment and the solutes investigated in these systems are relatively non-polar. Consequently, solvent-solute and solute-solute interactions will be weak and would not cause significant changes in the solution structure. With TBABF₄ dissolved in CH₂F₂ considerable solvent structuring will be required to solvate the ionic species, which will be considerably larger than the non-electrolyte solutes studied in the previous section. Ion-ion interactions will also cause the solute to aggregate; hence, it is not surprising that this ionic solute causes a larger increase in solution viscosity. High relative viscosities of this magnitude are not unprecedented and have been observed with polymers in sc fluids.¹⁸ Precedent has also been set using quaternary ammonium electrolytes in non-polar liquid solvents where relative viscosities up to 3.5 were reported over the same concentration range as that studied here.⁸⁸

Chapter Four – Determination of the Viscosity of Supercritical Solutions

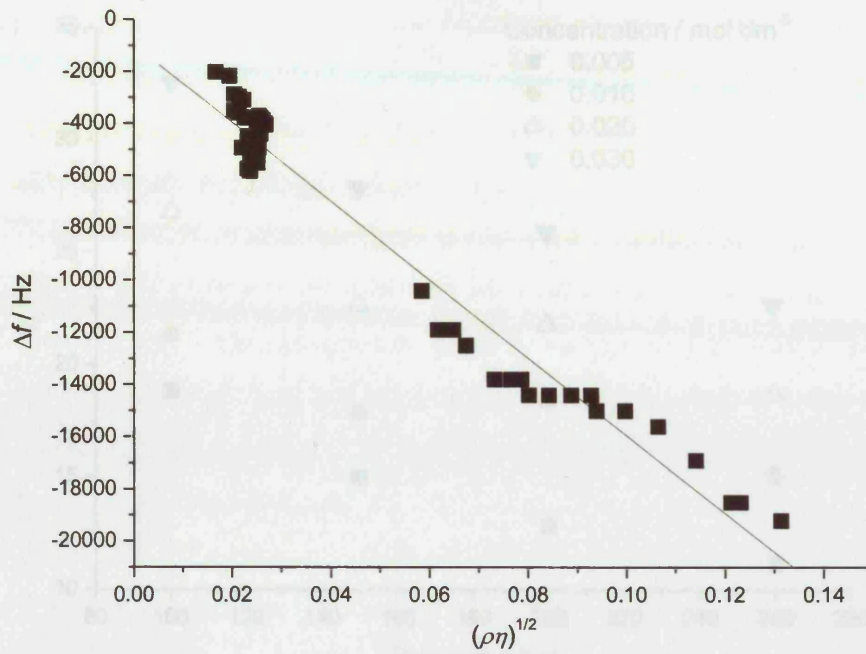


Figure 4.20 Calibration plot for electrolyte solutions using CH_2F_2 at 90°C and water and aqueous sucrose solutions at 25°C $\Delta f = -149630(\pm 4119)(\eta\rho)^{1/2} + -961(\pm 244)$

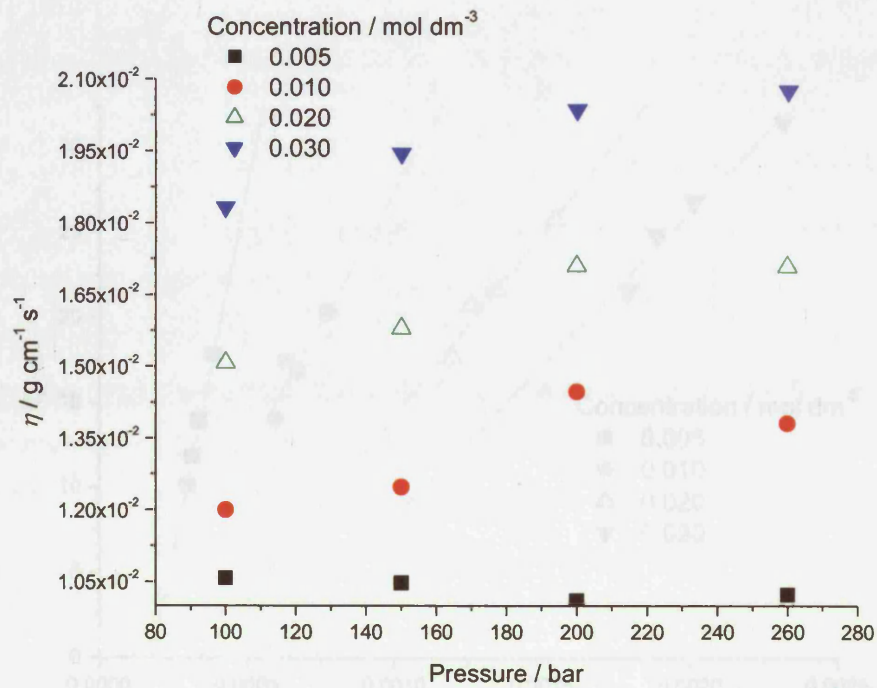


Figure 4.21 Viscosity for CH_2F_2 solutions at 90°C as a function of pressure and TBABF_4 concentration

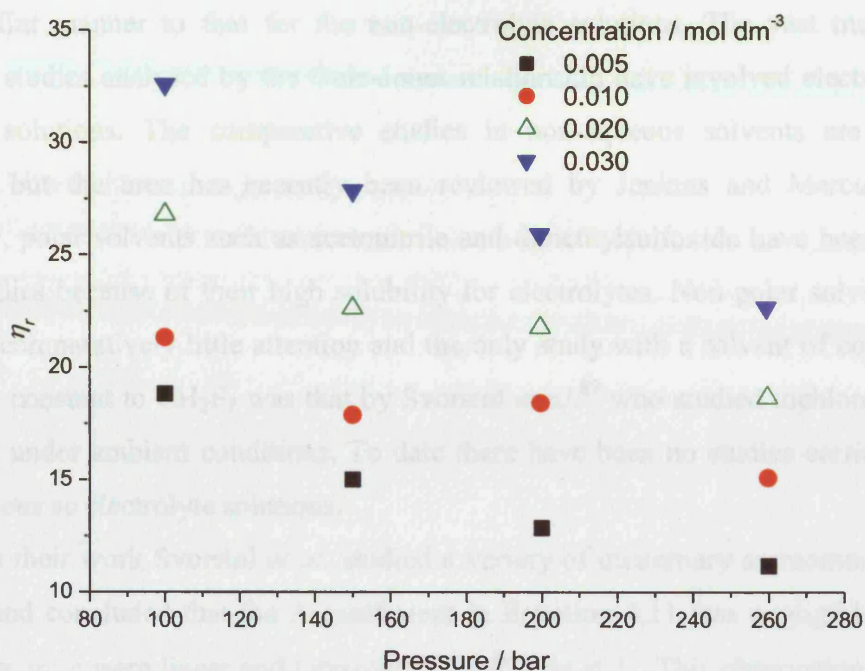


Figure 4.22 Relative viscosity ($\eta_r = \eta/\eta_0$) for CH_2F_2 solution at 90°C as a function of pressure and TBABF_4 concentration

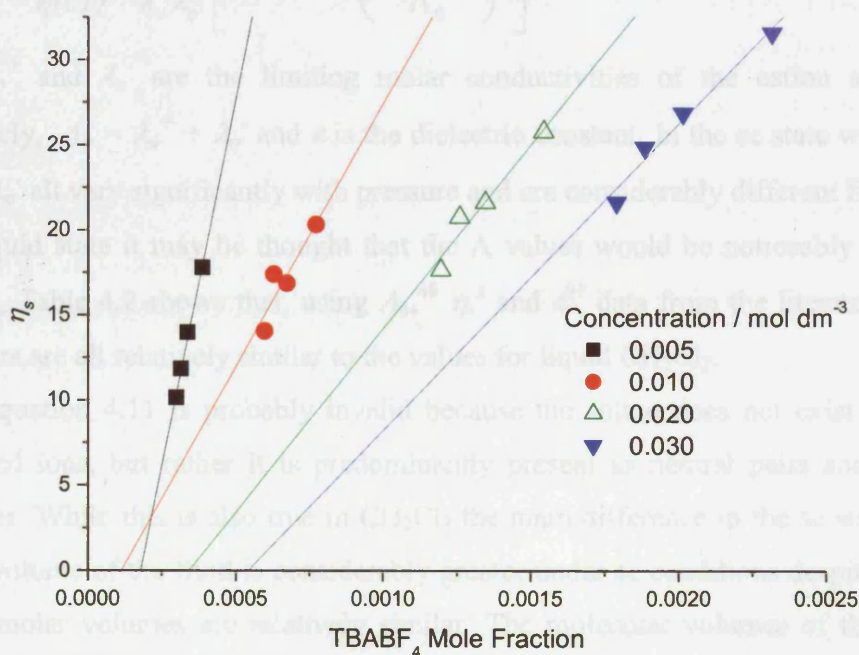


Figure 4.23 Specific viscosity ($\eta_s = \eta_r - 1$) for CH_2F_2 solution at 90°C as a function of pressure and TBABF_4 mole fraction. Comparable to Figure 4.17

These results can be evaluated by using the Dole-Jones equation (Equation 4.11) in a similar manner to that for the non-electrolyte solutions. The vast majority of viscosity studies analysed by the Dole-Jones relationship have involved electrolytes in aqueous solutions. The comparative studies in non-aqueous solvents are far less common but the area has recently been reviewed by Jenkins and Marcus *et al.*⁴ Primarily, polar solvents such as acetonitrile and dimethylsulfoxide have been used in these studies because of their high solubility for electrolytes. Non-polar solvents have received comparatively little attention and the only study with a solvent of comparable dielectric constant to CH₂F₂ was that by Svorstøl *et al.*⁸⁹ who studied dichloromethane (CH₂Cl₂) under ambient conditions. To date there have been no studies carried out on non-aqueous sc electrolyte solutions.

In their work Svorstøl *et al.* studied a variety of quaternary ammonium salts in CH₂Cl₂ and concluded that the A coefficient in Equation 4.11 was negligible because plots of η_r vs. c were linear and intercepted the Y axis at 1. This observation has been noted by other authors.⁹⁰

The A coefficient, which is a measure of long-range coulombic interactions between ions, can be predicted using the Falkenhagen-Vernon equation⁵⁷

$$A = \frac{0.2577 \Lambda_o}{\eta(\epsilon T)^{1/2} \lambda_o^+ \lambda_o^-} \left[1 - 0.6863 \left(\frac{\lambda_o^+ - \lambda_o^-}{\Lambda_o} \right)^2 \right] \quad (4.17)$$

where λ_o^+ and λ_o^- are the limiting molar conductivities of the cation and anion respectively, $\Lambda_o = \lambda_o^+ + \lambda_o^-$ and ϵ is the dielectric constant. In the sc state where ϵ , η , λ_o^+ and λ_o^- all vary significantly with pressure and are considerably different from those in the liquid state it may be thought that the A values would be noticeably different. However, Table 4.2 shows that, using Λ_o ,⁴⁹ η ,³ and ϵ ⁹¹ data from the literature, the A parameters are all relatively similar to the values for liquid CH₂Cl₂.

Equation 4.11 is probably invalid because the solute does not exist solely as dissociated ions, but rather it is predominantly present as neutral pairs and charged aggregates. While this is also true in CH₂Cl₂ the main difference in the sc state is that the free volume of the fluid is considerably greater under sc conditions despite the fact that the molar volumes are relatively similar. The molecular volumes of the species were calculated⁶⁵ to be $V_m(\text{CH}_2\text{Cl}_2) = 74.96 \text{ \AA}^3$ and $V_m(\text{CH}_2\text{F}_2) = 51.79 \text{ \AA}^3$. From these values the free volume of the fluids can be calculated using the molar volumes from the literature.^{3,92} Table 4.2 shows the percentage free volume for the systems studied here

and this is clearly related to the viscosity of the pure fluids. In CH₂F₂ the percentage free volume at 100 bar, 90 °C is twice that in CH₂Cl₂ at ambient conditions showing that the molecules have far more freedom to move around under sc conditions.

Table 4.2 Physical properties and molar conductivity of CH₂F₂ (90 °C) and CH₂Cl₂ (25 °C, 1 bar)^{3,49,91,92}

p / bar	$\eta / \text{g cm}^{-1} \text{s}^{-1}$	ϵ	V / cm ³ mol ⁻¹	$\Lambda_0 / \text{S cm}^2 \text{mol}^{-1}$	$\lambda_0^+ / \text{S cm}^2 \text{mol}^{-1}$	$\lambda_0^- / \text{S cm}^2 \text{mol}^{-1}$	A / cm ^{1/2} mol ^{-1/2}	V _{free} / %
100	5.63 x 10 ⁻⁴	7.39	77.3	0.770	0.202	0.568	0.501	59.7
150	6.98 x 10 ⁻⁴	8.29	67.4	0.622	0.163	0.459	0.473	53.7
200	7.87 x 10 ⁻⁴	8.99	63.0	0.551	0.145	0.406	0.454	50.5
260	9.19 x 10 ⁻⁴	9.59	59.8	0.499	0.131	0.368	0.416	47.9
CH ₂ Cl ₂	0.00401	8.93	64.5	0.108	0.028	0.080	0.505	30.0

Equation 4.11 may be simplified to Equation 4.12 by removal of the A coefficient. Figure 4.23 illustrates how specific viscosity ($\eta_s = \eta_r - 1$) varies with mole fraction of electrolyte and is comparable to the non-electrolyte data shown in Figure 4.17. B values obtained from this plot are shown in Table 4.3. As expected, they are greater than the values for the non-electrolytes (Table 4.1). At a concentration of 0.01 mol dm⁻³ the B coefficient for TBABF₄ is almost 18 times greater than that observed for salicylic acid.

According to Equation 4.15 the B coefficient can be related to the volume fraction of the solute. If the molecular volume of the species is considered ($V_m(\text{TBABF}_4) = 414.53 \text{ \AA}^3$) the calculated B value for the 0.01 mol dm⁻³ electrolyte system is very different to the value obtained from Figure 4.23 (Table 4.3). This indicates that this relationship is more complex for the electrolyte. This is probably because it may exist as both charged species and neutral pairs. These species will be different in size and hence B values would be different for the single ions, ion pairs and triple ions. To some extent this was seen with the non-electrolyte solutes where there was a slight discrepancy in the calculated and experimental values of the B coefficient for salicylic acid and toluic acid but not for the unassociated naphthalene.

Table 4.3 B coefficients for TBABF₄

c / mol dm ⁻³	B coefficient ^a
0.005	86266
0.01	30919
0.02	21585
0.03	17979

^amultiple regression of data in Figure 4.23 (R>0.91)

The dissolution of an electrolyte has been shown to cause a significant change in the structure of the sc fluid. It is thought that the charged species (both single and triple ions) will have the predominant effect on solution viscosity because electrostriction will produce a large increase in the local solvent density around the ions. This is already evident from the clathrate formation with the gas phase CH₂F₂ shown previously. The concentrations, *c*, of single ions *I_s* and triple ions, *I_t* can be obtained using the ion pair, *K_p* and triple ion *K_t* dissociation constants,

$$I_s = (K_p c)^{1/2} \quad (4.18)$$

$$I_t = (K_p c)^{1/2} c / K_t \quad (4.19)$$

The *K_p* and *K_t* data for this electrolyte system have been reported previously.⁴⁹ Hence the relative viscosity should be related to the ionic strength, (*I* = *I_s* + *I_t*). Figure 4.24 shows a plot of η_r vs. *I* for the data shown in Figure 4.21 and good correlation is observed for all pressures. It has previously been suggested that the association of the electrolyte can be accounted for by splitting the contribution of the electrolyte into ionic *B_i* and non-ionic components *B_p* by

$$\eta_r = 1 + A(\alpha c)^{1/2} + B_i \alpha c + B_p(1-\alpha)c \quad (4.20)$$

where α is the degree of dissociation and *c* is the concentration.⁹³⁻⁹⁵ Furthermore it has been noted that the effect of ion-pairing, *B_p*, is not significant and can be ignored.^{93,95}

This means that combining the ionic contributions Equation 4.20 becomes

$$\eta_r = 1 + A(I)^{1/2} + B_i I \quad (4.21)$$

which, since *A* is small, would account for the response shown in Figure 4.24.

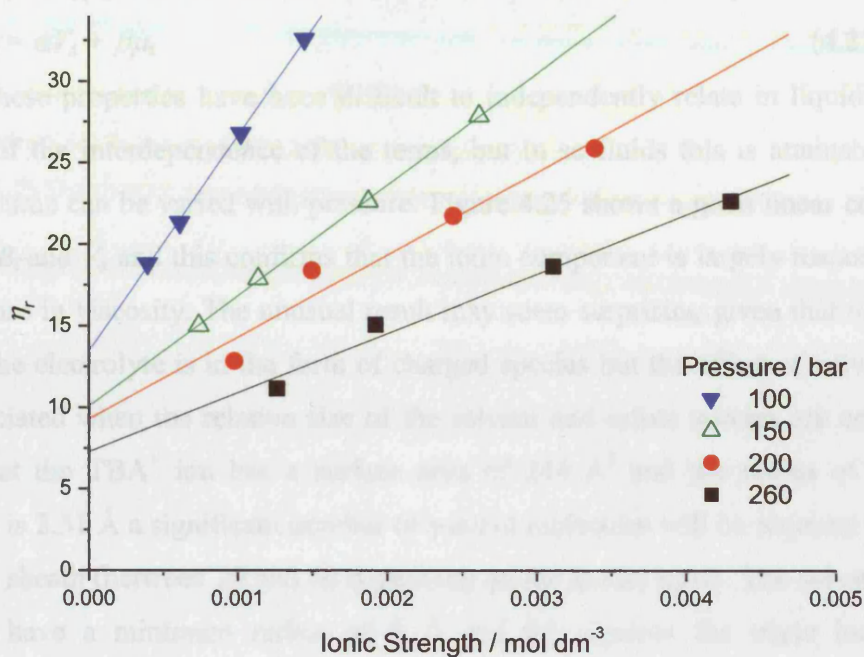


Figure 4.24 Relative viscosity and ionic strength (concentration of single and triple ions) as a function of pressure at 90 °C

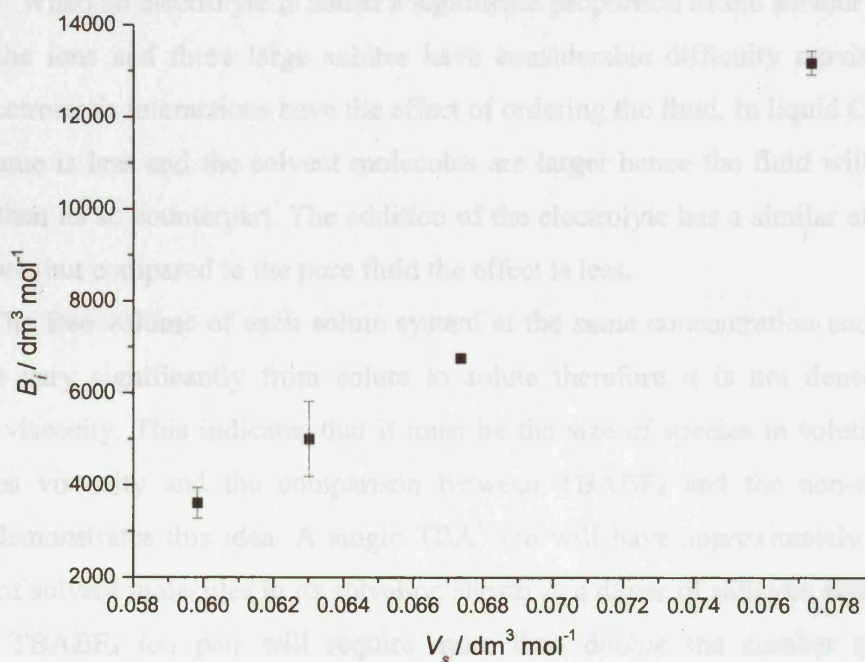


Figure 4.25 B_i parameter as a function of solvent molar volume, indicating ionic constituents are responsible for the increase in solution viscosity

It has been noted that a relationship exists between the B_i parameter and the dipole moment, μ_s and molar volume, V_s of the solvent, where α and β are constants^{4,89}

$$B_i = \alpha V_s + \beta \mu_s \quad (4.22)$$

These properties have been difficult to independently relate in liquid solvents because of the interdependence of the terms, but in sc fluids this is attainable as the molar volume can be varied with pressure. Figure 4.25 shows a good linear correlation between B_i and V_s and this confirms that the ionic component is largely responsible for the increase in viscosity. The unusual result may seem surprising given that only about 10% of the electrolyte is in the form of charged species but the effect of solvation can be appreciated when the relative size of the solvent and solute species are considered. Given that the TBA^+ ion has a surface area of 244 \AA^2 and the radius of a CH_2F_2 molecule is 2.31 \AA a significant number of solvent molecules will be required to fill the solvation sheath (between 20 and 60 depending on the model used). The solvated TBA^+ ion will have a minimum radius of 9 \AA and this ignores the triple ions whose contribution to the viscosity increase will be even larger.

Thus the qualitative comparison between sc CH_2F_2 and liquid CH_2Cl_2 explains the observed changes in relative viscosity. In the sc state there is a large free volume and a small solvent molecule, which is easily transported, hence the fluid has a low viscosity. When an electrolyte is added a significant proportion of the solvent is used to solvate the ions and these large solutes have considerable difficulty moving. Long-range electrostatic interactions have the effect of ordering the fluid. In liquid CH_2Cl_2 the free volume is less and the solvent molecules are larger hence the fluid will be more viscous than its sc counterpart. The addition of the electrolyte has a similar effect as in the sc state, but compared to the pure fluid the effect is less.

The free volume of each solute system at the same concentration and pressure does not vary significantly from solute to solute therefore it is not density which controls viscosity. This indicates that it must be the size of species in solution which influences viscosity and the comparison between TBABF_4 and the non-electrolyte solutes demonstrates this idea. A single TBA^+ ion will have approximately the same number of solvent molecules in its solvation sheath as a dimer of salicylic acid or toluic acid. A TBABF_4 ion pair will require more than double the number of solvent molecules and triples ions will require even more. Even the larger aggregates of non-electrolyte solutes are not able to order the same quantity of surrounding solvent

Chapter Four – Determination of the Viscosity of Supercritical Solutions

molecules and therefore influence the solvent structure to the same degree. The ionic species formed by TBABF₄ bring about the dramatic increase in solution viscosity and the interaction between these species and CH₂F₂ molecules arising through electrostriction are large and able to organize the molecules throughout the sc fluid. In contrast, the CH₂F₂ solvent has hydrogen bond donor properties and therefore capable of forming bonds with appropriate solutes; salicylic acid and toluic acid. These bonds will enhance the order of the surrounding solvent molecules but not to the same extent as the ionic species.

4.2.4 Electrochemistry in Supercritical Electrolyte Solutions

The bulk solvent property of viscosity, η , is commonly related to the diffusion of a species, D , by the Stokes-Einstein equation

$$D = kT/6\pi\eta r \quad (4.23)$$

where k is the Boltzmann constant, T is the temperature and r is the radius of the diffusing species. It is, therefore, possible to confirm these unusually large viscosity increases caused by dissolving an electrolyte in a sc fluid by establishing the diffusion coefficient of a standard redox couple via electrochemical studies. The chosen electroactive species was ferrocene as its redox behaviour is well understood and it is known to be soluble in the sc solvent.⁷⁷

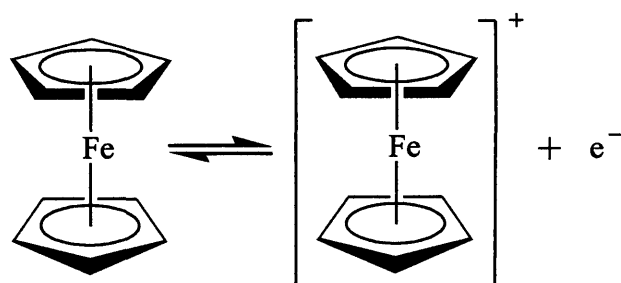


Figure 4.26 Standard redox couple for ferrocene

Figure 4.27 shows the voltammetric response of ferrocene at a 1 mm diameter Pt disc electrode in sc CH_2F_2 at 90 °C and a variety of pressures. It is evident that the oxidation current, and hence the diffusion coefficient, is not changed by pressure to the same extent as the viscosity of the pure fluid (viscosity changes from 5.63×10^{-4} to $9.19 \times 10^{-4} \text{ g cm}^{-1} \text{ s}^{-1}$ over the same pressure range). Furthermore it was observed that repeating the experiment using different electrolyte concentrations affected the oxidation current, which would not normally be expected. As the concentration of electrolyte is increased from 0.01 to 0.03 mol dm^{-3} the oxidation current decreases (Figure 2 in the Appendix). These preliminary findings confirm that the electrolyte concentration could change the viscosity of the solvent, which backs up the viscosity results obtained using the PQC. Qualitatively the trends in oxidation current follow those in viscosity shown in Figure 4.21.

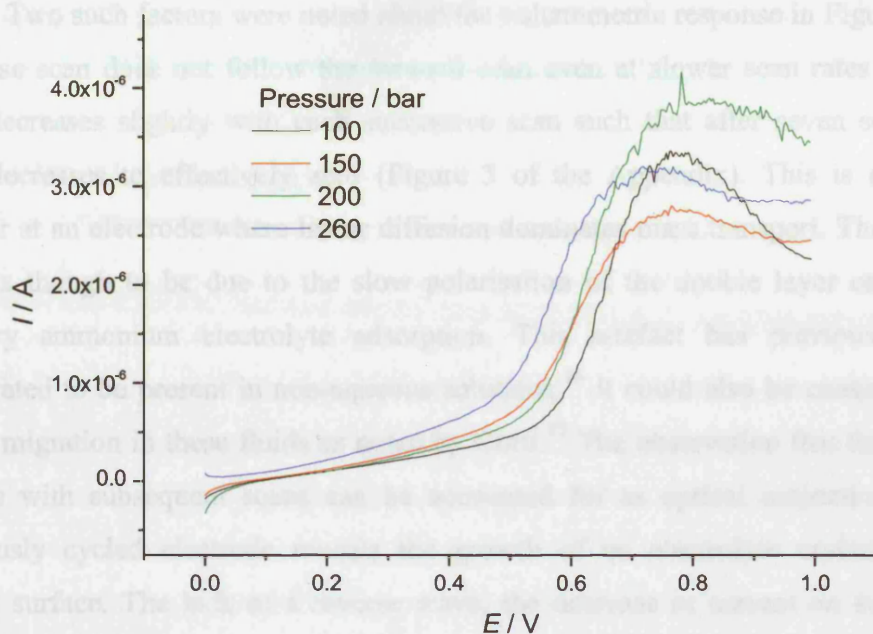


Figure 4.27 Voltammetric response of ferrocene at a 1 mm diameter Pt disc electrode in sc CH_2F_2 at 90°C as a function of pressures at 0.03 mol dm^{-3} TBABF_4 concentration

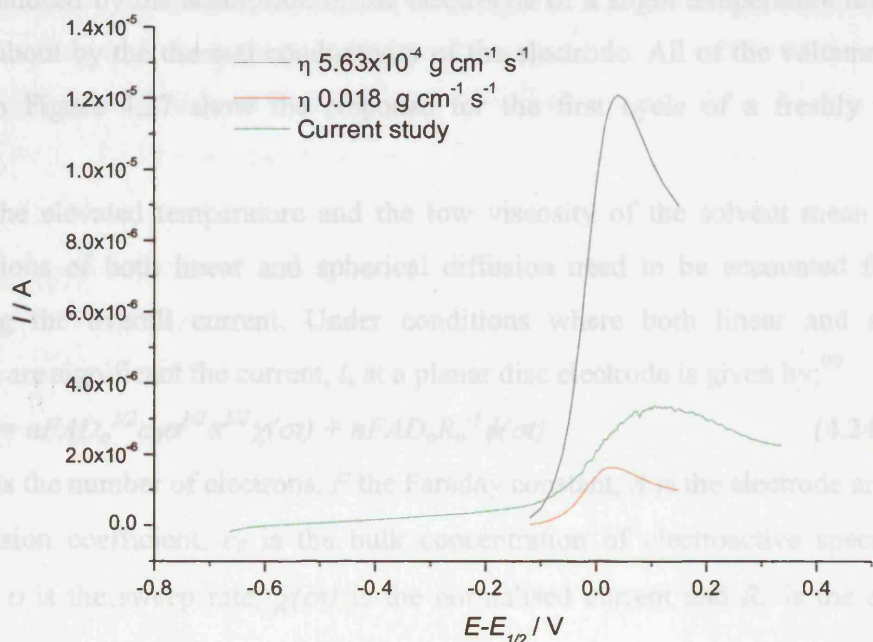


Figure 4.28 Comparison of the voltammetric response of ferrocene in sc CH_2F_2 containing 0.03 mol dm^{-3} TBABF_4 at 90°C and 100 bar, the theoretical voltammetric response for 100 bar assuming solution viscosity is the same as the pure solvent and the calculated voltammetric response using Equation 4.24

Unfortunately, electrochemical studies in sc fluids are somewhat prone to artefacts. Two such factors were noted about the voltammetric response in Figure 4.27; the reverse scan does not follow the forward scan even at slower scan rates and the current decreases slightly with each successive scan such that after seven scans the current decreases to effectively zero (Figure 3 of the Appendix). This is expected behaviour at an electrode where linear diffusion dominates mass transport. The former artefact is thought to be due to the slow polarisation of the double layer caused by quaternary ammonium electrolyte adsorption. This artefact has previously been demonstrated to be present in non-aqueous solutions.⁹⁶ It could also be caused by the effect of migration in these fluids as noted by Corti.⁹⁷ The observation that the current decreases with subsequent scans can be accounted for as optical inspection of the continuously cycled electrode reveals the growth of an electrolyte crystal on the electrode surface. The lack of a reverse wave, the decrease in current on successive scans, and the observation of a deposit on the electrode surface suggest that the Ferrocene oxidation product forms an insoluble salt with the electrode. Such effects have also been observed by Olsen and Tallman in sc chlorodifluoromethane.⁹⁸ This may also be induced by the adsorption of the electrolyte or a slight temperature differential brought about by the thermal conductivity of the electrode. All of the voltammograms shown in Figure 4.27 show the response for the first cycle of a freshly polished electrode.

The elevated temperature and the low viscosity of the solvent mean that the contributions of both linear and spherical diffusion need to be accounted for when modelling the overall current. Under conditions where both linear and spherical diffusion are significant the current, i , at a planar disc electrode is given by;⁹⁹

$$i = nFAD_o^{1/2}c_0\sigma^{1/2}\pi^{1/2}\chi(\sigma t) + nFAD_oR_o^{-1}\phi(\sigma t) \quad (4.24)$$

where n is the number of electrons, F the Faraday constant, A is the electrode area, D_o is the diffusion coefficient, c_0 is the bulk concentration of electroactive species, $\sigma = nFv/RT$, v is the sweep rate, $\chi(\sigma t)$ is the normalised current and R_o is the electrode radius.

Figure 4.28 shows the voltammetry of ferrocene at 100 bar in CH_2F_2 containing 0.03 mol dm^{-3} TBABF₄. The figure also shows the theoretical response obtained assuming the solution viscosity is the same as the bulk viscosity of the pure solvent calculated from Equation 4.24. It is clear that the current expected is almost three times

larger than that observed. It has previously been shown that in the absence of electrolyte the diffusion coefficient at a microelectrode corresponds to the value expected from the viscosity of the pure fluid.¹⁰⁰ The diffusion coefficient has, however, never been measured in solvents using typical electrolyte concentrations. In addition, it is noticeable that the current is significantly greater than that observed at any pressure presented in Figure 4.27. It is also noted that the electrolyte concentration has a significant effect upon the oxidation current, which could arise from a decrease in the diffusion coefficient of the electroactive species (Figure 1, Appendix).

The theoretical diffusion coefficient, D , can be calculated using the Stokes Einstein equation shown in Equation 4.23. Assuming that the radius of ferrocene is 3.8 \AA^{65} and the viscosity of the fluid is that of the pure solvent ($5.63 \times 10^{-4} \text{ g cm}^{-1} \text{ s}^{-1}$) a diffusion coefficient of $1.35 \times 10^{-4} \text{ cm}^2 \text{ s}^{-1}$ was calculated. The diffusion coefficient calculated using the experimentally measured voltammogram in Figure 4.28 is $8.60 \times 10^{-6} \text{ cm}^2 \text{ s}^{-1}$. This large discrepancy in D can only be explained by a larger than expected increase in solution viscosity. Figure 4.28 also shows the voltammogram calculated using equation 4.24 assuming a viscosity of $0.018 \text{ g cm}^{-1} \text{ s}^{-1}$. A diffusion coefficient of $4.14 \times 10^{-6} \text{ cm}^2 \text{ s}^{-1}$ is calculated using equation 4.23.

Good agreement between the maximum current for the experimentally measured and calculated voltammograms is obtained corroborating the viscosity data obtained using the PQC. This demonstrates for the first time that the dissolution of ionic solutes has a significant structuring effect on sc fluids. This leads to large relative viscosities in the electrolyte solutions and gives mass transport characteristics that are akin to liquid rather than sc fluids.

4.3 Conclusions

This study presents the first investigation into the solute effects on the viscosity of sc solutions. A piezoelectric quartz crystal has been shown to be an accurate analytical method for the measurement of solution viscosity in sc fluids.

The addition of a non-electrolyte solute has been shown to cause the viscosity to vary significantly from that of the pure sc fluid. In the region of low pressure the viscosity is significantly larger than the pure fluid and this is attributed to the enhanced degree of solute-solute clustering via hydrogen bonding interactions. As pressure is increased the solvation sheath becomes complete and the molar free volume of the system increases. This region is characterized by a decrease in solution viscosity. Above this point the molar volume increases further and the solute mole fraction becomes negligible. The viscosity in this region is shown to increase and at sufficient high pressures become the same as that of the pure sc fluid. Although the levels of solute-solute interactions are only speculated it is obvious that they play a role in structuring the sc fluid and influence the bulk viscosity. A modification of the Dole-Jones equation can be used to model the viscosity of sc solutions and it is shown that the volume fraction of the solute is the key factor in affecting solution viscosity.

Solutions of an electrolyte in CH_2F_2 were found to be inhomogeneous below 95 bar. A dense liquid phase was observed to exist under these conditions and is thought to be similar to a gas expanded ionic liquid. The affinity of the electrolyte for CH_2F_2 allows the gas to solvate the electrolyte and as a result the temperature required to melt the solid is reduced. As pressure is increased more gas dissolves in the dense liquid phase until a homogeneous sc solution is formed. Above 95 bar, the electrolyte causes an increase in the viscosity of CH_2F_2 of between 11 and 32-fold. This can be explained in terms of the structuring of the solvent that is brought about by the solvation of ionic aggregates and the equilibria that occur between neutral and charged species. These remarkable increases in solution viscosity have been confirmed using voltammetric measurements and account for the lower than expected peak currents.

4.4 References

1. Fenghour, A.; Wakeham, W. A.; Vesovic, V. *J. Phys. Chem. Ref. Data*, **1998**, *27*, 31.
2. Arp, V. D.; McCarty, R. D.; Friend, D. G. *Technical Note 1334*; National Institute of Standards and Technology; Boulder, CO, **1998**.
3. Tillner-Roth, R.; Yokozeki, A. *J. Phys. Chem. Ref. Data*, **1997**, *26*, 1273.
4. Jenkins, H. D. B.; Marcus, Y. *Chem. Rev.* **1995**, *95*, 2695.
5. Schaschke, C. *High Pressure Viscometry*; High Pressure Chemical Engineering Processes: Basics and Applications; Socrates Intensive Course, **2004**.
6. Yokoyama, C.; Nishino, T.; Takahashi, M. *Int. J. Thermophys.* **2004**, *25*, 71.
7. Yener, M. E.; Kashulines, P.; Rivzi, S. S. H.; Harriott, P. *J. Supercrit. Fluid.* **1998**, *11*, 151.
8. Tuan, D. Q.; Zollweg, J. A.; Harriott, P.; Rizvi, S. S. H. *Ind. Eng. Chem. Res.* **1999**, *38*, 2129.
9. Collings, A. F.; Mclaughlin E. *Trans. Faraday Soc.* **1971**, *67*, 340.
10. Vieira dos Santos, F. J.; Nieti de Castro, C. A. *Int. J. Thermophys.* **1997**, *18*, 367.
11. Cook, R. L.; King Jr, H. E.; Peiffer, D. G.; *Macromolecules*, **1992**, *25*, 2928.
12. Mertsch, R.; Wolf, B. A.; *Macromolecules*, **1994**, *27*, 3289.
13. Sen, Y. L.; Kiran, E. *J. Supercrit. Fluid.* **1990**, *3*, 91.
14. Llave, F. M.; Chung, F. T. H.; Burchfield, T. E. *SPE Reservoir Eng.* **1990**, 47.
15. Tilly, K. D.; Foster, N. R.; Macnaughton, S. J.; Tomasko, D. L. *Ind. Eng. Chem. Res.* **1994**, *33*, 681.
16. Peter, S.; Jakob, H. *J. Supercrit. Fluid.* **1991**, *4*, 166.
17. Xiong, Y.; Kiran, E.; *Polymer*, **1995**, *36*, 4817.
18. Dindar, C.; Kiran, E.; *Ind. Eng. Chem Res.* **2002**, *41*, 6354.
19. Yeo, S. D.; Kiran, E.; *J. Supercrit. Fluid.* **1999**, *15*, 261.
20. Yeo, S. D.; Kiran, E. *J. Appl. Polym. Sci.* **2000**, *75*, 306.
21. Lee, M.; Park, C. B.; Tzoganakis, C. *Ann. Tech. Con. Soc. Plastic. Eng.* **1998**, *56*, 1902.
22. Oh, J.; Lindt, T. J.; Ottoy, M. H. *Ann. Tech. Con. Soc. Plastic. Eng.* **2002**, *60*, 1920.
23. Vig, J. R. *A Tutorial on Quartz Crystal Resonators and Oscillators*; US Army Communications-Electronic Command, **2001**.
24. Shana, Z. A.; Josse, F. *Anal. Chem.* **1994**, *66*, 1955.

25. Buttry, D. A.; Ward, M. D. *Chem. Rev.* **1992**, *92*, 1355.
26. O'Sullivan, C. K.; Guilbault, G. G. *Biosens. Bioelectr.* **1999**, *14*, 663.
27. McKenzie, K. J. PhD Thesis, University of Loughborough, Loughborough, **2004**.
28. Hillman, A. R. In *The Electrochemical Quartz Crystal Microbalance*; Bard, A. J., Eds.; Encyclopaedia of Electrochemistry; Wiley: Chichester, **2003**, Vol. 3, pp 230-289.
29. Yang, M.; Thompson, M.; Duncan-Hewitt, W. C. *Langmuir*, **1993**, *9*, 802.
30. Lin, Z.; Yip, C. M.; Joseph, I. S.; Ward, M. D. *Anal. Chem.* **1993**, *65*, 1546.
31. Bruckenstein, S.; Shay, M. *Electrochim. Acta*, **1985**, *30*, 1295.
32. Kanazawa, K. K.; Gordon, J. *Anal. Chem.* **1985**, *57*, 1770.
33. Zhihong, M.; Lihua, N.; Shouzhou, Y. *J. Electroanal. Chem.* **1991**, *316*, 79.
34. Kurosawa, S.; Kitajima, H.; Ogawa, Y.; Muratsugu, M.; Nemoto, E.; Kamo, N. *Anal. Chim. Acta*, **1993**, *274*, 209.
35. Ash, D. C.; Joyce, M. J.; Barnes, C.; Booth, C. J.; Jefferies, A. C. *Meas. Sci. Tech.* **2003**, *14*, 1955.
36. Muramatsu, H.; Kimura, K.; Ataka, T.; Homma, R.; Miura, Y.; Karube, I. *Biosens. Bioelectron.* **1991**, *6*, 353.
37. Bandle, H. L.; Cernosek, R. W.; Lee, W. E.; Ondrovic, L. E. *Biosens. Bioelectron.* **2004**, *19*, 1657.
38. Stockbridge, C. D. In *Vacuum Microbalance Techniques*; Behrndt, K. H., Eds.; Plenum Press: New York, **1966**; Vol. 5, pp 147-205.
39. Park, K.; Koh, M.; Yoon, C.; Hakwon, K.; Kim, H. *J. Supercrit. Fluids*, **2004**, *29*, 203.
40. Otake, K.; Kurosawa, S.; Sako, T.; Sugeta, T.; Hongo, M.; Sato, M. *J. Supercrit. Fluid.* **1994**, *7*, 289.
41. Guigard, S. E.; Hayward, G. L.; Zytner, R. G.; Stiver, W. H. *Fluid Phase Equilib.* **2001**, *187*, 233.
42. Tsionsky, V.; Daikhin, L.; Urbakh, M.; Gileadi, E. *Langmuir*, **1995**, *11*, 674.
43. Wu, Y.; Akoto-Ampaw, P.; Elbaccouch, M.; Hurrey, M. L.; Wallen, S. L.; Grant, C. S. *Langmuir*, **2004**, *20*, 3665.
44. Aubert, J. H. *J. Supercrit. Fluid.* **1998**, *11*, 163.
45. Eltringham, W. E. PhD Thesis, University of Leicester, Leicester, **2004**.
46. Oag, R. M.; King, P. J.; Mellor, C. J.; George, M. W.; Ke, J.; Poliakov, M. *Anal. Chem.* **2003**, *75*, 479.

47. Ke, J.; King, P. J.; George, M. W.; Poliakoff, M. *Anal. Chem.* **2005**, *77*, 85.
48. Hillman, A. R.; Daisley, S. J. University of Leicester, **2005**, *unpublished*.
49. Abbott, A. P.; Eardley, C. A. *J. Phys. Chem. B*, **2000**, *104*, 9351.
50. Abbott, A. P.; Corr, S.; Durling, N. E.; Hope, E. G. *J. Chem. Eng. Data*, **2002**, *47*, 900.
51. Ulman, A. *Chem. Rev.* **1996**, *96*, 1533.
52. Abbott, A. P.; Eardley, C. A. *J. Phys. Chem. B*, **1999**, *103*, 2504.
53. Abbott, A. P.; Eardley, C. A.; Scheirer, J. E. *Phys. Chem. Chem. Phys.* **2001**, *3*, 3722.
54. Abbott, A. P.; Corr, S.; Durling, N. E.; Hope, E. G. *J. Phys. Chem. B*, **2003**, *107*, 10628.
55. Tucker, S. C. *Chem. Rev.* **1999**, *99*, 391.
56. Jones, G.; Dole, M. *J. Am. Chem. Soc.* **1929**, *51*, 2950.
57. Jones, G.; Talley, S. K. *J. Am. Chem. Soc.* **1933**, *55*, 624.
58. Patil, K. J.; Pawar, R. B.; Patil, P. D. *J. Mol. Liquids*, **2000**, *84*, 223.
59. Yoshida, K.; Tsuchihashi, N.; Ibuki, K.; Ueno, M. *J. Mol. Liquids*, **2005**, *119*, 67.
60. Tominaga, T. *J. Phys. Chem.* **1975**, *79*, 1664.
61. Tyrrell, H. J. V.; Kennerley, M. *J. Chem. Soc. A*, **1968**, 2724.
62. Jahagirdar, D. V.; Arbad, B. R.; Walvekar, A. A.; Shankarwar, A. G. *J. Mol. Liquids*, **2000**, *85*, 361.
63. Herskovits, T. T.; Kelly, T. M. *J. Phys. Chem.* **1973**, *77*, 381.
64. Thompson, P. T.; Fisher, B.; Wood, R. H. *J. Sol. Chem.* **1982**, *11*, 1.
65. Spartan Pro, Wavefunction Inc., Irvine, CA, USA.
66. Abbott, A. P.; Corr, S.; Durling, N. E.; Hope, E. G. *Chem. Phys. Chem.* **2005**, *6*, 466.
67. Rhodes, T. A.; O'Shea, K.; Bennett, G.; Johnston, K. P.; Fox, M. A. *J. Phys. Chem.* **1995**, *99*, 9903.
68. Ellington, J. B.; Park, K. M.; Brennecke, J. F. *Ind. Eng. Chem. Res.* **1994**, *33*, 965.
69. Ellington, J. B.; Brennecke, J. F. *J. Chem. Soc., Chem. Comm.* **1993**, *13*, 1094.
70. Hou, Z.; Han, B.; Zhang, X.; Zhang, H.; Liu, Z. *J. Phys. Chem. B*, **2001**, *105*, 4501.
71. Thompson, R. L.; Gläser, R.; Bush, D.; Liotta, C. L.; Eckert, C. A. *Ind. Eng. Chem. Res.* **1999**, *38*, 4220.
72. Reaves, J. T.; Roberts, C. B. *Chem. Eng. Comm.* **1999**, *171*, 117.

73. Wang, B.; Han, B.; Jiang, T.; Zhang, Z.; Xie, Y.; Li, W.; Wu, W. *J. Phys. Chem. B*, **2005**, *109*, 24203.
74. Gupta, R. B.; Combes, J. R.; Johnston, K. P. *J. Phys. Chem.* **1993**, *97*, 707.
75. Abbott, A. P.; Eardley, C. A. *J. Phys. Chem. B*, **1999**, *103*, 6157.
76. Abbott, A. P.; Durling, N. E. *Phys. Chem. Chem. Phys.* **2001**, *3*, 579.
77. Abbott, A. P.; Eardley, C. A.; Harper, J. C.; Hope, E. G. *J. Electroanal. Chem.* **1998**, *457*, 1.
78. McHugh, M.; Krukonis, V. *Supercritical Fluid Extraction*, 2nd Ed.; Butterworth-Heinemann: Boston, **1994**.
79. Van Welie, G. S. A.; Diepen, G. A. M. *J. Phys. Chem.* **1963**, *67*, 755.
80. Rodrigues, A. B. J.; Kohan, J. P. *J. Chem. Eng. Data*, **1967**, *12*, 191.
81. McHugh, M. A.; Yogan, T. J. *J. Chem. Eng. Data*, **1984**, *29*, 112.
82. Lemert, R. M.; Johnston, K. P. *Fluid Phase Equilib.* **1989**, *45*, 265.
83. Hammam, H.; Sivik, B. *J. Supercrit. Fluid.* **1993**, *6*, 223.
84. Bothun, G. D.; Knutson, B. L.; Strobel, H. J.; Nokes, S. E. *Langmuir*, **2005**, *21*, 530.
85. Niehaus, D. E.; Philips, M. E.; Michael, A.; Wightman, R. M. *J. Phys. Chem.*, **1989**, *93*, 6232.
86. Niehaus, D. E.; Wightman, M. *Anal. Chem.* **1991**, *63*, 1728.
87. Pickett, C. J. *J. Chem. Soc. Chem. Comm.* **1985**, 323.
88. Abbott, A. P.; Griffith G.; Harper, J. C. *J. Chem. Soc. Faraday Trans.* **1997**, *93*, 577.
89. Svorstøl, I.; Sigvartsen, T.; Songstad, J. *J. Acta Chem. Scand.* **1988**, *B42*, 133.
90. Stokes, R. H.; Mills, R. In *Viscosity of Electrolytes and related properties*; Stokes, R. H., Eds.; The International Encyclopaedia of Physical Chemistry and Chemical Physics 16; Pergamon Press: Oxford, **1965**: Vol. 3.
91. Abbott, A. P.; Eardley, C. A.; Tooth, R. J. *J. Chem. Eng. Data*, **1999**, *44*, 112.
92. Svorstøl, I.; Sigvartsen, T.; Songstad, J. *J. Acta Chem. Scand.* **1987**, *B41*, 318.
93. Davies, C. W.; Malpass, V. E. *Trans. Faraday Soc.* **1964**, *60*, 2075.
94. Crudden, J.; Delaney, G. M.; Feakins, D.; O'Reilly, P. J.; Waghorn, W. E.; Lawrence, K. G. *J. Chem. Soc., Faraday Trans. 1*, **1986**, *82*, 2207.
95. Qunitana, C.; Llorente, M. L.; Sanchez, M.; Vivo, A. *J. Chem. Soc., Faraday Trans. 1*, **1986**, *82*, 3307.
96. Abbott, A. P.; Harper, J. C.; Stimson, G. *J. Electroanal. Chem.* **2002**, *520*, 6.

Chapter Four – Determination of the Viscosity of Supercritical Solutions

97. Corti, H. R.; Goldfarb, D. L.; Longinotti, M. P. *J. Electroanal. Chem.* **2001**, *509*, 155.
98. Olsen S. A.; Tallman, D. E. *Anal. Chem.* **1994**, *66*, 503.
99. Bard, A. J.; Falkner, L. R. *Electrochemical Methods; Fundamentals and Applications*, 2nd Ed.; Wiley: Chichester, **1980**, pp 218.
100. Goldfarb, D. L.; Corti, H. R. *J. Phys. Chem. B*, **2004**, *108*, 3368.

Chapter Five

SOLUTE PRECIPITATION FROM SUPERCRITICAL SOLUTIONS

-
- 5.1 Introduction
 - 5.1.1 Rapid Expansion of Supercritical Solutions (RESS)
 - 5.1.2 Design of Particle Formation System
 - 5.2 Results and Discussion
 - 5.2.1 Effect of Extraction Pressure
 - 5.2.2 Slow Expansion of Supercritical Solutions (SESS)
 - 5.2.3 Effect of Pre-expansion Temperature
 - 5.2.4 Effect of Supercritical Solvent
 - 5.3 Conclusions
 - 5.4 References
-

5.1 Introduction

Conventional processes for particle design such as crushing, grinding, sublimation and air micronisation involve extensive use of organic solvents as anti-solvents for recrystallisation, reaction media or as extracting agents. Practical problems associated with these conventional methods include thermal or chemical degradation of products and health concerns over the use of organic solvents. Trace residues can remain in the final product and waste solvent streams are produced. As a result there is a driving force for research aimed at developing more environmentally-benign processing techniques. An ideal particle formation process needs to use relatively small quantities of organic solvents, be a single-step scalable operation, be suitable for a wide range of chemical types and be capable of preparing multi-component systems. The final product must be solvent-free with direct and targeted properties, such as particle size distribution. One major focus has been the investigation of processes in which the traditional solvents are replaced with sc fluids.

Interest in using sc fluids for precipitation and crystallisation processes has steadily increased over recent years. A number of processes have been developed and can be classified depending on the way in which the sc fluid is employed. This can be either as an anti-solvent (supercritical anti-solvent systems, SAS or solution enhanced dispersion by supercritical fluids, SEDS), a solute (particles from gas-saturated solutions, PGSS) or as the primary solvent. As with most sc processes, CO₂ has been the solvent of choice but suffers from the low solubility of polar solutes. In this work, sc CH₂F₂ is employed as the sc solvent and is used for the first time in the process known as rapid expansion of supercritical solutions, more commonly referred to as RESS, to investigate particle formation as a function of material, pressure and temperature.

5.1.1 Rapid Expansion of Supercritical Solutions (RESS)

In the nineteenth century Hannay and Hogarth observed a snow-like precipitation when a sc solution of cobalt chloride in ethanol was depressurized.¹ This was the first description of how materials can be modified through expansion of a sc solution, yet it was not until the 1980s that this technique was developed into the process that is widely used today.² The concept is relatively simple and relies on the fact that solvent strength can be significantly decreased by reducing the sc fluid density. Figure 5.1 shows the typical apparatus set-up used in RESS. The sc fluid is pressurised and heated to the desired conditions and saturated with one or more materials in the

extraction unit. The solution is then depressurized through an orifice into a low pressure chamber in order to cause supersaturation of the material. Extremely high supersaturation is obtained from depressurisation because expansion leads to a reduction in density and cooling of the sc solutions. The final product can be collected for analysis from the gaseous stream in the precipitation unit.

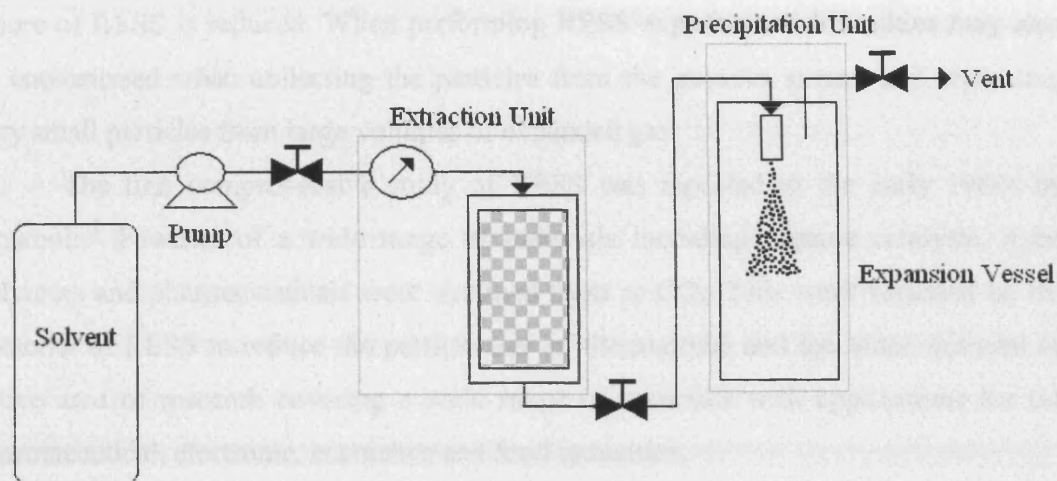


Figure 5.1 RESS apparatus⁸

RESS has been used for a wide variety of materials including polymers, pharmaceuticals, dyes and inorganic materials. The morphology of the final product depends on the crystallinity and purity of the material and on the RESS parameters employed. These include temperature, pressure and orifice or nozzle design. Varying the process parameters, and thus influencing supersaturation and nucleation rates, can result in particles which are quite different in size and morphology from the primary material.

The advantages of RESS are that very fine particles with controllable particle size and narrow size distribution can be produced. The major limitation is the solubility of the material in the sc fluid. This often means high ratios of gas/material and large quantities of sc fluid are required for increased product throughput. Consequently, it is important to know the solubility of the material near the upper critical end point in order to choose the process parameters that give the maximum amount of solute in the sc solution without the appearance of a liquid phase. This can be more complicated for binary systems as a variety of phase behaviours are possible. The solubility restriction is

very important for high molecular weight substances and, in particular, for polymers. Often bio-polymers used in the preparation of controlled-release systems are practically insoluble in sc fluids. One way of overcoming the low solubility issue is to use a co-solvent such as methanol. It has been shown that small amounts of co-solvent can considerably improve solubility as the local density around the solute molecules is higher than the bulk. However, even if only a small percent of organic solvent is necessary, the process becomes more complex and the environmentally-favourable nature of RESS is reduced. When performing RESS experiments difficulties may also be encountered when collecting the particles from the gaseous stream and separating very small particles from large volumes of expanded gas.

The first comprehensive study of RESS was reported in the early 1980s by Krukonis.² Powders of a wide range of materials including organic catalysts, dyes, polymers and pharmaceuticals were obtained from sc CO₂. This work focussed on the potential of RESS to reduce the particle size of the material and has since initiated an active area of research covering a wide range of materials with applications for the pharmaceutical, electronic, cosmetics and food industries.

Matson and co-workers showed ultrafine particles of SiO₂ could be produced by RESS and that it was possible to form homogeneous intimate mixtures of SiO₂ and GeO₂.³⁻⁵ These inorganic particles are important for the ceramic processing industry where small particles are desired because they will sinter faster and require lower processing temperatures. Ceramics are often composed of several constituents such as silicates, metal oxides and carbides. Intimate mixing of the components is necessary for uniformity of properties and reaction conditions during subsequent processing. Matson *et al.* used sc water and found that the concentration of silica in the sc water prior to expansion had the greatest influence on the final particle size. Lower concentrations yielded smaller and more uniformly dispersed particles whereas at higher concentrations the particles were found to be highly agglomerated. It was also noted that thin films of SiO₂ were obtained by operating at very low concentrations. Hence RESS could have applications in thin-film deposition. The type of nozzle employed also had an influence on the morphology. Nozzles with 'pinpoint' orifices produced oblong particles while capillary nozzles produced more spherical particles. Other studies of RESS with ceramics have examined polycarbosilanes, zirconium oxynitrate and α -alumina (Al₂O₃).^{5,6}

Chapter Five – Solute Precipitation from Supercritical Solutions

Conventional methods used to reduce the particle size of pharmaceuticals such as milling or grinding have been shown to have adverse effects on the crystallinity and chemical stability of the products. By selecting an appropriate sc fluid, RESS allows processing at much lower temperatures and will produce fine monodisperse particles, which are vital to meet high surface area, bioavailability and dissolution requirements of pharmaceuticals. In contrast to the liquid solvents used in conventional processes, sc fluids are easily separated leaving a pure final product. Organic compounds which are heat labile, decompose easily, require uniform size distribution or are shock sensitive, such as phospholipids or explosives can be successfully prepared by RESS. Furthermore, it is possible to produce intimate mixtures that are ideal for pharmaceuticals with formulations incorporating multiple drugs.

There are three main areas where the potential of RESS has been examined for pharmaceutical applications; the production of powders of pharmaceuticals to improve or modify their therapeutic action or enhance solubility; the production of polymers or bio-polymers that can be used as stationary phases, absorbents, catalyst supports or as matrices for drug impregnation; and the simultaneous precipitation (co-precipitation) of drugs and polymers for developing drug delivery systems. A wide range of organic materials with micro-particles ranging in size from a few microns to several hundred microns have been processed and a number of examples are shown in Table 5.1.

Table 5.1 Organic compounds processed by RESS⁶⁻⁸

Material	Sc Fluid	Particle Size / μm	Reference
β -estradiol	CO ₂	< 1	8
β -Sitosterol	CO ₂	1.6 – 2.1	20, 21
Lovastatin	CO ₂ (CO ₂ + methanol)	0.04 – 0.3 (10 – 50)	9
β -carotene	CO ₂ , C ₂ H ₆ , C ₂ H ₄ + toluene	0.3 – 2	11
Benzoic acid	CO ₂	2 – 10	16, 19, 20, 47
Stigmasterol	CO ₂	0.05 – 2	7
Aspirin	CO ₂	0.1 – 9	16, 17
Salicylic acid	CO ₂	< 4	12, 16
Griseofulvin	CHF ₃	0.9 – 3.2	13, 20, 21
Theophylline	CO ₂	0.4	8
Naproxen	CO ₂	1 – 20	28
Anthracene	CO ₂	20 – 45	9, 49, 50,
Caffeine	CO ₂	1 – 10	8
Naphthalene	CO ₂	1.5 – 3	10, 18, 19, 44, 47
Cholesterol	CO ₂	0.3 – 3	19
Ibuprofen	CO ₂	1.8 – 7.5	21, 22
Phenanthrene	CO ₂ , CHF ₃	1 – 25	16

In the study by Krukoniš the application of RESS for processing organic compounds such as ferrocene, β -estradiol (a steroid) and soy bean lecithin (phospholipid) was shown.² Following this work, Larson and King investigated the extraction and precipitation of the cholesterol-reducing drug lovastatin in sc CO₂.¹⁰ Later, Mohamed *et al.* examined lovastatin in sc CO₂ employing methanol as a co-solvent and concluded that smaller particles were produced using pure CO₂.¹¹ In the same study naphthalene was used to investigate how the operating conditions influence the morphology of the final product. The pre- and post-expansion temperature, pressure and composition were examined. It was found that the pre-expansion temperature had a pronounced effect on the particle size except at higher naphthalene concentrations, where higher temperatures produced larger particles. A five-fold decrease in particle size upon lowering the post-

expansion temperature was observed whereas increasing the post-expansion pressure only had a small effect on particle size. This was attributed to two competing processes. Increasing the post-expansion pressure is thought to decrease supersaturation, which causes lower nucleation and larger particles. In addition, the partial pressure of the solute is increased with post-expansion pressure resulting in higher nucleation and smaller particles. The group also characterised the effect of process conditions on the lovastatin-CO₂ system. In contrast to the naphthalene study, lovastatin particles were found to be insensitive to changes in the process conditions.

Other groups have examined the effect of process conditions on product morphology. Chang and Randolph studied the precipitation of β -carotene from ethylene.¹² They compared free expansion and expansion into gelatine solutions and found expansion into a gel solution decreased the amount of agglomeration, although a further separation step was required. They also showed that it was possible to use co-solvents and maintain a single solvent phase after expansion. The solubility of β -carotene was found to increase with co-solvent concentration. However, with high co-solvent concentrations, the expansion was not single phase and the particles obtained were larger with wider size distributions.

The effects of pre-expansion temperature and pressure, expansion temperature and solute concentration on salicylic acid particles from sc CO₂ were examined by Reverchon *et al.*¹³ It was found that increasing pre-expansion temperature led to larger particles and an increase in the particle size distribution (PSD). Increases in pre-expansion pressure also led to an increase in the PSD. It was also found that expansion temperature influenced the particle size and distribution. Decreases in temperature lead to a decrease in mean particle size and PSD. Mohamed *et al.* suggested that particle nucleation is influenced by pre-expansion temperature and particle growth by expansion chamber temperature.¹⁰ However, by measuring temperature at varying distances from the nozzle tip, Reverchon showed that the pre-expansion temperature greatly influences the temperature in the subsonic jet region. The pre-expansion temperature will then have an influence on the growth processes of salicylic acid crystals. In a later study Reverchon *et al.* examined the precipitation of griseofulvin from CHF₃ and observed two different types of morphologies dependent on the pre-expansion temperature.¹⁴ Quasispherical particles were obtained at high pre-expansion temperatures whereas at lower temperatures long needles were produced. Between these two temperatures an

intermediate region was found to exist where both types of particles were present. The formation of long needles was attributed to liquid droplets forming inside the nozzle, whereas the quasispherical particles were thought to result from precipitation in the free-jet region. This interpretation has also been proposed by other authors.^{15,16}

In an extensive study, Domingo and co-workers investigated the precipitation of benzoic acid, salicylic acid, aspirin and phenanthrene from sc CO₂.¹⁷ The effects of extraction temperature and pressure, pre- and post-extraction temperature and mass flow rate using two different types of nozzle were examined. The two nozzles employed were a sintered porous plate or 'frit' nozzle and the more commonly used capillary nozzle. The trends observed were solute-dependent, as both benzoic acid and salicylic acid particles were reduced in size when produced with the frit nozzle in comparison to particles produced using the capillary nozzle, but no significant modification was observed for phenanthrene. Under the conditions investigated they found that the extraction parameters did not influence the size and morphology of particles obtained. The pre-expansion temperature is thought to influence the point of nucleation. At lower temperatures, nucleation is thought to begin earlier and larger particles will be obtained. However, this effect was not observed with the capillary nozzle as the PSD was too large. With the frit nozzle no dependence on particle size was found although the PSD did vary. This was attributed to the influence of pre-expansion temperature on the mass flow rate and collection chamber temperature as reported by other authors.¹² Lower collection chamber temperatures, resulting from lower pre-expansion temperatures, gave particles with a narrower size distribution.

The formation of aspirin particles has been more recently examined by Huang *et al.*¹⁸ The pre-expansion temperature and nozzle geometry as well as the thermodynamic effects of extraction temperature and pressure were investigated. The results showed that a change in nozzle diameter did not lead to a significant change in particle size or morphology. This is similar to the findings by other authors.¹⁰ It was also noted that a longer nozzle may lead to an earlier crystallisation of particles inside the nozzle and hence yield larger particles. Both an increase in extraction temperature and pressure were found to decrease the particle size because the solubility of aspirin was increased. Variations in pre-expansion temperature were found not to have a significant effect on the particle size. This result was also observed by Mohamed and co-workers at high concentrations.¹⁰ However, Domingo reported lower pre-expansion temperatures cause early nucleation leading to larger particles¹⁶ whereas other authors have reported an

increase in pre-expansion temperature can result in larger particles due to the solution becoming sub-saturated upon pre-heating.¹⁹

More recently, Türk reported the precipitation of naphthalene, cholesterol and benzoic acid from sc CO₂.²⁰ The influence of pre-expansion temperature and pressure, nozzle diameter and nozzle temperature were examined by measuring the diameter and number concentration of particles using an *in situ* and online 3-wavelength-extinction measurement (3-WEM) technique. For the naphthalene systems it was found that increasing pre-expansion temperature decreased the particle size but had no influence on the number concentration. Increasing the pre-expansion pressure resulted in larger particles with a higher particle number concentration. For benzoic acid there was an increase in particle size with increasing pre-expansion temperature but no strong pressure dependence was observed. Cholesterol particles were found not to be dependent on pre-expansion conditions. This was thought to be due to the high levels of aggregation present. For each solute both the nozzle temperature and diameter were shown to influence the size of particle produced. A larger nozzle diameter and high nozzle temperatures gave much smaller particles. In a later study by Türk and co-workers, the precipitation of benzoic acid from sc CO₂ was reported and again found that lowering both the pre-expansion temperature and increasing the pre-expansion pressure lead to smaller particles.²¹ RESS experiments were also reported for β -sitosterol and ibuprofen using sc CO₂ and griseofulvin with sc CHF₃, due to its low solubility in sc CO₂.²² Under the conditions studied, no clear dependency of the particle size on the different pre-expansion conditions was observed. This was attributed to the low solubility of each solute in the respective sc solvents. In this work they also examined the potential of RESS to produce suspensions of water-insoluble drugs. This was done by spraying sc mixtures of β -sitosterol and CO₂ directly into an aqueous surfactant solution. The particles obtained were found to be smaller or equal in size to those produced by RESS into air.

The micronisation of ibuprofen in sc CO₂ has also been examined by Hortaçsu and co-workers.²³ The effects of extraction pressure, pre-expansion temperature, capillary length, spraying distance and collision angle on the size and morphology of the precipitated particles were investigated. It was concluded that increasing the pre-expansion temperature, capillary length and collision angle reduced the particle size collected. Although, low collision angle seemed to result in large deformation of

collected particles. Increasing the spraying distance was found to increase the particle size but no clear dependence of particle size on pressure was observed.

Conventional mechanical methods for the production of polymer microspheres, such as milling, produce non-uniform particles with wide size distributions. Monodispersed spheres with particle sizes in the micron range can be prepared by emulsion polymerisation of vinyl monomers or suspension polymerisation. However, these methods require surfactants, suspending agents and chemical initiators that need to be removed from the final product. RESS is a viable alternative to these methods and a wide range of polymers have been shown to be successfully processed (Table 5.2). In principle, any type of polymer may be processed using RESS; however polymers generally have low solubility in sc CO₂, which is the sc fluid most commonly applied.

In the pioneering work of Krukonis the precipitation of polypropylene from sc propylene was examined.² This was followed by work by Matson and co-workers who examined the processing of polystyrene, polypropylene and cellulose acetate in sc pentane and polyphenyl sulfone and polymethyl methacrylate in sc propane.^{4,5,16,24} In the 1990s biodegradable polymers such as poly-(L)-lactic acid (PLA), poly(glycolic acid) (PGA)^{26,27} and polysaccharides²⁸ were processed using sc CO₂. Nucleation of PLA produced microparticles and microspheres while nucleation of PGA produced both regular sized particles and needles.

Bio-polymers have been used to produce fine polymeric powders that, in conjunction with a drug, are the basis for the preparation of controlled drug delivery systems. Two approaches are common: one is the formation of pure biopolymer particles that are then impregnated with active ingredients. The other is the co-precipitation of the polymer and active ingredient. The active molecule is dispersed in the polymer carrier and either diffuses through pores in the non-erodable matrix or is released as the polymer disintegrates in the body. By adjusting the concentration of drug and polymer in the sc fluid streams, intimate drug/polymer mixtures are produced upon expansion of the combined streams. Debenedetti and co-workers reported the formation of composite PLA-pyrene and PLA-lovastatin particles by RESS.¹⁴ Pyrene was chosen because it is fluorescent and thus allowed observation and assessment of the effectiveness and uniformity of its distribution in the polymer matrix as a function of process conditions. Kim *et al.* reported the microencapsulation of the pharmaceutical molecule naproxen in PLA.²⁹ When PLA was co-precipitated with naproxen, microspheres loaded with the drug and some free naproxen was observed. The

solubilities of these compounds in CO₂ have often been enhanced by employing co-solvents such as acetone or ethanol.

Table 5.2 Polymers processed by RESS^{5,6,30,31}

Material	Sc Fluid	Particle Size / μm	Reference
Polypropylene	CO ₂ , Propane, Pentane	0.5 – 5 (spheres) 100 – 1000 (fibres)	4, 5, 15, 23
Polystyrene	Pentane	20 (spheres) 100 – 1000 (fibres)	4, 5, 15, 23
Polymethyl methacrylate	Propane, CCl ₂ F ₂	0.2 – 1 (spheres) 100 – 1000 (fibres)	4, 5, 24
Polyphenyl sulfone	propane,	0.5 (spheres)	4, 5, 23
Polydimethylsiloxane	CO ₂	2 – 3 (spheres)	31
Polycaprolactone	CHClF ₂	0.2 – 0.6 (spheres) < 1000 (fibres)	24
Polycarbosilane	Pentane	< 0.1 (spheres) 20 – 160 (fibres)	3, 4, 5, 23
Polyvinyl chloride	Ethanol	7 (spheres)	4, 5, 23
Cellulose acetate	Pentane	0.8 (fibres)	15
Hyaluronic acid	CO ₂	< 10 (spheres)	37
Perfluoropolyether diamide	CO ₂	2 – 4	33
Poly(vinylidene) fluoride	CO ₂	1 – 30 nm (film)	39
L-PLA (poly-L-lactic acid)	CO ₂ , CClF ₃ , (CO ₂ + acetone)	2 – 5 (10 – 25)	14, 24, 26
D-PLA (poly-D-lactic acid)	CO ₂	10 – 20	26
PGA (poly-glycolic acid)	CO ₂	10 – 20	26
Pyrene – L-PLA	CO ₂ + CHClF ₃	< 100 (spheres)	14
Naproxen – L-PLA	CO ₂	10 – 90	28

More recently, the application of RESS process for polymer coatings has gained interest.^{32,33} The formation of a thin layer of polymer coating does not require a large quantity of particles, therefore the low solubility of many polymers in sc fluids does not limit this process. One or more coating materials are dissolved in sc CO₂ and, by adjusting the temperature and/or pressure, the coating material becomes insoluble and goes onto the surface of the dispersed particles.

Fluidised bed coating technology is based on RESS. In this technique the coating material is dissolved in sc CO₂ and sprayed into the bulk of a fluidised bed containing the particles to coat. Polymers soluble in CO₂ such as siloxanes and fluoropolymers have received recent interest. Poly(dimethylsiloxane) films have been deposited onto sensing surfaces of microfabricated transducers³⁴ whereas fluoroacrylate polymers have been used to coat cardiovascular stents.³⁵ Fluoropolymer coatings have also been used to protect historic buildings and monumental civil infrastructures.³⁶ In addition to coating applications, particles and fibres of fluoropolymers have been produced by RESS to investigate the effect of polymer concentration and degree of saturation on particle size and morphology.³⁷ The size of polymer particles is reported to be controlled by the degree of saturation, whereas the morphology is controlled by the concentration.

A number of research groups have used mathematical models to predict particle size and to understand the mechanisms of particle formation and growth.^{19,21,38-41} The comparison of these theoretical models with experimental results shows good agreement in general trends but an exact match with the average particle sizes has not been obtained.

5.1.2 Design of Particle Formation System

The RESS apparatus used in this work is described in Section 2.2.4 and a schematic diagram is shown in Figure 5.1. The equipment is designed in a number of stages that can be broadly classified as delivery, extraction, pre-expansion, expansion and collection.⁴²

The delivery step requires heating and pressurising the gaseous solvent to sc conditions. The sc fluid is then brought in to contact with the material to be processed in the extraction vessel. Intimate mixing of the sc fluid and the material is a crucial step and there are a number of methods employed to maximise the interactions while limiting the entrainment of solute. The degree of interaction is often enhanced by mixing the material with glass beads or glass wool. Alternatively, stirring or agitation of the material and sc fluid can be used.

The extraction unit is connected to a pre-expansion line that feeds the sc solution to the expansion device. This line contains a valve so the pressure on the extraction side may be maintained until the system is depressurised. Occasionally a back pressure regulator is used to compensate for the loss of pressure upstream of the point of depressurisation. During the pre-expansion step the composition and phase of the sc solution from which particles precipitate is controlled and has a major effect on particle morphology. Phase changes in sc solutions may lead to premature precipitation and subsequent plugging of the line. It is, therefore, essential to have independent control of the pressure and temperature during the pre-expansion stage. The pre-expansion line is usually kept at 50 °C higher than the temperature of the extraction vessel using heated tape or a temperature bath/oven and may have a port for the addition of fresh solvent.

In the expansion step the solution is expanded through a restriction device. There are two aspects of rapid expansion that are of interest for controlling particle morphologies. These are the supersaturation profile of the solutes as temperature, pressure, phase and composition changes during the expansion (thermodynamics) and the mechanical shear that a particle undergoes in the subsonic and supersonic regions of the expanding sc fluid (aerodynamics).

The restriction device is designed to support the large pressure drop that will occur across it. Various configurations have been used such as capillaries, nozzles, laser-drilled discs and valves. Typical aspect ratios (length/diameter or L/D) of the restriction devices used have been in the range 6-20 with orifices from 30 to 1600 µm in

diameter. The geometry of the restriction device has been shown to influence the morphology of the particles to varying degrees and by different mechanisms.^{5,41,42} Joule-Thomson cooling resulting from the large volumetric expansion across the restriction device causes a drop in temperature. As a result, a phase change may occur and subsequently lead to plugging of the restriction device. Restriction devices are often heated to compensate for such effects.

The post-expansion conditions are thought to control particle growth by affecting the dynamics of jet expansion. However, the studies conducted so far have found such effects to be inconclusive or relatively insignificant. It is thought that this could be due to the conditions examined or inaccuracies arising from particle agglomeration.

Using computational fluid and aerosol dynamics, a number of authors have attempted to model the supersaturation and growth of particles during the rapid expansion.^{19,42,43} Although an absolute theoretical model does not exist the studies have considered which parameters affect particle size.

Retaining the original characteristics of the particles produced by RESS is of great importance as the distinct characteristics of the particle can be completely lost owing to a poor collection technique. The most commonly used collection devices are glass slides, filters and baskets, which can be easily removed for particle analysis. In the majority of cases collection vessels are maintained at atmospheric conditions. During RESS the rapidly expanding sc fluid imparts high kinetic energy to the particles produced. Insufficient path for expansion can therefore result in the agglomeration of particles. This can be even worse in the presence of residual amounts of co-solvent. Hence the particle collection vessel should be designed such that agglomeration is kept to a minimum by providing a sufficient path for expansion. However, if the collection vessel is made very large to prevent agglomeration the collection of small amounts of material can be difficult, resulting in low yields.

The most common techniques used to characterise the particles produced via RESS are optical microscopy and scanning electron microscopy (SEM). Changes in the crystallinity or amorphous nature of particles have been examined by X-ray diffraction and differential scanning calorimetry. Fluorescence spectroscopy has also been used to determine the homogeneity of precipitates from multiple solutes. A number of groups have used non-invasive, online and *in situ* techniques such as three-wavelength extinction measurements (3-WEM) and laser-based shadowgraphy (LABS).^{8-10,44} These

Chapter Five – Solute Precipitation from Supercritical Solutions

online techniques allow particle diameter, morphology, size distribution and concentration to be recorded.

5.2 Results and Discussion

It can be seen from the abovementioned studies that the majority of RESS experiments have employed sc CO₂ as the solvent. In some cases a co-solvent has been used to enhance the solubility of the material to be processed. However, this may introduce further separation steps and the problems of final product contamination. A number of organic compounds have been shown to exhibit relatively high solubility in sc hydrofluorocarbon solvents such as CH₂F₂.^{45,46} The authors have also shown CH₂F₂ to be more polar and have more tuneable solvent properties than CO₂.⁴⁷ This permits the use of solutes with limited solubility in CO₂ and allows a wider range of solvent properties to be investigated.

In this work sc CH₂F₂ has been used in RESS to examine the factors that influence particle formation. Process conditions such as extraction pressure and pre-expansion temperature have been varied for each solute. The solutes investigated were the polar compounds *o*-hydroxybenzoic acid (salicylic acid) and *p*-methylbenzoic acid (*p*-toluic acid). A number of authors have reported the precipitation of naphthalene particles from sc CO₂ and found it possible to examine the particles by optical microscopy.^{18,19,48} However, owing to the low sublimation pressure of naphthalene it was not possible to analyse the precipitate in the current study. For this reason anthracene was included as a non-polar compound for comparison. The electrolyte tetrabutylammonium tetrafluoroborate (TBABF₄) was also selected because it is known to be soluble and the precipitation of this salt has not previously been reported. The chosen compounds have similar melting points (Table 2.1) and their solubility in CH₂F₂ is known to be greater than in sc CO₂.^{45,49} Hence, the purpose of this work is to evaluate the use of sc CH₂F₂ to modify compounds by RESS that cannot be processed with sc CO₂ without the use of modifiers. It is anticipated that the solutes examined in this study will each cluster differently in solution and as a result crystallise in different ways when the solution is depressurised.

After the solutions had been depressurised, the material was collected and particle morphology was examined by scanning electron microscopy (SEM). SEM images of the unprocessed virgin solutes are shown in Figure 5.2. Anthracene and salicylic acid can be seen to exist in a range of particle shapes and sizes whereas toluic acid and TBABF₄ have a more even size and shape distribution.

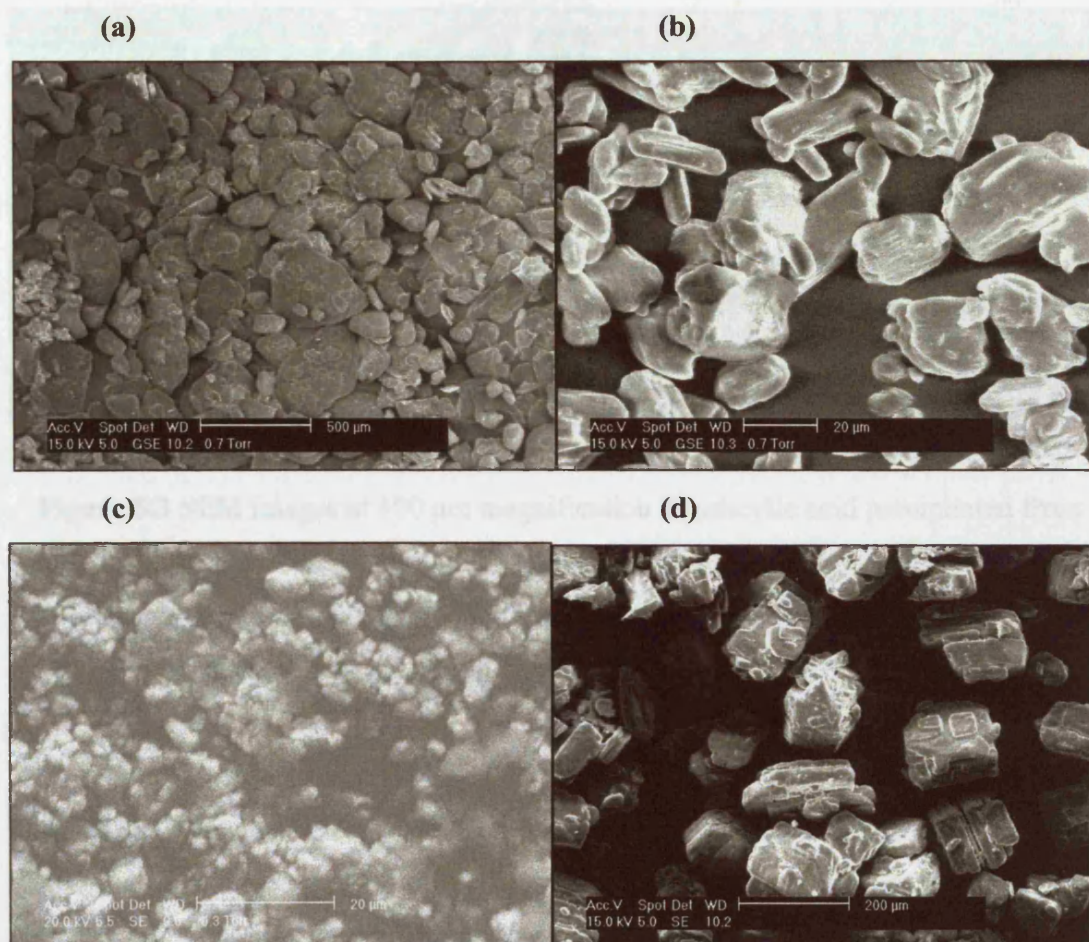


Figure 5.2 SEM images of unprocessed material at different magnifications

(a) anthracene

(b) salicylic acid

(c) *p*-toluic acid

(d) tetrabutylammonium tetrafluoroborate

Before performing high-pressure experiments, the precipitation of salicylic acid from liquid CH_2Cl_2 was performed. This was to ascertain particle size and shape obtained from a conventional organic solvent. SEM images of the crystals obtained are shown in Figure 5.3. Two cooling methods were used; rapid cooling was achieved by submerging a salicylic acid – CH_2Cl_2 solution into dry ice, whereas slow cooling was accomplished by allowing a solution to cool over 6 hours. Both types of cooling produced needle-shaped particles. Rapid cooling produced crystals with approximate lengths 100 – 300 μm whereas slow cooling formed crystals 50 – 150 μm in length. The needles obtained by slow cooling are more even in size and shape to those rapidly cooled. This is reasonable as slow cooling would allow slower and more even nucleation to take place.

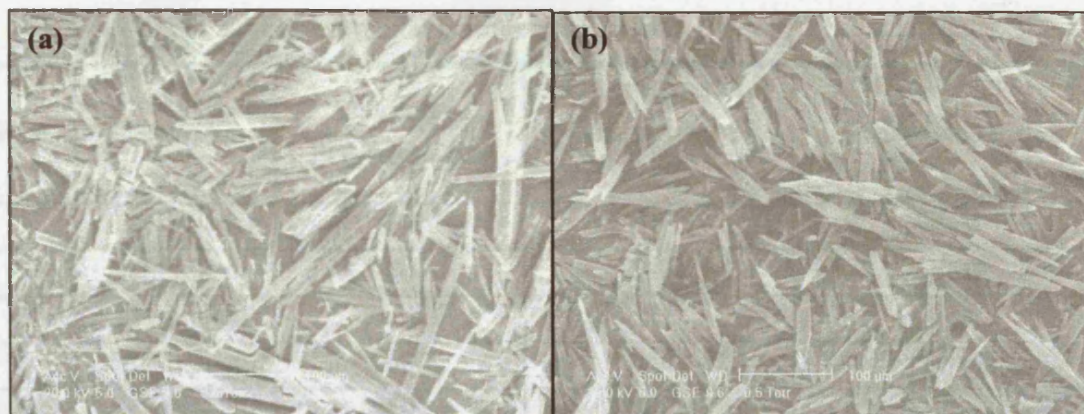


Figure 5.3 SEM images at 100 μm magnification of salicylic acid precipitated from liquid dichloromethane

(a) Particles produced by rapid cooling, lengths range from 100 – 300 μm

(b) Particles produced by slow cooling, lengths range from 50 – 150 μm

The process conditions varied in this work are shown in Table 5.3. In each experimental run the solvent was CH_2F_2 , extraction temperature was 90 $^\circ\text{C}$ and the restriction device was a 300 μm orifice (L/D aspect ratio = 6). The particles were collected on a carbon disc positioned 15 mm from the orifice. Expansion rate was controlled by employing two types of valve. Rapid expansion (RESS) was achieved by using a ball valve whereas slow expansion of sc solutions (SESS) was examined by employing a shut-off valve. Unfortunately plugging of the valve was experienced during SESS experiments. To overcome this issue the valve was opened further to increase the opening. Consequently, the accuracy of this method is questionable as a constant expansion rate was not achieved. It should be noted that it was not possible to quantitatively measure the expansion rate for either the fast or slow expansion. In addition, it was not possible to quantitatively measure particle size or particle size distribution. Hence this work describes the qualitative trends observed in particle size, morphology and amount of material collected. These trends are understood in terms of solute aggregation and the transport properties of solution.

Table 5.3 Experimental parameters varied in CH₂F₂ RESS studies

Run	Solute	Extraction Pressure / bar	Pre-expansion Temperature / °C ^a	Expansion rate ^b
1	Anthracene	60	NC	Fast
2	Anthracene	80	NC	Fast
3	Anthracene	200	NC	Fast
4	Anthracene	60	NC	Slow
5	Anthracene	80	NC	Slow
6	Anthracene	200	NC	Slow
7	Anthracene	60	140	Fast
8	Anthracene	80	140	Fast
9	Anthracene	200	140	Fast
10	Salicylic acid	60	NC	Fast
11	Salicylic acid	80	NC	Fast
12	Salicylic acid	200	NC	Fast
13	Salicylic acid	60	NC	Slow
14	Salicylic acid	80	NC	Slow
15	Salicylic acid	200	NC	Slow
16	Salicylic acid	60	140	Fast
17	Salicylic acid	80	140	Fast
18	Salicylic acid	200	140	Fast
19	<i>p</i> -Toluic acid	60	NC	Fast
20	<i>p</i> -Toluic acid	80	NC	Fast
21	<i>p</i> -Toluic acid	200	NC	Fast
22	<i>p</i> -Toluic acid	60	140	Fast
23	<i>p</i> -Toluic acid	80	140	Fast
24	<i>p</i> -Toluic acid	200	140	Fast
25	TBA BF ₄	100	NC	Fast
26	TBA BF ₄	200	NC	Fast
27	TBA BF ₄	100	NC	Slow
28	TBA BF ₄	200	NC	Slow
29	TBA BF ₄	100	140	Fast
30	TBA BF ₄	200	140	Fast

^a NC signifies no external control of pre-expansion line

^b expansion rate controlled by valve. Fast signifies ball valve, slow signifies shut-off valve

5.2.1 Effect of Extraction Pressure

Extraction temperature and pressure determine solution mole fraction prior to expansion. Extraction pressure will also influence the expansion profile and mass flow rate. In the region close to the critical point a large increase in solubility with pressure is observed. Above this point, an increase in pressure at constant temperature is found to lead to an almost constant solubility level. It is thought that many authors have not observed a significant change in morphology with extraction pressure for this reason. However several authors have reported an increase in the particle size distribution (PSD) with increasing pressure.^{12,19} Liu and Nagahama found decreasing the extraction pressure led to an increase in the particle size of naphthalene.¹⁸ This is thought to be due to a decrease in solvent density, naphthalene solubility and supersaturation ratio at the expansion chamber. Similar observations were made by Huang *et al.* who studied aspirin.¹⁷ It was thought this was caused by the increase in aspirin solubility at higher pressure (between 160 and 180 bar), which led to higher supersaturations and a faster nucleation rate. Above 180 bar a marked increase in particle size with an increase in extraction pressure was reported. This was attributed to a decoupling of nucleation and growth. At high aspirin concentrations particle growth may dominate, hence large particles are readily produced with a broad PSD. In general the effect of extraction pressure on particle size and morphology is inconclusive.

The terminal velocity, v , of a body with radius, r and density, ρ_s moving through a fluid of density, ρ_f is inversely proportional to the viscosity, η of the fluid.

$$v = \frac{2r^2 g(\rho_s - \rho_f)}{9\eta} \quad (5.1)$$

where g is the local gravitational acceleration. This relationship is the principle behind falling body viscometers.

Since expansion velocity will depend upon solution viscosity (Equation 5.1) it is appropriate to consider that the results shown in Chapter Four will have an affect upon particle growth. It is thought that if mass transport properties influence particle size and morphology, different morphologies will be obtained in the pressure regions of high and low viscosity. Furthermore the isentropic phase of the decompression and positive Joule-Thomson expanding coefficient causes significant cooling to occur in the expanding jet. It is possible for this cooling to have a predominant effect on particle

nucleation and growth. In this case it is thought that each pressure region would produce a different morphology.

In Chapter Four, sc solutions of TBABF₄ were only found to be homogeneous above approximately 90 bar. For this reason two pressures, 100 and 200 bar have been examined for TBABF₄. As shown in Table 5.3 three extraction pressures were examined for salicylic acid, toluic acid and anthracene. The pressures selected were 60, 80 and 200 bar. The data from the 80 bar studies should give interesting results as this corresponds to the minima in solution viscosity.

Figures 5.4 to 5.7 show SEM images of anthracene, salicylic acid and toluic acid at 60, 80 and 200 bar, respectively. TBABF₄ was examined at 100 and 200 bar. In these experiments the temperature of the pre-expansion line was not controlled (Table 5.3 experimental runs 1-3, 10-12, 19-21 and 25-26). Comparison of these images with the respective unprocessed solutes (Figure 5.2) clearly shows that precipitation from sc CH₂F₂ alters the size and shape of a material. In all cases, a reduction in particle size compared to the unprocessed virgin material is observed.

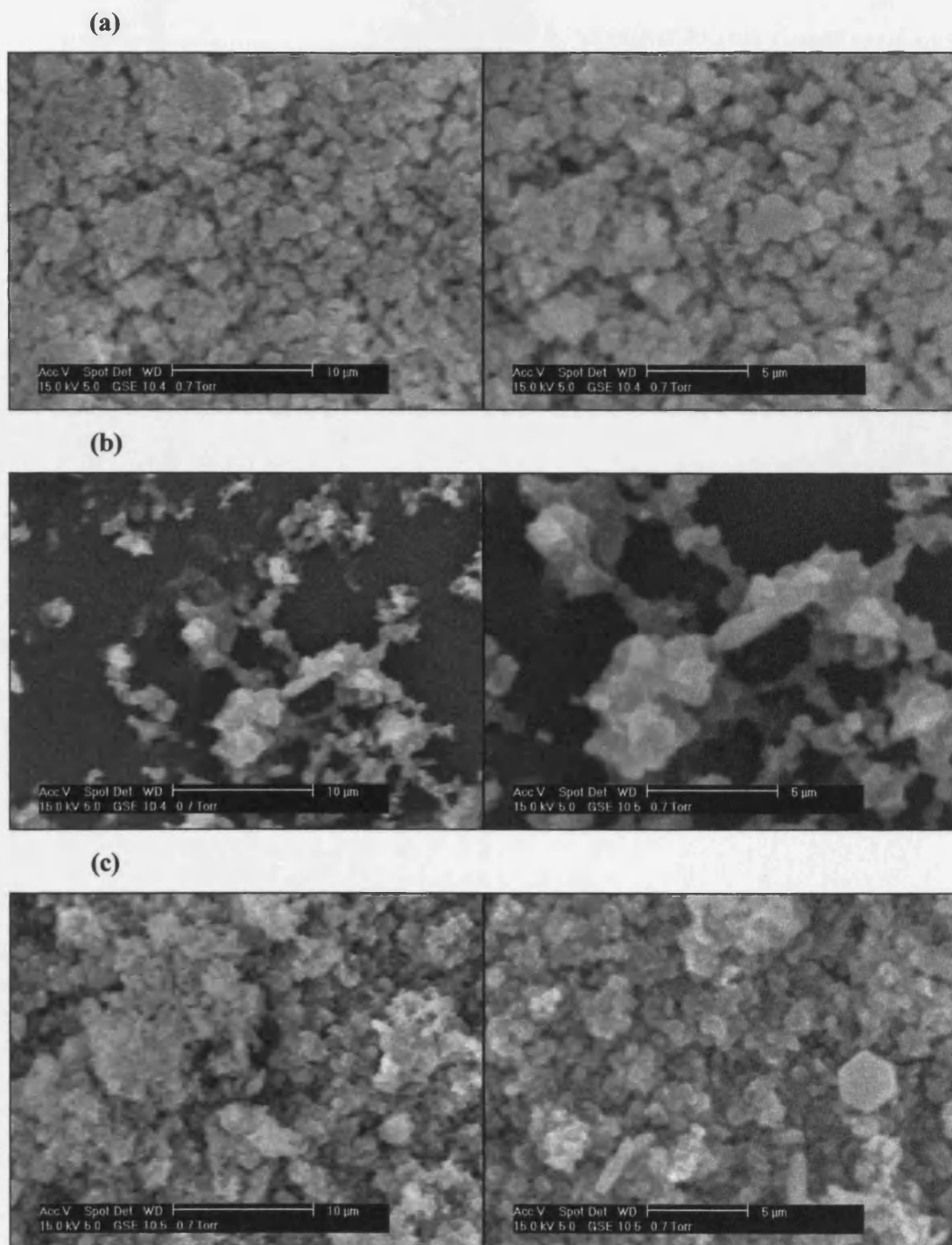
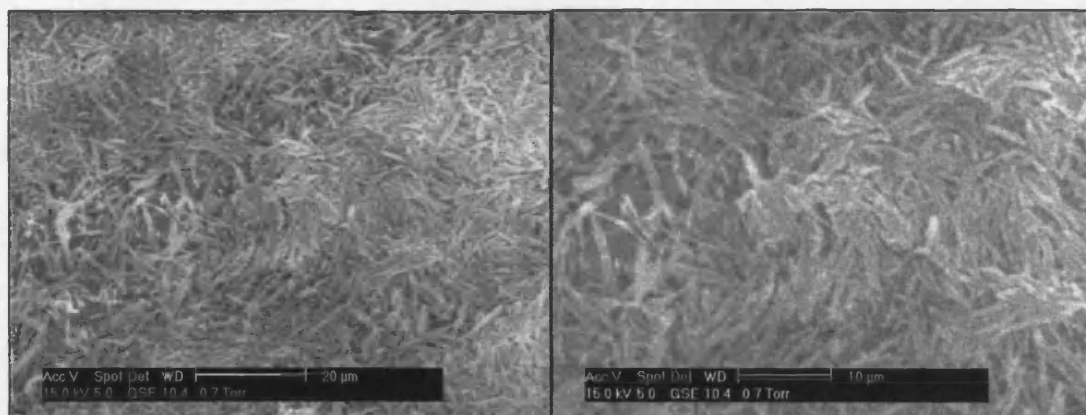


Figure 5.4 SEM images at different magnifications of RESS processed anthracene

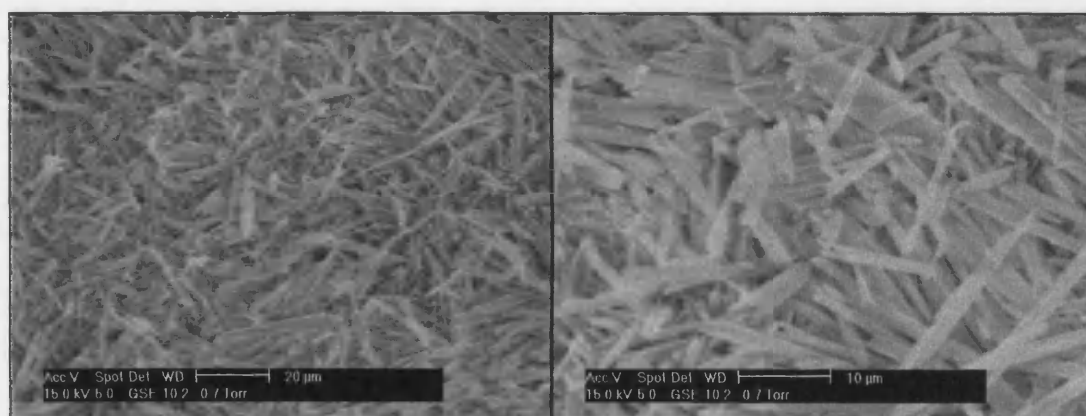
(a) 60 bar (b) 80 bar (c) 200 bar

Particle size range 1 – 2 µm. Note that the amount of material obtained at 80 bar is less than 60 or 200 bar, which corresponds to the region of viscosity minima

(a)



(b)



(c)

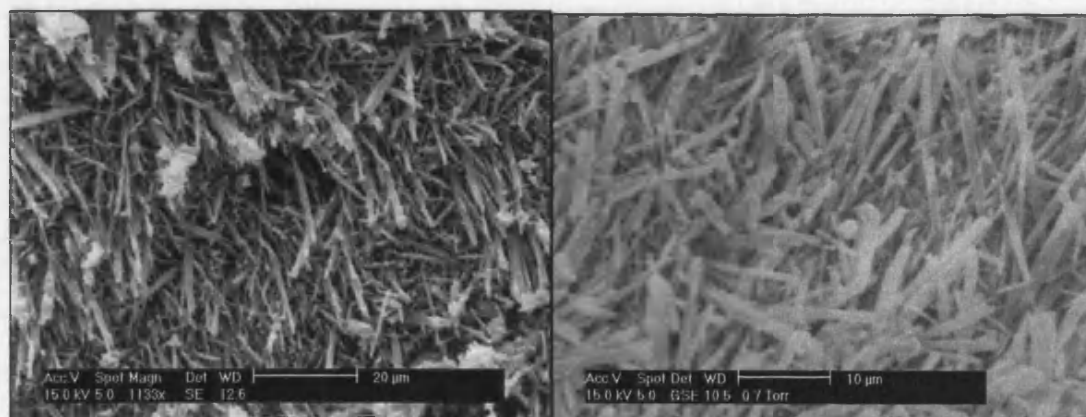
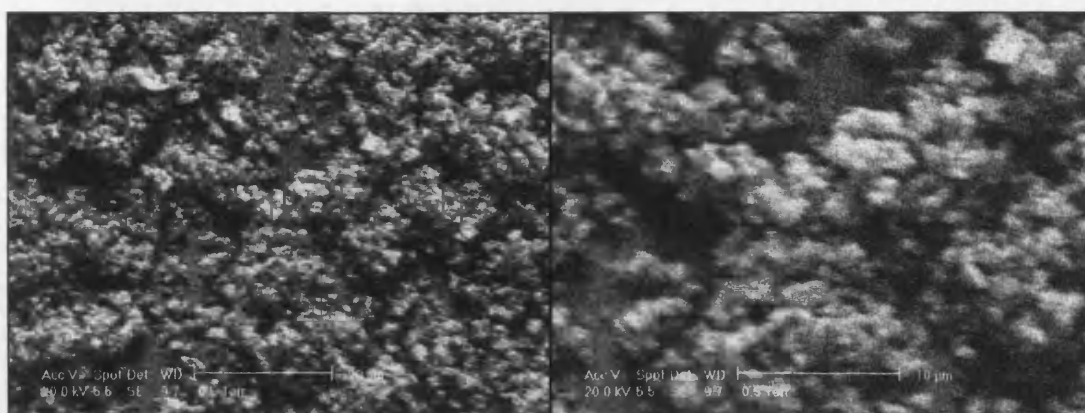


Figure 5.5 SEM images at different magnifications of RESS processed salicylic acid

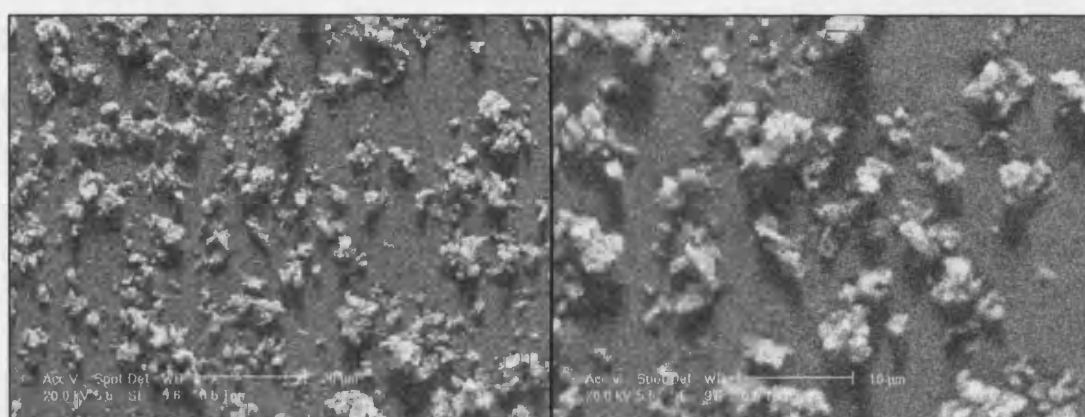
(a) 60 bar (b) 80 bar (c) 200 bar

Particle size ranges from 5 – 20 μm, finer particles are observed at 60 bar

(a)



(b)



(c)

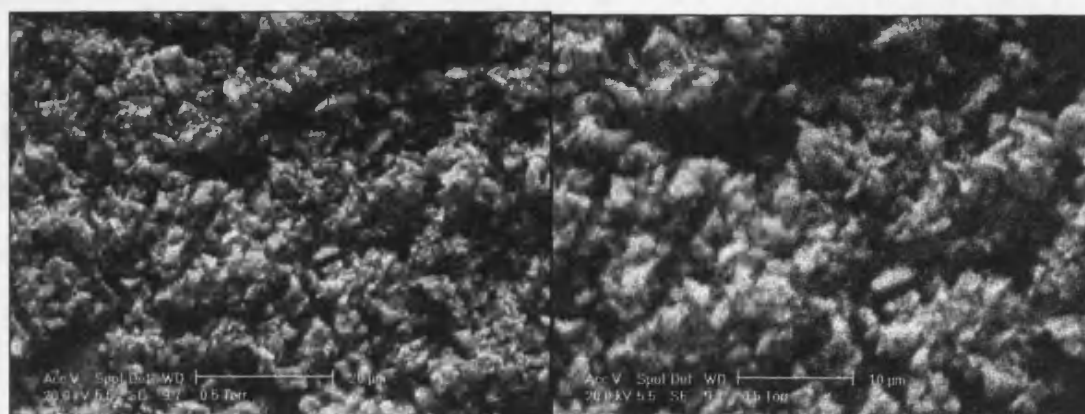


Figure 5.6 SEM images at different magnifications of RESS processed toluic acid

(a) 60 bar (b) 80 bar (c) 200 bar

Amount of material obtained at 80 bar is less than 60 or 200 bar, which corresponds to the region of viscosity minima

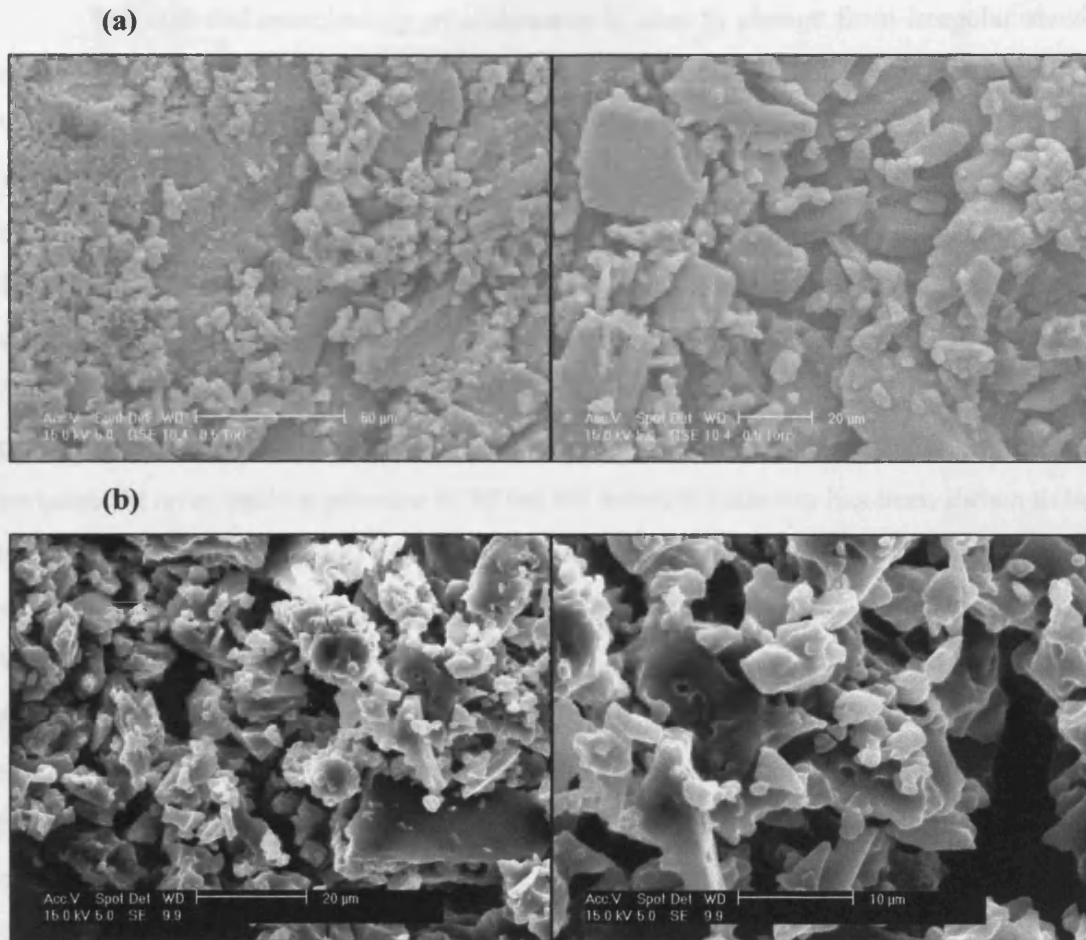


Figure 5.7 SEM images at different magnifications of RESS processed TBABF₄

(a) 100 bar (b) 200 bar

Irregular shaped particles obtain 5 – 20 µm diameter with a high degree of agglomeration present

The size and morphology of anthracene is seen to change from irregular sized plates to regular shaped spheres with a more even size distribution (Figures 5.2(a) and 5.4). Particle agglomeration is present at each pressure investigated, especially at 80 bar where there was a significant reduction in the amount of material collected on the sampling device. This could be attributed to changes in mass transport brought about by the variations in solution viscosity. Equation 5.1 shows how velocity can be related to viscosity. If this idea is applied to the motion of solute particles upon rapid expansion from a solution, it can be argued that solutions of low viscosity will give rise to particles with high velocities. This would result in the trend seen for anthracene particles. At an extraction pressure of 80 bar the solution viscosity has been shown to be much lower than at 60 or 200 bar. The particles will move from the solution with higher velocity and not as much will be collected on the sampling device. Other researchers have reported anthracene precipitated from sc CO₂. Bae and co-workers reported a reduction in mean particle size (approximately 10 µm at 150 bar to 6 µm at 250 bar) and a narrower PSD with increasing extraction pressure.⁵⁰ The morphology of precipitated anthracene particles was noted to be relatively spherical. Subra *et al.* observed tablet shaped particles of size 5 – 20 µm with a slight increase in PSD with increasing pressure.⁵¹ Smaller particles have been produced in the current work (Figure 5.4), approximately 1 – 2 µm in diameter.

Figure 5.3 shows salicylic acid particles obtained from crystallisation from CH₂Cl₂. Comparing these images to those in Figure 5.5 illustrates the advantage that the RESS process has over conventional liquid crystallisation. The particles produced via RESS are much smaller and more uniform in their shape and size distribution, with approximate lengths between 5 and 20 µm (RESS) and 50 and 300 µm (liquid).

Of the compounds examined, salicylic acid exhibits the most distinct alteration in morphology (Figures 5.2(b) and 5.5). Unprocessed salicylic acid is shown to exist as irregular sized blocks, whereas the material obtained via RESS can be described as needles. Comparing salicylic acid particles with extraction pressure, the needles obtained at an extraction pressure of 60 bar appear finer than those at 80 or 200 bar. This could be due to more agglomeration at higher extraction pressures where solubility is higher. Matson and co-workers explained that highly agglomerated particles are characteristic of more concentrated solutions.^{3,5} This is reasonable if particle size is related to the number of solute species experiencing collisions during expansion. It is

also possible that growth processes are more dominant at higher solute concentrations.¹⁷ An increase in extraction pressure from 60 to 200 bar will decrease the solute mole fraction from 0.0026 to 0.00077. Mohamed *et al.* found that increasing naphthalene mole fraction at constant extraction pressure lead to higher nucleation rates and smaller particles.¹⁰ A number of studies have examined precipitation of salicylic acid from sc CO₂.^{12,16} Due to its limited solubility, the salicylic acid mole fraction was lower than in the current work. Reverchon and co-workers found an increase in pressure gave a moderate increase in size and distribution of the needle shaped particles. Length of needles ranged from 5 to 15 μm at 200 bar and up to 50 μm in length at higher pressures.¹² The particle lengths reported in the current study vary from 5 – 10 μm (60 bar) to 20 μm (80 and 200 bar).

Unlike the previous compounds, there are no comparative studies of toluic acid processed by RESS. Figure 5.2(c) shows that unprocessed toluic acid has the smallest particle size of the solutes investigated. After RESS the particles are observed to decrease in size, but no distinct variation in morphology is clear (Figure 5.6). However, the quantity of particles collected can be seen to vary with extraction pressure. At 80 bar there was a significant reduction in the amount of material collected on the sampling device. The reason for this variation is thought to be same as that described for anthracene particles.

As with toluic acid, this is the first reported study to examine the precipitation of TBABF₄ by RESS. Of all the compounds studied, the largest degree of agglomerations can be seen with TBABF₄ particles. The unprocessed particles shown in Figure 5.2(d) can be described as irregular cubes of approximately 150 μm diameter. After processing, much smaller, less well-defined, irregular shaped particles are observed (Figure 5.7). At the two pressures employed (100 and 200 bar) a combination of small irregular particles (5-20 μm) and smooth, flat films are formed.

5.2.2 Slow expansion of Supercritical Solutions (SESS)

In the current work SESS experiments were conducted under the same conditions as RESS experiments with no external heating of the pre-expansion line. Figures 5.8 to 5.10 show SEM images of anthracene, salicylic acid and TBABF₄ produced by slow expansion of supercritical solutions (experimental runs 4-6, 13-15 and 27-28 in Table 5.3). During these experiments it was thought that the precipitated material would have more time to nucleate and result in longer growth times. This would produce particles that are larger and with a more even size distribution than those produced via RESS. This was seen in the work of Tai and Cheng, where experiments using RESS and SESS were conducted with sc CO₂. Larger naphthalene crystals were obtained with SESS as the nuclei were subject to growth for a longer period of time.⁴³

It was thought that no external heating of pre-expansion line would mean that the fluid has a higher density and may be liquid or sub-critical in the line. This would affect material solubility and particles produced upon expansion. At lower fluid temperatures a two-phase gas/liquid region is crossed during expansion and droplets are produced. Premature nucleation brought about by Joule-Thomson cooling could occur in the line under these conditions. This is also true for the aforementioned RESS experiments. However, with SESS the material will be under these conditions for a longer period of time.

Figure 5.8 shows anthracene at 60, 80 and 200 bar. The particles produced at 60 bar are smaller but more agglomerated than those at 80 bar, which appear to be large irregular plates. At 200 bar, more evenly distributed spherical particles are produced approximately 1-2 μm in diameter. Comparing these images with those for the RESS process (Figure 5.4) show particle shapes and sizes to be more even when the material has been produced by RESS, although there does not appear to be a distinct difference in particle size.

A combination of salicylic acid particles with different sizes was produced by SESS (Figure 5.9). At 60 and 80 bar, long needles approximately 20 μm in length and short oblongs about 5 μm in length are observed. At 200 bar the particles are more evenly distributed and 5 - 10 μm long oblongs are present. These are different to the needle-shaped particles obtained by RESS, (Figure 5.5) which may be due to early nucleation within the pre-expansion line.

Chapter Five – Solute Precipitation from Supercritical Solutions

Figure 5.10 shows TBABF₄ particles produced by SESS. The shape and size distribution of these particles are more even than seen by RESS in Figure 5.7. Although the material still appears to be agglomerated, the smooth flat film particle type is absent.

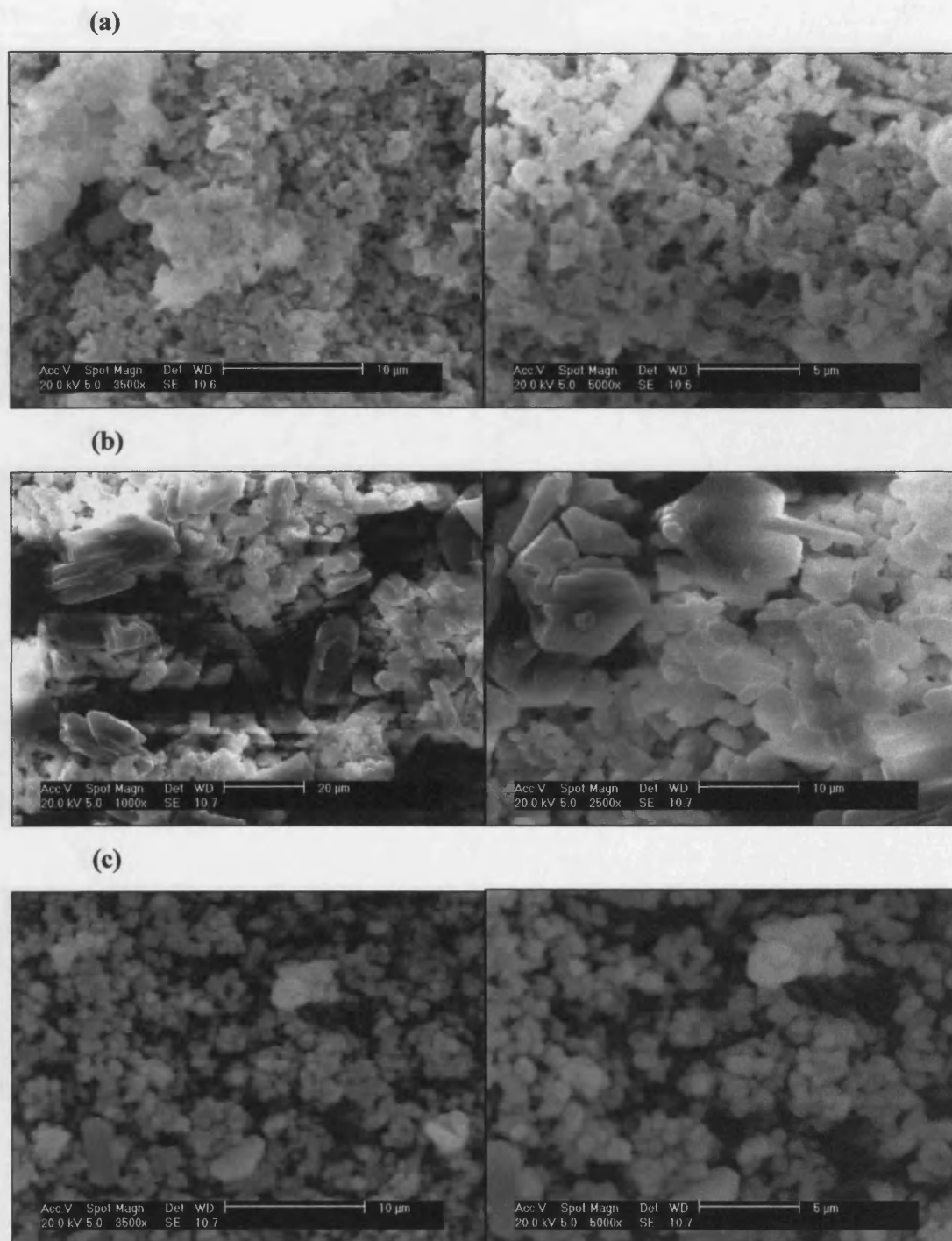


Figure 5.8 SEM images at different magnifications of SESS processed anthracene

(a) 60 bar (b) 80 bar (c) 200 bar

A larger degree of agglomeration is observed from 60 and 80 bar when compared to RESS process (Figure 5.4) and smaller particles with even shape have been obtained from 200 bar (1 – 2 µm)

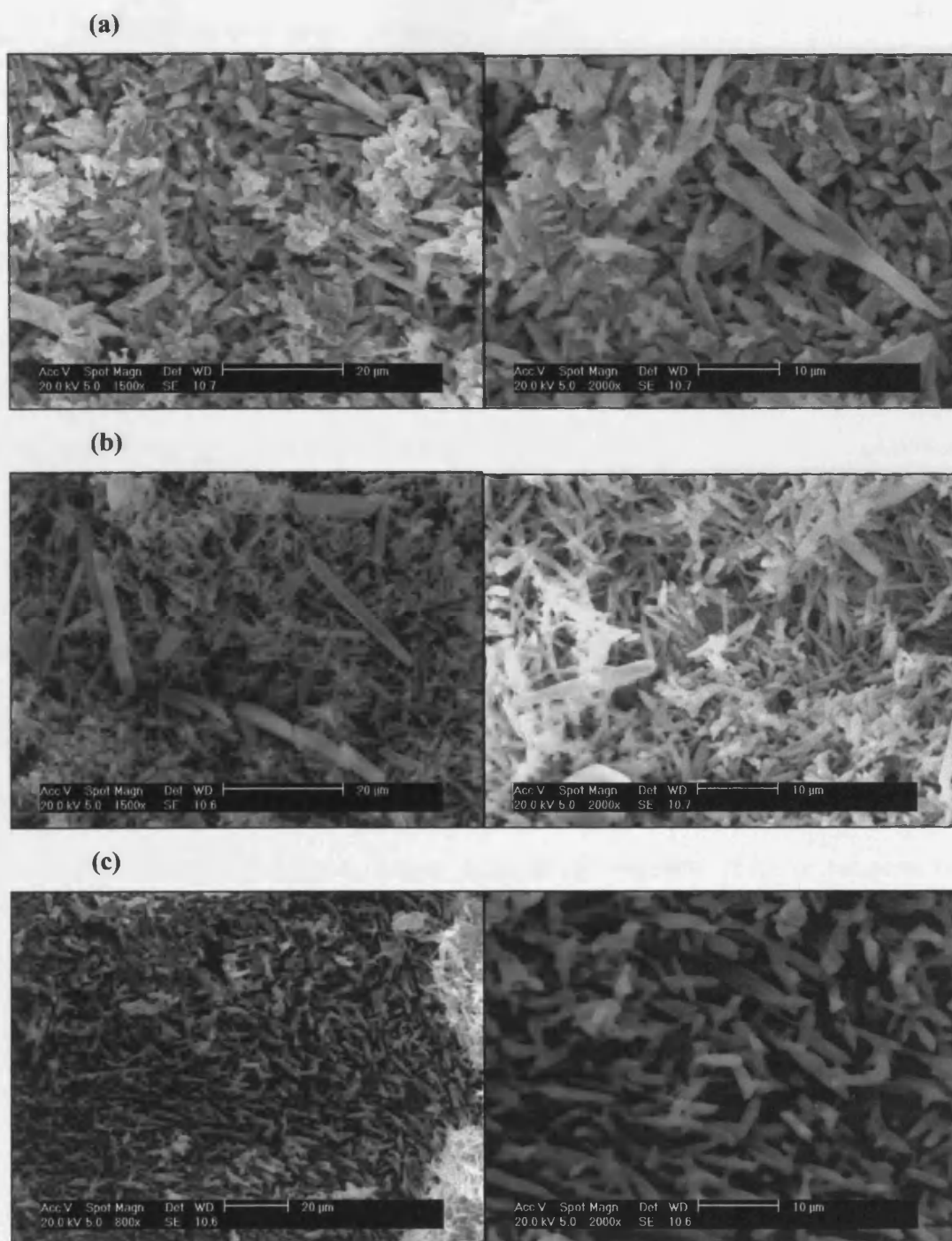


Figure 5.9 SEM images at different magnifications of SESS processed salicylic acid

(a) 60 bar (b) 80 bar (c) 200 bar

The observed variation in particle size and shape is thought to be caused by nucleation in the pre-expansion line. Note that more even sized particles were obtained from 200 bar

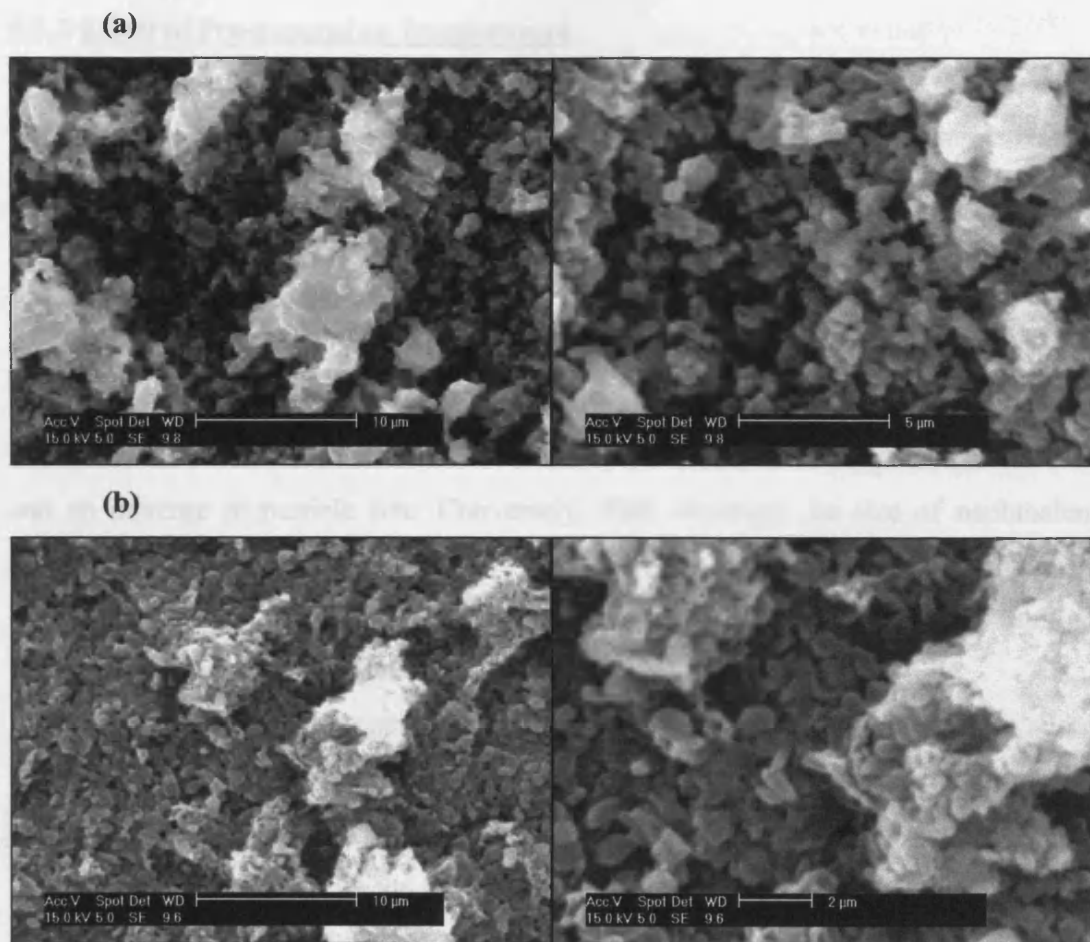


Figure 5.10 SEM images at different magnifications of SESS processed TBABF₄

(a) 100 bar (b) 200 bar

Compared to RESS material (Figure 5.7) size and shape are more even but the solute still agglomerates

5.2.3 Effect of Pre-expansion Temperature

The pre-expansion temperature is controlled in the region between the extraction unit and the expansion vessel. In the literature the dependence of particle characteristics on pre-expansion temperature is still unclear. Contradicting results have been reported, although this has commonly been attributed to the conditions employed. In the work of Mohamed *et al.*¹⁰ and Lui and Nagahama,¹⁷ an increase in pre-expansion temperature brought about an increase in the size of naphthalene particles. These studies were performed outside the retrograde region where an increase in pre-expansion temperature leads to a sub-saturated solution. This results in a decrease in the supersaturation ratio and an increase in particle size. Conversely, Türk observed the size of naphthalene particles to decrease with increasing pre-expansion temperature.¹⁹ This was thought to be due to the unsaturated solution preventing early particle formation in the capillary nozzle allowing shorter nucleation and growth times.

In studies of other organic materials similar ideas have been proposed. In a later publication Türk reported smaller benzoic acid particles were formed at lower pre-expansion temperatures and attributed this to higher fluid density and higher mass flow rates through the nozzle.²¹ In the study of Domingo *et al.* variations in particle size with pre-expansion temperature were explained in terms of the influence of temperature on the initial point of nucleation. Larger particles are expected at lower temperatures because nucleation starts earlier along the nozzle.¹⁶ Hortaçsu *et al.* also observed a decrease in the particle size of ibuprofen with increasing pre-expansion temperature.²³ Conversely, Reverchon and co-workers observed larger salicylic acid particles with higher pre-expansion temperatures.¹² In a later study it was observed that griseofulvin particles with different morphologies were produced according to the pre-expansion temperature.¹³ At high temperatures, where quasispherical particles were produced, the findings were interpreted as precipitation in the free-jet region and, at lower temperatures, liquid droplets were thought to form in the nozzle and produce long needle shaped particles.

Figures 5.4 to 5.7 display SEM images from the experiment runs 1-3, 10-12, 19-21 and 25-26 in which the pre-expansion line was not externally heated. In order to prevent plugging of material in the pre-expansion line it is recommended that the line should be heated to at least 50 °C higher than the temperature of the extraction cell.⁴⁴ In this work the extraction cell is kept at a constant temperature of 90 °C, hence in

Chapter Five – Solute Precipitation from Supercritical Solutions

experiment runs 7-9, 16-18, 22-24 and 29-30 the pre-expansion line is heated to 140 °C. Thermal decomposition of the compounds should not occur under these conditions.

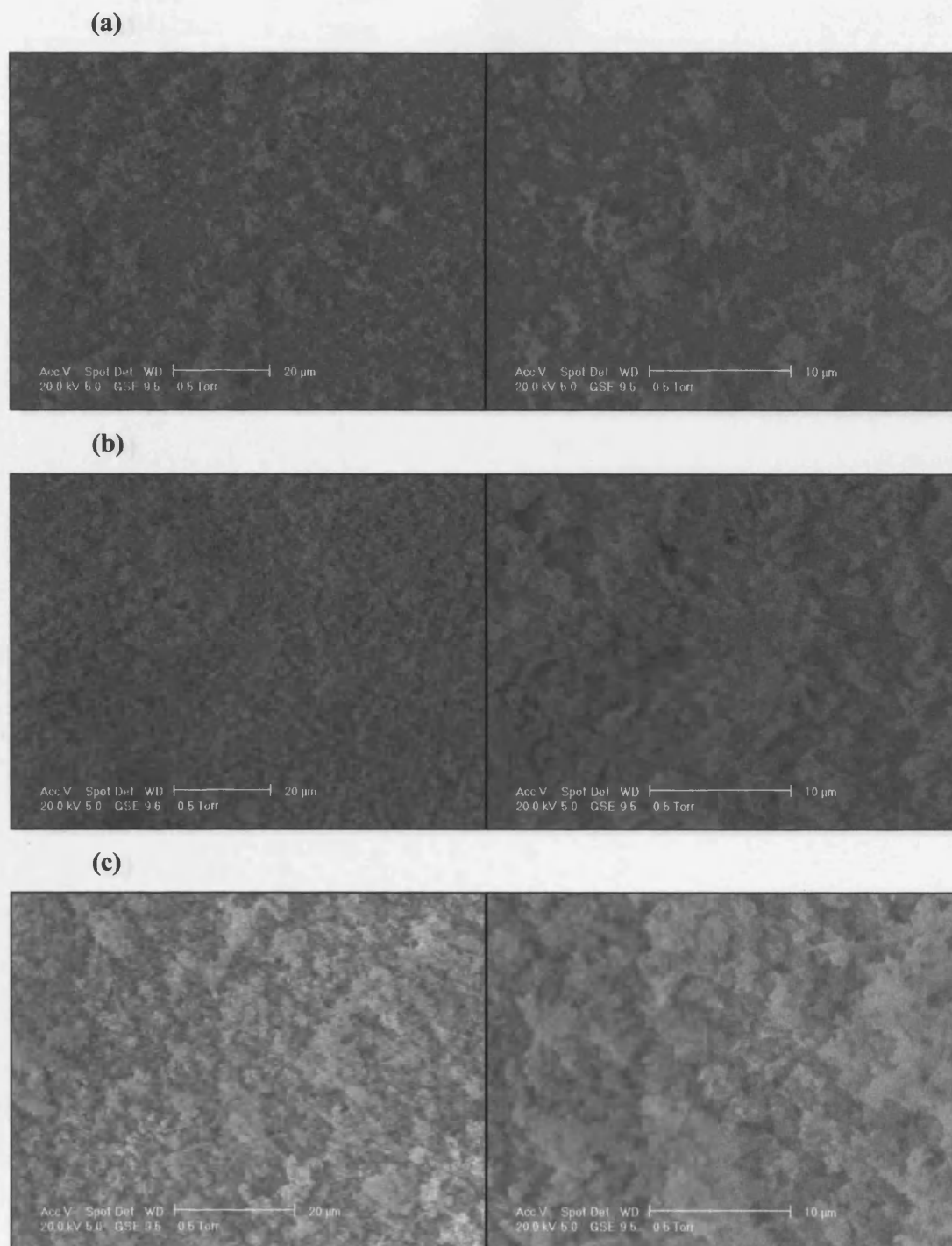
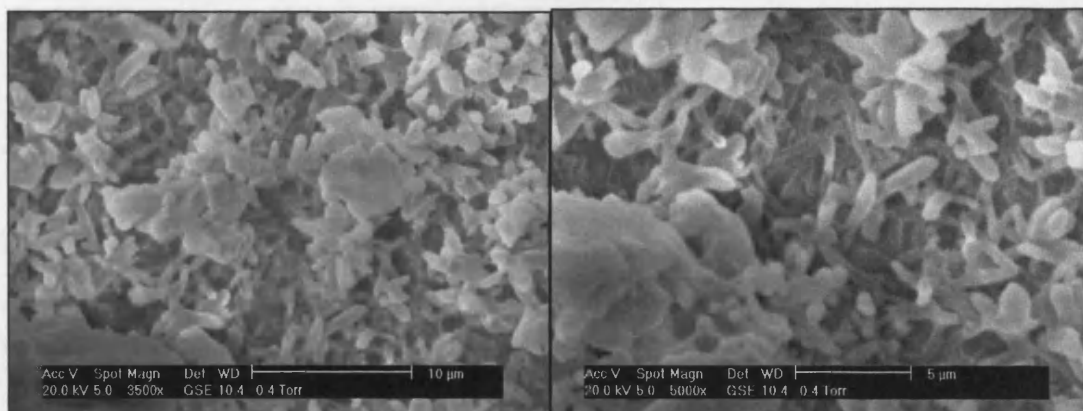


Figure 5.11 SEM images at different magnifications of RESS processed anthracene with pre-expansion temperature of 140 °C

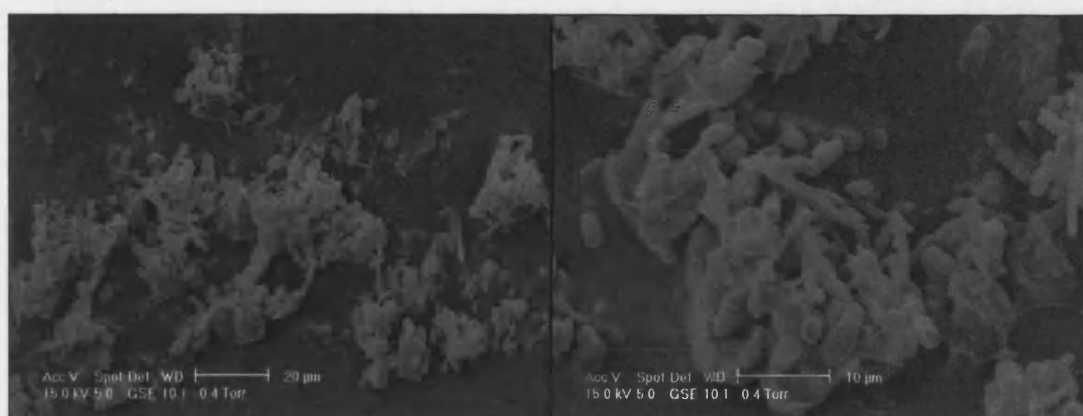
(a) 60 bar (b) 80 bar (c) 200 bar

Considerably smaller particles have been obtained when compared those from the to unheated pre-expansion line experiment (Figure 5.4)

(a)



(b)



(c)

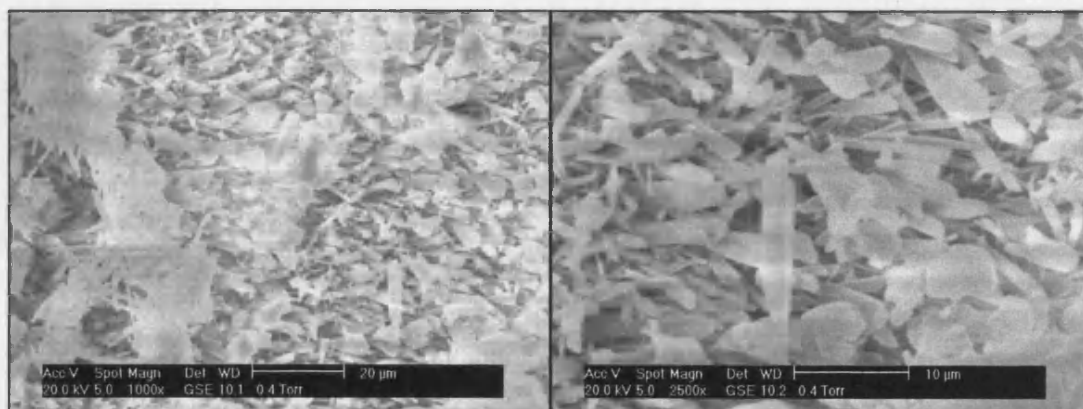


Figure 5.12 SEM images at different magnifications of RESS processed salicylic acid with pre-expansion temperature of 140 °C

(a) 60 bar (b) 80 bar (c) 200 bar

Particle size ranges from 2.5 – 10 µm. Note that the amount of material obtained at 80 bar is less than 60 or 200 bar, which corresponds to the region of viscosity minima

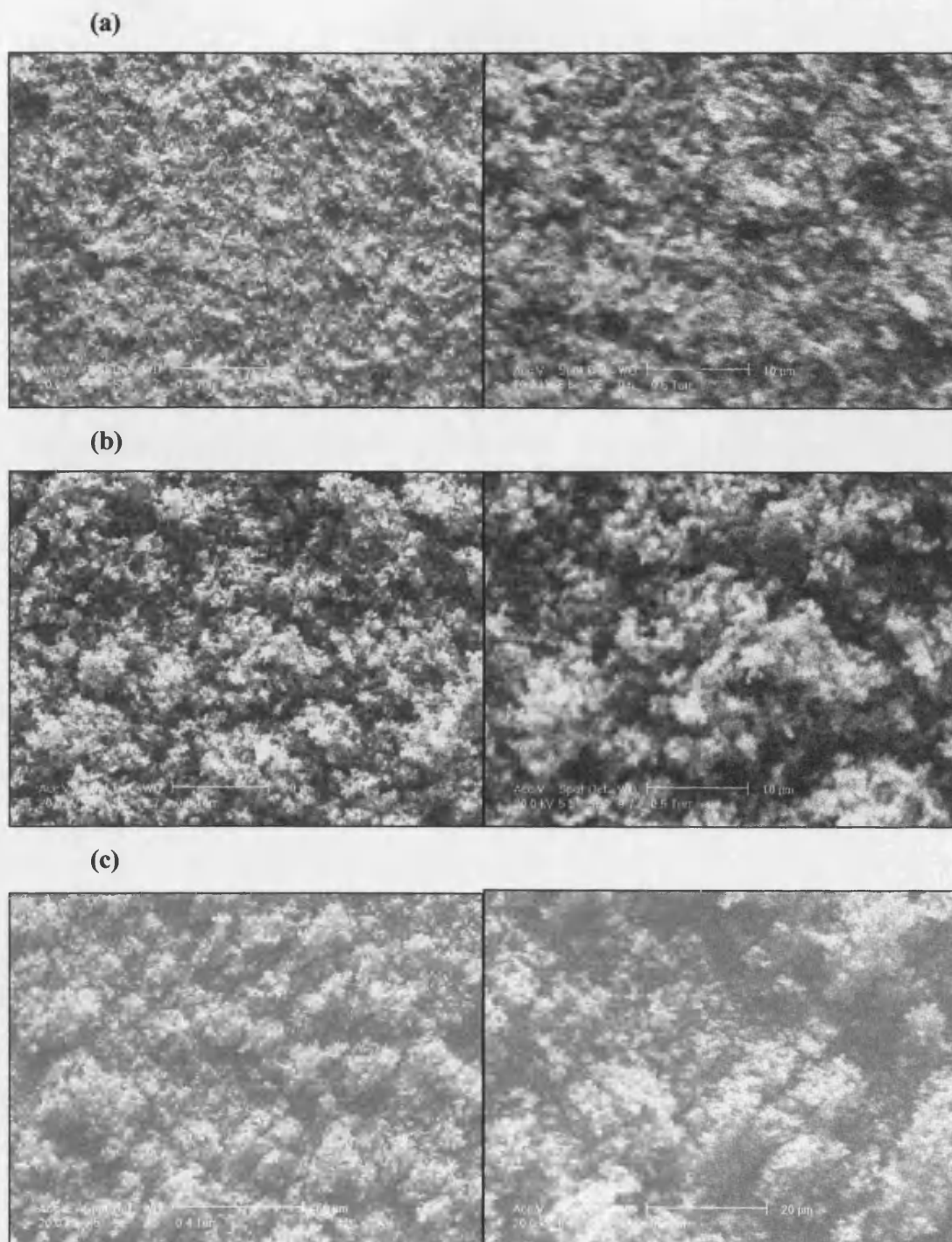
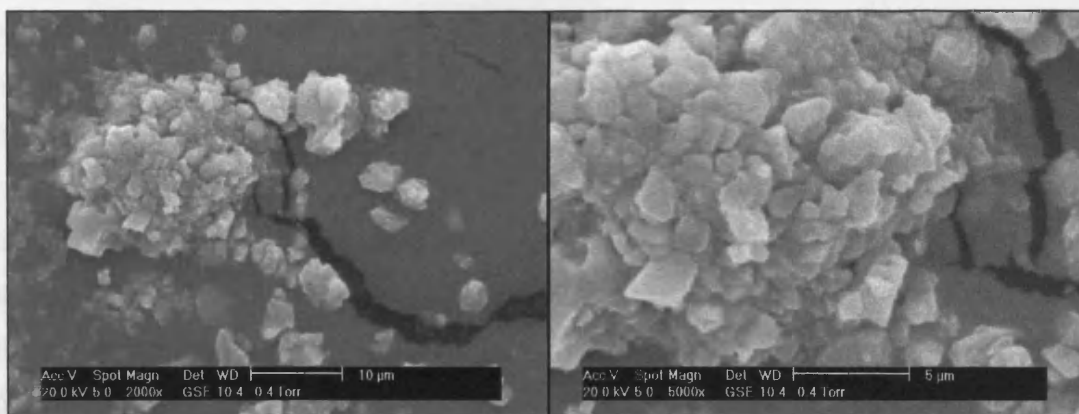


Figure 5.13 SEM images at different magnifications of RESS processed toluic acid with pre-expansion temperature of 140 °C
(a) 60 bar (b) 80 bar (c) 200 bar

No significant variations in particle size or shape have been observed

(a)



(b)

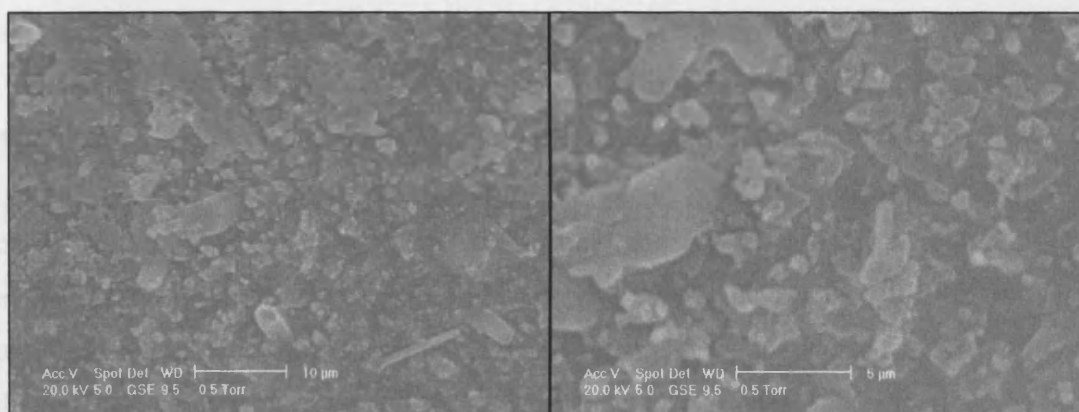


Figure 5.14 SEM images at different magnifications of RESS processed TBABF₄ with pre-expansion temperature of 140 °C

(a) 100 bar (b) 200 bar

Less material has been collected than observed for no heating of pre-expansion line (Figure 5.7)

Figure 5.11 to 5.13 show SEM images of anthracene, salicylic acid and toluic acid at extraction pressures of 60, 80 and 200 bar, respectively. Figure 5.14 shows TBABF₄ at 100 and 200 bar. Comparing these images with Figures 5.4 to 5.7 illustrates the effect of heating the pre-expansion line at each pressure.

Anthracene is shown in Figures 5.4 and 5.11. The particles collected under controlled pre-expansion temperature (Figure 5.11) are smaller at each pressure than those produced when the pre-expansion line is not heated. This is reasonable as heating the pre-expansion line ensures the solution is homogeneous and in the sc region until it passes through the orifice into the expansion chamber, preventing premature nucleation and growth of material in the line. Previous studies have also reported a reduction in particle size and narrower PSD with high pre-expansion temperatures.^{49,50}

The results for salicylic acid are shown in Figures 5.5 and 5.12. This material exhibits the largest change in size and morphology with an increase in pre-expansion temperature. At each extraction pressure under ambient pre-extraction conditions, needle shaped particles are produced with a small size variation, between 5 and 20 μm in length. When the pre-extraction temperature is maintained at 140 °C the particles produced are smaller (approximately 2.5 – 10 μm) and oblong in shape. This is more distinct at 60 bar, whereas at 200 bar a combination of oblong and longer needle-like particles are observed. In both cases an even coverage of the sampling device is obtained, however at 80 bar the quantity collected is significantly less and the average particle shape is less defined due to more agglomeration. The reason for the reduction in particle size is the same as that for anthracene. The variation in quantity of material collected with extraction pressure is thought to be due to the low viscosity of the solution under these conditions. As explained earlier the low viscosity allows the solution to move with higher velocity. The high velocity means material is lost and does not have sufficient time to nucleate. Previous authors have also examined the effect of pre-expansion temperature with salicylic acid. Reverchon *et al.* monitored the conditions of the expansion jet and found an increase in particle size was brought about by an increase in pre-extraction temperature when the liquid phase was not crossed.¹² Conversely, a slight decrease in particle size was observed (from 10 – 20 μm to 5 – 15 μm) with increasing pre-expansion temperature when liquid phase crossing conditions were realised. In the work by Domingo, Berends and van Rosmalen, the spread of salicylic acid crystals was found to be too large to prove any effect of pre-expansion temperature.¹⁶ The key difference between these two studies is the type of nozzle that

was employed. A capillary nozzle with aspect ratio of 5 was used by Domingo *et al.* and salicylic acid crystals 2 – 5 μm in size were observed. The aspect ratio for the nozzle employed by Reverchon and co-workers was 20. Consequently larger particles were observed.

Under conditions of controlled pre-expansion temperature, toluic acid particles do not appear to be significantly altered in shape or size and neither does the amount of material collected appear to vary with extraction pressure.

The TBABF_4 particles formed with a pre-expansion temperature of 140 $^\circ\text{C}$ (Figure 5.14) are sparser than with no control over pre-expansion temperature (Figure 5.7). At 100 bar the particles are fairly regular in size and grouped together in areas on the sampling device. An increase in pressure to 200 bar results in less regular shaped particles. The reduction in the quantity of material collected signifies the high kinetic energy imparted to the particles upon expansion and they do not have sufficient time to nucleate before reaching the sampling device. Furthermore TBABF_4 exhibits a high solubility in CH_2F_2 and has been shown to form a dense liquid phase under low pressures.

5.2.4 Effect of Supercritical Solvent

As mentioned earlier the majority of RESS studies have employed sc CO₂. Of the compounds examined in the current work only anthracene has sufficient solubility in sc CO₂ without the addition of a co-solvent. Figure 5.15 shows SEM image of anthracene precipitated from sc CO₂. The conditions used were similar to experimental runs 7-9 in Table 5.3 and can be directly compared to Figure 5.11(c) as shown in Figure 5.16. Anthracene particles precipitated from sc CH₂F₂ (Figure 5.16(b)) are smaller, more uniform and less agglomerated than those precipitated from sc CO₂. Under the experimental conditions (90 °C, 200 bar) the density of each solvent system is different ($\rho(\text{CO}_2)=0.533 \text{ g cm}^{-3}$ $\rho(\text{CH}_2\text{F}_2)=0.825 \text{ g cm}^{-3}$). This indicates that it is not just Joule-Thomson cooling which determines particle morphology and that the solvent also plays a role.

Although other authors have examined the precipitation of salicylic acid from sc CO₂ these experiments were limited by its solubility and cannot be directly compared with the current results. For this reason, 4 % methanol was used in the current work to enhance the solubility of salicylic acid in sc CO₂. After depressurisation the collection vessel was not found to have any observable precipitate and methanol was clearly present on the sample device. Once the methanol had evaporated the sample was imaged by SEM but no salicylic acid precipitate was observed.

Quaternary ammonium salts have been shown to be soluble in sc CO₂ with the addition of co-solvents.⁵² To enhance the solubility of TBABF₄ in sc CO₂ 4 % methanol was added to the solution. After depressurisation, similar observations to those from the salicylic acid experiment were made. The sample device was imaged by SEM and results are shown in Figure 5.17. The images are comparable to Figure 5.14(b) and it is evident that processing TBABF₄ with modified sc CO₂ produces larger particles than with unmodified sc CH₂F₂. This shows that CH₂F₂ can be used to dissolve solutes that unmodified CO₂ cannot.

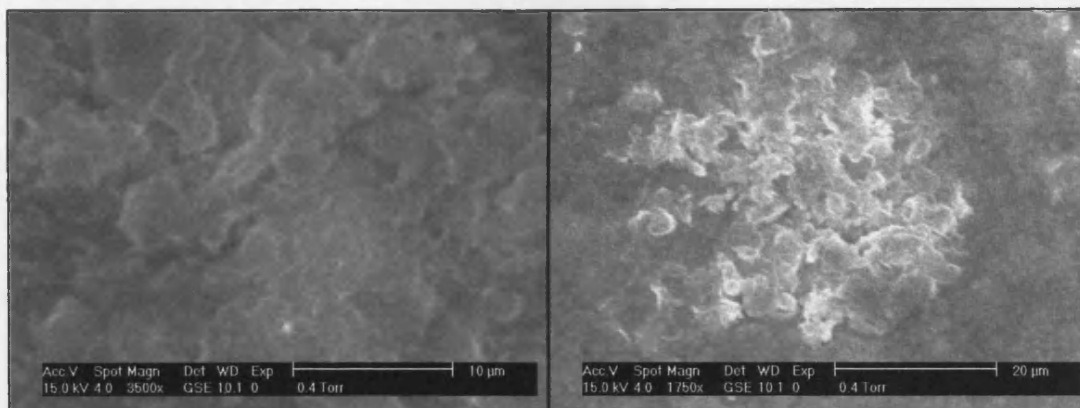


Figure 5.15 SEM images at different magnifications of RESS processed anthracene from CO₂ with pre-expansion temperature of 140 °C and extraction pressure of 200 bar

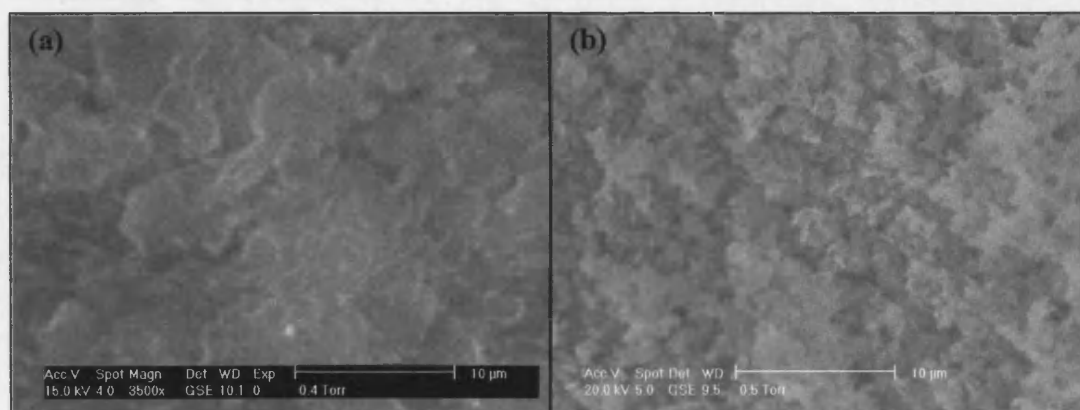


Figure 5.16 SEM images at 10 µm magnification of RESS processed anthracene with pre-expansion temperature of 140 °C and extraction pressure of 200 bar using (a) CO₂ and (b) CH₂F₂. Larger particles have been obtained by processing with CO₂ (left image)

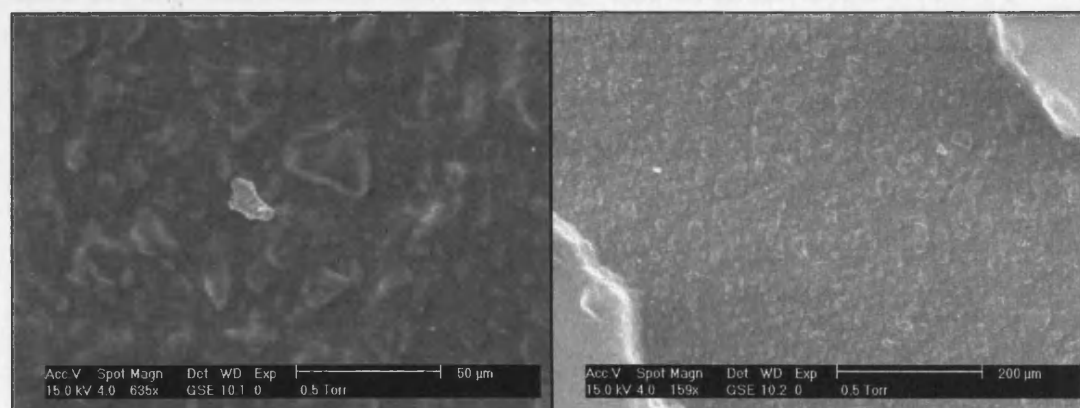


Figure 5.17 SEM images at different magnifications of RESS processed TBABF₄ from CO₂ and 4 % methanol with pre-expansion temperature of 140 °C and extraction pressure of 200 bar. Particles obtained are larger than those from CH₂F₂

5.3 Conclusion

This work has described the first use of sc CH_2F_2 for the precipitation of material using the RESS process. A number of compounds that cannot be processed using sc CO_2 without the addition of modifiers have been successfully precipitated. For anthracene, a different particle size and morphology are obtained using sc CH_2F_2 and CO_2 at the same physical conditions, showing that the solvent affects pre-saturation concentrations of nucleation. Variations in both extraction and expansion parameters are shown to influence size and morphology of the precipitated material and can be explained in terms of solution viscosity and solute aggregation.

It has been found that the viscosity of solutions has a marked effect on morphology and quantity of deposits recovered. In supersonic expansion, material growth is dependent on viscosity. At lower viscosity the fluid moves at a faster velocity and the material has less chance to grow into larger particles. When the solutions are depressurised the fluid travels at a high velocity and the material has high kinetic energy. This is evident when little sample is collected on the sampling device. For example, at 80 bar the solution viscosity has been shown to be significantly lower than at 60 or 200 bar and an amorphous material is obtained.

Control of the pre-expansion temperature has been shown to influence the precipitated material. This is because solution density determines solubility and variations in fluid temperature throughout the system lead to nucleation. Under heated pre-expansion conditions, sufficient thermal energy remains to suppress fluid droplet formation during expansion. This prevents the increase in density and the fluid remains under sc conditions until it reaches the orifice. This means nucleation will not occur in the pre-expansion line. A pre-extraction temperature of 140 °C has been shown to maintain the temperature of the reservoir preventing the material pre-concentrating in the line. Subsequently, smaller particles are observed to be produced.

5.3 References

1. Hannay, J. B.; Hogarth, J. *Proc. R. Soc. London*, **1879**, 29, 324.
2. Krukonis, V. *AIChE. Annual Meeting, San Francisco, USA*, **1984**.
3. Matson, D. W.; Petersen, R. C.; Smith, R. D. *Mat. Lett.* **1986**, 4, 429.
4. Petersen, R. C.; Matson, D. W.; Smith, R. D. *J. Am. Chem. Soc.* **1986**, 108, 2100.
5. Matson, D. W.; Fulton, J. L.; Petersen, R. C.; Smith, R. D. *Ind. Eng. Chem. Res.* **1987**, 26, 2298.
6. Tom, J. W.; Debenedetti, P. G. *J. Aerosol Sci.* **1991**, 22, 555.
7. Subramaniam, B.; Rajewski, R. A.; Snavely, K. *J. Pharm. Sci.* **1997**, 86, 855.
8. Jung, J.; Perrut, M. *J. Supercrit. Fluid.* **2001**, 20, 179.
9. Nagahama, K.; Liu, G.-T. *Proceedings of the 4th meeting on Supercritical Fluids*, **1997**, 43-46.
10. Larson, K. A.; King, M. L. *Biotechnol. Prog.* **1986**, 2, 73.
11. Mohamed, R. S.; Debenedetti, P. G.; Prud'homme, R. K. *AIChE J.* **1989**, 35, 325.
12. Chang, C. J.; Randolph, A. D. *ALChE. J.* **1989**, 35, 1876.
13. Reverchon, E.; Donsi, G.; Gorgoglione, D. *J. Supercrit. Fluid.* **1993**, 6, 241.
14. Reverchon, E.; Della Porta, G.; Taddeo, R.; Pallado, P.; Stassi, A. *Ind. Eng. Chem. Res.* **1995**, 34, 4087.
15. Tom, J. W.; Debenedetti, P. G.; Jerome, R. *J. Supercrit. Fluid.* **1994**, 7, 9.
16. Petersen, R. C.; Matson, D. W.; Smith, R. D. *Polym. Eng. Sci.* **1987**, 27, 1693.
17. Domingo, C.; Berends, E.; van Rosmalen, G. M.; *J. Supercrit. Fluid.* **1997**, 10, 39.
18. Huang, Z.; Sun, G-B.; Chiew, Y. C.; Kawi, S. *Powder Technol.* **2005**, 160, 127.
19. Lui, G. T.; Nagahama, K. *Ind. Eng. Chem. Res.* **1996**, 35, 4626.
20. Türk, M. *J. Supercrit. Fluid.* **1999**, 15, 79.
21. Türk, M.; Hils, P.; Helfgen, B.; Schaber, K.; Martin, H-J.; Wahl, M. A. *J. Supercrit. Fluid.* **2002**, 22, 75.
22. Türk, M.; Helfgen, B.; Hils, P.; Lietzow, R.; Schaber, K. *Part. Part. Syst. Charact.* **2002**, 19, 327.
23. Kayrak, D.; Akman, U.; Hortaçsu, Ö. *J. Supercrit. Fluid.* **2003**, 26, 17.
24. Matson, D. W.; Petersen, R. C.; Smith, R. D. *J. Mater. Sci.* **1987**, 22, 1919.
25. Lele, A. K.; Shine, A. D. *Ind. Eng. Chem. Res.* **1994**, 33, 1476.
26. Debenedetti, P. G. *AIChE J.* **1990**, 36, 1289.
27. Tom, J. W.; Debenedetti, P. G. *Biotechnol. Prog.* **1991**, 7, 403.
28. Benedetti, L.; Bertucco, A.; Pallado, P. *Biotechnol. Bioeng.* **1997**, 53, 232.

29. Kim, J. H.; Paxton, T. E.; Tomasko, D. L. *Biotechnol. Prog.* **1996**, *12*, 650.
30. Yeo, S. D.; Kiran, E. *J. Supercrit. Fluid.* **2005**, *34*, 287.
31. Cooper, A. I. *J. Mater. Chem.* **2000**, *10*, 207.
32. Hay, J. N.; Khan, A. *J. Mater. Sci.* **2002**, *37*, 4743.
33. Cansell, F.; Aymonier, C.; Loppinet-Serani, A. *Curr. Opin. Solid State Mater. Sci.* **2003**, *7*, 331.
34. Tepper, G.; Levit, N. *Ind. Eng. Chem. Res.* **2000**, *39*, 4445.
35. Fulton, J. L.; Deverman, G. S.; Yonker, C. R.; Grate, J. W.; de Young, J.; McLain, J. B. *Polymer*, **2003**, *44*, 3627.
36. Chernyak, Y.; Henon, F.; Harris, R. B.; Gould, R. D.; Franklin, R. K.; Edwards, J. R.; DeSimone, J. M.; Carbonell, R. G. *Ind. Eng. Chem. Res.* **2001**, *40*, 6118.
37. Blasig, A.; Shi, C.; Enick, R. M.; Thies, M. C. *Ind. Eng. Chem. Res.* **2002**, *41*, 4976.
38. Shaub, G. R.; Brennecke, J. F.; McCreedy, M. J. *J. Supercrit. Fluid.* **1995**, *8*, 318.
39. Helfgen, B.; Türk, M.; Schaber, K. *J. Supercrit. Fluid.* **2003**, *26*, 225.
40. Debenedetti, P. G.; Tom, J. W.; Kwauk, X.; Yeo, S. D. *Fluid. Phase. Equil.* **1993**, *82*, 311.
41. Weber, M.; Russell, L. M.; Debenedetti, P. G. *J. Supercrit. Fluid.* **2002**, *23*, 65.
42. Vemavarapu, C.; Mollan, M. J.; Lodaya, M.; Needham, T. E. *Int. J. Pharm.* **2005**, *292*, 1.
43. Helfgen, B.; Türk, M.; Schaber, K. *Powder Technol.* **2000**, *110*, 22.
44. Oum, K.; Harrison, J. J.; Lee, C.; Wild, D. A.; Luther, K.; Lenzer, T. *Phys. Chem. Chem. Phys.* **2003**, *5*, 5467.
45. Abbott, A. P.; Eltringham, W.; Hope, E. G.; Nicola, M. *Green Chem.* **2005**, *7*, 210.
46. Abbott, A. P.; Corr, S.; Durling, N. E.; Hope, E. G. *J. Chem. Eng. Data*, **2002**, *47*, 900.
47. Abbott, A. P.; Corr, S.; Durling, N. E.; Hope, E. G. *J. Phys. Chem. B*, **2003**, *107*, 10628.
48. Tai, C. Y.; Cheng, C. S. *Trans. IChemE*, **1997**, *75*, 228.
49. Abbott, A. P.; Eardley, C. A. *J. Phys. Chem. B*, **2000**, *104*, 9351.
50. Kwauk, H.; Jung, J. W.; Bae, S. Y.; Kumazawa, H. *Korean, J. Chem. Eng.* **2004**, *21*, 1245.

Chapter Five – Solute Precipitation from Supercritical Solutions

51. Subra, P.; Boissinot, P.; Benzaghoul, S. *Proceeding of the 5th Meeting on Supercritical Fluids*, **1998**, 307-312.
52. Niehaus, D.; Philips, M.; Michael, A.; Wightman, R. M. *J. Phys. Chem.* **1989**, *93*, 6232.

Chapter Six

SUMMARY AND FUTURE WORK

6.1 Summary

6.1.1 Probing Clustering in Supercritical Solutions Using Solvatochromic Parameters

6.1.2 Determination of the Viscosity of Supercritical Solutions

6.1.3 Solute Precipitation from Supercritical Solutions

6.2 Future Work

6.2.1 Probing Clustering in Supercritical Solutions

6.2.2 Analysis of the Conductivity and Viscosity of Supercritical Solutions

6.2.3 Particle Size Analysis

6.1 Summary

This study has shown polar solutes significantly affect the physical properties of sc solutions when difluoromethane is used as a solvent. Local solvent properties of polarisability and hydrogen bond donor ability around an indicator molecule have been determined and are found to have implications on bulk solution properties. It has been shown that solution viscosity can be easily measured by employing a piezoelectric quartz crystal over a range of pressures and solvent polarities. A series of rapid expansion of supercritical solutions (RESS) experiments were carried out to determine the influence of these properties when the sc solutions are depressurised.

6.1.1 Probing Solute Clustering in Supercritical Solutions Using Solvatochromic Parameters

It has been demonstrated that the addition of a solid solute to a sc fluid affects the polarisability and hydrogen bond donor properties of the solution. For the first time, the effects of solute polarity and pressure have been examined and the ability of a solute molecule to influence the solvent structure is emphasised.

A model for solvation is proposed and variations in solvent polarisability and hydrogen bond donor ability are explained by considering relative solute-solute and solute-solvent interactions. A decrease in the polarisability parameter and the HBD properties of the solvent is brought about by a solute forming highly self-associated aggregates, which result in a significant reduction in the solvent free density. Conversely, a positive increase in the polarisability parameter with respect to the pure sc fluid indicates the solute molecule is included in the solvation sheath. This behaviour is characteristic of solvent molecule reorientation to complete the solvation sheath of the indicator molecule because association between solute aggregates has been weakened by an increase in pressure.

6.1.2 Determination of the Viscosity of Supercritical Solutions

The first viscosity measurements of solutes in sc difluoromethane over a range of pressures have been reported. A piezoelectric quartz crystal has been shown to be an accurate analytical method for the measurement of solutions viscosity in sc fluids. It has been shown to be a quick, simple and precise *in situ* technique that can be applied to measure the viscosity of polar and non-polar solutes dissolved in sc fluids.

The addition of a non-electrolyte solute has been shown to cause the viscosity to vary significantly from that of the pure sc fluid, with high solution viscosity at pressures close to the critical pressure. The increase in relative viscosity has been modelled using a modified Dole-Jones equation and it is shown that the change in relative viscosity is related to the volume fraction occupied by the solute. A general model is presented for simple solutes whereby the viscosity of a sc solution can be calculated from the molecular volume of the solute and the viscosity of the pure fluid.

Solutions of a quaternary ammonium electrolyte were found to be inhomogeneous below 95 bar. A dense liquid phase was observed to exist under these conditions and is thought to be similar to a gas expanded ionic liquid. Above 95 bar, solutions are homogeneous and the viscosity is found to be significantly greater than that of the pure fluid. This is understood in terms of the structuring of the solvent that is brought about by the solvation of ionic aggregates and the equilibria that occur between neutral and charged species. Voltammetric measurements have been performed and confirm the significant increase in viscosity caused by dissolution of an electrolyte.

6.1.3 Solute Precipitation from Supercritical Solutions

The first RESS experiments employing sc difluoromethane are presented in the current work. Effects of solute polarity, extraction pressure and pre-expansion temperature have been investigated and comparisons are made with RESS from sc carbon dioxide.

It has been found possible to process compounds using sc difluoromethane that would normally require a co-solvent to be present with carbon dioxide. Extraction pressure has been found to influence the amount of material collected for sampling. This is thought to be due to variations in viscosity over the pressure range investigated. Pre-expansion temperature is shown to influence particle morphology. Smaller particles are obtained with a higher pre-expansion temperature. This is because early nucleation in the pre-expansion line is prevented.

6.2 Future Work

6.2.1 Probing Solute Clustering in Supercritical Solutions

The solvatochromic parameters reported in this study show that solutes are capable of forming aggregates in sc solutions and the size of these species vary with solute polarity and pressure. In the future it would be beneficial to perform experiments that can provide information about the cluster size of the species in solution. This will present specific information on solute aggregation and how it is affected by process conditions. There are a number of *in situ* techniques available including neutron scattering, dynamic light scattering or NMR imaging of the sc solution.

6.2.2 Analysis of the Conductivity and Viscosity of Supercritical Solutions

Conductivity is affected by the nature, number and mobility of charge carriers present in solution. Clustering of species in solution will influence conductivity, as larger species will have lower mobility and the number of charge carriers will be reduced. The conductivity of TBABF₄ in sc CH₂F₂ has previously been measured however the solution viscosity was taken to be that of the pure sc fluid.

The viscosity measurements reported in this work show that the addition of TBABF₄ to sc CH₂F₂ is found to significantly increase the solution viscosity. Future research could use this data and re-examine solution conductivity. By combining conductivity and viscosity measurements it would be possible to determine the cluster size of the ionic species in solution.

6.2.3 Particle Size Analysis

The investigation into the precipitation of solutes from sc fluids reported in the present work has demonstrated that the pressure, temperature and solvent affect the morphology of the material collected.

Future work in the area could assess the influence of other process conditions such as nozzle size, geometry and temperature. A range of extraction and pre-expansion temperatures could also be examined. If the precipitated material could be analysed by *in situ* particle size and shape determining methods, quantitative data could be collected. A number of particles from the sample are measured, statistical parameters generated and the mean particle size and distribution can be obtained. Dynamic light scattering is a technique commonly employed to characterise particle size.

Appendix

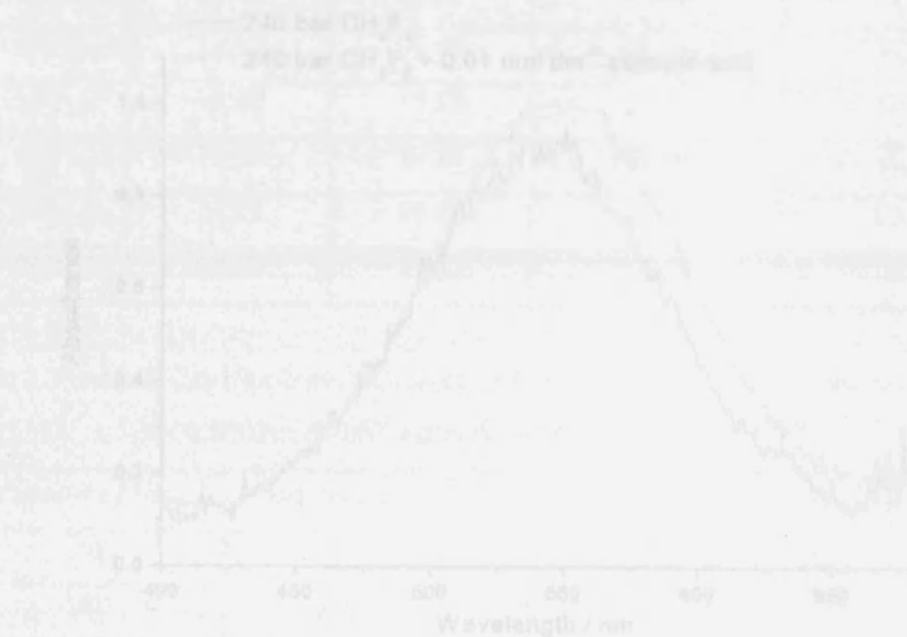


Figure 1. UV-visible absorption spectra of phenol blue in CH_2F_2 taken at 50°C and 240 bar with and without 0.01 mol dm^{-3} salicylic acid. The addition of salicylic acid causes a bathochromic shift in λ_{max} towards longer wavelengths and results in an increase in both ϵ^* and n values.

Table 1. Comparison between experimental and calculated λ_{max} values

Pressure / bar	Nile red expt / kK	Nile red calc / kK	Phenol blue expt / kK	Phenol blue calc / kK
50	21.26	21.26	20.29	20.02
55	20.59	20.59	19.31	19.19
60	20.41	20.41	19.07	18.96
80	20.02	20.05	18.43	18.40
100	20.00	19.99	18.41	18.30
120	19.95	19.95	18.36	18.25
140	19.90	19.89	18.29	18.22
160	19.36	19.37	18.24	18.15
180	19.35	19.34	18.14	18.13
200	19.83	19.82	18.10	18.10

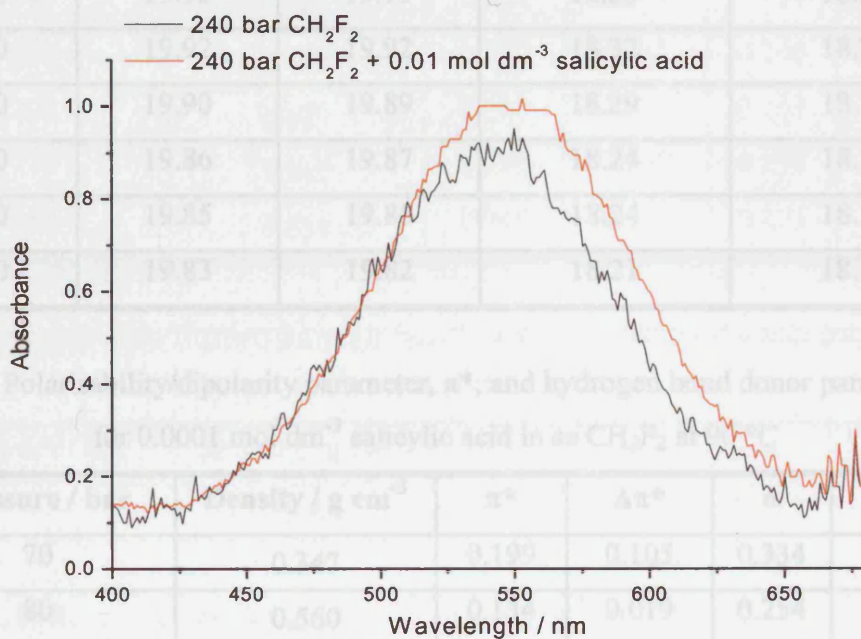


Figure 1. UV-visible absorption spectra of phenol blue in CH_2F_2 taken at $90\text{ }^\circ\text{C}$ and 240 bar with and without 0.01 mol dm^{-3} salicylic acid. The addition of salicylic acid causes a bathochromic shift in λ_{max} towards longer wavelengths and results in an increase in both π^* and α values

Pressure / bar	Density / g cm ⁻³	π^*	$\Delta\pi^*$	α	$\Delta\alpha$
70	0.745	0.199	0.103	0.234	0.111
80	0.560	0.309	0.079	0.254	0.022
100	0.673	0.170	0.037	0.273	0.045
180	0.825	0.309	0.066	0.281	0.047
220	0.847	0.321	0.054	0.278	0.044
240	0.856	0.146	0.077	0.283	0.061

Table 1. Comparison between experimental and calculated v_{\max} values

Pressure / bar	Nile red expt / kK	Nile red calc / kK	Phenol blue expt / kK	Phenol blue calc / kK
50	21.26	21.26	20.29	20.07
55	20.59	20.59	19.31	19.19
60	20.41	20.41	19.07	18.96
80	20.02	20.05	18.43	18.40
100	20.00	19.99	18.41	18.30
120	19.95	19.95	18.36	18.25
140	19.92	19.92	18.32	18.22
160	19.90	19.89	18.29	18.19
180	19.86	19.87	18.24	18.15
200	19.85	19.85	18.24	18.13
220	19.83	19.82	18.21	18.10

Table 2. Polarisability/dipolarity parameter, π^* , and hydrogen bond donor parameter, α , for 0.0001 mol dm⁻³ salicylic acid in sc CH₂F₂ at 90 °C

Pressure / bar	Density / g cm ⁻³	π^*	$\Delta\pi^*$	α	$\Delta\alpha$
70	0.347	0.199	0.105	0.334	0.111
80	0.560	0.134	0.019	0.254	0.032
100	0.673	0.170	0.037	0.273	0.045
120	0.724	0.221	0.049	0.284	0.051
140	0.758	0.252	0.059	0.288	0.055
160	0.785	0.252	0.045	0.271	0.037
180	0.807	0.298	0.065	0.284	0.054
200	0.825	0.309	0.066	0.281	0.047
220	0.842	0.321	0.064	0.278	0.044
240	0.856	0.346	0.077	0.283	0.061

Table 3. Polarisability/dipolarity parameter, π^* , and hydrogen bond donor parameter, α , for 0.0001 mol dm⁻³ *p*-toluic acid in sc CH₂F₂ at 90 °C

Pressure / bar	Density / g cm ⁻³	π^*	$\Delta\pi^*$	α	$\Delta\alpha$
70	0.347	0.211	0.117	0.402	0.179
80	0.560	0.134	0.019	0.269	0.047
100	0.673	0.175	0.041	0.283	0.055
120	0.724	0.186	0.014	0.277	0.044
140	0.758	0.212	0.019	0.268	0.035
160	0.785	0.207	-0.00065	0.238	0.005
180	0.807	0.250	0.017	0.246	0.016
200	0.825	0.282	0.039	0.263	0.028
220	0.842	0.296	0.039	0.259	0.025
240	0.856	0.340	0.072	0.273	0.051

Table 4. Polarisability/dipolarity parameter, π^* , and hydrogen bond donor parameter, α , for 0.0001 mol dm⁻³ naphthalene in sc CH₂F₂ at 90 °C

Pressure / bar	Density / g cm ⁻³	π^*	$\Delta\pi^*$	α	$\Delta\alpha$
70	0.347	-0.009	-0.103	0.176	-0.047
80	0.560	-0.0007	-0.116	0.152	-0.070
100	0.673	0.074	-0.060	0.183	-0.045
120	0.724	0.101	-0.071	0.189	-0.044
140	0.758	0.197	0.003	0.250	0.016
160	0.785	0.237	0.029	0.267	0.033
180	0.807	0.285	0.052	0.290	0.059
200	0.825	0.307	0.064	0.293	0.059
220	0.842	0.336	0.079	0.305	0.071
240	0.856	0.349	0.081	0.298	0.076

Table 5. Actual and relative viscosity for 0.001 mol dm⁻³ salicylic acid in sc CH₂F₂ at 90 °C

Pressure / bar	Density / g cm ⁻³	Viscosity / x 10 ⁻³ g cm ² s ⁻¹	Relative viscosity
60	0.200	0.766	3.71
65	0.252	0.760	3.32
70	0.347	0.512	1.83
75	0.483	0.453	1.21
80	0.561	0.390	0.88
85	0.603	0.465	0.96
90	0.632	0.469	0.91
95	0.655	0.478	0.88
100	0.673	0.439	0.78
120	0.724	0.523	0.83
140	0.759	0.598	0.88
160	0.785	0.654	0.91
180	0.807	0.700	0.93
200	0.826	0.768	0.98

Table 6. Actual and relative viscosity for 0.001 mol dm⁻³ *p*-toluic acid in sc CH₂F₂ at 90 °C

Pressure / bar	Density / g cm ⁻³	Viscosity / x 10 ⁻³ g cm ² s ⁻¹	Relative viscosity
60	0.200	0.517	2.51
65	0.252	0.505	2.21
70	0.347	0.466	1.67
75	0.483	0.352	0.93
80	0.561	0.317	0.71
85	0.603	0.410	0.84
90	0.632	0.412	0.80
95	0.654	0.419	0.77
100	0.673	0.464	0.82
120	0.701	0.559	0.89
140	0.724	0.637	0.94
160	0.743	0.6578	0.92
180	0.759	0.717	0.95
200	0.785	0.767	0.98

Table 7. Actual and relative viscosity for 0.001 mol dm⁻³ naphthalene in sc CH₂F₂ at 90 °C

Pressure / bar	Density / g cm⁻³	Viscosity / x 10⁻³ g cm² s⁻¹	Relative viscosity
60	0.200	0.532	2.58
65	0.252	0.497	2.16
70	0.347	0.495	1.77
75	0.483	0.451	1.20
80	0.561	0.443	1.00
85	0.603	0.418	0.86
90	0.632	0.428	0.82
95	0.655	0.474	0.88
100	0.673	0.471	0.84
120	0.724	0.516	0.82
140	0.759	0.579	0.86
160	0.785	0.638	0.89
180	0.807	0.719	0.95
200	0.826	0.801	1.02

Table 8. Actual and relative viscosity for 0.01 mol dm⁻³ salicylic acid in sc CH₂F₂ at 90 °C

Pressure / bar	Density / g cm ⁻³	Viscosity / x 10 ⁻³ g cm ² s ⁻¹	Relative viscosity
60	0.201	0.762	3.69
65	0.254	0.757	3.30
70	0.348	0.577	2.06
75	0.484	0.452	1.20
80	0.562	0.398	0.90
85	0.604	0.410	0.84
90	0.634	0.441	0.85
95	0.656	0.466	0.86
100	0.674	0.473	0.84
120	0.725	0.548	0.87
140	0.760	0.597	0.88
160	0.786	0.653	0.91
180	0.808	0.714	0.95
200	0.827	0.780	0.99

Table 9. Actual and relative viscosity for 0.01 mol dm⁻³ *p*-toluic acid in sc CH₂F₂ at 90 °C

Pressure / bar	Density / g cm ⁻³	Viscosity / x 10 ⁻³ g cm ² s ⁻¹	Relative viscosity
60	0.201	0.588	2.85
65	0.254	0.570	2.48
70	0.348	0.555	1.98
75	0.484	0.459	1.22
80	0.562	0.429	0.97
85	0.604	0.458	0.94
90	0.633	0.510	0.99
95	0.656	0.530	0.98
100	0.674	0.569	1.01
120	0.703	0.588	0.93
140	0.725	0.639	0.94
160	0.744	0.710	0.99
180	0.760	0.781	1.03
200	0.786	0.803	1.02

Table 10. Actual and relative viscosity for 0.01 mol dm⁻³ naphthalene in sc CH₂F₂ at 90 °C

Pressure / bar	Density / g cm ⁻³	Viscosity / x 10 ⁻³ g cm ² s ⁻¹	Relative viscosity
60	0.201	0.532	2.58
65	0.254	0.495	2.16
70	0.348	0.463	1.66
75	0.484	0.450	1.20
80	0.562	0.425	0.95
85	0.604	0.471	0.97
90	0.633	0.493	0.95
95	0.656	0.507	0.94
100	0.674	0.524	0.93
120	0.725	0.568	0.91
140	0.760	0.661	0.98
160	0.786	0.688	0.96
180	0.808	0.78	1.04
200	0.827	0.842	1.07

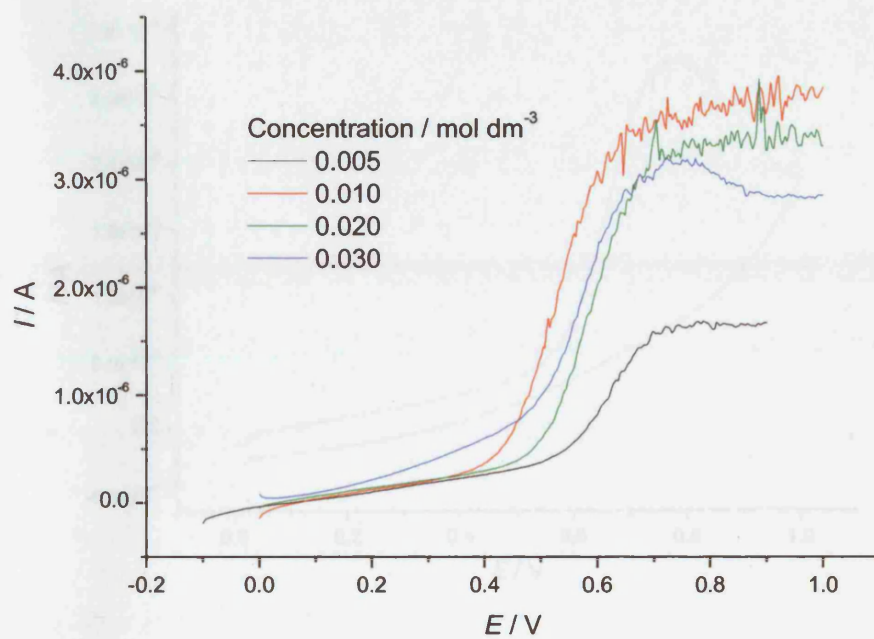


Figure 2. Voltammetric response of ferrocene at a 1 mm diameter Pt disc electrode in sc CH_2F_2 at 90 °C as a function of TBABF_4 concentration at 260 bar

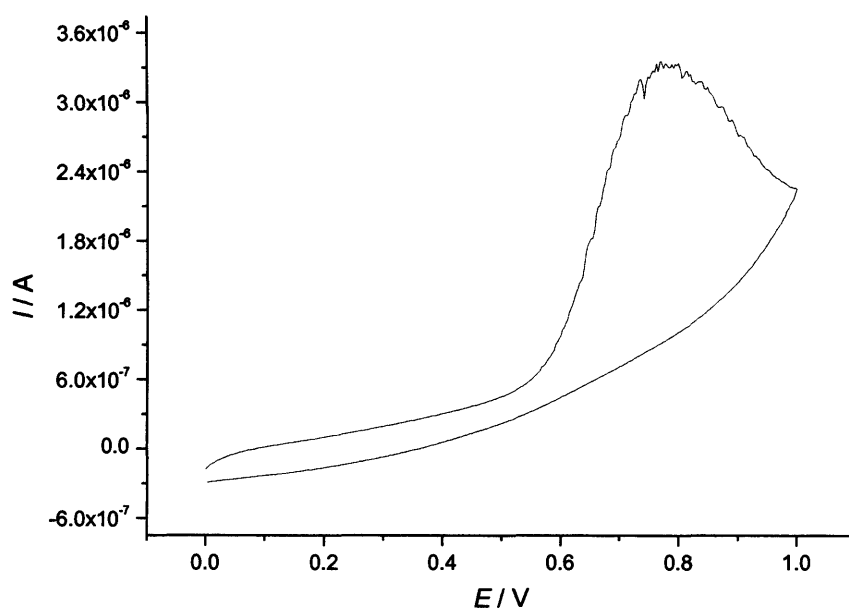


Figure 3. Forward and reverse voltammetric response of ferrocene at a 1 mm diameter Pt disc electrode in sc CH_2F_2 at 90°C at 100 bar at 0.03 mol dm^{-3} TBABF₄ concentration. Irreversible voltammetry was thought to be due to the formation of an insoluble salt on the electrode